

UNIVERSITY OF BIRMINGHAM

THE EFFECT OF NUCLEAR HORMONE RECEPTOR STIMULATION IN ORAL EPITHELIA

by

BENJAMIN JOHN HEWITT

A thesis submitted to the University of Birmingham for the degree of DOCTOR OF PHILOSOPHY

School of Dentistry
Institute of Clinical Sciences
College of Medical and Dental Sciences
University of Birmingham

December 2023

UNIVERSITY OF BIRMINGHAM

University of Birmingham Research Archive
e-theses repository



This unpublished thesis/dissertation is under a Creative Commons Attribution 4.0 International (CC BY 4.0) licence.

You are free to:

Share — copy and redistribute the material in any medium or format

Adapt — remix, transform, and build upon the material for any purpose, even commercially.

The licensor cannot revoke these freedoms as long as you follow the license terms.

Under the following terms:



Attribution — You must give appropriate credit, provide a link to the license, and indicate if changes were made. You may do so in any reasonable manner, but not in any way that suggests the licensor endorses you or your use.

No additional restrictions — You may not apply legal terms or technological measures that legally restrict others from doing anything the license permits.

Notices:

You do not have to comply with the license for elements of the material in the public domain or where your use is permitted by an applicable exception or limitation.

No warranties are given. The license may not give you all of the permissions necessary for your intended use. For example, other rights such as publicity, privacy, or moral rights may limit how you use the material.

Unless otherwise stated, any material in this thesis/dissertation that is cited to a third-party source is not included in the terms of this licence. Please refer to the original source(s) for licencing conditions of any quotes, images or other material cited to a third party.

ABSTRACT

Gingivitis is a plaque-mediated, inflammatory periodontal disease of the gingival mucosa with high prevalence in the modern population. The gingival mucosa is covered by the gingival epithelium, which plays a significant role in the pathogenesis of periodontal diseases by instigating inflammatory signalling and recruiting immune cells in response to bacteria. Importantly, the gingival epithelia act as a barrier, maintaining homeostasis and preventing bacterial ingress into the deeper tissues. Gingivitis itself poses little risk to the patient but may progress to periodontitis in susceptible individuals. This is a hyperactive immune response to the plaque stimulus, leading to destruction of the deeper tissues and a loss of attachment of the tooth. This thesis aimed to study these inflammatory and barrier function responses to bacteria *in vitro* in monolayer cells and novel organotypic models, and then investigate the nuclear hormone receptor peroxisome proliferator activated receptor gamma (PPARγ) as an anti-inflammatory agent.

RT-qPCR, transepithelial electrical resistance and fluorescent macromolecular tracer assays were employed to identify a suitable inducer of inflammation and barrier function failure for use in successive studies. Additionally, two reporter cell lines were generated to validate PPARγ agonists in epithelial cells, with western blotting and PCR performed to identify differential expression of PPARγ tissue isoforms. Finally, a novel culture device was designed, tested and utilised to generate organotypic gingival epithelial cultures, enabling comparison of the response of monolayer and organotypic cultures to an inflammatory agent and PPARγ agonists.

Bacterial lipopolysaccharide (LPS) was shown to effectively induce pro-inflammatory cytokine expression. Treatment with a validated PPARγ agonist (GW1929) abrogated

this effect, reducing the expression of pro-inflammatory cytokines and increasing anti-inflammatory cytokines. Barrier function was also significantly reduced by LPS, with this effect appearing to be partially abrogated by PPARγ treatment.

The buoyant epithelial culture device (BECD) was shown to generate stratified, differentiated gingival epithelial mimics, with minimal user input compared to alternative approaches due to a unique floating design. BECD-cultured cells showed minimal pro-inflammatory cytokine expression following LPS treatment, indicating marked differences in inflammatory signalling compared to monolayer cultures.

In conclusion, this thesis demonstrated the usage of LPS as an inducer of inflammation and barrier function failure, whilst showing that PPARγ agonists may pose significant utility in curbing inflammatory responses in gingival epithelia, with the potential to aid in the maintenance of epithelial barrier function. The efficacy of the novel BECD was also demonstrated by showing the marked difference in response between simple monolayer cultures and more complex organotypic cultures. This system may also find use in further studies of other stratified epithelial tissues.

ACKNOWLEDGMENTS

I'd like to say a huge thank you to my supervisors; Professor Michael Milward, Dr Malgorzata Wiench, Dr Richard Shelton, Professor Paul Cooper and Dr Robert Lucas. I couldn't have asked for a better team to guide me through the process of this PhD, and to help me to become a better scientist – I've valued every meeting, every word of advice and all the support you gave me. A big thank you also goes to the Innovation team at Haleon for supporting me and providing me with the opportunity to work with you all. I'd also like to thank the technical staff at the School of Dentistry; Dr Helen Wright, Dr Jianguo Liu, Dr Jonathan James, Gay Smith, Michelle Holder and Lisa Shriane. All of you were always willing to help, listen to moans about failed experiments or provide a late afternoon sugar kick.

A huge thank you goes to the PGR office at the School of Dentistry, and to the wonderful group of people that I was lucky enough to become friends with – I can't possibly thank you enough. With all the laughs, espressos and hours working together, you really did make my time working on the PhD a fantastically fun experience. I feel immensely fortunate to have ended up here at the same time as you all, and I'm so excited to see what we all do next!

Of course, none of this would be possible without my family – Mom, Dad, and Em for always encouraging me to do what inspires me and makes me happy. Thank you for always putting up with my vague complaints about things not working in the lab and making me laugh with jokes about me pipetting things! I can't thank enough every one of my climbing partners – Tom, Dave, Mirf, Phil and Paula, to name but a few - for keeping me sane and happy, be it out in the mountains or drinking tea at Redpoint. Similarly, a huge thanks to Zach, who's shared many a car ride with me complaining and ranting about biology; but has always been there to suggest a day out climbing to make me realise everything will be okay. A big thank you too to Anthony, who's always been able to make me laugh and keep me sane, even when it's a tough ask!

Finally, I'd like to thank the wonderful Amelia, who I've been incredibly lucky to have with me through the highs and lows of obtaining a PhD, both as a friend and partner. Thank you for all your endless support, encouragement, and love – it really has made the journey an exciting and happy one.

TABLE OF CONTENTS

THE EFFECT OF NUCLEAR HORMONE RECEPTOR STIMULATION IN ORAL EPITHELIA i

ABSTRACT ii

ACKNOWLEDGMENTS iv

TABLE OF CONTENTS v

LIST OF FIGURES x

LIST OF TABLES xiii

1. INTRODUCTION 1

1.1. Periodontal disease 2

1.1.1. Periodontal tissues and plaque 3

1.1.2. Symptoms, scoring and epidemiology of periodontal disease 3

1.1.3. Mechanism of gingival inflammation and progression to periodontitis 7

1.1.4. Current approaches to prevention and treatment of periodontal diseases 9

1.2. Gingival epithelia: structure and function 11

1.2.1. Epithelial intercellular junctions 14

1.2.1.1. Desmosomes and hemidesmosomes 14

1.2.1.2. Adherens junctions 15

1.2.1.3. Tight junctions 16

1.2.2. Interplay between inflammation and barrier function 19

1.2.3. *In vitro* assessment of barrier function 22

1.2.4. Organotypic culture of gingival epithelia *in vitro* 24

1.3. Nuclear hormone receptors (NHRs) 27

1.3.1. Nuclear hormone receptor classification and structure 29

1.3.1.1. Class I nuclear hormone receptors 29

1.3.1.2. Class II nuclear hormone receptors 30

1.3.1.3. Class III and IV nuclear hormone receptors 31

1.3.2. Peroxisome proliferator activated receptor gamma (PPARγ) 32

1.3.2.1. PPARγ structure and function 32

1.3.2.2. PPARγ in health and disease 34

1.4. Aims and objectives 37

2. MATERIALS AND METHODS 39

2.1. Cell culture 40
2.2. Culture treatments and stock solutions 41
2.2.1. *Escherichia coli* lipopolysaccharide supplementation 41
2.2.2. PPARγ agonists and antagonists 41
2.2.3. Cosmetic compounds under investigation as PPARγ agonists 42
2.2.1. Compound 43
2.2.2. Cell counting kit 8 (CCK-8) cytotoxicity assay 45
2.2.3. Combined LPS and PPARγ agonist treatment 46
2.3. H400 cell growth and viability curves 47
2.4. Production of PPARγ reporter cell lines in H400 oral squamous cell carcinoma cells. 48
2.4.1. Stable genetic transfection with PPRE-H2B-eGFP reporter 48
2.4.1.1. Extraction and purification of PPRE-H2B-eGFP plasmid DNA from DH5α *E. coli* ... 48
2.4.1.2. Diagnostic restriction enzyme digest of PPRE-H2B-eGFP plasmid DNA 49
2.4.1.3. Transfection of H400 oral squamous carcinoma cells with PPRE-H2B-eGFP plasmid 50
2.4.1.4. Culture of H400:PPRE-H2B cells 51
2.4.1.5. Selection of transfected cells for stable plasmid integration into H400 cell genome ... 51
2.4.1.6. Initial verification of eGFP fluorescence in transfected H400:PPRE-H2B-eGFP cells 52
2.4.1.7. Polyclonal to monoclonal selection of PPRE-H2B-eGFP transfected cells 52
2.4.2. Transient transfections with PPRE-pNL1.3 reporter system 53
2.4.2.1. Extraction and purification of PPRE-pNL1.3 plasmid DNA from DH5α *E.coli* 53
2.4.2.2. Diagnostic restriction enzyme digest of PPRE-pNL1.3 plasmid DNA 54
2.4.2.3. Transfection of H400 Oral Squamous Carcinoma cells with PPRE-pNL1.3 plasmid . 55
2.4.2.4. NanoGlo nanoluciferase assay 56
2.5. Development of a novel 3D printed device for the culture of gingival epithelial equivalents 57
2.5.1. Buoyant epithelial culture device (BECD) design and fabrication 57
2.5.2. Production of stratified epithelia using BECDs 58
2.5.3. Histological processing 60
2.5.4. Immunofluorescence staining 61
2.5.5. Image processing and analysis 63
2.5.6. Replicate definitions for BECD validation studies 63
2.6. Gene expression analysis 64

2.6.1. RNA isolation 64
2.6.1.1. Monolayer cells 64
2.6.1.2. Organotypically cultured cells 64
2.6.2. cDNA synthesis 65
2.6.3. RT-qPCR 65
2.6.4. Sequencing of GW9662-modifiable region of PPARG ligand binding domain 70
2.6.4.1. Reverse transcription PCR and DNA electrophoresis 70
2.6.4.2. PCR product gel extraction 71
2.6.4.3. Preparation of samples for sequencing 72
2.6.5. Semi-quantitative RT-PCR of PPARγ transcript variants 72
2.7. Protein expression analysis 73
2.7.1. Western blotting 73
2.7.1.1. Protein isolation and quantification 73
2.7.1.2. Sodium dodecyl sulphate polyacrylamide gel electrophoresis (SDS-PAGE) 75
2.7.1.3. Protein transfer to western blot membrane 76
2.7.1.4. Ponceau staining 76
2.7.1.5. Immunodetection 77
2.7.2. Enzyme-linked immunosorbent assays (ELISAs) for interleukins 6 and 11 79
2.8. Epithelial barrier function assays 79
2.8.1. Transepithelial electrical resistance (TEER) assay 79
2.8.2. Fluorescein-isothiocyanate (FITC) tagged dextran macromolecular tracer assay 80
2.8.3. Barrier function assays in organotypically cultured tissues 81
2.9. Combined LPS challenge and PPARγ activation in H400 cells 82
2.9.1. Epithelial barrier function: identifying optimal concentration of LPS 82
2.9.2. Epithelial barrier function: combined LPS stimulation and PPARγ agonist treatment 82
2.9.3. Culture setup for gene and protein expression analysis following combined LPS and PPARγ agonist exposure 83
2.9.3.1. 2D cultured H400 OSCC cells 83
2.9.3.2. 3D culture of stratified H400 OSCC cells with BECD system 83
2.10. Statistical analysis and replicate definitions 84
3. CHARACTERISING THE RESPONSE OF ORAL EPITHELIAL CELLS TO BACTERIAL LIPOPOLYSACCHARIDE 85
3.1. Introduction 86

3.2. Growth curves and cytotoxicity testing 87
3.3. Modification of epithelial barrier function with LPS: TEER and macromolecular tracer assays 89
3.4. Analysis of LPS treatment induced changes in gene expression 92
3.5. Verification of PPARγ expression in H400 OSCC cells 94
3.6. Discussion 96
4. DEVELOPMENT AND APPLICATION OF PPARγ REPORTER SYSTEMS IN ORAL EPITHELIAL CELLS 101
4.1. Introduction 102
4.2. PPRE-H2B-eGFP and PPRE-pNL1.3 plasmid validation with restriction enzyme digests 103
4.3. H400:PPRE-H2B-eGFP reporter line generation and testing 110
4.4. H400:PPRE-pNL1.3 reporter line generation and testing 113
4.5. Screening of compounds for PPARγ agonist activity 116
4.6. Investigation of paradoxical PPARγ activation by the irreversible antagonist GW9662 120
4.7. Discussion 122
5. DEVELOPMENT OF A NOVEL 3D PRINTED DEVICE FOR THE ORGANOTYPIC CULTURE OF GINGIVAL EPITHELIA EQUIVALENTS 133
5.1. Introduction 134
5.2. BECD design and geometry 136
5.3. Material selection trials and generation of stratified epithelia at the ALI 137
5.4. Assessment of BECD-cultured epithelial tissue thickness and reproducibility 142
5.5. Assessment of BECD-cultured epithelial tissue differentiation 144
5.6. Discussion 147
6. THE ROLE OF PPARγ ACTIVATION IN REDUCING THE EFFECTS OF LPS ON ORAL EPITHELIAL CELLS 153
6.1. Introduction 154
6.2. Analysis of gene and protein expression in LPS-challenged H400 cells treated with PPARγ agonists 155
6.2.1. LPS/GW1929 double treatment in monolayer H400 OSCC cells 156
6.2.2. LPS/GW1929 double treatment in organotypically cultured H400 OSCC cells 164
6.2.3. Comparison of gene expression between monolayer- and organotypically cultured cells 166

6.3. Barrier function assays in LPS-challenged H400 cells treated with a PPARγ agonist 173
6.4. Discussion 175
7. CONCLUSIONS AND FUTURE WORK 183
7.1. Summary of findings 184
7.2. Future work 187
7.3. Concluding remarks 189
8. LIST OF REFERENCES 190
9. APPENDICES 217
9.1. Publications arising from this thesis 217

LIST OF FIGURES

Figure 1.1 – Diagrammatic representation of the architectural organisation of the gingival epithelia.. 12
Figure 1.2 - Diagrammatic representation of simplified tight junction structure in epithelial cells. 17
Figure 1.3 - Diagram depicting transepithelial electrical resistance (TEER) measurement system.. 23
Figure 1.4 – Diagram depicting a generic macromolecular tracer barrier function assay. 24
Figure 1.5 - Diagram of simple air-liquid interface (ALI) culture of keratinocytes in tissue culture inserts. 26
Figure 1.6 - Nuclear hormone receptor schematic diagram.. 27
Figure 1.7 - Diagrammatic representation of nuclear hormone receptor activation pathways. 32
Figure 2.1 - Schematic diagrams depicting the steps involved in the production and processing of 3D printed BECDs. 58
Figure 2.2 - Steps applied for the use of BECDs in establishing a fibroblast-seeded collagen gel and seeding keratinocytes on the surface for stratification via ALI culture. 60
Figure 2.3 - Photographs of steps involved in organotypic gingival epithelium sample preparation for barrier function assays. 81
Figure 3.1 - H400 oral squamous cell carcinoma cell growth plot, comparing cells exposed to LPS at three different concentrations to untreated controls. No statistically significant difference was identified between any tested concentration and untreated control at any timepoint. 88
Figure 3.2 - H400 oral squamous cell carcinoma cell viability plot, showing cell viability over 9 days of LPS treatment.. 89
Figure 3.3 - Transepithelial electrical resistance (TEER) measurements of designated wells A) prior to LPS addition and B) after 24 hours of LPS exposure. 90
Figure 3.4 - FITC-dextran macromolecular tracer assay of LPS exposed (24 hours) H400 cells. 91
Figure 3.5 – RT-qPCR analysis of RNA extracted from H400 cell cultures exposed to *E.coli* LPS for 24 hours at 20, 200 and 2000 ng/ml. A) Inflammatory cytokines B) PPARγ and barrier function related genes. 93

Figure 3.6 – Comparison of the expression of PPARγ transcript variants γ1 and γ2 at the RNA level by semiquantitative RT-PCR (A, B) and protein level by western blot (C, D). 95
Figure 4.1 - Plasmid map of PPRE-H2B-eGFP, showing restriction enzyme recognition sites and key features or inserts.. 105
Figure 4.2 – Gel image of restriction enzyme digestion of PPRE-H2B-eGFP isolated from cultured, transformed DH5α *E.coli.* 106
Figure 4.3 - Plasmid map of PPRE-pNL1.3, showing restriction enzyme recognition sites and key features or inserts.. 108
Figure 4.4 - Restriction enzyme digestion of PPRE-pNL1.3 isolated from cultured, transformed DH5α *E.coli.* 109
Figure 4.5 -Merged widefield epifluorescence and phase contrast photomicrograph of H400 cells transiently transfected with PPRE-H2B-eGFP plasmid. 110
Figure 4.6 – Cell growth curves of untransfected (blue) and PPRE-H2B-eGFP transfected (red) H400 cells, exposed to 500 µg/ml Geneticin G418. 111
Figure 4.7 – eGFP fluorescence of untransfected control and PPRE-H2B-eGFP transfected H400 cells exposed to GW1929 at indicated concentrations. 113
Figure 4.8 - Analysis of PPARγ activation using H400 cells (left, black) and HaCaT cells (right, orange) transfected with PPRE-pNL1.3. 115
Figure 4.9 - PPARγ activation in H400:PPRE-pNL1.3 cells in charcoal stripped serum (CSS) supplemented media. 116
Figure 4.10 – CCK-8 cytotoxicity assay of cosmetic compounds under investigation as PPARγ agonists, following 24 hours of exposure. 117
Figure 4.11 – NanoGlo assay of H400 cells transfected with PPRE-pNL1.3 reporter and treated with cosmetic compounds for 24 hours (1 µg/ml for all), showing that no tested compound generated a significant increase in PPARγ activation. 119
Figure 4.12 - DNA electrophoresis of PCR products for sequencing of the GW9662-modifable region of the PPARγ ligand binding domain in H400 cells. 121
Figure 4.13 – Sanger sequencing of PCR product aligned to canonical PPARG-217 coding sequence (CDS). 122
Figure 5.1 – Engineering drawings depicting the features and geometry of the BECD system. 137

Figure 5.2 - PLA-based BECDs, demonstrating the two different failure modes observed in this study. 138
Figure 5.3 – Images of polypropylene (PP) 3D-printed BECD as used for *in vitro* trials. 139
Figure 5.4 - Images of steps involved in the production and use of BECDs for stratified epithelial culture. 139
Figure 5.5 - Representative photomicrographs of H&E-stained sections of BECD-cultured H400 cells on a collagen-3T3 fibroblast gel for 7 (A), 14 (C) and 21 (E) days. 141
Figure 5.6 – A) Maximum epithelial thickness (MET) 'superplot' for H400 cells cultured at the ALI using BECDs. 144
Figure 5.7 - Confocal micrographs of control human gingival tissue (A, C, E) and epithelia cultured in BECDs for 21 days (B, D, F).. 146
Figure 6.1 - RT-qPCR analysis of gene expression in monolayer cultured H400 cells, stimulated with LPS (2 µg/ml) and treated with GW1929 (5 µM). 158
Figure 6.2 - Human IL-6 ELISA standard curve. 160
Figure 6.3 - IL-11 ELISA performed on H400 cells exposed to LPS and GW1929. 161
Figure 6.4 – Western blots and quantification of protein expression for tight junction proteins ZO-1 (A, B), claudin (C, D) and occludin (E, F). 163
Figure 6.5 - RT-qPCR analysis of gene expression in BECD cultured H400 cells (14 days ALI), stimulated with LPS (2 µg/ml) and treated with GW1929 (5 µM). 165
Figure 6.6 – Comparison of inflammation-related gene expression in monolayer (blue) and organotypic (red) H400 cells. 167
Figure 6.7 - Comparison of PPARγ and PPRE gene expression in monolayer (blue) and organotypic (red) H400 cells. 169
Figure 6.8 - Comparison of barrier function related gene expression in monolayer (blue) and organotypic (red) H400 cells. 171
Figure 6.9 - Comparison of epithelial differentiation marker gene expression in monolayer (blue) and organotypic (red) H400 cells. 172
Figure 6.10 – Barrier function assays performed in monolayer H400 cells exposed to 2 µg/ml LPS and the PPARγ agonist GW1929 (5 µM).. 174
Figure 6.11 - TEER assay performed on organotypically cultured H400 cells exposed to 2 µg/ml LPS and the PPARγ agonist GW1929 (5 µM).. 175

LIST OF TABLES

Table 2.1 - Final concentration of O127:B8 *E.coli* LPS in culture media, and volume of LPS stock added to 3 ml supplemented HamsF12:DMEM.....41
Table 2.2 - Volumes of test compounds and DMSO added to 3 ml of supplemented HamsF12 culture media for PPARγ studies.....42
Table 2.3 – GRAS compounds used in cosmetics and oral care products which were selected for screening for PPARγ activation.....43
Table 2.3 - Culture designation matrix, showing supplementation with GW1929 or LPS.....47
Table 2.4 - FastDigest restriction enzymes employed in producing a diagnostic digest of plasmid DNA.....49
Table 2.5 - FastDigest restriction enzymes employed in producing a diagnostic digest of PPRE-pNL1.3 plasmid DNA.....54
Table 2.6 - Volumes of Lipofectamine 3000 reagents and OptiMEM media used for transfection of H400 cells with pNL1.3......55
Table 2.8 - Antibodies used for immunofluorescence staining......62
Table 2.8 - Primer sequences used for RT-qPCR throughout the present work, detailing target gene, gene symbol, product size and forward and reverse primer sequences.....66
Table 2.9 - LightCycler 480 II (Roche, USA) reaction conditions used for RT-qPCR throughout the present work.....69
Table 2.10 - RT-PCR conditions for amplification of PPAR ligand binding domain, prior to sequencing.....71
Table 2.11 - PCR primers used for amplification and sequencing of the PPARG ligand binding domain region of interest.....72
Table 2.12 – Primers used for isoform-specific RT-sqPCR in H400 cells.....73
Table 2.13 – Constituents of RIPA buffer for protein isolation.....74
Table 2.14 - Components of protein-buffer mixtures for SDS-PAGE.....75
Table 2.15 - Constituents of Ponceau staining solution, as used for assessing protein transfer to western blotting membranes.....76
Table 2.16- Constituents of 10x Tris-buffered saline (TBS).....77
Table 2.17 - Antibodies used for western blotting.....78

Table 2.18 - ELISA kits and manufacturer details used to assess changes in interleukins 6 and 11 production in H400 cells.....79
Table 5.1 - Materials selection matrix depicting the outcome of printing, sterilisation and *in vitro* trials of PLA, PC, PETG and PC. 142
Table 6.1 - Human IL-6 ELISA, recorded absorbance values of sample wells (450 - 570 nm).. 160

1. INTRODUCTION

1.1. Periodontal disease

Gingival inflammation (gingivitis) is a form of periodontal disease with remarkable prevalence across the modern population, with upper estimates suggesting that 93.9% (Li *et al.*, 2010) to 100% (Idrees *et al.*, 2014) of adults present with mild to severe clinical gingivitis. This inflammation can range from slight changes in colour of the soft gum tissues, through to marked spontaneous bleeding and ulceration.

Gingivitis can be reversed by removal of the pathogenic stimulus – plaque – while continued inflammation may progress to periodontitis in susceptible individuals. This is inflammation of, and damage to, the periodontal tissues – an irreversible and serious condition which may lead to the loss of the tooth (Flemmig, 1999). Furthermore, recent research has revealed evidence of correlation between periodontal disease and increased risk of serious systemic disease, including cancer (Dizdar *et al.*, 2017; Michaud *et al.*, 2017), coronary heart disease (Bahekar *et al.*, 2007) and diabetes mellitus (Preshaw *et al.*, 2012). Indeed, patients presenting with periodontal disease may show elevated systemic inflammatory markers (Nibali *et al.*, 2007; Hajishengallis, 2014), which may result in exacerbation of other inflammatory conditions such as atopic dermatitis and psoriasis (MacKlis *et al.*, 2020).

As gingivitis is almost entirely a plaque-driven pathology (Page, 1986), strict oral hygiene routines are widely accepted as the best preventative approach (Chapple *et al.*, 2015). Improved management of gingivitis may result in a reduction in the number of individuals showing progression to periodontitis, a more serious disease state. A great deal of research has been performed into both further preventative measures and possible treatments for gingivitis as additions to oral hygiene awareness and education; aiming to prevent the onset of gingivitis, or to reduce the degree of inflammation and periodontitis. However, with the

extreme prevalence of the disease, and the increasing burden of gingivitis-mediated disease on health services, novel strategies are required to help in disease management.

1.1.1. Periodontal tissues and plaque

The periodontal tissues comprise the alveolar bone, covered in the gingival mucosa and connected to the cementum of the tooth by the periodontal ligament (Hassell, 1993). The gingival mucosa attaches to the tooth surface with the junctional epithelium, which prevents the ingress of microbes and particles into the periodontal ligament. Additionally, the external surface of the gingival mucosa is covered in gingival epithelium, a keratinised stratified epithelial tissue which acts to forms a barrier between the deeper tissues and the oral cavity (Takahashi *et al.*, 2019). These periodontal tissues are constantly exposed to the oral environment, including its diverse microbiome. These bacteria typically form oral biofilms (plaque), which are multispecies communities of bacteria within a secreted extracellular matrix, which often inhabit the sub- and supra-gingival margin (Jakubovics *et al.*, 2021). This close association between the periodontal tissues and plaque biofilm produces the potential for an inflammatory host response of the periodontal tissues.

1.1.2. Symptoms, scoring and epidemiology of periodontal disease

Periodontal disease describes an inflammatory disease process which may occur in both the soft tissues of the gums, and in the deeper periodontal tissues. Periodontal disease is typically divided into two stages – the earlier, reversible gingivitis, and the later, irreversible periodontitis. As previously discussed, gingivitis has been shown to affect a majority of the population at any given time and is widely seen and recognised both by dental professionals and the general public. To the lay person, the first indication of gingivitis is typically bleeding after brushing. However, to the dental professional, gingivitis can be identified by the

presence of redness, swelling, changes in gum appearance, bleeding on probing or exudate (Armitage, 2004). To screen for periodontal problems, practitioners use the basic periodontal exam (BPE) that utilises systematic probing and a defined scoring system. The BPE comprises dividing the dentition into 6 regions and walking a standardised examination probe around the margin between gingiva and tooth. Periodontal pocket probing depth, bleeding and calculus formation are recorded on a scale from 0-4, with 0 indicating no pocket formation and periodontal health, through to 4 indicating a probing depth greater than 5.5 mm (British Society of Periodontology, 2016). Additionally, gingival index (GI), for example with the Löe-Silness GI, can be documented to specifically record the inflammatory status of the gingiva by combining visual observations and mechanical stimulation by probing (Löe, 1967). Once the BPE indicates potential for periodontitis (scores 3 &4) further investigation (radiographic assessment and detailed probing charts) is used to determine a diagnosis (The British Society of Periodontology, 2018).

While periodontal disease is relatively common within the general population, several risk factors can significantly increase both the chance of periodontal disease occurring and the severity of the disease state. Poor oral hygiene has consistently been linked with increased periodontal disease risk, with a buildup of plaque and calculus leading to a greater burden of pathogenic biofilm (Timmerman and van der Weijden, 2006). Oral hygiene is generally a modifiable behaviour which may be improved by patient education in effective manual brushing and by professional interventions including supra and subgingival professional mechanical plaque removal (PMPR) to remove supra and sub-gingival calculus (Cugini *et al.*, 2000). Another such high-risk behaviour is smoking, which has long been correlated with a reduction in periodontal health (Peruzzo *et al.*, 2016). In epidemiological studies, smoking has been shown to significantly increase attachment loss and the rate of tooth loss (Axelsson,

Paulander and Lindhe, 1998) and increase plaque scoring (Preber and Bergström, 1985). Early attempts to identify the mechanism of smoking-related periodontal disease often blamed the vasoconstrictive effect of nicotine (Clarke, Shephard and Hirsch, 1981). However, more recent evidence has shown that, while the vasoconstrictive effect of smoking may be overridden by a simultaneous increase in blood pressure, transient and repeated vasoconstriction may contribute to periodontal disease pathogenesis (Mavropoulos, Aars and Brodin, 2003). Smoking has also been associated with a reduction in viability of neutrophils, which are immune cells crucial to the innate immune response within the gingival crevice (Güntsch *et al.*, 2006). Further *ex vivo* research has shown that cigarette smoke may inhibit the activation and immune responses of neutrophils, potentially contributing to the worsened periodontal health in smokers (White *et al.*, 2018).

However, while smoking and oral hygiene are modifiable behaviours, there is an increasing body of evidence suggesting a non-modifiable genetic and microbiome component to the severity of periodontal disease. An aberrant, overactive immune response to bacterial stimulus has been linked with polymorphisms of genes encoding inflammatory cytokines, leading to severe, chronic periodontal disease (Tarannum and Faizuddin, 2012; Kozak *et al.*, 2020). Additionally, due to the important role of bacterial dysbiosis in periodontal disease, the oral microbiome is increasingly understood as a key contributor to individual disease risk. Early studies identified the presence of complexes of bacteria (widely referred to as Socransky complexes), which tightly correlate with periodontitis severity (Socransky *et al.*, 1998). More recently, high throughput 16S ribosomal RNA sequencing has enabled the characterisation of these bacterial shifts in greater detail. The microbiome has been shown to differ greatly between individuals (Schwarzberg *et al.*, 2014) and this may result in differences in susceptibility to the onset of periodontal disease. For example, studies of gingivitis

pathogenesis identified a marked increase in microbiome complexity in gingivitis sufferers compared with periodontally healthy subjects (Huang *et al.*, 2014).

In addition, neutrophil function has been shown to differ between healthy patients and those who are susceptible to periodontal disease, with hyperresponsive neutrophil function strongly associated with aggressive periodontitis (Kantarci, Oyaizu and Van Dyke, 2003). Studies have suggested a link between oral microbiome and neutrophil function, potentially impairing the neutrophil-mediated killing of pathogenic bacteria while simultaneously increasing neutrophil-mediated tissue destruction (Hajishengallis, 2020).

Moreover, a growing body of evidence has shed light on the links between periodontal disease and systemic diseases, especially as gingival index has previously been shown to correlate with markers of systemic inflammation (Wohlfeil *et al.*, 2009). For example, the metabolic disorder type II diabetes mellitus (T2DM) has long been linked with periodontitis. T2DM has been associated with overactive inflammatory pathways and greater oxidative stress (Iacopino, 2001; Brownlee, 2005), which in turn may lead to an increase in the rate and severity of periodontal damage in persons living with T2DM. While inflammatory pathways may be hyperactive due to the presence of a sub or supra-gingvial biofilm, neutrophil function may be impaired, as has been shown in diabetic patients, potentially reducing the microbial killing effect of these cells (Shetty, Thomas and Ramesh, 2008). The severity of periodontal damage in these patients has also been proposed to correlate with the degree of hyperglycaemia (Preshaw *et al.*, 2012), highlighting the importance of both education regarding oral hygiene and blood glucose maintenance to minimise the severity of periodontal disease (Preshaw and Bissett, 2019). Interestingly, the elevation in systemic inflammation associated with periodontal disease has been shown to exacerbate T2DM by impairing insulin

signalling (Polak and Shapira, 2018), leading to a bi-directional relationship between periodontal disease and T2DM.

Individual susceptibility to periodontal disease has been demonstrated to be complex and multifactorial. However, it is important to note that gingivitis acts as a useful indicator of general oral hygiene, and gingivitis is both reversible and easy to manage. Indeed, gingivitis may act to prime the local immune system to clear a bacterial challenge, with studies showing marked, transient increases in inflammatory signalling in gingivitis (Offenbacher *et al.*, 2009). The progression of gingivitis to periodontitis is generally regarded as much more serious due to a loss of attachment of the tooth. For this reason, an understanding of the pathogenesis of gingivitis and its progression to periodontitis is important in the process of modelling or managing periodontal disease.

1.1.3. Mechanism of gingival inflammation and progression to periodontitis

Gingivitis is initially triggered by the response of oral keratinocytes to pathogenic oral bacteria. Gingival epithelial cells and gingival fibroblasts express membrane-linked pattern recognition receptors (PRRs), including those of the Toll-like receptor (TLR) family. These specialised receptors act to recognise components of pathogenic microbes, known as pathogen-associated molecular patterns (PAMPs), and trigger an inflammatory response, with the goal of removing the pathogenic stimulus (Groeger and Meyle, 2019). PAMPs, ranging from the bacterial endotoxin lipopolysaccharide (LPS) through to bacterial DNA, bind to PRRs and activate PRR response elements as part of the innate immune system. In keratinocytes, this innate immunity typically comprises activation and nuclear translocation of the transcription factor nuclear factor kappa beta (NFkβ) with subsequent upregulation of inflammatory cytokine production (Pivarcsi, Kemény and Dobozy, 2004). These cytokines act to guide specialised immune cells to the site of the bacterial insult, in addition to increasing

the permeability of blood vessels (Piipponen, Li and Landén, 2020). For example, the production of the pro-inflammatory cytokine interleukin 8 (CXCL8) encourages recruitment and migration of polymorphonuclear leukocytes, also known as neutrophils (De Oliveira, Rosowski and Huttenlocher, 2016). Neutrophils may kill bacteria by several mechanisms, including the release of neutrophil extracellular traps (Papayannopoulos, 2017) and by the generation of reactive oxygen species (ROS); typically the hydroxide radical ·OH, superoxide radical $O_2^{\cdot-}$ or hypochlorous acid (HOCl) (Krumova and Cosa, 2016). Additionally, neutrophils directly engage and engulf bacteria via the process of phagocytosis.

ROS are characterised by an unpaired electron in the outer electron shell, which leads to extreme reactivity. While the exact mechanism of bacterial killing by ROS is not yet understood, ROS have been shown to damage cellular fatty acids, DNA and proteins, increasing oxidative stress and preventing normal cellular functions (Al-Shehri, 2021). However, these effects are not limited to bacteria, and ROS have long been understood to cause oxidative stress in eukaryotic cells, leading to cell death and tissue damage (Bandyopadhyay, Das and Banjeree, 1999). Unresolved early gingivitis may progress in severity as the innate immune response escalates and continues to damage epithelial tissues, eventually resulting in the formation of an ulcerated pocket and microbial invasion of the deeper tissues (Preethanath, Ibraheem and Anil, 2020). Persistent, untreated gingivitis has been identified as a crucial indicator of periodontal inflammation and loss of tooth attachment (Lang, Schätzle and Löe, 2009), as has increased pro-inflammatory cytokine expression (Ellis *et al.*, 1998).

Nonetheless, the host response to bacteria is ultimately initiated and propagated by the presence of plaque, a bacterial biofilm. As the oral cavity is a microbially densely populated environment, the balance of commensal and pathogenic bacteria is increasingly being

understood as an important factor in gingival health. Studies with gingival epithelial models have indicated that epithelia exposed to reconstructed, non-pathogenic bacterial biofilms have increased epithelial thickness, keratinocyte proliferation and keratinization compared with those not exposed to biofilm (Shang *et al.*, 2018). These data suggested that the presence of a healthy, commensal bacterial microbiome improved epithelial maturity, in addition to preventing overgrowth of pathogenic bacteria (referred to as dysbiosis). Gingival microbiome analyses have previously shown that inflammatory gingival disorders may be marked by a distinct shift in the oral microbiome (Schincaglia *et al.*, 2017). For example, a reduction in the abundance of *Rothia dentocariosa* and an increase in *Fusobacterium nucleatum* subsp. *polymorphum* has been associated with a shift from periodontal health to disease (Kistler *et al.*, 2013). For this reason, treatment of gingivitis often focusses on rebalancing dysbiosis by mechanical removal of the pathogenic plaque biofilm, with limited usage of pharmaceuticals, especially antibiotic or antimicrobial therapies.

1.1.4. Current approaches to prevention and treatment of periodontal diseases

Prevention of gingivitis is largely driven by education of the patient in effective plaque removal by means of a suitable oral hygiene routine. Brushing of the teeth with an appropriate fluoridated dentifrice is widely accepted as the most effective tool to prevent periodontal disease by removal of bacterial plaque (Chapple *et al.*, 2015). In addition to regular effective brushing, chemical mouthwashes are a commonly used adjunct to improve plaque removal, with chlorhexidine-based formulations generally recognised as the most effective (Van der Weijden *et al.*, 2015). However, while gingivitis and periodontitis are bacteria-driven disease states, antibiotic therapy is rarely used in patients with chronic gingivitis. Indeed, studies of NHS general dental practitioners found that only 3% of respondents prescribed antibiotics for chronic gingivitis (Palmer *et al.*, 2000). Overuse of antibiotic therapy may lead to the removal

of commensal bacteria, allowing for an overgrowth of biofilm-bound (and thus more antibiotic resistant) pathogenic bacteria. Therefore, systemic antibiotics are typically only prescribed in cases of acute necrotising ulcerative gingivitis (ANUG), an acute presentation of infective gingivitis (Summers, 2009; Malek *et al.*, 2017).

As previously discussed in Section 1.1.3, gingivitis is an appropriate response to bacterial insult, which may result in an excessive host response in susceptible individuals, leading to periodontitis. Modulation of this immune response by reducing pro-inflammatory cytokine production, reducing ROS production or improving host antioxidant defences may all act to reduce the collateral damage caused to the gingival tissues. Non-steroidal anti-inflammatory drugs (NSAIDs) pose an appealing treatment option, with readily available access, low cost and widely accepted safety. NSAIDs typically function by inhibition of cyclooxygenase 2 (COX-2), which usually responds to circulating pro-inflammatory cytokines by the synthesis of prostaglandins, exacerbating the inflammatory response (Vane and Botting, 1998; Osafo *et al.*, 2017).

Systematic reviews of the literature have shown good evidence for the efficacy of systemic NSAIDs on gingival inflammation, both as single doses and adjuncts to conventional therapies (Polak *et al.*, 2015). Regarding topical NSAID administration, studies in dogs (Howell *et al.*, 1991) and humans (Sapna and Vandana, 2011; Funosas *et al.*, 2012) have shown some reductions in gingival index and bleeding following probing in patients treated with topically applied NSAIDs when compared with control populations. However, NSAIDs are rarely used for the treatment of gingivitis due to undesirable side effects when applied systemically, and issues with application and absorption of a suitable dose when applied topically (Heasman and Hughes, 2014). Similarly, steroidal anti-inflammatory drugs, such as corticosteroids, are not used clinically to control gingivitis, with data linking chronic

corticosteroid use with increased incidence of periodontal disease (Brasil-Oliveira *et al.*, 2020), likely due to the immunosuppressive effect of these drugs enabling deeper bacterial invasion (Coutinho and Chapman, 2011). This association between steroidal drugs and periodontal disease highlights the fine, paradoxical balance of reducing inflammation without excessive immunosuppression, as would be required of potential novel drug treatments for gingivitis.

Studies have also previously been performed to identify the role of diet on gingivitis, with clinical trials examining the use of an anti-inflammatory diet on gingival bleeding and inflammatory cytokine production. These data showed that changing to a diet rich in antioxidants, omega-3 fatty acids and vitamins generated a reduction in gingival bleeding scores, however no significant change in the production of inflammatory cytokines was observed (Woelber *et al.*, 2019). Such studies highlight the close association between oral health and systemic wellbeing, diet and other sources of inflammation and disease, as discussed previously (Section 1.1).

1.2. Gingival epithelia: structure and function

Epithelia are a group of tissues ubiquitous throughout the internal and external bodily surfaces, including the skin, oral mucosa, cornea and gut. Within the oral cavity, there are two distinct sub-types of epithelial tissues; stratified non-keratinized (as found in buccal tissues and soft palate) and stratified keratinized (located in the gingiva and hard palate) (Presland and Jurevic, 2002).

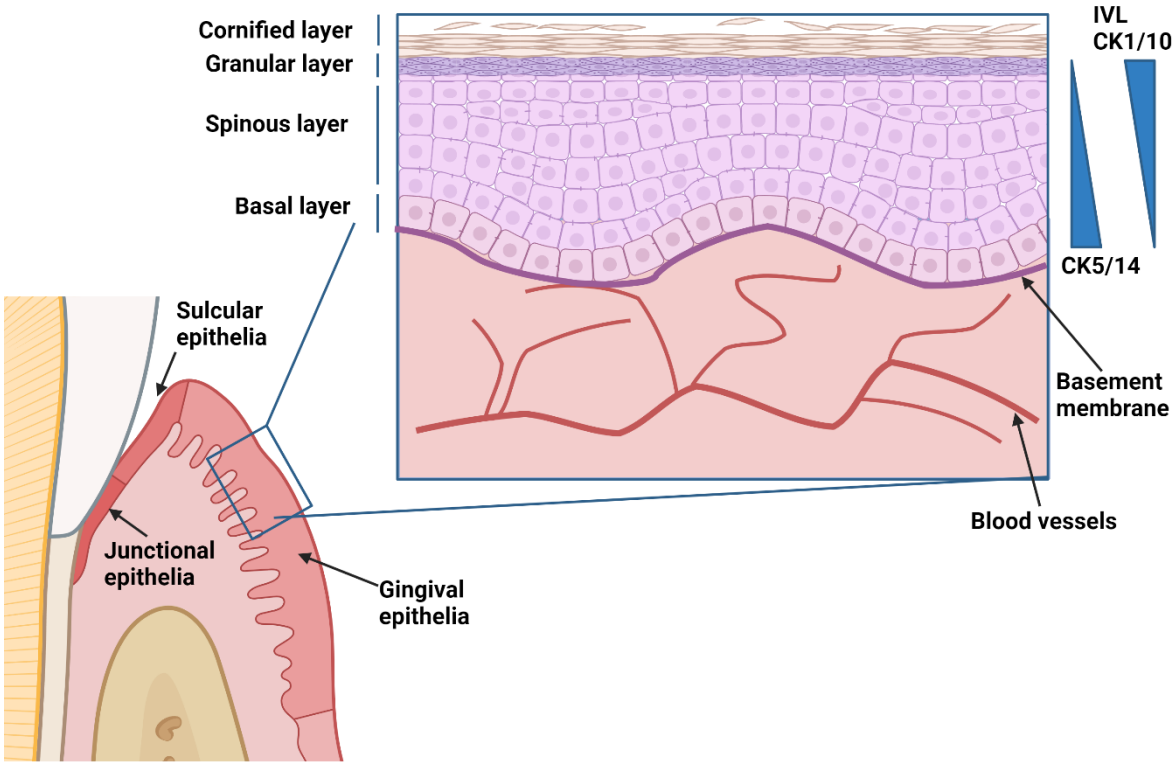


Figure 1.1 – Diagrammatic representation of the architectural organisation of the gingival epithelia. Four distinct layers are shown, including the undifferentiated basal layer which characteristically expresses cytokeratins 5 and 14 and the terminally differentiated granular layer, which expresses involucrin and cytokeratins 1 and 10. Superficial to the granular layer sits the cornified layer, comprising anuclear cells which slough off with abrasion. IVL - involucrin, CK - cytokeratin. Diagram created using BioRender.com.

Stratified epithelia share a common substructure, with a collagenous basement membrane separating a proliferative basal epithelial layer from the deeper connective tissue and blood vessels. In the stratified keratinized epithelial subtype seen in the gingiva, successive layers of cells form above the basal cell layer, with these layers becoming increasingly differentiated towards the apex in a process of spatial differentiation. As depicted in Figure 1.1, cells directly adjacent to the basal cell layer form spinous cells (Lechler and Fuchs, 2005), which express cytokeratins 5 and 14, markers of undifferentiated epithelial cells (Koster and Roop, 2007). Cells located at a further distance from the basement membrane exhibit a more mature phenotype, differentiating into granular and cornified cells, with a corresponding switch to

increased expression of cytokeratins 1 and 10 (Khan *et al.*, 2012). The cornified layer, comprised of terminally differentiated, anuclear cells, provides resistance to physical and chemical attack. This uppermost cell layers slough off under physical stress, providing abrasion resistance and protection for the deeper tissues, thus constant replenishment of these differentiated layers is critical for the health of the deeper epithelium. Involucrin is a key marker of these terminally differentiated epithelial cells, forming a protein precursor for the insoluble cornified cell envelope (Banks-Schlegel and Green, 1981; Watt, 1983).

Epithelia typically take on a protective, homeostatic role, with the multi-layered tissue architecture protecting against particle and fluid ingress, as well as abrasion (Steinert, 2000), and providing both a passive and active role in the immune system by preventing bacterial ingress and colonisation (Presland and Jurevic, 2002). The gingival epithelium (GE) is continually exposed to the microbe-rich environment of the oral cavity, necessitating the formation and maintenance of an effective protective barrier between the oral environment and the underlying periodontal tissues. This high microbial load also means that the onset of gingival inflammation can be rapid, with resultant failure of the gingival barrier leading to the ingress of bacteria and bacterial products, leading to inflammation in the deeper periodontal tissues.

These protective, homeostatic roles are often termed barrier function, a defining property of stratified epithelia describing the function of these tissues to form a competent, water-tight barrier, through which the migration of molecules can be controlled (Kalinin, Kajava and Steinert, 2002). This barrier may be compromised by physical, chemical, and microbial insults, ranging from burns and abrasions to sustained bacterial infection. Failure of barrier function is likely to result in unchecked paracellular migration of molecules and microbes across the epithelial membrane, leading to a loss of homeostatic balance and the possible

infection of deeper tissues. Failure of gingival epithelial barrier function is also observed in the process of epithelial-mesenchymal transition (EMT), characterised by a change in both cell phenotype and genotype from epithelial to a more mesenchymal type, leading to a reduction in barrier function of the affected cells, as is described below. This pathological process has been shown to occur following exposure to both whole bacteria and LPS (Abdulkareem et al., 2018), highlighting the diverse impacts that bacterial colonisation may have on the oral soft tissues.

1.2.1. Epithelial intercellular junctions

Barrier function is maintained and regulated by intercellular junctions; highly specialised protein complexes bound to the epithelial plasma membrane (Green *et al.,* 2010). Most important to barrier function are desmosomes, hemidesmosomes, adherens junctions and tight junctions, which have been shown to play different roles. Additionally, the lipid coating of the cornified cell layer also acts to regulate epithelial permeability in much the same way as in the epidermis, though with a lower lipid concentration, resulting in slightly higher permeability of the gingival epithelia than the skin (Wertz, 2021).

1.2.1.1. Desmosomes and hemidesmosomes

Desmosomes and hemidesmosomes are protein complexes which act to connect the cellular intermediate filaments at cell-cell and cell-substrate junctions, respectively (Green and Jones, 1996). Desmosomes comprise an extracellular cadherin component, which interacts with the desmogleins (a family of cadherins) expressed by the neighbouring cell desmosomes. These desmogleins are linked to intermediate filaments by desmoplakin and plakophilin, forming a desmosome—intermediate filament complex (DIFC) (Garrod and Chidgey, 2008). Hemidesmosomes typically link intermediate filaments to integrins within the extracellular matrix (ECM) via a protein complex including plectin and collagen type XVII (de Pereda *et*

al., 2009). Hemidesmosomes are often associated more with the junctional epithelium (connecting between the gingiva and tooth surface) than the gingival epithelium, likely due to the requirement for a mechanically strong dento-epithelial connection (Hormia, Owaribe and Virtanen, 2001). However, hemidesmosomes are also present in the basal cell layer of the gingival epithelium, connecting this cell layer with the deeper ECM (Bartold, Walsh and Narayanan, 2000).

While hemidesmosomes are crucial to the barrier function of epithelial tissues (Salas, Forteza and Mashukova, 2016), no studies identified have explored the possibility of hemidesmosome downregulation by bacteria. Desmosomes, however, have been shown to play a role in maintaining epithelial integrity in gingival epithelia which is susceptible to attack by bacterial infection. For example, studies of gingival epithelial cultures challenged with bacterial biofilm have shown marked downregulation of desmocollin-2 and desmoplakin, resulting in potential compromise in barrier integrity (Belibasakis *et al.*, 2015).

1.2.1.2. Adherens junctions

Adherens junctions are responsible for coupling the actin cytoskeleton of adjacent cells to one another, controlling the intercellular adhesion which holds the epithelial tissues together (Brandner, Haftek and Niessen, 2010). Adherens junctions comprise a complex of α- and β-catenin, which acts to bridge between actin cytoskeletal filaments intracellularly, and E-cadherin extracellularly (Niessen, 2007). Competent adherens junction formation has been shown to be essential in life, due to the crucial role of these intracellular junctions in controlling 'inside-out' barrier function, preventing the unchecked paracellular migration of water and solutes from within an epithelial tissue to the outside (Tunggal *et al.*, 2005). The same work showed that knockout of E-cadherin in mice resulted in perinatal death due to the inability of tissues to form an appropriate barrier to the external environment. Additionally,

these studies also identified the importance of E-cadherin expression in regulating the localization of tight junction proteins via a process of mechanotransduction (Rübsam *et al.*, 2017). This demonstrates the importance of E-cadherin in epithelial barrier function, with direct control over 'inside-out' barrier formation, and an influential role in the formation of 'outside-in' barrier formation (mediated by tight junctions).

1.2.1.3. Tight junctions

Tight junctions (TJs) are intra-cellular junctions found at the apical border of the lateral epithelial cell membrane and are responsible for forming a contiguous, sealed epithelial sheet with tightly apposed plasma membrane junctions, often referred to as kissing points (Brandner *et al.*, 2002).

TJs are typically described as having both a 'fence function' and 'gate function', both of which are critical to epithelial health. In combination, these functions enable the formation of a tight, selectively permeable epithelial layer with diffusion gradients maintained. These gradients enable the transepithelial migration of small molecules in a regulated manner, mediated by cell transport proteins (Omonijo *et al.*, 2019).

Epithelial fence function describes the role of TJs in forming and maintaining epithelial polarity. Gingival epithelial cells are highly polarised (Hodgkins, Watkins and Walker, 1978), with distinct functions and protein distributions between the apical, lateral and basal plasma membranes. The localisation of TJs to the apical edge of the lateral membrane effectively separates the apical and lateral membrane domains and forms two asymmetric membrane compartments, preventing the migration of membrane-bound proteins between these (Sawada, 2013). This allows for the containment of specific functions to each domain, which is crucial in the maintenance of ion concentration gradients and the normal functioning of the epithelial

cell. Loss of epithelial polarity has been linked to pathological processes including aggressive carcinomas (Tanos and Rodriguez-Boulan, 2008) and to the process of EMT in carcinogenesis (Royer and Lu, 2011). This link to EMT is of relevance to periodontal disease, as EMT has been noted as a pathogenic mechanism in periodontitis (Abdulkareem *et al.*, 2018b).

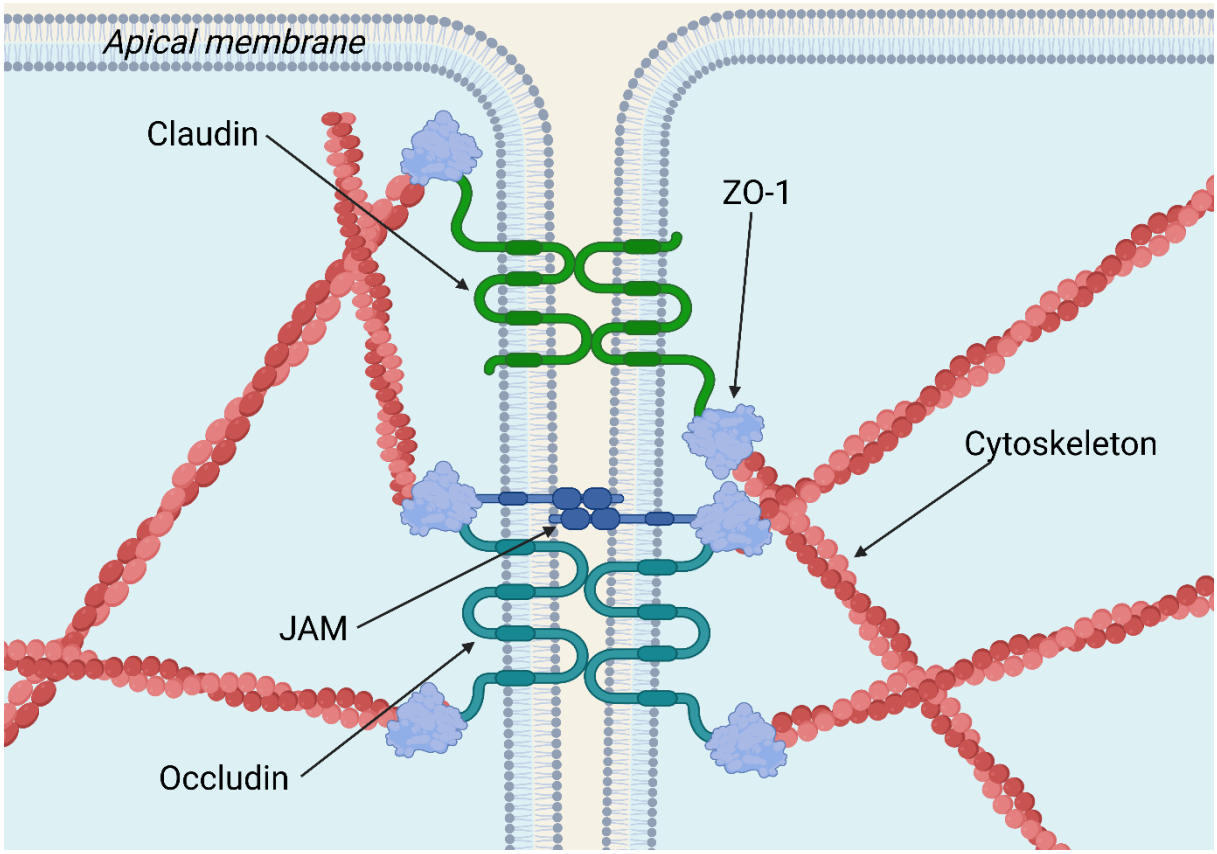


Figure 1.2 - Diagrammatic representation of simplified tight junction structure in epithelial cells. Key proteins shown, with the apical edge of the epithelial cells located at the top of the figure. The membrane proteins claudin and occludin form epithelial tight junction pores, bound to the cellular cytoskeleton by the linker protein ZO-1
JAM – Junctional adhesion molecule, ZO-1 – Zona occludens 1. Diagram created using BioRender.com.

Epithelial gate function describes the ability of cells to directly control the paracellular migration of molecules (Giepmans and van IJzendoorn, 2009). This selective permeability is driven by the architectural arrangement of proteins (shown in

Figure 1.2) within the TJ complex, forming two separate pores. A charge-selective 'small' pore is formed by the tetraspanning transmembrane protein claudin. The claudin mediated pore is responsible for the regulation of paracellular ion migration (Krug, Schulzke and Fromm, 2014) and claudin-2 has also been shown to be involved in the formation of a paracellular water channel (Rosenthal *et al.*, 2010). Conversely, a size-selective 'large' pore is formed by junctional adhesion molecules (JAMs), which allow for paracellular migration of larger molecules (>4 kDa) than would be permitted through a claudin-dependent pore (Otani *et al.*, 2019). Additionally, a third protein – occludin – is commonly found in TJs, though it has been suggested that occludin may not be required for TJ assembly. Instead, research has shown that occludin may play a regulatory role in TJ function, with post-translational modification by phosphorylation modulating the interaction between occludin and ZO-1 (Rao, 2009).

The dual-action (size and charge selective) of the tight junction mediated by JAM-1 and occludin enables exclusion and defence against harmful macromolecules and microbes, while allowing controlled migration of immune cells, such as leukocytes (Ostermann *et al.*, 2002). Simultaneously, charge-selective claudin pores enable the maintenance of concentration gradients, essential to the function of intramembrane ion channels and other transport systems. Disruption of epithelial tight junctions is suggested to have a significant effect on gradient-dependent processes and the overall tissue health (O'Neill and Garrod, 2011).

In addition, the transmembrane protein ZO-1 (zona occludens 1 / tight junction protein 1), acts as a key bridging protein between claudin, occludin and JAM-1 and the cytoskeletal actin filaments (Fanning *et al.*, 1998), as depicted in Figure 1.2. Disruption of ZO-1 expression resulted in delayed tight junction complex assembly, and continued suppression has been shown to lead to partial failure of the tight junction-mediated epithelial barrier (Roehlen *et al.*,

2020; Kuo *et al.*, 2021). Therefore, any stimulus which downregulates ZO-1 expression, or directly impacts ZO-1 integrity, is likely to cause a reduction in the barrier function of the epithelial tissue. However, there is also some indication that the TJs may not be critical to membrane integrity in cultured human gingival epithelial cells (Damek-Poprawa *et al.*, 2013). However, such a finding may depend on the cell type or culture conditions, as other research shows appropriate localisation of TJ-associated proteins from cells cultured *in vitro* (Richter *et al.*, 2016). Interestingly, protein expression of claudin, occludin and ZO-1 has been shown to vary from the basal to cornified cell layers, suggesting that the distribution of proteins within tight junctions may not be homogenous within different layers of the epithelia (Kirschner and Brandner, 2012).

1.2.2. Interplay between inflammation and barrier function

Bacterial infection may lead to a loss of barrier function due to both the direct influence of bacteria, and the host immune response. Bacterial LPS has not only been shown to trigger EMT, as discussed in Section 1.2.1, but also has been shown to directly impact the integrity of tight junctions in a range of epithelial cell types. For example, 1 µg/ml LPS has been shown to significantly downregulate claudin and occludin expression at both the gene and protein levels in intestinal epithelial cells, with a corresponding increase in barrier permeability (He *et al.*, 2019). Studies in cultured oral epithelial cells have indicated similar reductions in occludin expression following 4 hours of exposure to LPS isolated from the periodontopathogenic bacterium *Porphyromonas gingivalis*, though no barrier permeability studies were performed in this work, preventing a direct comparison between gingival TJ gene expression and barrier function (Guo *et al.*, 2018). In addition to modifying the expression of TJ-linked proteins, LPS has also been shown to increase epithelial cell apoptosis and directly disrupt ZO-1 protein complexes through a caspase-dependent

mechanism (Chin *et al.*, 2006), though these studies were again performed in intestinal epithelial cells and used high doses of LPS (up to 50 µg/ml).

Within the gingival epithelia, lipopolysaccharides from *P. gingivalis* have been shown to reduce the expression of E-cadherin, a key component of adherens junctions, with this downregulation correlating with reduced barrier function (Abe-Yutori *et al.*, 2017). As previously discussed (Section 1.2.1.2), E-cadherin has been shown to play crucial roles in the formation and localisation of tight junctions, in addition to being directly involved in adherens junction formation. Studies examining the expression of E-cadherin in the gingival epithelia of periodontally healthy and diseased patients have revealed a significant reduction in E-cadherin expression in diseased patients compared with healthy ones (Ye, Cheryl C. Chapple, *et al.*, 2000; Nagarakanti *et al.*, 2007). These investigations suggest that both the formation of both tight and adherens junctions may be compromised in periodontal disease, negatively affecting gingival barrier function.

Aside from direct interactions with tight junctions, both by modifying expression of TJ proteins and by disrupting TJ complexes, bacterial challenge may also damage barrier function by triggering an immune response. Following bacterial insult, both epithelial and specialised immune cells may secrete pro-inflammatory cytokines such as tumour necrosis factor alpha (*TNFα*), which has been shown in endothelial cells to generate a rapid increase in the phosphorylation of the TJ protein occludin, corresponding with an increase in TJ permeability and downregulation of occludin expression (Ni *et al.*, 2017). The increased epithelial permeability enabled leukocyte diapedesis, flooding bacterially challenged regions with immune cells which aim to destroy the invading pathogens. However, sustained or egregious inflammatory responses may ultimately lead to excessive tissue damage, leading to

a cycle of host cell and tissue damage and barrier compromise resulting in an exacerbated inflammatory response (Ivanov, Parkos and Nusrat, 2010).

This host cell damage is often mediated by reactive oxygen species (ROS), (see Section 1.1.3). This mechanism is a highly effective anti-microbial defensive mechanism generated by neutrophils but is also likely to damage host cells. Previous work has shown significant and marked increases in ROS production in oral epithelial cells following *P. gingivalis* LPS exposure, whilst also generating a significant reduction in epithelial barrier function (Maquera-Huacho *et al.*, 2023). Additionally, ROS have been suggested as a key mechanism via which LPS exposure triggers a pro-inflammatory response in gingival fibroblasts, with overproduction of these ROS leading to damage to host cells and increased cellular stress (Li *et al.*, 2016). Continued inflammation and ROS-production may produce an accumulation of cellular damage, which may begin to extend from the gingival epithelia into the deeper and underlying tissues leading to periodontitis (Waddington, Moseley and Embery, 2008).

1.2.3. *In vitro* assessment of barrier function

Significant research has been performed on assessing both treatments and preventative measures for barrier function, highlighting the importance of the use of repeatable, accurate *in vitro* and *in vivo* measurements of this defining property of epithelia.

Typically, barrier function assays have identified changes in the transepithelial flux of an ion or macromolecule, as is employed in transepithelial electrical resistance (TEER) and macromolecular tracer assay (MMT) measurement. TEER has been used to identify changes in ion flux through a tissue section, with a reduction in TJ tightness increasing the ease with which ions can permeate the junctions and flow between the apical and basal aspects of the tissue. A decrease in TEER value (typically presented as ohms of resistance multiplied by the tissue surface area) has been shown to act as a marker of a reduction in barrier function (Srinivasan *et al.*, 2015). TEER is widely used within the existing literature and has been validated in a range of cell types from cutaneous epithelial models (Guth *et al.*, 2015) through to oesophageal tissues (Poenar *et al.*, 2020).

TEER measurement systems typically comprise a 'chopstick' style electrode pair and tissue culture insert as shown in Figure 1.3, with requirements for the operator to ensure exact, consistent placement of handheld electrodes, as changes in depth, angle or distance have been shown to lead to marked experimental variability (Srinivasan *et al.*, 2015) . These factors may enable a substantial degree of bias – unconscious or otherwise – to occur with handheld 'chopstick' style TEER electrodes. For this reason, alternative TEER measurement systems may be employed, including measurement cups and Ussing chambers (Thomson *et al.*, 2019), which may provide a more reproducible and bias-free methodology. TEER electrodes have also been integrated into biochip / organ-on-a-chip systems in order to increase assay throughput (Poenar *et al.*, 2020).

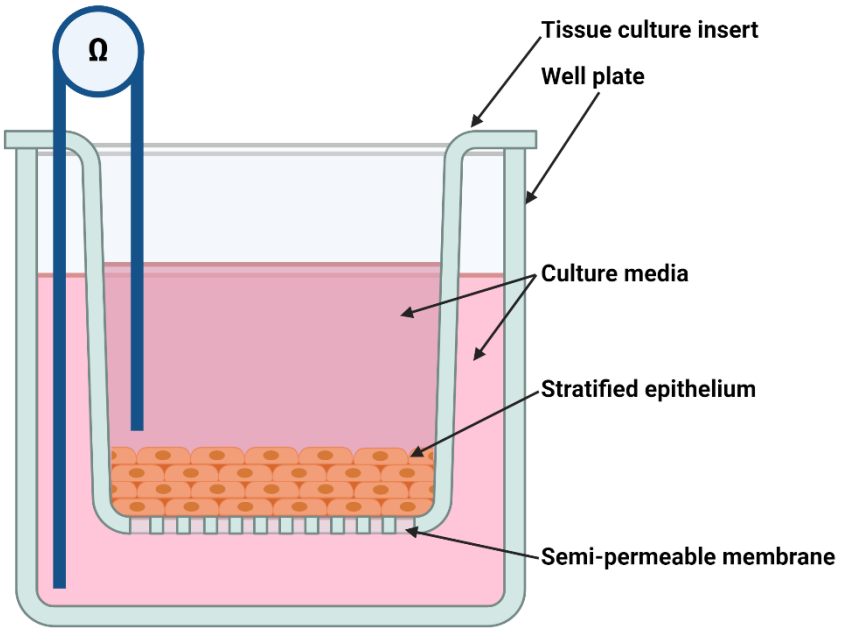


Figure 1.3 - Diagram depicting transepithelial electrical resistance (TEER) measurement system. Tissue culture inserts are used to provide two compartments separated by a semipermeable membrane. Cells are cultured on this membrane until confluent, or at the air-liquid interface until appropriately stratified. An appropriate conductive medium (typically phosphate buffered saline or culture media) is added to the top chamber, and a reading of electrical resistance across the membrane and cell layer is taken. Diagram created using BioRender.com.

MMTs (shown in Figure 1.4) are often used as an alternative, or adjunct, to TEER assays, employing a tagged molecule which can migrate through the epithelial tissue. Historically, a range of macromolecules and tracers have been employed, including early studies using the enzyme horseradish peroxidase (Colony and Neutra, 1985), or radioisotope-tagged serum proteins in microvascular studies (Studer and Potchen, 1971). However, most contemporary methodologies utilize a fluorescently tagged molecule, commonly a fluorescein isothiocyanate (FITC)-tagged dextran, due to the ease with which these can be assessed with common laboratory multimode plate readers. When added to the top chamber of an equilibrated tissue culture insert and incubated, FITC-dextran concentration in the bottom chamber has been shown to be inversely proportional to the barrier integrity of the epithelial

cell layer (Srinivasan *et al.*, 2015).

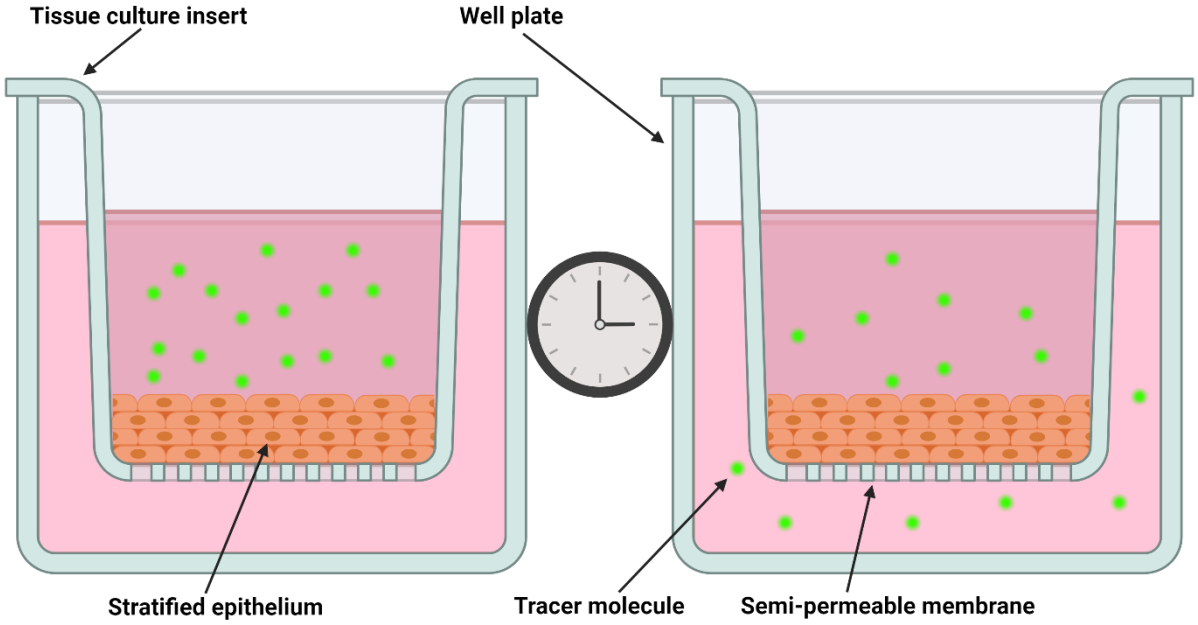


Figure 1.4 – Diagram depicting a generic macromolecular tracer barrier function assay. As for TEER measurements, tissue culture inserts are used to provide two compartments separated by a semipermeable membrane, upon which cells are cultured. An appropriate tracer is added to the apical compartment, and incubated for a set period, after which media is taken from the bottom chamber and assessed for the presence of the macromolecular tracer. Diagram created using BioRender.com

More complex macromolecular tracer assays have also been devised, using multiple tracer molecules to enable the tracking and imaging of tight junction permeability at the single cell level. This approach allows for the localisation of leaky TJs within the epithelia and improving understanding of the spatial characteristics of barrier function failure (Richter *et al.*, 2016; Reiche, Schumann and Richter, 2018).

1.2.4. Organotypic culture of gingival epithelia *in vitro*

The production of stratified epithelial tissue *in vitro* provides a useful and robust model for studying the function of normal epithelium as well as the changes that accompany a wide range of epithelial diseases. It also allows for more representative cytotoxicity and biocompatibility testing than is provided by simple monolayer culture (Pezzulo *et al.*, 2011),

as cell differentiation, morphology and signalling have been shown to represent *in vivo* cells or tissue more closely when cultured in 3D (Breslin and O'Driscoll, 2016; Tatara *et al.*, 2018). For this reason, organotypic oral mucosal equivalents (OMEs) are generally considered more advanced in the study of oral cancers, periodontal disease, drug absorption and *in vitro* drug efficacy studies.

The generation of stratified epithelial *in vitro* typically makes use of air-liquid interface (ALI) cultures, wherein a monolayer of epithelial cells is supplied with culture media from the bottom, with the top surface exposed to air (Prunieras, Regnier and Woodley, 1983). While the exact mechanism of ALI-induced stratification is still not known, this approach is widely used as an effective method to produce stratified epithelia in the laboratory. One proposed mechanism is that direct exposure to oxygen in the air increases oxidative stress in epithelial cells, leading to increases in cellular glutathione levels and promoting cell growth and differentiation (Kameyama *et al.*, 2009).

A wide range of ALI induction techniques have been described, varying from the use of stainless steel meshes (MacCallum and Lillie, 1990) to tissue culture inserts as shown in Figure 1.5 (Bals *et al.*, 2004) and microfluidic-based systems (Nalayanda *et al.*, 2009; Alexander, Eggert and Wiest, 2018).

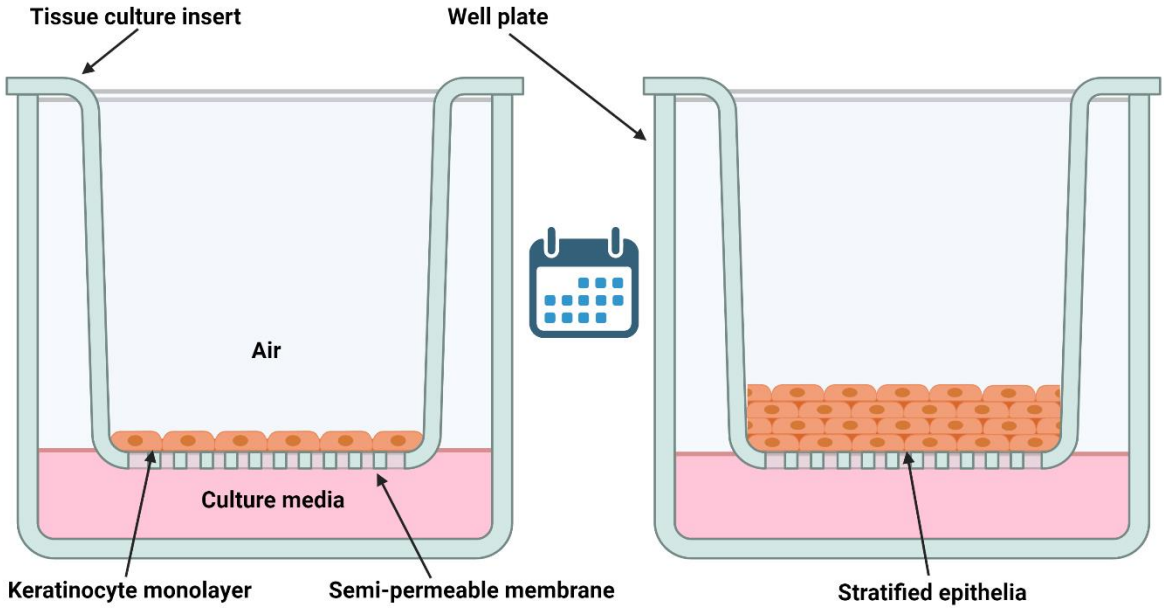


Figure 1.5 - Diagram of simple air-liquid interface (ALI) culture of keratinocytes in tissue culture inserts. Keratinocyte monolayers are seeded and grown to confluency on the semi-permeable membrane of the insert. Cell monolayers are supplied with culture media by diffusion from below the membrane, while the upper surface of cells is exposed to air. Several days or weeks of incubation at the ALI encourages the formation of a stratified (multi-layered) epithelium.

ALI culture has been identified as an important tool in adequately recapitulating both the phenotype and gene expression of several cell types, including airway epithelial cells (Yeh *et al.*, 2007; Pezzulo *et al.*, 2011) and female reproductive tract cells (Chen and Schoen, 2019). Importantly, early studies also revealed the importance of ALI culture techniques in generating a stratified gingival epithelial tissue with expression of cytokeratins indicating epithelial differentiation (Delcourt-Huard *et al.*, 1997). ALI cultures incorporating scaffolds or specific substrates have been widely used, including fibroblast-seeded hydrogels (Chinnathambi *et al.*, 2003), de-epithelialized dermis (Colley *et al.*, 2013) or traditional tissue culture plastics. Organotypic gingival epithelial cultures have been shown to differ widely in both cellular morphology and tissue architecture when cultured in/on different substrates (Khan *et al.*, 2012). These architectural differences may result in a marked difference in cell

differentiation and response to stimuli, highlighting the importance of substrate choice in the generation of organotypic tissue equivalents.

The generation of an appropriately stratified and terminally differentiated tissue equivalent may be highly important when studying inflammatory responses. For example, research has shown that the distribution of cell membrane pattern recognition receptors (responsible for detecting and responding to pathogenic microbes, as discussed in Section 1.1.3) is spatially dependent within stratified epithelia (Jiang *et al.*, 2020). Failure to properly recapitulate this differentiation pattern in a model system may result in suppressed innate immune responses.

1.3. Nuclear hormone receptors (NHRs)

Nuclear hormone receptors (NHRs) are a family of intracellular, ligand-activated transcription factors, responsible for mediating the transcriptional control and influence of multiple species of small, lipophilic signalling molecules (Bain *et al.*, 2007). These molecules are involved in a diverse range of processes relevant to metabolism, differentiation and reproduction of eukaryotic cells. Transcriptional regulation by NHRs occurs by direct interaction between the NHR and target sequences on DNA, referred to as hormone response elements (HREs) (Aranda and Pascual, 2001).

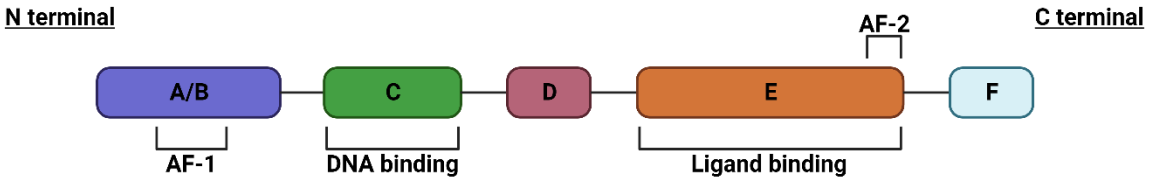


Figure 1.6 - Nuclear hormone receptor schematic diagram. Ligand independent activation functions are controlled by the AF-1 domain within the variable A/B region. NHR-DNA binding occurs via the DNA binding domain (DBD) in the highly conserved C region, connected to the ligand binding domain (LBD, region E) by the variable linking region (D). The LBD contains the ligand-dependent activation function (AF-2) domain, close to the C terminal of the protein. Diagram adapted from Aranda and Pascual, 2001.

NHRs typically comprise five regions (as depicted in Figure 1.6), with a variable A/B region at the NH_2 terminus containing the ligand-independent activation function (AF-1) domain. The roles of the AF-1 domain are as diverse as the NHR family, with evidence that residues in the AF-1 domain are targeted for post-translational modification by phosphorylation (Weigel, 1996) and by SUMOylation (modification with the small ubiqutin-related modifier-1) (Treuter and Venteclef, 2011), with these modifications aiding in the regulation of NHR function. Additionally, the role of the AF-1 domain in interacting with both basal transcription machninery and co-activator proteins has been widely reported on (Lavery and Mcewan, 2005).

In contrast to the variable A/B region, the C region is highly conserved between members of the NHR superfamily. This region contains the DNA binding domain (DBD), containing zinc-finger binding motifs responsible for the recognition and binding of the NHR to HREs within promoters and thus exerting control over the transcription of target genes (Khorasanizadeh and Rastinejad, 2001). Binding of NHRs to DNA is dependent on the presence of a hexamer recognition sequence within the HRE. This sequence is typically either monomeric or dimeric, allowing for the attachment of both NHR hetero/homodimers and monomers (Helsen *et al.*, 2012). The DBD has also been shown to function as a nuclear export signal in steroid receptors (particularly the glucocorticoid receptor), wherein NHRs are exported from the nucleus to the cytoplasm following removal of the NHR ligand (Black *et al.*, 2001).

The hinge region (region D) is a flexible link between the DBD and ligand binding domain (LBD), with increasing evidence demonstrating that it plays a role in regulating transcriptional activity via a range of post-translational modifications. For example, SUMOylation of the hinge region of the oestrogen receptor α (ERα) has been shown to be critical to enable ERα-dependent transcription (Sentis *et al.*, 2005). Similarly, acetylation of

different residues within the ERα hinge region increases transactivation and hormone sensitivity (Wang *et al.*, 2001). This highlights the complex pathway of activation, modification and downstream signalling required for effective NHR function.

Crucial to the function of NHRs as a family of ligand-dependent transcription factors is the E region, comprising the ligand binding domain (LBD) and AF-2 domain. Binding of a suitable ligand to the LBD leads to the recruitment of co-activators or co-regulators, regulating binding to, and transcription of, target genes (Jin and Li, 2010). While the primary structure of the LBD is variable, structural features such as receptor domains are generally conserved across the NHR superfamily, suggesting that the activation mechanism is similar in all NHRs (as summarised by Nagy and Schwabe, 2004). Following ligand binding, recruited transcriptional co-activators/repressors bind to the ligand-dependent activation function (AF-2) domain within the LBD (Moras and Gronemeyert, 1998; Westin, Rosenfeld and Glass, 1999).

The C-terminal F region varies in function within the NHR superfamily, with evidence that the F region is crucial to the activity of the oestrogen receptor (ERα). Truncation of this region has been shown to modify the activity of ERα-promoter transactivation and the sensitivity of ligand-receptor binding as well as altering the response of ERα to variations in coactivator availability (Koide *et al.*, 2007).

1.3.1. Nuclear hormone receptor classification and structure

1.3.1.1. Class I nuclear hormone receptors

Class I nuclear receptors, known as steroid hormone receptors, play fundamental roles in homeostatic and metabolic pathways. Examples of class I NHRs include the progesterone, glucocorticoid and androgen receptors (Bain *et al.*, 2007). In a basal state, class I receptors are

anchored in the cytoplasm by chaperone proteins (as depicted in Figure 1.7). Binding of a suitable ligand to the ligand binding domain (LBD) triggers a conformational shift, leading to detachment of the chaperone protein. A nuclear receptor homodimer is then formed between two ligand-bound receptor molecules, providing a suitable target for the binding of a nuclear localisation sequence (NLS) (Picard and Yamamoto, 1987). Binding and activation of the NLS enables translocation of the homodimer-ligand complex into the nucleus, where DNA binding occurs. The DNA binding process is facilitated by recognition of inverted DNA repeats in the HRE by the DBD (Mangelsdorf *et al.*, 1995). NHR-DNA binding is facilitated by nuclear co-activators, which may function by modification of chromatin accessibility, methylation or acetylation of HREs or by binding to RNA (McKenna and O'Malley, 2002).

1.3.1.2. Class II nuclear hormone receptors

Class II NHRs are defined as all non-steroid receptors with a known endogenous ligand, and include the thyroid hormone receptor, peroxisome proliferator activated receptor (PPAR) family and retinoid receptors. Unlike homodimer-forming class I receptors, class II receptors may bind DNA as monomers, homodimers or heterodimers, dependent on the orientation and spacing of the DNA HRE site (Forman *et al.*, 1992). Most typically however, class II receptors form heterodimers with the retinoid X receptor (RXR), improving DNA binding stability (Bugge *et al.*, 1992). The class II receptor / RXR complex is found to bind to response elements in DNA via direct repeat sequences, in contrast to the inverted repeats bound to by Class I receptors (Rastinejad *et al.*, 2013).

Inactive NHR-RXR heterodimers are bound to DNA HREs, unlike class I NHRs which only translocate to the nucleus and bind to DNA upon activation by a ligand. However, the class II NHR-RXR heterodimer is also bound to by corepressor molecules, which act to maintain chromatin condensation, preventing access by the NHR. This leads to quenching of

transcriptional activity of the NHR as a form of gene silencing (Baniahmad, 2005). Ligand binding triggers dissociation of the corepressor molecules and replacement with coactivators (Kraus and Wong, 2002). NHR coactivators function by a wide range of mechanisms. However, one key group of coactivators are histone acetyl-transferases; enzymes responsible for manipulating and decondensing the structure of chromatin, potentially exposing relevant response elements in the genome (Sever and Glass, 2013).

1.3.1.3. Class III and IV nuclear hormone receptors

Whilst Class I and II nuclear receptors have known endogenous ligands, Classes III and IV receptors are those that share some structural homology with Class I and II receptors but have no known naturally present endogenous ligands (Safe *et al.*, 2016).

While initially not well studied, these orphan receptors have now been shown to have utility in the treatment of disease (Evans, 2005). The origin of these orphan receptors, and their coexistence with classical receptors (defined as classes I and II), is a widely discussed topic in the literature with no current consensus on their biological role (Escriva, Delaunay and Laudet, 2000; Owen and Zelent, 2000).

Efforts to find synthetic ligands for these orphan nuclear receptors have identified therapeutic targets for anti-cancer therapies (Hermann-Kleiter *et al.*, 2015; Wenzl *et al.*, 2015), which have been shown to improve barrier function in gastrointestinal disease (Klepsch *et al.*, 2018) and may also have utility as anti-fibrotic treatments (Palumbo-Zerr *et al.*, 2015).

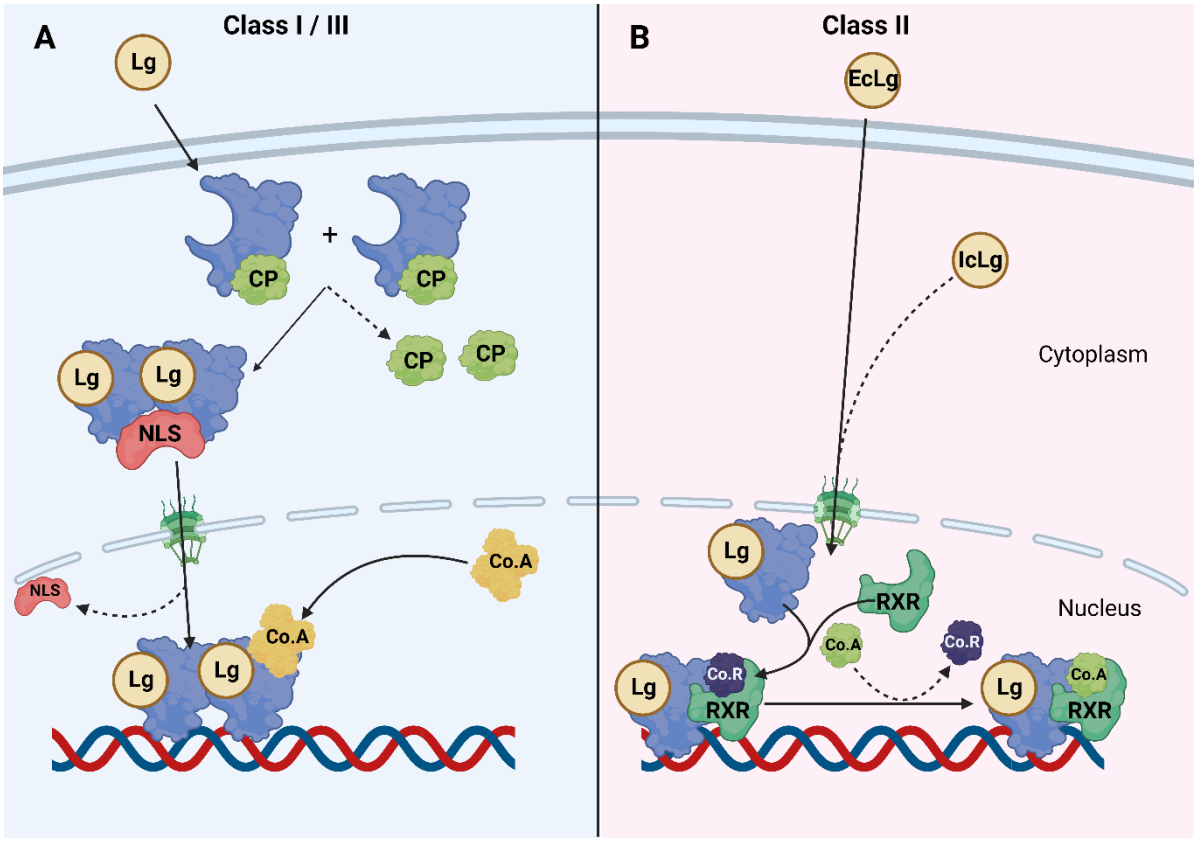


Figure 1.7 - Diagrammatic representation of nuclear hormone receptor activation pathways.
A) Class I and III nuclear hormone receptors (NHRs) are bound to the cytoplasm by chaperone proteins (CP). Binding of a suitable ligand (L) leads to the formation of an NHR homodimer and a conformational shift revealing a nuclear localisation signal (NLS). The homodimer translocates into the nucleus via nuclear pores, and bind to hormone response elements (HREs) on DNA strands. Activation then occurs via coactivator molecules and proteins.
B) Typically, class II NHRs are bound to their hormone response elements as a heterodimer with the retinoid X receptor (RXR). Ligands (Ecl / IcL) translocate to the nucleus before binding to the NHR, triggering the successive dissociation of co-repressors and replacement with coactivator molecules and proteins.
L = Ligand, NHR = Nuclear Hormone Receptor, CP = Chaperone Protein, RXR = Retinoid X Receptor, EcL = Extracellular Ligand, IcL = Intracellular Ligand, NLS = Nuclear Localisation Signal.
Created with BioRender.com

1.3.2. Peroxisome proliferator activated receptor gamma (PPARγ)

1.3.2.1. PPARγ structure and function

Peroxisome proliferator activated receptor gamma (PPARγ) is a class II nuclear hormone receptor, predominantly expressed in adipose tissue and pre-adipocytes (Chawla, 1994).

PPARγ typically functions as a regulator of insulin sensitivity and glucose metabolism by controlling fatty acid uptake into adipocytes (Montaigne, Butruille and Staels, 2021). Additionally, PPARγ (and other members of the PPAR family) have been shown to be closely involved in the differentiation of adipose and placental tissues during vertebrate development (Michalik *et al.,* 2002).

PPARγ is activated by a range of endogenous ligands, including micromolar concentrations of polyunsaturated fatty acids (Xu *et al.,* 1999), likely linked to the endogenous role of PPARγ as an insulin sensitizing transcription factor. 15-deoxy-Δ-12,14-prostaglandin-J2 (15d-PGJ2) was the earliest endogenous PPARγ ligand described and characterized (Forman *et al.,* 1995), exerting anti-inflammatory, anti-tumour and antioxidant effects in a PPARγ-dependent manner (Li, Guo and Wu, 2019). Binding of a ligand to the PPARγ ligand binding domain (LBD) triggers the formation of a PPARγ-RXR heterodimer, facilitating the replacement of co-repressor molecules with co-activators, which enables chromatin remodelling. This activated PPARγ-RXR complex is then able to bind to PPARγ response elements (PPREs) in the promoter region of target genes, producing ligand-dependent transactivation (IJpenberg *et al.,* 1997). Aside from this expected function, PPARγ has also been demonstrated to mediate ligand-dependent transrepression. In such a case, activation of PPARγ by a suitable ligand leads to antagonism of other transcription factors, further widening the widespread effects PPARγ may exert (Ghisletti *et al.,* 2007).

In addition, this transactivation and transrepression is further modified by alternative mRNA splicing of the PPARγ gene (*PPARG*), which gives rise to multiple transcript variants with different transcriptional potency due to differences in the activation function (AF-1) domain. This splicing generates parallel expression of two main protein isoforms, PPARγ1 and PPARγ2 (Zhu *et al.,* 1995). PPARγ1, a 475 amino acid protein, is relatively widely expressed

in a range of cells and tissues, including epithelia, liver and skeletal muscle. Conversely, expression of PPARγ2, a 505 amino acid protein, is limited to adipose tissue (Mukherjee *et al.*, 1997; Grygiel-Górniak, 2014). This tissue-specific expression is explained by studies showing that PPARγ2 is more specifically involved in the regulation of adipocyte deposition, differentiation and insulin sensitivity (Zhang *et al.*, 2004), as these tissues are tightly involved in glucose metabolism. The modified AF-1 domain within the A/B region of PPARγ2 has been shown to be involved in recruiting cofactors and enabling transactivation of specific target genes which are not typically activated by PPARγ1 (Bugge *et al.*, 2009), widening the potential targets of PPARγ2 beyond those activated by the more widely expressed variant. Additionally, the ability of PPARγ2 to stimulate downstream transcription has been shown to be up to 6-fold greater than the PPARγ1 isoform, suggesting that PPARγ2 is the more potent transcription factor (Fajas *et al.*, 1997). This combination of multiple PPAR isoforms, multiple PPARγ splice variants and the potential for both transactivation and transrepression of response elements may explain the involvement of PPARγ in such a wide variety of tissues and pathways.

1.3.2.2. PPARγ in health and disease

PPARγ has been implicated in a range of important pathways regulating lipid and glucose homeostasis, with particular focus given to the role of PPARγ in insulin sensitization as a treatment for insulin-resistant (type II) diabetes mellitus (Rangwala and Lazar, 2004). Activation of PPARγ in adipocytes, liver and skeletal muscle by thiazolidinediones (TZDs) such as rosiglitazone has been shown to increase the oxidation of glucose and reduce free fatty acid content in the blood, improving sensitivity to insulin (Olefsky, 2000; Cha *et al.*, 2001). For this reason, rosiglitazone was widely used in the early 2000s as a powerful and effective tool for diabetic therapy in patients with insulin-resistant diabetes mellitus

(Malinowski and Bolesta, 2000). However, the strong influence of PPARγ on systemic pathways controlling lipid storage, lipid metabolism and insulin sensitivity (Grimaldi *et al.*, 2010), as well as the relatively widespread expression of PPARγ throughout the tissues of the body, led to concerns regarding its safety for the treatment of disease (Watkins *et al.*, 2002). A host of undesirable side effects and potentially major adverse cardiac events were observed in patients treated with TZD-class drugs (Richter *et al.*, 2007; Mittal *et al.*, 2009), ultimately leading to the European Medicines Agency (EMA) issuing a ban on the use of rosiglitazone for this purpose (European Medicines Agency, 2010). These adverse events highlight the potential drawbacks of treating disease with systemically applied PPARγ ligands, as expression of PPARγ amongst a wide range of cell types, and involvement in many metabolic and signalling pathways, may produce increased risk of side effects.

In addition to diabetes, PPARγ has wide-ranging effects on inflammation and wound healing. PPARγ has been reported to repress the activation of nuclear factor kappa beta (NFκβ), a major transcription factor involved in inflammatory signalling, by binding to and blocking the promoters of NFκβ response element (typically inflammatory response genes, including cytokines) (Pascual *et al.*, 2005). This transrepression results in a PPARγ-dependent dampened inflammatory response, which has since been explored extensively. In macrophages, the expression of key inflammatory signalling molecules, including inducible nitric oxide synthase (iNOS) and matrix metalloproteinase-9 (MMP-9), have previously been shown to be markedly reduced following activation of PPARγ with both endogenous (15d-PGJ2) and synthetic ligands (Ricote *et al.*, 1998). Similarly, PPARγ activation has been demonstrated as an effective tool to reduce the synthesis of pro-inflammatory interleukins and improving *in vivo* survival in rat models of systemic sepsis (Zingarelli *et al.*, 2003; Celinski *et al.*, 2011).

In addition to reducing pro-inflammatory signalling, PPARγ stimulation has been shown to increase both the proliferation and migration of endothelial progenitor cells *in vitro* (Pistrosch *et al.*, 2005). This indicates the potential utility of PPARγ ligands for improving wound healing. For this reason, PPARγ ligands have been explored as possible treatments for inflammatory skin conditions. For example, both psoriatic arthritis and dermal plaque-type psoriasis (both forms of auto-immune disorder) have been effectively treated in a clinical trial setting using pioglitazone, a thiazolidinedione class synthetic PPARγ ligand (Bongartz *et al.*, 2005; Mittal *et al.*, 2009). Interestingly, clinical trials treating inflammatory skin disorders have shown significant differences in treatment efficacy between molecularly similar TZD-class drugs, including rosiglitazone, troglitazone and pioglitazone (Kuenzli and Saurat, 2003; Shafiq *et al.*, 2005).

Of particular importance to the present work is the potential role of PPARγ stimulation in maintaining epithelial barrier function, especially in the gingiva. As has previously been discussed, bacterial challenge can lead to a reduction in gingival barrier function, leading to bacterial ingress and homeostatic imbalance. Previous work has shown that 24 hours of activation of PPARγ by 0.1 μM rosiglitazone significantly increased RNA and protein level expression of key tight junction proteins claudin and occludin in nasal epithelial cells (Ogasawara *et al.*, 2010). Additionally, the observed regulatory changes translated to an increase in barrier function within 8 hours of PPARγ activation, as assessed by both TEER and macromolecular tracer assay.

Investigations have also been performed examining the function of PPARγ-stimulation in mouse dermal models, assessing transepidermal water loss (TEWL) recovery following physical insult by tape stripping. TEWL is widely used in *in vivo* studies to assess barrier permeability in a similar manner to the use of TEER *in vitro*. Indeed, it has been shown that

TEWL recovered faster in tape-stripped mouse dermis treated with ciglitazone, a TZD-class PPARγ ligand, compared with control mice (Man *et al.*, 2004). Ciglitazone has also been investigated in human foreskin-derived keratinocytes, where 24 hours of supplementation with 10mM ciglitazone generated significant upregulation of the aquaporin 3 (*AQP3*) gene (Jiang *et al.*, 2011). *AQP3* has previously been linked to epidermal barrier function, due to the role of these molecules in moderating water transport across barriers (Hara-Chikuma and Verkman, 2005). While relatively few specific studies have been performed on PPARγ as a target for treating or preventing the inflammatory signalling and reduction in barrier function associated with gingivitis, these studies suggest that PPARγ-activation may be therapeutically beneficial.

However, many of the previous studies have employed either recombinant endogenous or TZD-class PPARγ ligands, which are likely to have non-specific or off-target effects. For example, both 15d-PGJ2 and ciglitazone have been shown to modulate the mitogen-activated protein kinase cascade in a PPARγ-independent manner (Lennon *et al.*, 2002). This suggested that some of the anti-inflammatory and pro-barrier function effects observed in these studies may not be entirely PPARγ specific and may be due to activation of an alternative pathway. The use of specific PPARγ ligands with minimal cross-reactivity may improve the confidence in the data generated. For example, GW1929, first described in 1998, is a highly selective ligand for PPARγ with a greater potency than TZD-class ligands (Henke *et al.*, 1998).

1.4. Aims and objectives

The present work aimed to explore the potential role of PPARγ stimulation in models of inflammation in gingival epithelia. It was hypothesized that PPARγ activation may lead to a reduction in pro-inflammatory cytokine expression, whilst increasing anti-inflammatory

cytokine expression, and improving or maintaining barrier function. An additional aim was to identify any potential differences between the response of gingivitis models in monolayer cultures and more complex organotypic models. These aims were addressed with the following objectives:

Objective 1 – To identify a suitable stimulus to induce inflammation (defined here as an increase in pro-inflammatory cytokine expression and a reduction in barrier function) in monolayer-cultured oral epithelial cells.

Objective 2 – Develop a reporter system to identify suitable ligands to activate PPARγ in keratinocytes *in vitro*. The sensitivity of this system was optimised by comparison with other cell lines and a range of reporter systems trialled. Following this, the system was applied to selected compounds commonly found in cosmetic and oral care products, screening for PPARγ-agonist or antagonist activity.

Objective 3 – Develop a methodology to produce stratified, differentiated gingival epithelial equivalents *in vitro*. Confirm epithelial differentiation and quantify epithelial thickness at multiple timepoints in order to identify suitable culture periods for further studies.

Objective 4 – Trial PPARγ ligands as anti-inflammatory treatments in oral keratinocyte model systems, cultured as both monolayer and 3D-culltured epithelial equivalents. Efficacy was assessed by using RT-qPCR to identify changes in expression of cytokines and barrier function-related genes, barrier function assays and enzyme linked immunosorbent assays (ELISAs).

2. MATERIALS AND METHODS

2.1. Cell culture

All cell culture was performed aseptically in a ScanLaf Mars Class 2 microbiological safety cabinet, and cultures incubated in a HeraCell 150i CO_2 incubator (Thermofisher, UK) at 37°C and 5% CO_2. Unless stated otherwise, H400 oral squamous cell carcinoma (ECACC 06092006) cells were cultured in 1:1 Hams F12 nutrient mix and Dulbecco modified Eagle's media (DMEM) (11330-032, Gibco, USA), supplemented to final concentrations of 10% foetal calf serum (FCS), 100U /ml penicillin, 100 µg/ml streptomycin and 1mM L-glutamine – referred to as 'supplemented HamsF12:DMEM'.

Murine 3T3 Fibroblasts (ECACC 93061524) and HaCaT (300493, Cell Lines Services, Germany) were cultured in DMEM (D5796, Sigma, USA), supplemented to final concentrations of 10% FCS, 100 U/ml penicillin, 100 µg/ml streptomycin and 1mM L-glutamine.

Routine cell culture was performed in filtered T75 flasks (Nunc EasYFlask, ThermoFisher, UK). Cell passaging was performed whenever cell confluency approached 80%, with cell dissociation performed by incubation (37°C, 5% CO_2) in trypsin solution (0.25% trypsin-EDTA, 25200056, Gibco, USA) for 10 minutes. Mycoplasma testing was performed every 6 months by PCR using a commercially available testing kit (EZ-PCR mycoplasma testing kit, Geneflow, UK). All mycoplasma tests performed throughout the course of the present work were negative.

2.2. Culture treatments and stock solutions

2.2.1. *Escherichia coli* lipopolysaccharide supplementation

To produce stock solutions, 1mg O127:B8 *Escherichia coli* lipopolysaccharide (LPS) (Sigma Aldrich, UK) was reconstituted in 1 ml HamsF12:DMEM, producing a 1 mg/ml stock solution. From this, a 1:10 dilution was also performed to produce a 100 µg/ml stock solution for use at a lower final concentration when required. Siliconized, low retention microcentrifuge tubes (Eppendorf, USA) and pipette tips were used for all handling steps with LPS to maximise sample recovery.

Table 2.1 - Final concentration of O127:B8 *E.coli* LPS in culture media, and volume of LPS stock added to 3 ml supplemented HamsF12:DMEM.

Final concentration of LPS (ng/ml)	Volume of LPS stock added to 3 ml media
0	No LPS added
20	0.6 µl of 100µg/ml LPS
200	0.6 µl of 1mg/ml LPS
2000	6 µl of 1mg/ml LPS

2.2.2. PPARγ agonists and antagonists

3ml aliquots of HamsF12:DMEM supplemented with 10% FCS and 1mM L-glutamine were prepared, and test compounds added to final concentrations as shown (Table 2.2), with one compound per aliquot. All test compounds were dissolved in cell culture grade dimethylsulfoxide (DMSO) (Hybri-Max DMSO, Sigma Aldrich, UK). All media aliquots were then supplemented with DMSO as required to ensure the final DMSO concentration was consistent in all samples.

Table 2.2 - Volumes of test compounds and DMSO added to 3 ml of supplemented HamsF12 culture media for PPARγ studies.

Test compound	Stock concentration	Volume of stock added	Volume of DMSO	Manufacturer reference
Control group	N/A	0 µl	30 µl	N/A
1µM GW1929 (Agonist)	1mM	3 µl	27 µl	2057-5, Cayman Chemical, USA
5µM GW1929 (Agonist)	1mM	15 µl	15 µl	2057-5, Cayman Chemical, USA
10µM GW9662 (Antagonist)	10mM	3 µl	27 µl	M6191, Sigma Aldrich, UK
1µM rosiglitazone (Agonist)	15mM	0.6 µl	29.4 µl	R2408, Sigma Aldrich, UK

2.2.3. Cosmetic compounds under investigation as PPARγ agonists

Samples of pterostilbene, hydroxystearic acid, palmitoylethanolamide (PEA), MAXnolia™, vitamin E acetate, chia oil, SabiWhite™, sulfradex and retinol were received as gifts from Haleon, UK as part of the working agreement of the PhD studentship, and are detailed in

Table 2.4. Candidate compounds (Table 2.3) were selected following a literature search, either for activation of other members of the PPAR family (α or δ) or for evidence of interplay with the molecular pathways controlling epithelial barrier function and/or inflammation. Many of these compounds are classified as being 'generally recognised as safe' (GRAS), and so regulatory approval for use may be more easily achieved.

Table 2.3 – GRAS compounds used in cosmetics and oral care products which were selected for screening for PPARγ activation.

2.2.1. Compound	Justification
Palmitoylethanolamide (PEA)	Fatty acid amide which binds to PPARα (LoVerme *et al.*, 2005), interaction with PPARα and δ has also been reported in neuronal cells, producing an anti-inflammatory effect (Paterniti *et al.*, 2013).
Pterostilbene / pTeropure®	Reported as activating PPARα *in vitro* and lowering serum cholesterol *in vivo* in Syrian hamsters in a PPARα-dependent manner (Rimando *et al.*, 2005).
Hydroxystearic acid (HSA)	Isomers of HSA have been previously investigated as PPARα agonists (Rawlings *et al.*, 2021), and so were included in the present work to identify any cross-activation of PPARγ.
Retinol (vitamin A)	Shown to be crucial to epithelial barrier function, and highly dependent on the presence of the retinoic acid receptor (RARγ) and retinoic X receptor (RXRα) (Kubota *et al.*, 2001). RXRα has been widely described as a key coactivator to PPARγ, with the two proteins forming a heterodimer prior to

	binding to DNA response elements (Aranda and Pascual, 2001).
Sulfradex	Sulfradex, a cyclodextrin-stabilised sulforaphane, has been reported to modulate PPARγ signalling (Patel, Mann and Chapple, 2018).
MAXnolia	Honokiol (a derivate of magnolia bark) has been shown both *in silico* and *in vitro* to activate PPARγ-dependent signalling pathways without the adipogenic side effects often associated with synthetic thiazolidinedione-class PPARγ agonists (Atanasov *et al.*, 2013). MAXnolia® is a stabilised magnolia bark extract suited to use in cosmetics.
SabiWhite®	Curcumin (a constituent of the spice turmeric) has been shown to exert anti-inflammatory effects *in vivo* and *in vitro*, with a suggested PPARγ-dependent mechanism (Jacob *et al.*, 2007). Due to this, SabiWhite®, a colourless curcumin derivative intended for use in cosmetics, was included in the present work.
Chia oil **Vitamin E acetate (tocopherol acetate)**	Expression of PPARγ has been shown to be upregulated *in vivo* by chia oil (Batista *et al.*, 2023), and by vitamin E (α-tocopherol) both *in vivo* in mice (Hsieh, Huang and Lin, 2006) and *in vitro* in human keratinocytes (De Pascale *et al.*, 2006). Increased PPARγ expression may lead to increased

	PPARγ activation by endogenous or exogenous ligands, enhancing the effects of PPARγ ligands.

10 mg/ml stock solutions of each were prepared in DMSO and vortexed to ensure complete dissolution of the material before sterilisation with a 0.22 µm syringe filter. All compounds except for MAXnolia and PEA showed excellent dissolution – MAXnolia and PEA produced slightly turbid solutions. These solutions were warmed to 37°C prior to filter sterilising and complete dissolution was noted. For each cosmetic compound tested, a 10 µg/ml solution was prepared via a 1:1000 dilution of stock (10 mg/ml) solution in culture media. Following aspiration of culture media, 100 µl of 10 µg/ml stock was added to the first test column, and serially diluted into the remaining columns to produce dilutions of 1000, 100, 10, and 1 ng/ml. All dilutions were performed to generated equal final volumes of culture media in all wells. Identical dilutions were also performed for control wells containing no cells, allowing later calculation to compensate for any differences in absorbance caused by the test compounds.

2.2.2. Cell counting kit 8 (CCK-8) cytotoxicity assay

Subconfluent H400 cells were trypsinised and diluted 1:1 with trypan blue (0.4% solution, Gibco, UK). Viable cells were counted with a haemocytometer and diluted to a concentration of $5x10^5$ cells / ml in supplemented HamsF12:DMEM. 100 µl of this cell suspension was added to the required wells of four 96 well cell culture plates and incubated overnight at 37˚C, 5% CO_2. Media was then aspirated, and all wells washed with 100 µl OptiMEM (Gibco, USA) three times to ensure removal of all traces of FBS-supplemented media. 100 µl of OptiMEM

was then added to each well to initiate a serum starvation period. Cells were then incubated for a further 24 hours at 37°C, 5% CO_2.

Following addition of test compounds as described in Section 2.2.3, cells were incubated for a further 24 hours at 37°C, 5% CO_2. 10 µl of cell counting kit 8 (CCK-8) reagent (Abcam, UK) was then added to each well and incubated again at 37°C, 5% CO_2 for 1 hour. Absorbance at 450 nm was recorded using a BioTek ELx800 plate reader (BioTek, USA). Absorbance of each well was calculated as: $Final\ absorbance = Abs(cells + media + test\ agent) - Abs(media + test\ agent)$.

2.2.3. Combined LPS and PPARγ agonist treatment

Two aliquots of media were prepared and assigned to either control or LPS challenge groups. The latter was supplemented with 2 µg/ml LPS as per Table 2.1. Cultures were then treated with control or LPS challenge media and incubated for 24 hours as a 'pre-challenge' prior to treatment with PPARγ agonists.

LPS-supplemented (2 µg/ml) or control media was prepared again and split into four groups (A-D) to receive either supplementation with the known PPARγ agonist GW1929 or DMSO as a solvent control, in addition to LPS, as shown in Table 2.4. Cultures selected for PPARγ agonist treatment were supplemented with GW1929 at a final concentration of 5 µM (as described in Section 2.2.2), with non-GW1929 cultures supplemented with the same volume of DMSO. LPS was again supplemented at 2 µg/ml if required. Cultures were incubated (37°C, 5% CO_2) for a final 24 hours prior to assay.

Table 2.4 - Culture designation matrix, showing supplementation with GW1929 or LPS

	Culture designation			
	A	**B**	**C**	**D**
GW1929 in DMSO	-	-	5 µM	5 µM
LPS	-	2 µg/ml	-	2 µg/ml
DMSO only	+	+	-	-

2.3. H400 cell growth and viability curves

Subconfluent H400 cells were dissociated with trypsin, and cell suspensions diluted 1:1 with trypan blue (0.4% solution, Gibco, UK). Viable cells were counted using a haemocytometer and diluted to a concentration of $1.66x10^3$ cells/ml. 3 ml of this cell suspension was added to each well of a six well plate, with three technical replicate wells per condition. Cells were incubated overnight at 37˚C, 5% CO_2 to allow for attachment. Following incubation, aliquots of supplemented HamsF12:DMEM were treated with LPS to final concentrations of 20, 200 and 2000 ng/ml, or left untreated (control group). Culture media was aspirated from the culture plates and replaced with LPS-supplemented media. Culture media were aspirated and replaced at 48hr intervals with freshly produced LPS-supplemented media. Control group media was aspirated and replaced with supplemented HamsF12:DMEM without LPS at the same intervals.

Cells were counted at 48-hour intervals, with culture media aspirated to labelled falcon tubes to include both detached and dead cells. Monolayers were washed with 500 µl trypsin, which was then aspirated to the same Falcon tube as the culture supernatant. 500 µl of trypsin was then added and incubated for 15 minutes at 37˚C, 5% CO_2, with complete removal of all

attached cells confirmed using phase contrast microscopy. Cell suspensions were then centrifuged at 180 x *g* for 5 minutes (5804R centrifuge, Eppendorf, USA), the supernatant removed to waste, and cell pellets resuspended in 100 µl culture media. 100 µl trypan blue was added, the suspension briefly vortexed, and incubated at room temperature for 10 minutes. For counts on days 7 and 9 post-LPS addition, 600 µl of sterile PBS was also added to trypan blue treated cell suspension after the 10-minute incubation period to reduce the counted cell numbers. Cell suspensions were vortexed briefly again and counted in Tecan Cell Chips using a Tecan Spark multimode plate reader (Tecan, Switzerland).

2.4. Production of PPARγ reporter cell lines in H400 oral squamous cell carcinoma cells

2.4.1. Stable genetic transfection with PPRE-H2B-eGFP reporter

2.4.1.1. Extraction and purification of PPRE-H2B-eGFP plasmid DNA from DH5α *E. coli*

DH5α *Escherichia coli* containing PPRE-H2B-eGFP plasmid DNA were obtained from the non-profit plasmid repository AddGene. DH5α *E. coli* were plated to LB Agar containing 50 µg/ml kanamycin antibiotic (ThermoFisher, UK) and incubated for 48 hours at 37°C, 5% CO_2, 100% relative humidity. Isolated colonies were selected and used to produce overnight cultures in 4 Falcon tubes containing 50 ml LB Broth (produced from LB broth base (ThermoFisher, UK) and supplemented with 50 µg/ml kanamycin) to produce 200 ml of total culture volume and incubated for 18 hours in a shaking incubator (NB-205, N-Biotek Inc., South Korea) at 37˚C and 100 RPM.

Overnight cultures were centrifuged at 3500RPM for 5 minutes (Jouan R35i, AB50.10 rotor), producing bacteria pellets, which were thoroughly mixed in PureLink resuspension buffer (ThermoFisher, UK) and individual Falcon tubes combined together. Bacteria were then lysed

and plasmid DNA eluted following manufacturers specifications (PureLink HiPure Plasmid Miniprep Kit, ThermoFisher, UK), with the exception of using elution buffer warmed to 50˚C for the elution step instead of the recommended room temperature. Following elution in a 15 ml centrifuge tube, 3.5 ml chilled molecular biology grade isopropanol (Sigma Aldrich, UK) was added, and the solution cooled at -80˚C for 30 minutes. This solution was centrifuged at 12000 x *g* for 30 minutes at 4˚C, before removing the supernatant to waste. 3 ml of chilled 70% ethanol was added and centrifuged at 12000 x *g* for 30 minutes, 4˚C. A white DNA pellet was identified, and the supernatant gently pipetted off, tube opened and allowed to air dry for 15 minutes before resuspending in 200 µl TE buffer (ThermoFisher, UK).

Purity and concentration of isolated plasmid DNA was quantified via spectrophotometry (Genova Nano spectrophotometer, Jenway) providing $Abs\frac{260}{280}$ and $Abs\frac{260}{230}$ ratios of 1.927 and 2.237 respectively, with a concentration of 357 µg/ml.

2.4.1.2. Diagnostic restriction enzyme digest of PPRE-H2B-eGFP plasmid DNA

Three single cutting restriction enzymes were employed to perform a diagnostic digest of the plasmid DNA, as shown in Table 2.5.

Table 2.5 - FastDigest restriction enzymes employed in producing a diagnostic digest of plasmid DNA. ^ = enzyme cut site.

Restriction Enzyme	**Manufacturer**	**Reaction temperature (˚C)**	**5'-3' Cut Site**
FastDigest VspI (AseI Isoschizomer)	ThermoFisher	37	AT^TAAT
FastDigest NheI	ThermoFisher	37	G^CTAGC
FastDigest BamHI	ThermoFisher	37	G^GATCC

Manufacturer's specifications were followed to perform a diagnostic digest, with 5 minutes of incubation at 37˚C (Veriti 96-well thermal cycler, Applied Biosystems, California, USA). Reaction mixtures for single and double restriction enzyme digests comprised 1 µl of each restriction enzyme, 2 µl Green FastDigest buffer (ThermoFisher) and 2 µl of DNA, made up to a final volume of 20 µl with water. Triple enzyme digests (NheI/VspI/BamHI) used 4 µl of DNA to improve the intensity of the resulting agarose gel electrophoresis band.

Following incubation, 6 µl of each sample was loaded onto a 1% agarose gel and electrophoresis performed at 120 V for 1 hour. Uncut plasmid DNA was also loaded onto the gel, using 2.7 µl DNA with 0.6 µl Green FastDigest buffer as a loading dye.

2.4.1.3. Transfection of H400 oral squamous carcinoma cells with PPRE-H2B-eGFP plasmid

H400 oral squamous carcinoma cells were cultured for 2 passages without addition of penicillin / streptomycin to the culture media. These cells were then trypsinised and seeded to 6 well plates at $1x10^4$ cells/well and incubated at 37˚C, 5% CO_2 until approximately 75% confluent. Culture media was then aspirated, and cultures rinsed twice with sterile, un-supplemented Opti-MEM (31985062l, ThermoFisher, UK). 800 µl of Opti-MEM was then added to each well.

'High' and 'low' concentration dilutions of Lipofectamine 3000 transfection reagent (L3000001, ThermoFisher, UK) were prepared, with 22.5 µl and 11.3 µl Lipofectamine added to 375 µl Opti-MEM respectively. Solutions were then mixed by brief vortexing.

A DNA mastermix was prepared with 1.5 ml Opti-MEM, 30 µg plasmid DNA and 60 µl P3000 transfection reagent (L3000001, Thermofisher, UK), giving a ratio of 2 µl P3000 per 1µg of DNA. This diluted DNA mastermix was added to the two lipofectamine dilutions in a

1:1 ratio (375 µl DNA mastermix to 375 µl diluted lipofectamine). This DNA-Lipofectamine solution was then incubated for 15 minutes at room temperature, after which 250 µl of the solution added dropwise to each well designated for transfection. Untransfected control wells were untreated with DNA-lipid complexes. Cultures were then incubated at 37˚C, 5% CO_2.

Following 4 hours of incubation, Opti-MEM media was aspirated and replaced with HamsF12:DMEM culture media (supplemented to a final concentration of 10% FCS). A greater number of detached, floating cells were noted in the cultures treated with high concentration Lipofectamine, though some cells remained attached to the culture surface.

2.4.1.4. Culture of H400:PPRE-H2B cells

Genetically modified H400 cells were cultured in HamsF12:DMEM, supplemented to final concentrations of 10% FCS, 1 mM L-Glutamine, and 500 µg/ml Geneticin G418 antibiotic (10131027, Gibco, UK). No penicillin or streptomycin were supplemented to avoid competitive inhibition of G418.

2.4.1.5. Selection of transfected cells for stable plasmid integration into H400 cell genome

48 hours post-transfection, all wells were trypsinised and individually transferred to T25 flasks for expansion. This expansion step employed HamsF12:DMEM, supplemented with 10% FCS, 1 mM L-Glutamine, 1.372 µM sodium hydrocortisone and 500 µg/ml Geneticin G418 antibiotic.

All cultures were maintained separately, with daily monitoring via phase contrast microscopy to identify the formation of G418-resistant cell islands and the death of non-resistant cells. Cell islands were identified in transfected cultures after 3 days of culture while the untransfected control cultures resulted in no viable, attached cells as seen by phase contrast. Once cultures were observed to have formed islands of ~100 cells, these were then passaged

and expanded into T75 flasks until near-confluent, and stocks frozen in cryogenic media (final concentrations of 70% HF12:DMEM, 20% FCS, 10% DMSO) for storage in liquid nitrogen.

2.4.1.6. Initial verification of eGFP fluorescence in transfected H400:PPRE-H2B-eGFP cells

Following expansion of transfected H400 cultures into T25 flasks, one flask of each transfection condition (high and low concentration Lipofectamine reagent) was stimulated with a known PPARγ agonist, GW1929, at a final concentration of 1µM as described in Section 2.2.2. After 24 hours of incubation with GW1929, the cultures were examined using a phase contrast / fluorescence microscope (Nikon Eclipse TE300, Nikon, Japan) with an LED excitation system (CoolLED pE-100) and an excitation wavelength of 490nm.

2.4.1.7. Polyclonal to monoclonal selection of PPRE-H2B-eGFP transfected cells

A limiting dilution was performed by seeding H400:PPRE-H2B-eGFP cells to a 96 well plate at a concentration of 10 cells per ml, with 100 µl of suspension added to each well. Following 24 hours of incubation, each well was inspected using phase contrast microscopy. The number of cells and locations within the wells were noted, and cells cultured for a further 4 days. These cultures were examined again with phase contrast microscopy, noting wells containing a single colony of cells. Next, all wells were treated with complete growth media containing 1 µM GW1929 hydrate and incubated for 24 hours. Cultures were examined as previously described by both phase contrast and fluorescence microscopy, imaging all single-colony wells (Nikon D3000 DSLR) with identical camera settings. The well showing the most eGFP fluorescence was noted and selected for further expansion. This well was allowed to grow to ~50% confluency, after which it was dissociated with 100 µl of trypsin-EDTA and the cell population subcultured by transferring to 12 well plates for expansion.

These cells were then used for further validation of reporter activity in response to GW1929, seeded at a density of $1x10^5$ cells/well in a 96-well opaque black, clear bottomed optical culture plate (Nunclon, ThermoFisher, UK). Culture media comprised HamsF12:DMEM, containing 10% FCS, 1 mM L-glutamine, no penicillin or streptomycin and 500 µg/ml G418. Following seeding of cells, cultures were incubated for 24 hours prior to addition of GW1929 in DMSO (Section 2.2.2).

2.4.2. Transient transfections with PPRE-pNL1.3 reporter system

2.4.2.1. Extraction and purification of PPRE-pNL1.3 plasmid DNA from DH5α *E.coli*

DH5α *Escherichia coli* containing PPRE-pNL1.3 plasmid DNA were obtained from the non-profit plasmid repository AddGene. DH5α *E.coli* were plated to LB Agar containing 100µg/ml ampicillin antibiotic and incubated for 48 hours at 37˚C, 5% CO_2. Isolated colonies were selected and used to produce overnight cultures in 8 Falcon tubes containing 40 ml LB Broth (supplemented with 100µg/ml ampicillin) to produce 320 ml of total culture volume. Cultures were incubated for 18 hours in a shaking incubator at 37°C and 120RPM.

Cell lysis was performed as previously described for the PPRE-H2B-eGFP reporter system (Section 482.4.1.1), with the overnight cultures pooled following resuspension. Plasmid isolation and precipitation protocols required modification to produce an acceptable yield. A PureLink MaxiPrep kit (K210007, ThermoFisher, UK) was employed, following manufacturer's specifications. It was deemed critical to use warmed elution buffer (40°C) and avoid drying of the column membrane at any point. 10.5 ml of molecular biology grade isopropanol (I9516, Sigma Aldrich, UK) was added to the eluate at room temperature, mixed by repeated inversion and passed through a PureLink HiPure plasmid filter (K210016, ThermoFisher, UK). 500 µl of warmed (40°C) TE buffer was then used to elute plasmid DNA, with this flowthrough then passed back through the HiPure filter once more to improve

the yield. Purity and concentration of isolated plasmid DNA was quantified via spectrophotometry (Genova Nano spectrophotometer, Jenway) providing and $Abs\,\frac{260}{280}$ ratio of 1.895, with a concentration of 493.38 µg/ml.

2.4.2.2. Diagnostic restriction enzyme digest of PPRE-pNL1.3 plasmid DNA

Four single cutting restriction enzymes were employed to perform a diagnostic digest of the plasmid DNA, as shown below (Table 2.6).

Table 2.6 - FastDigest restriction enzymes employed in producing a diagnostic digest of PPRE-pNL1.3 plasmid DNA. ^ = enzyme cut site.

Restriction Enzyme	Manufacturer	Reaction temperature (˚C)	5'-3' Cut Site
FastDigest KpnI	ThermoFisher	37	GGTAC^C
FastDigest BglII	ThermoFisher	37	A^GATCT
FastDigest BamHI	ThermoFisher	37	G^GATCC
FastDigest HindIII	ThermoFisher	37	A^AGCTT

Manufacturer's specifications were followed to perform a diagnostic digest, with 10 minutes of incubation at 37˚C (Veriti 96-well thermal cycler, Applied Biosystems, California, USA). Reaction mixtures for single and double restriction enzyme digests comprised 1 µl of each restriction enzyme, 2 µl Green FastDigest buffer (B72, ThermoFisher, UK) and 5 µl of DNA, made up to a final volume of 20 µl with water.

Following incubation, 6 µl of each sample was loaded onto a 1% agarose gel and electrophoresis performed at 100 V for 115 minutes. Uncut plasmid DNA was also loaded onto the gel, using 2.7 µl DNA with 0.6 µl Green FastDigest buffer as a loading dye. For quadruple enzyme digests (BamHI/BglII/HindIII/KpnI), 12 µl of reaction product was loaded into the agarose gel to increase the intensity of the resulting agarose gel electrophoresis bands.

2.4.2.3. Transfection of H400 Oral Squamous Carcinoma cells with PPRE-pNL1.3 plasmid

Transient transfection with isolated PPRE-pNL1.3 plasmid DNA (pDNA) was performed at the point of seeding cells to 96 well assay plates, to minimise variability in plasmid DNA uptake. Prior to seeding, H400 cells were cultured in HamsF12, supplemented with 10% FCS, 1mM L-glutamine, with no addition of penicillin or streptomycin. At 80% confluency, H400 cells were trypsinised, resuspended and counted. A dilution to $5x10^5$ cells/ml was prepared in HamsF12, +10% FCS, 1mM L-glutamine, with sufficient media for 100 µl per well of a 96 well plate. Transfection reagents (L3000001, Thermofisher, UK) were prepared as shown below.

Table 2.7 - Volumes of Lipofectamine 3000 reagents and OptiMEM media used for transfection of H400 cells with pNL1.3. Volumes per well of a 96 well plate.

Reagent	**Volume /well**
OptiMEM for each lipofectamine dilution	5 µl
Lipofectamine 3000 (High concentration)	0.3 µl
Lipofectamine 3000 (Low concentration)	0.15 µl
OptiMEM for DNA dilution	5 µl
P3000 Reagent	0.2 µl
Plasmid DNA – 0.1µg/well	0.2 µl
Total volume per well of cells to be transfected	10.85 µl

DNA-lipid complexes were produced by mixing Lipofectamine reagents, plasmid DNA and OptiMEM as per manufacturer's instructions, and incubated at room temperature for 15 minutes. 10.85 µl of DNA-lipid complexes was added to the prepared cell suspensions for every required well of a 96 well plate. 100 µl of transfected cell suspension was then added to

each well (resulting in a seeding density of $5x10^4$ cells/well) and incubated for 18 hours at 37°C, 5% CO_2. These cells were then used for analysis of the reporter response to PPARγ agonists (Section 2.2.2) and cosmetic compounds (Section 2.2.3) using a NanoGlo nanoluciferase assay (Promega, UK).

2.4.2.4. NanoGlo nanoluciferase assay

Following 18 hours of incubation of H400 cells with DNA-lipid complexes, culture media containing DNA-lipid complexes were aspirated and replaced with 100 µl test compound-supplemented media per well, and incubated overnight at 37°C, 5% CO_2. This same approach was employed both for studies on known PPARγ agonists, and studies investigating cosmetic compounds as PPARγ agonists. Culture plates were then placed on a shaker table for 3 minutes at room temperature to evenly distribute any local accumulations of secreted nanoluciferase. 10 µl of culture media was removed from each well and added to an opaque white 96 well plate (ThermoFisher, UK), and diluted with 40 µl of deionised water. A Nano-Glo nanoluciferase assay system (N1120, Promega, UK) was then prepared, with 50 µl of assay reagent prepared per well, following manufacturers protocols for the dilution of Nano-Glo substrate in assay buffer. 50 µl of assay reagent was then applied to each well of diluted culture supernatant and incubated for 5 minutes at room temperature. Where lytic Nano-Glo assays were performed, 100 µl of Nano-Glo substrate in buffer was added directly to cells, mixed by pipetting and 100 µl of the media then added to an opaque white 96 well plate.

Luminescence was then recorded with a Tecan Spark multimode plate reader (Tecan, Switzerland), with 1000ms integration time and a 5 second orbital shaking step prior to reading.

2.5. Development of a novel 3D printed device for the culture of gingival epithelial equivalents

The following methods were published in part in a publication, entitled “A novel 3D printed buoyant device for *in vitro* generation of stratified epithelial rafts at the air-liquid interface” (Hewitt *et al.*, 2022).

2.5.1. Buoyant epithelial culture device (BECD) design and fabrication

ALI culture devices were developed to fit within a standard 6-well plate culture dish using a computer aided design (CAD) package (Fusion 360, Autodesk, USA) with an internal diameter of 15mm and outer diameter of 33mm. STL (stereolithography) files for the devices were exported by slicing into. gcode format (Ultimaker Cura 4.6, Ultimaker, Netherlands). Engineering drawings and 3D renderings of the devices were generated within the same CAD package (Fusion 360, Autodesk, USA).

BECDs and submerging rings were fabricated on a bespoke fused filament fabrication (FFF) system with a brass 0.6mm diameter nozzle (E3D, United Kingdom), 0.5mm initial layer height, 0.32mm successive layer height, 40mm/s print speed, 240˚C extrusion temperature, and 80˚C bed in 1.75mm PP filament (UltraFuse / BASF, Netherlands). Three top layers and one skin layer were incorporated to reduce the risk of voids forming in the upper surface, which could allow media ingress. The heated borosilicate bed was covered with polypropylene (PP) tape for increased part adhesion.

Following printing, BECDs and submerging rings were immersed in 70% ethanol overnight to aid in removal of any build surface residue and begin the decontamination process prior to sterilisation (Figure 2.1 A-C). 25mm wide Kapton tape (RS Electronics, UK) was applied

across the base of the BECD to prevent leakage during the collagen matrix gelling process (Figure 2.1 D). The submerging rings and BECDs – with tape *in* situ – were then autoclaved (MLS-3781L, Sanyo, Japan) at 121˚C, 101kPa for 15 minutes.

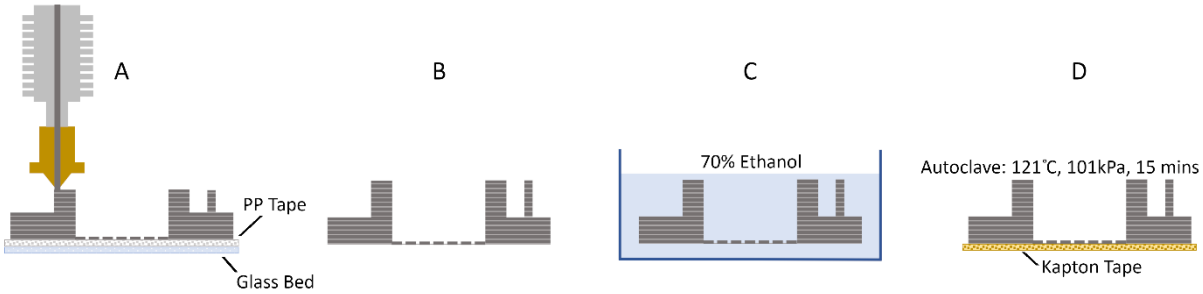


Figure 2.1 - Schematic diagrams depicting the steps involved in the production and processing of 3D printed BECDs.

(A) 3D printing via fused filament fabrication with polypropylene material on a heated borosilicate glass bed. Heated bed was coated in polypropylene (PP) tape for increased part adhesion.
(B) Construct with polypropylene (PP) tape removed.
(C) Immersion in 70% ethanol for removal of tape residue and initial decontamination.
(D) Addition of Kapton polyamide tape before sterilisation by autoclave. Kapton tape provided a sealing film, preventing the leakage of collagen solution prior to gelling.
Figure used with permission from publisher (Hewitt *et al.*, 2022).

2.5.2. Production of stratified epithelia using BECDs

To prepare the necessary stock solutions for generating collagen hydrogels, 10x reconstitution buffer was produced by addition of 1.1g $NaHCO_3$ and 2.385g HEPES (both Sigma Aldrich, UK) to 50 ml dH_2O. 10x DMEM (Gibco, UK) and 10x reconstitution buffer were sterilised by passing through a 0.22 µm syringe filter. 1 ml 3 mg/ml rat tail collagen (ThermoFisher, UK) was then added to 100 µl 10x DMEM and 100 µl 10x reconstitution buffer. 1M NaOH was added dropwise to produce a pink coloured solution, at pH 6.9, measured using a Beckman Φ40 pH meter (Beckman Coulter, USA). Viable 3T3 fibroblasts were counted using a haemocytometer and trypan blue dye exclusion. 3T3 fibroblasts were added to the solution

immediately after preparation to a final concentration of $5x10^4$ cells/ml and the solution mixed well by pipetting on ice.

Devices were placed in 6-well plates and 1.2 ml buffered collagen solution with fibroblasts was added per BECD (Figure 2.2A). Devices were incubated at 37˚C, 5% CO_2 for 90 minutes until a firm gel had formed, Kapton tape was aseptically removed and devices were placed into a new 6-well plate (Figure 2.2B). 3ml DMEM was added to each well. The BECDs were then incubated at 37˚C, 5% CO_2 for 24 hours to allow initial growth of 3T3 fibroblasts (Figure 2.2C).

Culture medium was replaced with 2ml supplemented Hams F12:DMEM. H400 cells were counted and diluted to a final concentration of $8x10^4$ cells/ml, with 1 ml of suspension added to the upper gel surface, to a final 3ml total media volume. Submerging rings were placed on top of the BECDs submerging the devices once the plate lid was applied (Figure 2.2 D), and incubated for 72 hours at 37˚C, 5% CO_2.

The submerging rings were removed and BECDs transferred to a plate containing 3 ml of Hams F12:DMEM per well. Removal of the submerging rings allowed the devices to float on the culture media, exposing the confluent H400 cell layer to air (Figure 2.2 E). Devices were cultured at the ALI for 7, 14 or 21 days, with media changes every second day. Five independent biological replicates were produced, with two technical replicates (BECD cultured rafts) for each biological replicate and timepoint.

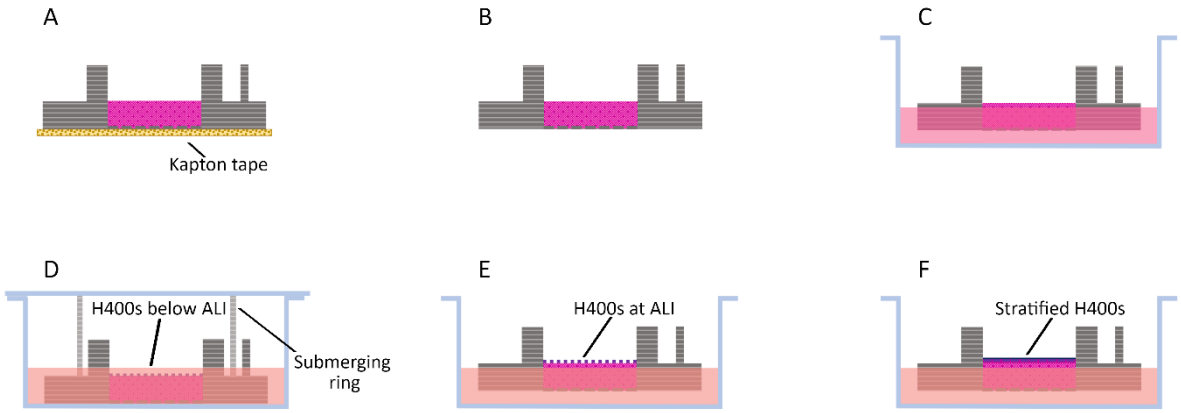


Figure 2.2 - Steps applied for the use of BECDs in establishing a fibroblast-seeded collagen gel and seeding keratinocytes on the surface for stratification via ALI culture.
A) Addition of 1.2ml fibroblast seeded collagen.
B) 90 min incubation to allow for gelling, followed by removal of Kapton tape.
C) Overnight incubation in supplemented DMEM.
D) Addition of H400 cells onto surface to final concentration of $8x10^4$ cells /ml, followed by 3-day submersed incubation using 3D printed forced submersion ring.
E) Removal of submersion ring to enable ALI culture.
F) Incubation at 37°C, 5% CO2 to enable epithelial stratification. Diagrams are not to scale.
Figure used with permission from publisher (Hewitt *et al.*, 2022).

Cultures were then processed by fixation, dehydration, embedding, sectioning and H&E staining as described in Section 2.6.4.

2.5.3. Histological processing

Hydrogels were fixed in 10% neutral buffered formalin (CellStor, CellPath, UK) for 24 hours, followed by dehydration in 10% graded solutions of ethanol, starting at 10% and finishing at 100% (10 minutes each). This 100% step was repeated three times, followed by two 10-minute immersions in xylene (Sigma Aldrich, UK). Samples were then impregnated with paraffin wax overnight at 60°C, moved into fresh paraffin wax after 18 hours, and then embedded at 60°C. A rotary microtome (RM2035, Leica Instruments, Germany) was used to cut 4 µm sections, which were floated onto glass slides and dried at room temperature. Immediately prior to staining, slides were heated in a 60°C oven for 1 hour, dewaxed in

xylene and stained with haematoxylin and eosin (H&E), following standard protocols (Feldman and Wolfe, 2014).

Sections of healthy gingival tissue were used as control samples for comparison with BECD cultured tissues and were sectioned and H&E stained as previously described. Ethical approval for studies with human waste surgical tissue was provided by NHS South West-Central Bristol Research Ethics Committee (code 19/SW/0198).

2.5.4. Immunofluorescence staining

Sections were dewaxed as described above, and cells permeabilised by exposure to 0.25% Triton X-100 (Sigma Aldrich, USA) in phosphate buffered saline (PBS), 10 minutes, at room temperature (RT), washed with PBS and blocked with goat serum (Sigma Aldrich, UK) diluted 1:5 in PBS for 10 minutes at RT. Primary antibodies were diluted (Table 2.8) in PBST-BSA (10 mg/ml BSA in PBS with 0.1% Tween 20 (P1379, Sigma Aldrich, UK)), applied to samples and incubated at RT for 1 hour, prior to washing 3x in PBST for 5 minutes each. Fluorophore-conjugated secondary antibodies were diluted (Table 2.8) in PBST-BSA supplemented to a final concentration of 10% type AB human plasma. Samples were incubated with secondary antibodies for 1 hour at RT, washed three times in PBST for 2 minutes each and mounted in Fluoroshield mounting media containing DAPI (Ab104139, Abcam, UK).

Table 2.8 - Antibodies used for immunofluorescence staining. Manufacturer reference and dilution from stock shown.

Primary antibodies		
Antibody	**Manufacturer reference**	**Dilution from stock**
Anti-E-cadherin, recombinant rabbit anti-human, monoclonal	Ab76319	1:100
Anti-involucrin, mouse, monoclonal	Ab80530	1:100
Anti-cytokeratin 5, recombinant rabbit anti-human, monoclonal	Ab52635	1:100
Secondary antibodies		
Antibody	Manufacturer reference	Dilution from stock
Anti-rabbit IgG, goat, polyclonal, Alexa Fluor 488 conjugated	Ab150077	1:200
Anti-mouse IgG, goat, polyclonal, Alexa Fluor 488 conjugated	Ab150113	1:1000

Samples were imaged using a Zeiss LSM700 confocal microscope, maintaining the same imaging settings for all samples.

2.5.5. Image processing and analysis

Following H&E staining, sections were imaged using a Nikon D3000 camera (Nikon, Japan) and inverted microscope (Nikon Eclipse TE300, Nikon, Japan). Images were processed using Fiji (Schindelin *et al.*, 2012), with the simple interactive object extraction (SIOX) plugin utilised for segmentation of the epithelial cell layer. A SIOX preset was generated and applied to all images, ensuring unbiased segmentation. Approximately 5% of SIOX-segmented images presented some regions with false-positive selection and segmentation was manually modified in these cases for these regions only.

The SIOX image was then processed via a macro within Fiji, wherein any holes in the segmented epithelium were filled and the Euclidean Distance Transform (EDT) was used to compute the distance from each epithelial tissue pixel to the closest epithelial boundary (i.e. superficial or basal). Since the maximum value of the EDT occurs at the thickest location(s) in the epithelium and its position is equidistant to both superficial and basal tissue boundaries, the EDT value was multiplied by 2 to give the maximal epithelial thickness and a precalculated pixel:µm calibration factor applied to produce thickness measurements in micrometres.

2.5.6. Replicate definitions for BECD validation studies

For each biological replicate, two devices were cultured per time point, established with the same population of cells to provide technical replicates.

Two slides were produced for each technical replicate at each time point, with one section obtained ~2 mm and a second section obtained ~10 mm from the block face. This approach was employed to identify any changes in epithelial thickness across the diameter of the

hydrogel. Data from both sections were incorporated into the final average for each biological replicate, giving four total technical replicates.

2.6. Gene expression analysis

2.6.1. RNA isolation

2.6.1.1. Monolayer cells

RNA isolation of cell monolayers was performed using a RNeasy plus mini kit (Qiagen, Germany), following manufacturer's instructions. Briefly, cell monolayers were washed twice with PBS, lysed with 350 µl RLT buffer and an equal volume 70% molecular grade ethanol added. Lysate was then applied to the gDNA eliminator spin column and centrifuged at 12,000 x g for 30 seconds. Flowthrough was then applied to an RNeasy spin column and centrifuged at 12,000 x *g* for 30 seconds. Flowthrough was discarded, the column washed with 350 µl buffer RW1 and centrifuged again. Flowthrough was again discarded and the column washed twice with buffer RPE, with centrifugation and flowthrough removal between washings. The columns were then centrifuged 13,200 x *g* for two minutes to dry the membrane, with 40 µl RNase free water then added and the column centrifuged again at 12,000 x *g* for 30 seconds. RNA purity and concentration was quantified (Jenway Genova spectrophotometer, Fisher Scientific, UK).

2.6.1.2. Organotypically cultured cells

Cells cultured in hydrogels required a different approach for RNA isolation to ensure appropriate tissue homogenisation and cell disruption. TRI reagent (Sigma Aldrich, UK) was added to each BECD-cultured hydrogel (1 ml each) and homogenised via repeated mixing in sterile 5 ml syringes fitted with 18-gauge blunt fill needles (BD Microlance, Appleton Woods,

UK). 200 µl chloroform (Sigma Aldrich, UK) was then added to each sample, each tube capped and shaken vigorously and allowed to stand at room temperature for 5 minutes before being centrifuged at 12,000 x *g* for 15 minutes at room temperature. The upper organic phase was then removed, an equal volume of 70% molecular-grade ethanol (Sigma Aldrich, UK) added, mixed by pipetting, and the solution then applied to a RNeasy RNA mini extraction kit (Qiagen, Germany). The manufacturer-provided protocol was followed, using a 40 µl RNA elution volume.

2.6.2. cDNA synthesis

cDNA was synthesised using a Tetro cDNA synthesis kit (Meridian Bioscience, USA) following manufacturers protocols for oligo (dT)18 primers. Each reaction was carried out on ice using 2 µg of RNA and made up to a final volume of 20 µl with molecular biology grade water (Corning, USA). The reaction mixture was maintained at 45°C for 1 hour and the reaction terminated at 85°C for 5 minutes, using a Biometra TAdvanced Twin 48G thermocycler (Analytik Jena, Germany).

2.6.3. RT-qPCR

A reaction mastermix of each primer was produced, comprised 100 µl SYBR Green I Master (50-720-3180, ThermoFisher, USA), 78 µl molecular biology grade water (W4502, Sigma, UK) and 1 µl of each of the forward and reverse primers, at a stock concentration of 100 µM. 10 µl reaction volumes were used, comprising 9 µl reaction mastermix and 1 µl of cDNA. qPCR was performed with a LightCycler 480 II (Roche, USA), with reaction conditions shown in Table 2.10.

Table 2.9 - Primer sequences used for RT-qPCR throughout the present work, detailing target gene, gene symbol, product size and forward and reverse primer sequences.

Gene	Gene Symbol	Size (bp)	Forward Primer (5'-3')	Reverse Primer (5'-3')
Peroxisome proliferator activated receptor gamma	*PPARG*	132	AGCCCAAGTTTGAGTTTGCT	TGTCTTCAATGGGCTTCACA
Aquaporin 3	*AQP3*	99	GGGGCTCTGCAGTCTTCA	TCAGCTGGTACACGAAGACA
Glyceraldehyde 3-phosphate dehydrogenase	*GAPDH*	104	GACAGTCAGCCGCATCTTCT	GCGCCCAATACGACCAAATC
Beta Actin	*ACTB*	70	CCTCGCCTTTGCCGATCC	CGCGGCGATATCATCATCC
Tyrosine 3-Monooxygenase/ Tryptophan 5-Monooxygenase Activation Protein Zeta	*YWHAZ*	132	AGACGGAAGGTGCTGAGAAA	CTTGTGAAGCATTGGGGATCA
Tight junction protein 1 / zona occludens 1	*TJP1*	101	GGCGTGCTGAGTTCCATAGA	TCCCGGCAGACCTTGAAATA
Occludin	*OCLN*	134	GAGGAATTTTGACACTGGCCT	CAGCAGCCATGTACTCTTCAC
Nuclear factor kappa beta	*NFKB*	121	AGCAATCACAACACTGGCTG	AACGTAGCAGAGGGACAACA
Transforming growth factor beta 1	*TGFB1*	108	GCTGTACATTGACTTCCGCA	TCCAGGCTCCAAATGTAGGG
E-cadherin	*CDH1*	89	TGAAGAAGGAGGCGGAGAAG	CGTTACGAGTCACTTCAGGC

Matrix metalloproteinase 1	*MMP1*	112	CGACAGAGATGAAGTCCGGT	TCTAGGGAAGCCAAAGGAGC
Prostaglandin-endoperoxide synthase 2	*PTGS2*		ATCACAGGCTTCCATTGACC	GAGTGCTTCCAACTCTGCA
Interleukin 6	*IL6*	125	AGACAGCCACTCACCTCTTC	AGTGCCTCTTTGCTGCTTTC
Interleukin 8	*CXCL8*	132	TCCAAACCTTTCCACCCCAA	CCAGTTTTCCTTGGGGTCCA
Caspase 3	*CASP3*	146	AGCGAATCAATGGACTCTGGA	GCTGCATCGACATCTGTACC
Interferon gamma	*IFNG*	150	CAGATGTAGCGGATAATGGAACT	CACTCTTTTGGATGCTCTGGT
Tumour necrosis factor alpha	*TNFA*	123	AACCCCGAGTGACAAGCC	TGGTTATCTCTCAGCTCCACG
Involucrin	*IVL*	150	GCACTCCACCAAAGCCTCT	TGGGTATTGACTGGAGGAGG
Cytokeratin 10	*KRT10*	107	AGCCTCGTGACTACAGCAAA	GGCATTGTCGATCTGAAGCA
Ribosomal protein L27	*RPL27*	133	ATGGGCAAGAAGAAGATCGC	AGACATCCTTATTGACGACAGTT
Ribosomal protein S20	*RPS20*	135	GCGACTCATTGACTTGCACA	CTCAAAGTGTACTGCTGGCC
Interleukin 11	*IL11*	115	GAGTTTCCCCAGACCCTCG	CCGTCAGCTGGGAATTTGTC

Tight junction protein 2 / zona occludens 2	*TJP2*	146	ATCAGTCCTGGGCAAAGTCA	GCGTTTTGATTGGAACTGCA
Claudin	*CLDN1*	112	CTATGACCCTATGACCCCAGT	GGAACAGCAAAGTAGGGCAC
Junctional adhestion molecule (JAM) 1	*JAM1*	211	CTTTGATCCCCTGTCAGCCT	ATCAGGGTTACAAGGACGGC
Junctional adhestion molecule (JAM) 3	*JAM3*	185	CTGATCACGTTGGGCATCTG	TGGTTTCCCTGGGTTCTTGT

All reactions were carried out with triplicate technical replicates (wells of the same sample and primer, pipetted identically), with all biological replicates dispensed on the same plate, and all plates contained negative template controls (NTCs) and positive template controls (PTCs) for each primer tested. Each plate also contained a housekeeping gene (*GAPDH*) as an inter-plate calibrator (IPC), with this reaction performed with both undiluted pooled cDNA and the same cDNA diluted 1:10. NTCs were produced by combining 9 µl of the reaction mastermix with 1 µl molecular grade water. PTCs were produced by combining 9 µl reaction mastermix with 1 µl undiluted, pooled cDNA, as used for generating efficiency values via standard curves. IPCs used 9 µl *GAPDH* housekeeping gene mastermix and 1µl undiluted, pooled cDNA. All RT-qPCR reaction mixes were prepared in 96-well PCR plates (04729692001, Roche, USA) sealed with LightCycler 480 sealing foil (04729757001, Roche, USA), and reactions performed using a LightCyler 480 II (Roche, USA).

Table 2.10 - LightCycler 480 II (Roche, USA) reaction conditions used for RT-qPCR throughout the present work.

Reaction step	Temperature (°C)	Ramp rate (°C/s)	Hold time (mm:ss)	Cycles
1 – Preincubation	95	4.4	05:00	1
2 - Amplification	-	-	-	45
2a	90	4.4	00:10	-
2b	60	2.2	00:10	-
2c	72	4.4	00:10	-
3 – Melting Curve	-	-	-	1
3a	95	4.4	00:05	-
3b	65	2.2	01:00	-
3c – Acquisition (5 acquisitions / °C)	65-97	0.11	-	Continuous
4 - Cooling	4	2.2	30:00	1

Data analysis was performed by generating Cp (crossing point) values within the LightCycler 480 software (Roche, USA) via the second derivative method. Cp values were imported into QBase+ (Biogazelle, Belgium) for analysis using the calibrated normalised relative quantity (CNRQ) method. Crossing point (Cp) values greater than 40 amplification cycles were taken as zero expression of the gene of interest, and any reactions meeting these criteria were repeated at least once to eliminate the possibility of operator error.

Five housekeeping genes were assessed with the geNorm algorithm within QBase+, and the three housekeeping genes with the lowest variability were used as reference genes for sample normalisation.

2.6.4. Sequencing of GW9662-modifiable region of PPARG ligand binding domain

2.6.4.1. Reverse transcription PCR and DNA electrophoresis

PCR was performed on cDNA produced from unstimulated, sub-confluent H400 cells. Primer mastermix was produced by dilution of 10 µl forward primer and 10 µl reverse primer in 60 µl molecular biology grade water, resulting in primers at a concentration of 12.5 µM.

Reaction mixtures (per reaction) comprised 12.5 µl MyTaq Red mix (BIO-25043, Meridian Bioscience, USA), 9.5 µl molecular biology grade water (W4502, Sigma, UK), 2 µl primer set mastermix and 1 µl cDNA. PCR was then performed in duplicate at 25 and 32 cycles to optimise PCR conditions, with no template controls (NTCs) for each reaction. PCR was performed on a Biometra TAdvanced twin 48G (Analytik Jena, Germany), with reaction conditions described in Table 2.11.

Table 2.11 - RT-PCR conditions for amplification of PPAR ligand binding domain, prior to sequencing.

Reaction step	Temperature (°C)	Ramp rate (°C/s)	Hold time (mm:ss)	Cycles
1 – Preincubation	94	6	05:00	1
2 - Amplification	-	-	-	25/32
2a	94	6	00:20	-
2b	60.5	6	00:20	-
2c	68	6	00:20	-
3 – Termination	72	6	10:00	1
3 - Cooling	4	6	Infinite	1

DNA electrophoresis was performed using a 1.5% (w/v) agarose gel. Agarose (16500500, ThermoFisher, UK) was dissolved in Tris-acetate EDTA buffer (TAE) (J63931.K2, ThermoFisher, UK) and heated until molten, and stained with SYBR safe DNA gel stain (S33102, ThermoFisher, UK) diluted 1:10,000. 25 µl of PCR product was added to each well, in addition to 6 µl of 1kb ladder (SM0311, ThermoFisher, UK) and 6 µl of 100bp ladder (SM0241, ThermoFisher, UK) and electrophoresis performed at 120 V for 30 minutes. Imaging of DNA electrophoresis gels was performed using a GBox imaging system (Syngene, UK).

2.6.4.2. PCR product gel extraction

Following imaging, PCR products were dissected out of the agarose gel, weighed and added to microcentrifuge tubes, with two wells of 32 cycle PCR product combined. A DNA gel

extraction kit (Monarch T1020, New England Biolabs, USA) was used to extract DNA following the manufacturer's protocol. Gel dissolution was performed using a thermal mixer (13687711, ThermoFisher, UK) at 50°C for 10 minutes. 15 µl of molecular biology grade water was used to elute DNA, with the eluate then passed back through the column a second time to maximise DNA yield. All centrifugation steps were performed at 10,000 x *g* for 1 minute. DNA concentration was then quantified (Jenway Genova spectrophotometer, Fisher Scientific, UK).

Table 2.12 - PCR primers used for amplification and sequencing of the PPARG ligand binding domain region of interest.

Primer	**Size (bp)**	**Forward Primer (5'-3')**	**Reverse Primer (5'-3')**
PPARG LBD	298	AGGGCGATCTTGACAGGAAA	AGGAGGCCAGCATTGTGTAA

2.6.4.3. Preparation of samples for sequencing

PCR product sequencing was performed using a third-party (Source Bioscience, Cambridge, UK). Extracted DNA was diluted in molecular biology grade water to a final concentration of 10 ng/µl, and forward sequencing primer (Table 2.10) diluted to a concentration of 10 pMol/µl. 6 µl of each was added to microcentrifuge tubes, sealed and delivered to the sequencing supplier (Source Bioscience, UK). Following receipt of sequencing data, alignments were performed with Benchling (Biology Software, 2023).

2.6.5. Semi-quantitative RT-PCR of PPARγ transcript variants

RNA was isolated from healthy, control H400 cells, cDNA synthesised and 1 µl of cDNA used in an RT-PCR reaction as previously described (Section 2.6.4.1). Specific

oligonucleotide primers were designed for PPARγ1 and γ2, shown in Table 2.13. PCR reaction conditions were the same as shown in Table 2.11, but employing 35 amplification cycles. DNA electrophoresis was performed as previously described in Section 2.6.4.1. Band intensity was then quantified, calibrated to a housekeeping gene (*GAPDH*) and an expression ratio between PPARγ1 and γ2 calculated.

Table 2.13 – Primers used for isoform-specific RT-sqPCR in H400 cells.

Primer	Size (bp)	Forward Primer (5'-3')	Reverse Primer (5'-3')
PPARγ1	71	TGAAAGAAGCCAACACTAAACCA	CGTTAAAGGCTGACTCTCGT
PPARγ2	134	TCCTATTGACCCAGAAAGCGA	TTACGGAGAGATCCACGGAG

2.7. Protein expression analysis

2.7.1. Western blotting

2.7.1.1. Protein isolation and quantification

Western blotting was performed for 2D cultured cells only. Culture medium was removed and stored at -80°C, with technical replicates pooled. Cells were washed twice with ice cold (4°C) DPBS (D8537, Sigma Aldrich, UK), and 300 µl of radioimmunoprecipitation assay (RIPA) lysis buffer (produced as shown in Table 2.14) was added to each well, incubated for 15 minutes on ice.

Table 2.14 – Constituents of RIPA buffer for protein isolation.

Stock solution	**Volume of stock (ml)**
5M NaCl	3
0.5M EDTA, pH 8.0	1
1M Tris, pH 8.0	5
Triton X-100	1
10% sodium deoxycholate	5
10% SDS	1
dH20	84
cOmplete protease inhibitor tablets (Roche, USA)	x2 tablets
Final volume	**100 ml**

Cell lysis was ensured using scrapers and the cell lysate pooled before removal into sterile microcentrifuge tubes with combined technical replicates. These tubes were incubated for 1 hour on a rotator at 4°C, before centrifugation to pellet cellular debris (13,000 x *g*, 30 seconds). Supernatant (containing isolated protein in suspension) was aliquoted into microcentrifuge tubes for long term storage at -80°C.

Protein solution was then quantified using a Qubit protein assay (Q33211, ThermoFisher, UK) and a Qubit Flex Fluorometer (ThermoFisher, UK) following manufacturer's instructions.

2.7.1.2. Sodium dodecyl sulphate polyacrylamide gel electrophoresis (SDS-PAGE)

10 well, 12% Bis-tris mini-PAGE gels (NP0341BOX, ThermoFisher, UK) were prepared by washing in 1x MOPS-SDS running buffer, prepared from 20x NuPAGE MOPS-SDS running buffer concentrate (NP0001, ThermoFisher, UK), supplemented with 1ml of NuPAGE antioxidant (NP0005, ThermoFisher) per litre of running buffer. Reducing protein-buffer solutions were prepared as shown in Table 2.15.

Table 2.15 - Components of protein-buffer mixtures for SDS-PAGE.

Component	**Volume (µl)**
Protein sample (5 µg)	x
NuPAGE LDS Sample Buffer 4x (NP0007, ThermoFisher, UK)	5 µl
NuPAGE Reducing agent (NP0004, ThermoFisher, UK)	2 µl
dH20	Adjusted to give final volume of 20 µl
Total volume	**20 µl**

Protein-buffer solutions were mixed by pipetting and incubated at 70°C for 10 minutes (Biometra TAdvanced 48g, Analytik Jena, Germany) before loading 20 µl of each sample into the prepared PAGE gel, in addition to a dual colour protein standard ladder (1610374, BioRad, USA). 1x MOPS-SDS running buffer with antioxidant was then added. Electrophoresis was performed at 180 V for 70 minutes in an XCell SureLock electrophoresis system (ThermoFisher, UK) using a VWR electrophoresis power supply (VWR, USA).

2.7.1.3. Protein transfer to western blot membrane

PAGE gels were opened and washed with 1x transfer buffer, prepared from 20x NuPAGE transfer buffer (NP0006, ThermoFisher, UK). A transfer stack was prepared, which comprised one nitrocellulose blotting membrane (Whatman Protran BA85, 0.45 um, Whatman, UK) and two western blotting filter papers (84784, ThermoFisher, UK) in an XCell II blot module (ThermoFisher, UK). The blot module was filled with 1x transfer buffer, and electrophoresis performed at 25 V for 1 hour, utilising the same power supply and tank as SDS-PAGE.

2.7.1.4. Ponceau staining

The efficiency of protein transfer from the PAGE gel to western blotting membranes was qualitatively assessed using Ponceau staining. Briefly, membranes were immersed in Ponceau stain for 10 minutes before washing three times in distilled water, 2 minutes per wash.

Table 2.16 - Constituents of Ponceau staining solution, as used for assessing protein transfer to western blotting membranes.

Glacial acetic acid	25 ml
Ponceau S tetrasodium salt	0.5 g
Distilled water	475 ml
Total volume	**500 ml**

Stained membranes could then be reviewed and imaged as required. De-staining was then performed by washing twice in distilled water, 10 minutes per wash.

2.7.1.5. Immunodetection

Tris-buffered saline (TBS) was prepared as a 10x solution as described in Table 2.17.

Table 2.17- Constituents of 10x Tris-buffered saline (TBS)

Component	Quantity
Tris-HCl	24 g
NaCl	88 g
Tris Base	5.6 g
HCl (12N)	to pH 7.6
H20	to 1000 ml final volume

10x TBS was diluted 1:10 in distilled water and TWEEN-20 (P1379, Sigma Aldrich, UK) added to a final concentration of 0.1% (v/v) to produce 1x Tris-buffered saline with TWEEN 20 (TBST).

Membranes were blocked at room temperature for 1 hour in 5% (w/v) skimmed milk powder (Sainsburys, UK) dissolved in TBST, with constant agitation. Each membrane was exposed to the desired primary antibody, diluted as described, in 5ml 5% (w/v) skimmed milk in TBST. Incubation took place either overnight at 4°C or for 1 hour at room temperature, with constant agitation in a sealed, sterile container. Three TBST washes were then performed at room temperature, 15 minutes each. Secondary antibody was diluted 5ml 5% (w/v) skimmed milk in TBST and the membrane incubated in antibody solution for 1 hour at room temperature, again with constant agitation. Three TBST washes (10 minutes each) were performed at room temperature with constant agitation, before the dropwise addition of 200 µl chemiluminescent substrate (WesternSure Premium, 926-95000, Licor, USA) per manufacturer instructions. Imaging was then performed using a LiCor C-DiGit blot scanner (Licor, USA).

Table 2.18 - Antibodies used for western blotting.

Antibody	Manufacturer reference	Dilution from stock
Anti-PPARγ, Rabbit anti-human, polyclonal	Abcam, Ab59256	1:1000
Anti-beta actin, recombinant rabbit anti-human, monoclonal	Abcam, Ab213262	1:10,000
Goat anti-rabbit IgG-HRP conjugated	Abcam, Ab6721	1:5000
Anti-claudin-1, recombinant rabbit anti-human, monoclonal	Abcam, Ab211737	1:1000
Anti-occludin, recombinant rabbit anti-human, monoclonal	Abcam, Ab216327	1:1000
Anti-ZO-1, recombinant rabbit anti-human, monoclonal	Abcam, Ab216880	1:1000

Western blot data were analysed within Licor Image Studio (Licor, USA). Target protein band intensity was quantified and normalised to loading control band intensity (beta actin) for each sample.

2.7.2. Enzyme-linked immunosorbent assays (ELISAs) for interleukins 6 and 11

Culture supernatant was removed to centrifuge tubes, centrifuged at 5000 x *g* for 5 minutes, and the cell debris pellet discarded. Culture supernatant was then applied to ELISAs as per manufacturer's instructions (Table 2.19**)**. Four technical replicates were performed and averaged, with each plate (MaxiSorb ELISA plates (ThermoFisher, UK)) containing a five-point standard curve prepared from protein standard provided within the ELISA kit.

Table 2.19 - ELISA kits and manufacturer details used to assess changes in interleukins 6 and 11 production in H400 cells.

Target	Kit	Manufacturer	Supernatant dilution
Interleukin 6 (IL-6)	Human IL-6 DuoSet ELISA, DY206	BioTechne, USA	None
Interleukin 11 (IL-11)	Human IL-11 DuoSet ELISA, DY218	BioTechne, USA	None

Following completion of the manufacturers recommended protocol, optical density was recorded at 450 nm and 540 nm using a Tecan Spark plate reader (Tecan, Switzerland), subtracting the latter from the former. Interpolation of standard curves was performed using a simple linear regression within GraphPad Prism (GraphPad Software, San Diego, California USA).

2.8. Epithelial barrier function assays

2.8.1. Transepithelial electrical resistance (TEER) assay

Cultured media were aspirated and cells washed twice with warmed (37°C) PBS. 500 µl warmed PBS was then added to both the upper and lower chambers of each Transwell insert.

Initial pre-treatment TEER measurements were then taken using an EVOM2 epithelial voltohmeter with STX2 chopstick electrodes (both World Precision Instruments, UK), with the electrodes pre-cleaned by 20 minutes of immersion in 70% ethanol. Electrodes were immersed and washed in PBS between each measurement. Each well was measured three times and the average TEER reading recorded per well. Following initial readings, PBS was aspirated and 500 µl of LPS-supplemented HamsF12:DMEM added to the lower chamber of each Transwell, with LPS added as per Table 2.1.

Following a further 24-hour incubation period at 37°C, 5% CO_2, media was aspirated, wells washed twice with warmed (37°C) PBS, and 500 µl PBS added to both chambers of each Transwell. TEER readings were then taken as per the pre-treatment reading protocol detailed previously. TEER values for technical replicates (identical wells) were averaged, and the TEER value of a blank well subtracted to account for the electrical resistance of the membrane and PBS.

2.8.2. Fluorescein-isothiocyanate (FITC) tagged dextran macromolecular tracer assay

100 mg of FITC-tagged, 40 kDa dextran (Sigma Aldrich, UK) was resuspended in 10 ml of PBS to produce a 10mg/ml stock solution. Following a 24-hour incubation with LPS (+/- GW1929) and TEER readings being acquired, media in the lower tissue culture insert chamber was aspirated and replaced with 1 ml of HamsF12, with 500 µl HamsF12 added to the top chamber. Cells were then incubated at 37°C, 5% CO_2 for 30 minutes to allow for equilibration of hydrostatic pressure between the two chambers.

50 µl of 10 mg/ml FITC-dextran stock was then added to the top chamber and incubated again at 37°C, 5% CO_2. After 90 minutes of incubation, 100 µl of culture media was removed from the lower chamber and added to a black, clear bottomed 96-well plate (Corning, USA).

Fluorescence was recorded using a Tecan Spark multimode plate reader (Tecan, Switzerland), at an excitation wavelength of 485 nm and emission wavelength of 544 nm with a 20nm bandwidth for both.

2.8.3. Barrier function assays in organotypically cultured tissues

Following culture and treatment with LPS and PPARγ agonist, BECD-cultured hydrogels were removed from culture and carefully placed on a petri dish, with care taken to maintain the orientation of the hydrogel raft (Figure 2.3 A and B). A 7 mm inside diameter biopsy punch (WellTech Rapid-Core 7.0, WellTech, Taiwan) was then used to take a core biopsy from the centre of the hydrogel (Figure 2.3 C), with this sample then deposited into a 24-well tissue culture insert (662641 ThinCert 0.4 µm PET, Greiner BioOne, UK) (Figure 2.3 D). Each raft was then checked for gaps between the outside diameter of the hydrogel and inside wall of the tissue culture insert (Figure 2.3 E).

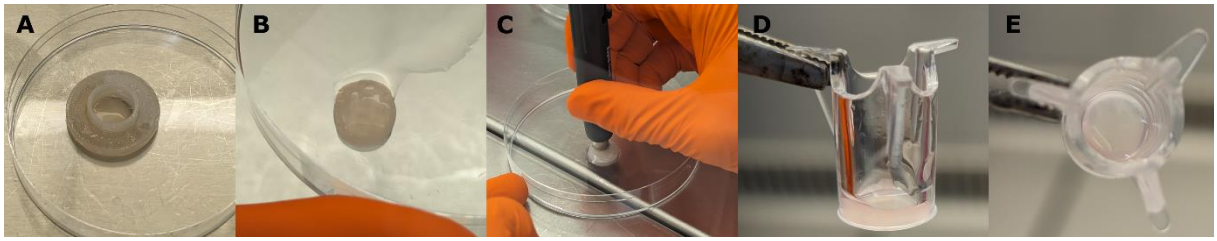


Figure 2.3 - Photographs of steps involved in organotypic gingival epithelium sample preparation for barrier function assays.
A) BECD removed from culture, with hydrogel *in situ*.
B) Hydrogel removed from BECD onto plastic petri dish.
C) 7mm biopsy taken from centre of hydrogel.
D) Hydrogel inserted into 24-well tissue culture insert.
E) Sample in place in tissue culture insert and checked for gaps around margin.

Both TEER and FITC-dextran assays were performed as described for monolayer epithelial cells (Sections 2.8.1 and 2.8.2), following washing of the hydrogel section with 100 µl warmed PBS.

2.9. Combined LPS challenge and PPARγ activation in H400 cells

2.9.1. Epithelial barrier function: identifying optimal concentration of LPS

Prior to the introduction of a PPARγ agonist, a range of concentrations of LPS was trialled in barrier function assays. $1x10^4$ H400 cells were seeded in 1 ml of supplemented HamsF12:DMEM to the upper chamber of 12mm diameter, 0.4µm polycarbonate membrane Transwell devices (CLS3401-48EA, Corning, USA) in 12 well culture plates. 1 ml supplemented HamsF12:DMEM was added to the lower chamber, and cells incubated for 72 hours at 37°C, 5% CO_2. Culture media was aspirated, replaced and incubated for a further 24 hours under the same conditions. LPS was then added as described in Section 2.2.1 and incubated for 24 hours prior to testing with barrier function assays.

2.9.2. Epithelial barrier function: combined LPS stimulation and PPARγ agonist treatment

Due to the unavailability of the 12mm diameter, 0.4 µm polycarbonate membrane Transwell devices (Corning, USA) used for identifying the optimal LPS concentration for barrier function challenge (Section 2.9.1), 0.4 µm PET, 24-well ThinCerts (662641 Greiner Bio-One, UK) were used for the following assays. $5x10^4$ H400 cells were seeded to the upper chamber of 24-well ThinCerts (Greiner Bio-One, UK) in 100 µl supplemented HamsF12, with 1 ml supplemented HamsF12 added to the lower chamber. Cells were incubated at 37°C, 5% CO2 for 72 hours, culture media aspirated and replaced and incubated for a further 24 hours under the same conditions. Cultures were then supplemented as described in Section 2.2.3, and barrier integrity assessed with both TEER and a macromolecular tracer assay, described in Sections 2.8.1 and 2.8.2 respectively.

2.9.3. Culture setup for gene and protein expression analysis following combined LPS and PPARγ agonist exposure

2.9.3.1. 2D cultured H400 OSCC cells

$1x10^5$ H400 cells were seeded to each well of a 6 well plate in 3 ml HamsF12:DMEM with duplicate technical replicates. Within each biological replicate, one group of cells was plated for RT-qPCR analysis, and another plated for ELISA / western blot analysis. These two groups were treated and supplemented identically. Cultures were designated into 4 groups; control, LPS only, GW1929 only and LPS + GW1929. Culture groups were treated as described in Section 2.2.3 and then processed according to the assigned assay.

2.9.3.2. 3D culture of stratified H400 OSCC cells with BECD system

Organotypic H400 cultures were established as previously described (Section 2.5.2) with the modification of using a 48-hour submersion to produce confluent a H400 cell layer, instead of the 72 hours previously used. A 14-day ALI period was employed, counted from the day of ALI-induction to the day of first LPS treatment, and culture media was changed every second day.

Following 14 days of ALI culture, cultures were split into four groups (in duplicate technical replicates, with each technical replicate defined as a separate epithelial raft cultured in the same plate) and exposed to LPS-treated culture media as appropriate. Cultures were treated as described in Section 2.2.3, with treated media added to wells containing BECDs. Cultures designated for both RT-qPCR and histological analysis were supplemented identically. Following supplementation, both hydrogel and monolayer cultures were lysed for RNA extraction, as described in Section 2.6.1.

2.10. Statistical analysis and replicate definitions

All statistical analysis was carried out using GraphPad Prism (GraphPad Software, San Diego, California USA), with versions ranging from 8.7.0 to 10.1.0 over the course of the research. Within the present work, biological replicates were depicted as separate experimental cultures, established from different cell passages on different days. Technical replicates were depicted as experimental cultures treated identically within the sample culture plate. Within technical replicates, the mean of measured values was used as the value for that biological replicate. Unless stated otherwise, data displayed in figures are the mean of multiple biological replicates with standard deviation shown. Details of specific statistical tests performed are shown in all figure legends.

3. CHARACTERISING THE RESPONSE OF ORAL EPITHELIAL CELLS TO BACTERIAL LIPOPOLYSACCHARIDE

3.1. Introduction

The bacterial endotoxin lipopolysaccharide (LPS) has been widely used to instigate the production of inflammatory cytokines in cells, *ex vivo* models and *in vivo* (Angrisano *et al.*, 2010; Chae, 2018; He *et al.*, 2019). This chapter describes the response of H400 oral squamous cell carcinoma (OSCC) cells to *E.coli* 0127:B8 LPS, with a focus on inflammatory cytokines and monolayer barrier function. While LPS has been extensively used for *in vitro* studies of inflammation, toxicity, and barrier function, these responses may differ between models (Pezzulo *et al.*, 2011). Therefore, initial work was performed to identify a suitably non-toxic concentration (using growth curves and viability assays) which also produced a reduction in barrier function (TEER and MMT assays) and an increase in pro-inflammatory cytokine expression (RT-qPCR). LPS concentrations from 20 to 2000 ng/ml were selected initially based upon previous publications (Loryman and Mansbridge, 2008; Nishio *et al.*, 2013; Zheng, Zhang and Hu, 2018). Continuous exposure of H400 cells to LPS throughout the 9-day culture period was tested to screen for toxicity after chronic exposure, more closely mimicking the clinical scenario, as gingival epithelial cells are continuously exposed to bacteria and bacterial products, as opposed to a single acute challenge.

An extensive panel of genes was assessed by RT-qPCR, which included a range of inflammation associated, barrier function-linked and PPARγ-related transcripts. This selection of genes allowed for validation of the role of LPS on the expression of pro-inflammatory signalling molecules (*IFNG* (Kim and Moudgil, 2008; Zaidi, 2019), *IL6* (Scheller, Garbers and Rose-John, 2014), *CXCL8* (Celik *et al.*, 2016), *TNFa* (Kim and Moudgil, 2008) and *TGFB1* (Takahara *et al.*, 2022)), a wound repair gene (*MMP1* (Stevens and Page-McCaw, 2012)), an inflammatory linked transcription factor (*NFKB* (Yamamoto and Gaynor, 2005))

and apoptosis marker (*CASP3* (Asadi *et al.*, 2022)). In addition, genes known to be regulated by PPARγ (*PTGS2* (Hotta *et al.*, 2010) and *AQP3* (Jiang *et al.*, 2011)) were assessed to identify any potential impact of LPS exposure on their expression. The expression of key barrier genes (*CDH1* (Van Roy and Berx, 2008), *OCLN* (Feldman, Mullin and Ryan, 2005), *TJP1* (Fanning *et al.*, 1998)) were also analysed.

Due to the intended application of PPARγ agonists to models of gingival inflammation induced with LPS, PPARγ expression was confirmed with RT-qPCR and western blotting, as failure to choose a PPARγ-expressive cell line could result in sub-optimal responses to receptor stimulation. Overall, these steps aimed to provide an initial understanding of the effect of LPS on the H400 cell line when cultured in a monolayer and generate an evidence base for further studies incorporating LPS and PPARγ agonists to study the possible anti-inflammatory role of PPARγ.

3.2. Growth curves and cytotoxicity testing

Growth curves from H400 cells exposed to LPS indicated no significant difference in live cell number between the control and any LPS-treated population at any of the tested timepoints or LPS concentrations (Figure 3.1).

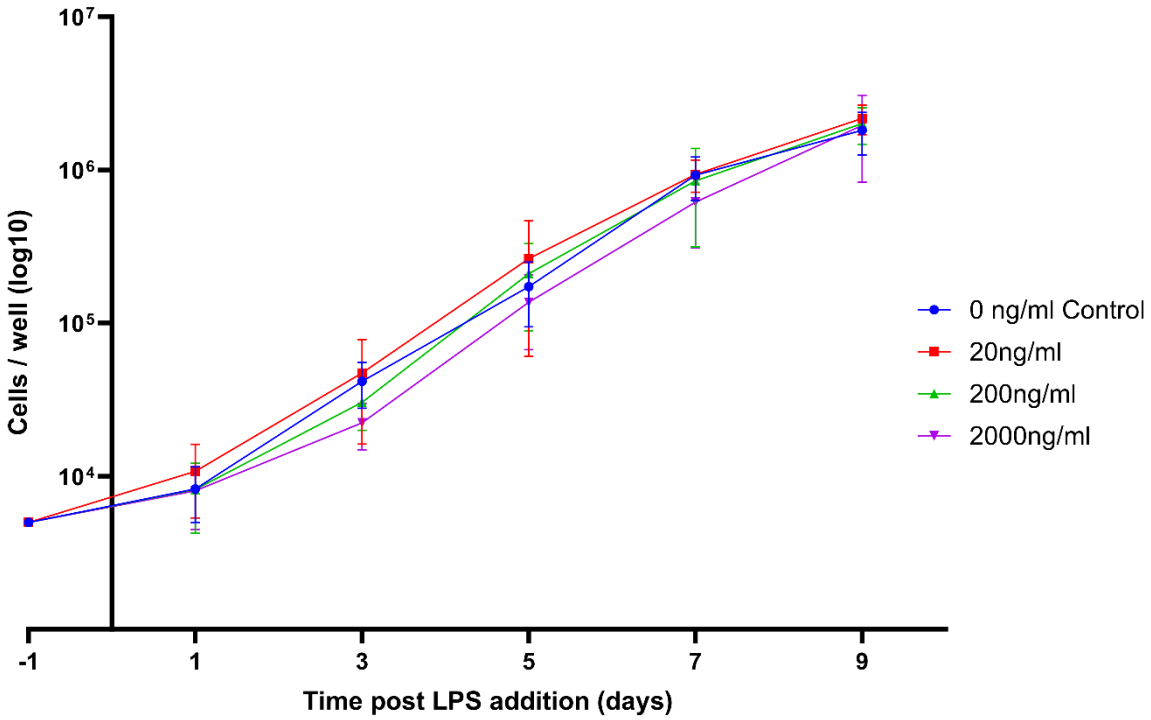


Figure 3.1 - H400 oral squamous cell carcinoma cell growth plot, comparing cells exposed to LPS at three different concentrations to untreated controls. No statistically significant difference was identified between any tested concentration and untreated control at any timepoint. N=3, mean ±SD, two-way ANOVA with Tukey's multiple comparisons post-hoc test (all to control).

From the same cell populations, cell viability data again showed no significant difference between cells exposed to the tested concentrations of LPS and untreated controls at any timepoint (Figure 3.2). Initial cell viability at day 1 post-LPS addition was variable between biological replicates, with the mean fraction of viable cells ranging from 85% (200 ng/ml LPS) to 90% (2000 ng/ml LPS). Cell viability appeared to peak and plateau at approximately 97% for all tested concentrations on day 5.

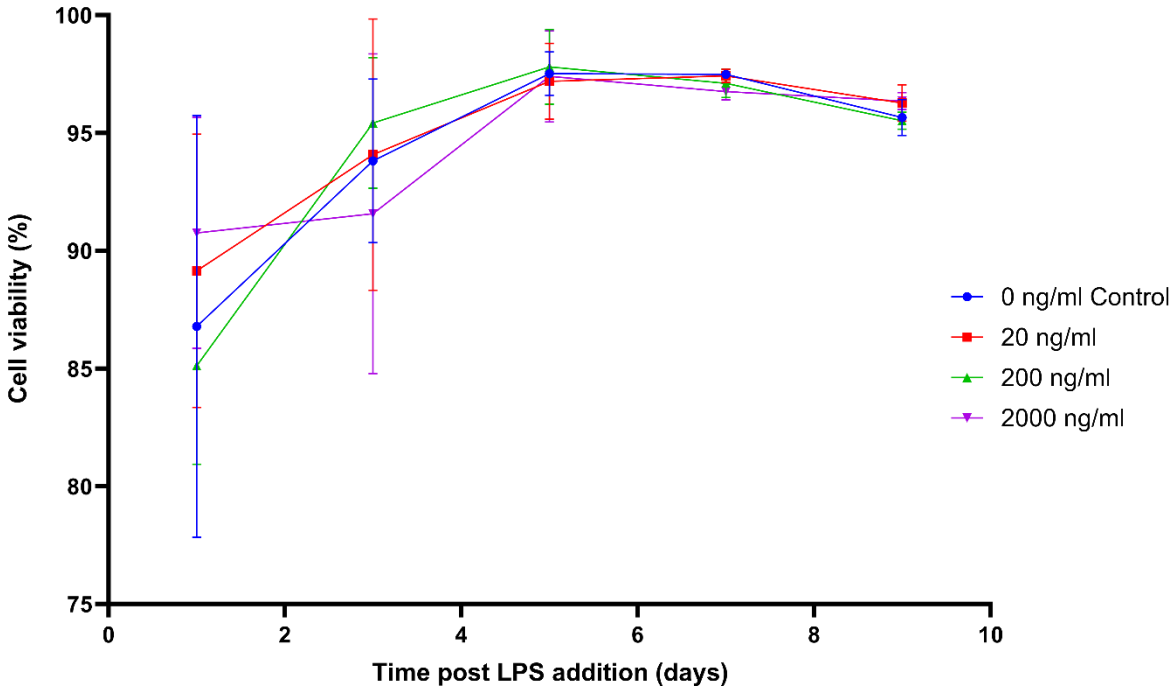


Figure 3.2 - H400 oral squamous cell carcinoma cell viability plot, showing cell viability over 9 days of LPS treatment. No statistically significant difference was identified between any tested concentration and untreated control at any timepoint.
N=3, mean ±SD, two-way ANOVA with Dunnett's multiple comparisons post-hoc test (all to control).

3.3. Modification of epithelial barrier function with LPS: TEER and macromolecular tracer assays

TEER testing prior to LPS exposure showed no significant difference between wells designated as control (no LPS) and those designated for treatment with 20, 200 and 2000 ng/ml LPS. After 24 hours of exposure to LPS at the same concentrations, a statistically significant reduction in TEER was detected between the control and cultures exposed to all test concentrations of LPS. Mean TEER reduced from 158.8 $\Omega.cm^2$ to 150.3 ($p = 0.0006$), 152 ($p = 0.002$) and 151 $\Omega.cm^2$ ($p = 0.0009$) for LPS concentrations of 20, 200 and 2000 ng/ml respectively (Figure 3.3).

The greatest reduction in mean TEER was identified with 20 ng/ml LPS, however there was no statistically significant difference in TEER value between the LPS-exposed cultures ($p > 0.05$). These data do not suggest a dose-dependent relationship between LPS concentration and TEER at the concentrations of LPS used.

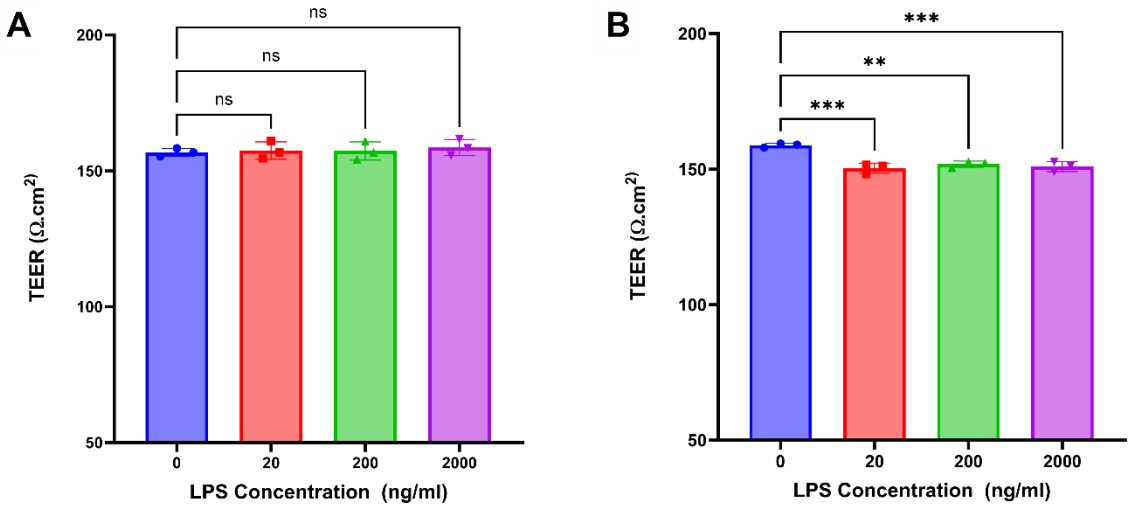


Figure 3.3 - Transepithelial electrical resistance (TEER) measurements of designated wells A) prior to LPS addition and B) after 24 hours of LPS exposure. LPS treated cells show a significant reduction in TEER relative to control at all tested concentrations.
N=3, mean ±SD, one-way ANOVA with Tukey's multiple comparisons post-hoc test (all to all). NS = not significant ($p > 0.05$), ** = $p < 0.01$. *** = $p < 0.001$.

Due to a shortage of the devices used for this assay, only one biological replicate of the MMT assay was possible. These N=1 MMT results are included as the data directed future work, indicating the utility of such an assay in combination with TEER. Recorded fluorescence increased for all LPS-exposed cultures compared with controls, from 513.3 to 610, 584.7 and 591.7 RFU at 20, 200 and 2000 ng/ml LPS respectively (Figure 3.4).

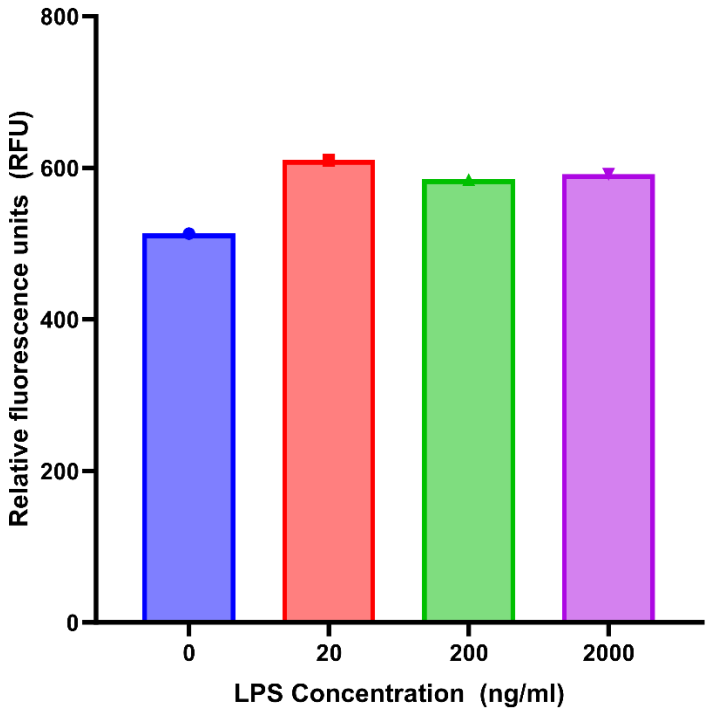


Figure 3.4 - FITC-dextran macromolecular tracer assay of LPS exposed (24 hours) H400 cells. H400 OSCC cells treated with 20, 200 and 2000 ng/ml LPS generated an increase in recorded fluorescence compared with untreated control cells. Cell layers exposed to FITC-dextran (40 kDa) for 90 minutes prior to measurement of fluorescence. N=1, no statistical analysis performed due to sample size of 1.

3.4. Analysis of LPS treatment induced changes in gene expression

H400 cells were treated with three LPS concentrations for 24 hours prior to RNA extraction. RT-qPCR analysis demonstrated that treatment with LPS statistically significantly increased the expression of interleukin 8 (*CXCL8*) and decreased aquaporin 3 expression(*AQP3*) relative to untreated controls (Figure 3.5).

Calibrated normalised relative quantity (CNRQ) of *CXCL8* increased from 3.13 to 22.45 and 28.90 with 200 and 2000 ng/ml LPS respectively ($p < 0.0001$ for both). (Figure 3.5A). AQP3 CNRQ decreased from 1.66 to 0.897 with 2000 ng/ml LPS ($p < 0.05$) (Figure 3.5 B).

PPARG expression is present and consistent between the control and LPS-exposed groups. No other tested genes showed a statistically significant change expression between the control and any LPS-exposed treatment group.

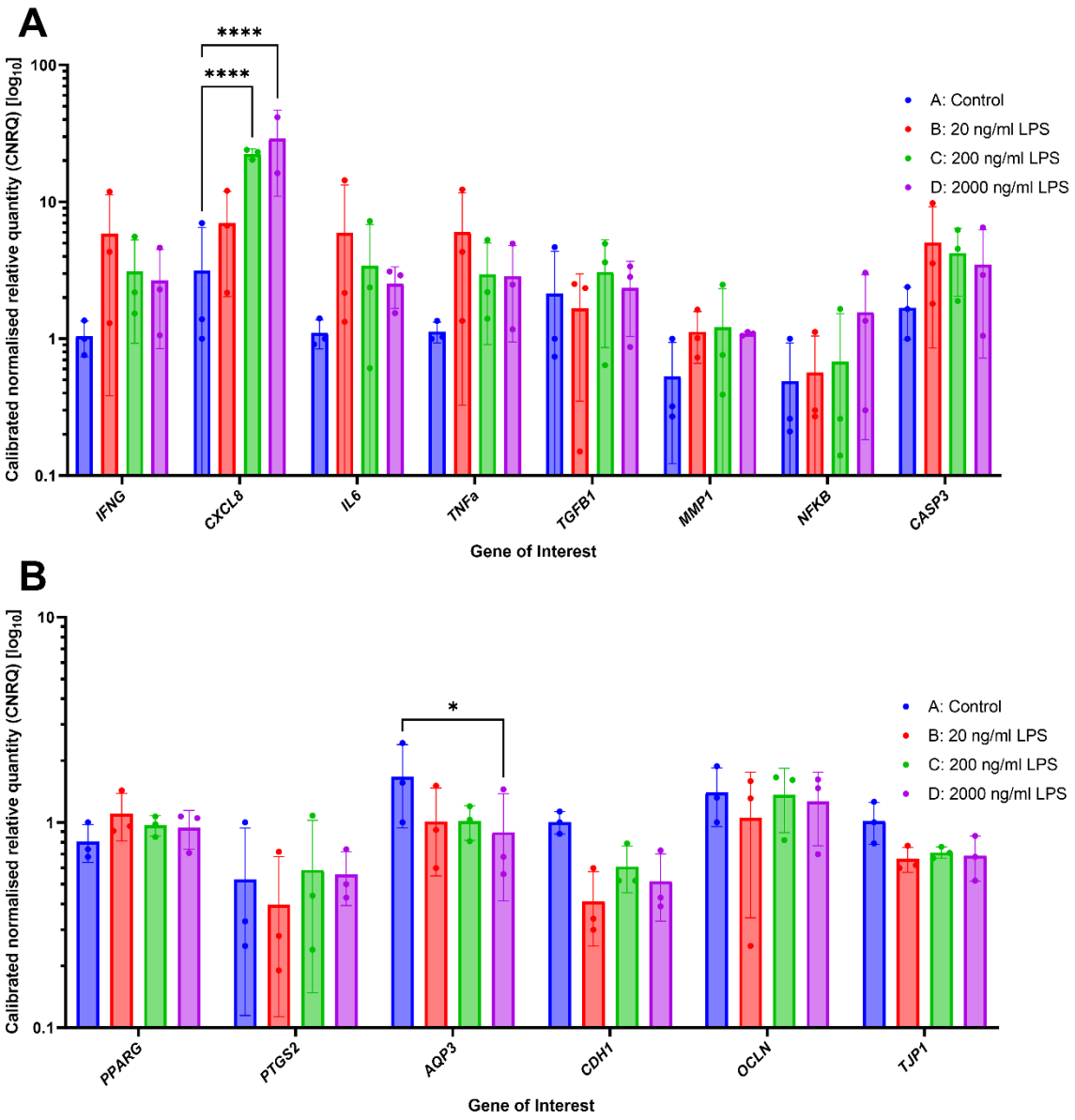


Figure 3.5 – RT-qPCR analysis of RNA extracted from H400 cell cultures exposed to *E.coli* LPS for 24 hours at 20, 200 and 2000 ng/ml. A) Inflammatory cytokines B) PPARγ and barrier function related genes.

All data normalised and scaled to control group, displayed with $\log_{10}$ y-axis.

IFNG – Interferon gamma, *CXCL8* – Interleukin 8, *IL6* – interleukin 6, *TNFa* – tumour necrosis factor alpha, *MMP1* – matrix metalloproteinase 1, *NFKB* – nuclear factor kappa beta, *CASP3* – caspase 3, *PPARG* – peroxisome proliferator activated receptor gamma, *PTGS2* - prostaglandin-endoperoxide synthase 2, *AQP3* – aquaporin 3, *CDH1* – e-cadherin, *OCLN* – occludin, *TJP1* – zona occludens 1, *YWHAZ* - Tyrosine 3-Monooxygenase/Tryptophan 5-Monooxygenase Activation Protein Zeta, *ACTB* – beta actin, *GAPDH* - Glyceraldehyde 3-phosphate dehydrogenase.

N=3, mean calibrated normalised relative quantity (CNRQ) ±SD, two-way ANOVA with Dunnett's multiple comparisons post-hoc test (all to control). * = $p < 0.05$. **** = $p < 0.0001$.

3.5. Verification of PPARγ expression in H400 OSCC cells

Following initial confirmation of PPARγ expression by qPCR (as shown in Figure 3.4), isoform specific semiquantitative RT-PCR analysis for PPARγ1 (PPARG-217, ENST00000651735.1) produced a markedly higher signal than for PPARγ2 (PPARG-201, ENST00000287820.10) (Figure 3.6 C), in a statistically significant ratio of 3:1 ($p = 0.0007$) (Figure 3.6 D). PCR products also matched the expected product size for the oligonucleotide primers used. Western blotting of protein isolated from untreated control H400 OSCC cells revealed two distinct bands above 50 kDa in size. The lower molecular weight band, of approximately 55 kDa, closely matched the predicted molecular weight of PPARγ1 (UniProt E9PFV2, 54.4 kDa). A second, higher molecular weight band was noted closer to 60 kDa and was suspected to be the PPARγ2 isoform (UniProt P3721-1, 57.6 kDa). Semi quantitative

analysis of these two fragments showed a statistically significant expression differential between PPARγ1 and γ2 ($p = 0.0226$) at a ratio of 2.6:1 (Figure 3.6 B).

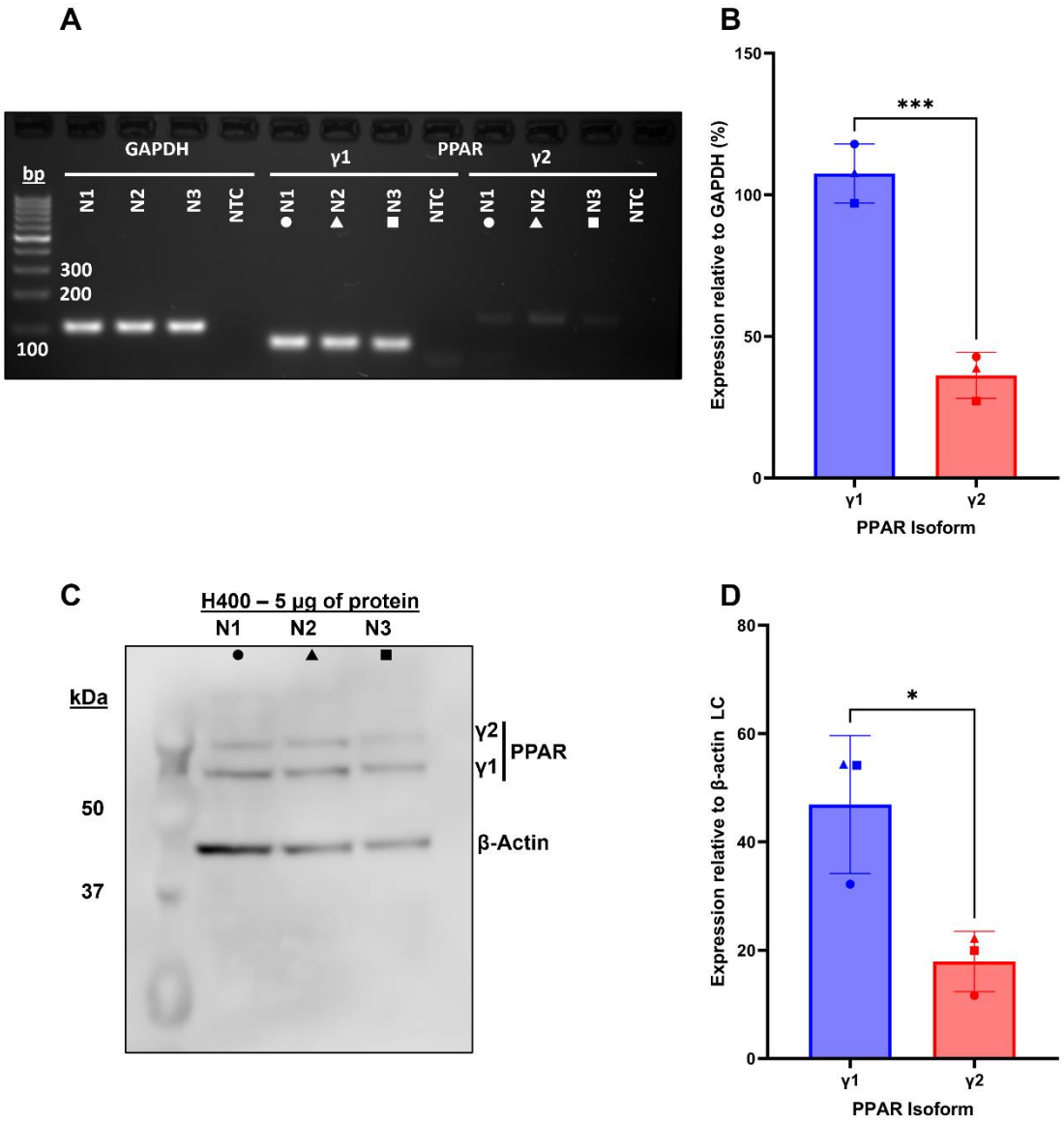


Figure 3.6 – Comparison of the expression of PPARγ transcript variants γ1 and γ2 at the RNA level by semiquantitative RT-PCR (A, B) and protein level by western blot (C, D).
A) Annotated DNA electrophoresis of RT-PCR products. Primers specific to PPARγ1 and PPARγ2 were used, in addition to GAPDH product used as a housekeeping loading control.
B) Semi-quantitative analysis of isoform expression as measured by RT-PCR. Expression of γ1 and γ2 fragments normalised to GAPDH expression.
C) Annotated, unedited western blot for PPARγ and β-actin loading control. Two PPARγ fragments were noted, with a higher signal lighter fragment and lower signal heavy fragment.
D) Semi-quantitative analysis of PPARγ isoform expression. Expression of γ1 and γ2 fragments normalised to loading control (β-actin) expression.

N=3 for all, mean ±SD. Statistical analyses performed with two-tailed, unpaired t-tests, *=p < 0.05, ***=p < 0.001.

3.6. Discussion

The work described in this chapter aimed to characterise the response of H400 OSCC cells to bacterial LPS, in order to identify a suitable pro-inflammatory stimulus for use in further studies. These data indicated that *E.coli* LPS treatment exerted no statistically significant change in cell growth (Figure 3.1) or viability (Figure 3.2) after a maximum of 9 days of exposure at 20, 200 and 2000 ng/ml concentrations. This finding was consistent with the literature, with concentrations as high as 1 µg/ml (He *et al.*, 2019) to 200 µg/ml (Sharifi, Hoda and Noor, 2010) used with no significant cytotoxicity observed. However, it is likely that different cell types have unique tolerances or susceptibility to LPS exposure, though such information is rarely reported in the literature, so characterisation of growth rates and cytotoxicity for each cell line is important to ascertain.

With evidence that the tested LPS concentrations were not cytotoxic, it was then important to identify if the pro-inflammatory stimulus influenced epithelial barrier function and the expression of pro-inflammatory cytokines. LPS is a well characterised pro-inflammatory stimuli, with evidence that some cells may be responsive to concentrations in the tens of picogram per millilitre range (Chae, 2018). However, as with cell growth and viability studies, cells are likely to vary in response to LPS – especially when comparing a cell line *in vitro* to cells *in vivo*.

TEER data showed a statistically significant reduction in epithelial resistance at all tested concentrations of LPS compared with unexposed cells, indicating an increase in the paracellular flux of ions (Srinivasan *et al.*, 2015). TEER is a commonly used tool for *in vitro* barrier function studies, and *E.coli* LPS has been shown to effectively reduce TEER in

intestinal epithelial cells at 1 µg/ml (He *et al.*, 2019) and previously in H400 oral squamous cell carcinoma cells (OSCC) at 20 µg/ml (Abdulkareem *et al.*, 2018a). Data in Figure 3.3 show significant reductions in TEER values of H400 OSCC cells with three orders of magnitude (20 ng/ml) lower LPS concentration than used by Abdulkareem et al., (2018a), suggesting that even low-dose LPS effectively reduces TEER.

However, while the data in Figure 3.3 show a significant reduction in TEER value with LPS stimulation, this reduction was only a relatively small proportion of the overall TEER reading (ranging between 4.5% (200 ng/ml LPS) and 5.5% (20 ng/ml LPS)) below the control. It is likely that the reduction in TEER is unique to the model system, stimuli and cells used; studies with differentiated intestinal epithelial cells showed a decrease in TEER of approximately 50% with a 1 µg/ml LPS stimulus (He *et al.*, 2019) and 30% in lung endothelial cells with 5 µg/ml LPS (McClenahan *et al.*, 2008).

Data within this chapter used an H400 OSCC monolayer as a simple model with high ease of use, but these findings may vary when applied in more complex model systems. Tight junctions are present through all levels of stratified epithelia except for the upper most keratinised layer (stratum corneum), but the distribution and localisation of relevant TJ-linked proteins varies spatially (Kirschner and Brandner, 2012). Consequently, more exhaustive studies of barrier function may require recapitulation of this stratified epithelium. It is expected that the use of a stratified, differentiated epithelium would result in both a greater absolute TEER value and increased percentage reduction with LPS stimulation, due to a higher number of tight junctions being present with multiple epithelial layers.

In addition to TEER data, preliminary FITC-dextran macromolecular data (Figure 3.4) indicated an increase in FITC-dextran flux at these same concentrations of LPS. This

indicates that LPS may have increased the paracellular flux of both ions (indicated by a reduction in TEER (Srinivasan *et al.*, 2015)) and FITC-dextran – suggesting an overall reduction in epithelial barrier function with LPS stimulation.

With an understanding of the effect of LPS on H400 cell growth, viability and monolayer barrier function, RT-qPCR was employed to begin to develop a mechanistic understanding of these effects and identify changes in cytokine production indicating an inflammatory response. Pro-inflammatory cytokine interleukin 8 (*CXCL8*) showed a statistically significant upregulation at two the tested LPS concentrations, relative to unstimulated cells. LPS has been widely documented to significantly increase the expression of inflammatory markers in a variety of cell types, including *IL8* in dental pulp cells (He *et al.*, 2013) and gingival keratinocytes (Johnson *et al.*, 2010), and *IL6* and *TNFA* are reportedly increased in gingival keratinocytes (Hagiu *et al.*, 2019).

With regards to barrier function gene expression, Figure 3.5 shows that LPS may have an effect on the expression of genes responsible for intercellular junction function, as expression of both E-cadherin (*CDH1*) and tight junction protein 1 / ZO-1 (*TJP1*) showed a slight trend towards reduction with LPS treatment, though this was non-significant. LPS has previously been shown to downregulate the expression of ZO-1 (*TJP1*) (Bein *et al.*, 2017; Zou *et al.*, 2022) and claudin (*CLDN1*), which encodes the charge-selective tight junction protein (Bein *et al.*, 2017). Notably, research has shown significant reductions in claudin expression and TEER *in viv*o in rats, employing an LPS-exposed periodontal epithelium as a model of chronic periodontitis (Fujita *et al.*, 2012). Studies with cultured oral epithelial cells exposed to 1 µg/ml *P. gingivalis* LPS indicated reductions in ZO-1 and occludin gene expression (Guo *et al.*, 2018). However, this study examined gene expression after 4 hours of LPS exposure, compared to the 24 hours of exposure in the present work (Figure 3.5). The relatively limited

response of TJ-linked gene expression to LPS shown in the present work may be due to the timepoints used and further work may aid in elucidating the optimal timepoint for such studies.

Finally, due to the intended application of LPS-stimulated H400 OSCC cells in models of gingivitis treated with PPARγ agonists, confirmation of expression of PPARγ was required. PPARγ has previously been reported to be predominantly expressed in adipose tissue (Chawla, 1994) and thus expression may be lower in a non-adipose tissue such as the gingival epithelium. The use of RT-PCR and western blotting enabled confirmation of PPARγ expression in H400 OSCC cells at both the transcript and protein levels respectively. Additionally, two isoforms were identified with western blotting. Alternative splicing of PPARγ has been shown to lead to the generation and expression of two key tissue isoforms – PPARγ1 and PPARγ2 (Elbrecht *et al.*, 1996; Ren *et al.*, 2002). Western blotting and RT-PCR of H400 OSCC cells revealed differential expression of these two isoforms (Figure 3.6) in a ratio of 2.62:1 (western blotting) and 2.97:1 (RT-PCR) (both ratios γ1:γ2). These two isoforms have been shown to have different activation function 1 (AF-1) domains, with the PPARγ2 variant having an additional 30 amino acids at the N-terminal end (Bateman *et al.*, 2023). This co-expression may result in unexpected responses to PPARγ ligands, as will be discussed in further detail (Chapter 6).

In summary, the data presented in the current chapter, combined with the existing literature, indicate that *E.coli* LPS reliably induced inflammatory cytokine production in H400 OSCC cells and resulted in reductions in TEER in these cells, as a marker of epithelial barrier function. This reduction in TEER may occur via downregulation of genes coding for key tight junction proteins, though further work across additional timepoints and LPS concentrations may make this relationship clearer. Additionally, PPARγ expression was confirmed

experimentally in H400 OSCC cells, enabling the use of LPS-challenged H400 cells as a model of PPARγ agonist-treated gingivitis.

4. DEVELOPMENT AND APPLICATION OF PPARγ REPORTER SYSTEMS IN ORAL EPITHELIAL CELLS

4.1. Introduction

The present chapter describes studies undertaken to identify a PPARγ reporter system suitable for screening potential PPARγ ligands. Two systems were assessed; PPRE-H2B-eGFP and PPRE-pNL1.3 (Degrelle, Shoaito and Fournier, 2017). Initial studies were performed with the PPRE-H2B-eGFP reporter, which utilised a human apolipoprotein CIII promoter as a PPARγ response element (PPRE), with activation of this response element leading to expression of an eGFP gene. Additionally, the presence of a selection gene (Neo*R*) enabled the generation of stably transfected cell populations, though this presented considerable challenges. For this reason, PPRE-pNL1.3 was also investigated, in which the same PPRE controlled expression of a secreted nanoluciferase. This system is characterised by high sensitivity and allows for higher throughput quantification of PPARγ activation (Degrelle, Shoaito and Fournier, 2017).

Bacterial transformation with plasmids can be unstable, with the likelihood and rate of plasmid loss depending on plasmid size and culture conditions (Smith and Bidochka, 1998). Therefore, restriction enzyme digestion were performed to identify that the correct plasmid was present and contained key inserts and transgenes. Function was confirmed by exposure of transfected cells to GW1929, a known PPARγ agonist (Degrelle, Shoaito and Fournier, 2017), to induce expression of the PPRE-linked eGFP. A stable transfectant was generated by supplementing cultures with G418, a cytotoxic antibiotic to which resistance is conferred by the *NeoR* gene included in the PPRE-H2B-eGFP plasmid.

Initial verification of the PPRE-pNL1.3 reporter system was performed in both H400 cells (H400:PPRE-pNL1.3) and HaCaT cells, a spontaneously immortalised skin keratinocyte cell line (HaCaT:PPRE-pNL1.3), to identify how transfection efficiency varied between keratinocyte cell lines. The TZD-class PPARγ agonist rosiglitazone (Camp *et al.*, 2000) was

included in these studies, in addition to GW1929 as used in previous studies, both acting as positive controls. The PPARγ antagonist GW9662 (Seargent, Yates and Gill, 2004) was also included to identify the effect of blocking activation of PPARγ on the expression of the reporter. Finally, charcoal-stripped serum (CSS) was also trialled. CSS is commonly used in the study of steroid hormones and steroid receptors, containing fewer endogenous hormones which may interfere with treatments (Cao *et al.*, 2009; Sikora *et al.*, 2016).

Validated PPARγ reporter systems were then applied to the testing of compounds commonly used in cosmetic or oral care products. Cytotoxicity testing of these compounds was performed using a CCK-8 assay (Ishiyama *et al.*, 1996), relying on a redox-based chemistry similar to MTT (3-[4,5-dimethylthiazol-2-yl]-2,5-diphenyltetrazolium bromide) assay (Ciapetti *et al.*, 1993; Supino, 1995).

Following studies of H400 cells transfected with PPRE-pNL1.3, evidence of paradoxical activation of PPARγ by the antagonist GW9662 was observed. Therefore, PCR-product Sanger sequencing was performed to confirm the nucleotide sequence and predicted primary structure of the PPARγ ligand binding domain (LBD) in H400 OSCC cells (Section 4.6).

4.2. PPRE-H2B-eGFP and PPRE-pNL1.3 plasmid validation with restriction enzyme digests

Upon receipt, PPRE-H2B-eGFP and PPRE-pNL1.3 plasmids were expanded in DH5α *E.coli*, isolated and purified, as described previously (Section 2.4).

A plasmid map (

Figure **4.1**) was used to identify insert and transgene position and expected fragment sizes. Restriction enzyme digests performed on purified PPRE-H2B-eGFP with three single-cutting

enzymes (NheI, VspI and BamHI) in isolation produced single, distinct bands following DNA electrophoresis between 5 and 6 kb (Figure 4.2, lanes 3-5), and these were of the expected plasmid size of 5.5 kb when in a linear conformation, as shown in lane 2.

Dual digestion with NheI and VspI (an AseI isoschizomer) was performed to isolate the apolipoprotein C3 (ApoCIII) insert, a response element promoter activated by PPARγ The ApoCIII insert spanned from base 95 to 1236, an expected product size of 1141 bp, with a resultant 4519 bp backbone fragment. As expected, dual digestion produced two bands of approximately 1.1 and 4.5 kb (Figure 4.2, lane 6).

Triple digestion with NheI, VspI and BamHI was performed to identify both the ApoCII sequence and the histone 2B (H2B) sequence, responsible for localisation of the produced eGFP to the cell nucleus. Expected fragments included the ApoCIII insert from base 95 to 1236 (1141 bp fragment), the H2B sequence from base 1302 to 1679 (377bp) and a backbone of 4080bp. Accordingly, RE digestion produced three bands of approximately 400 bp, 1.1 kb

and 4.1 kb (Figure 4.2, lane 7).

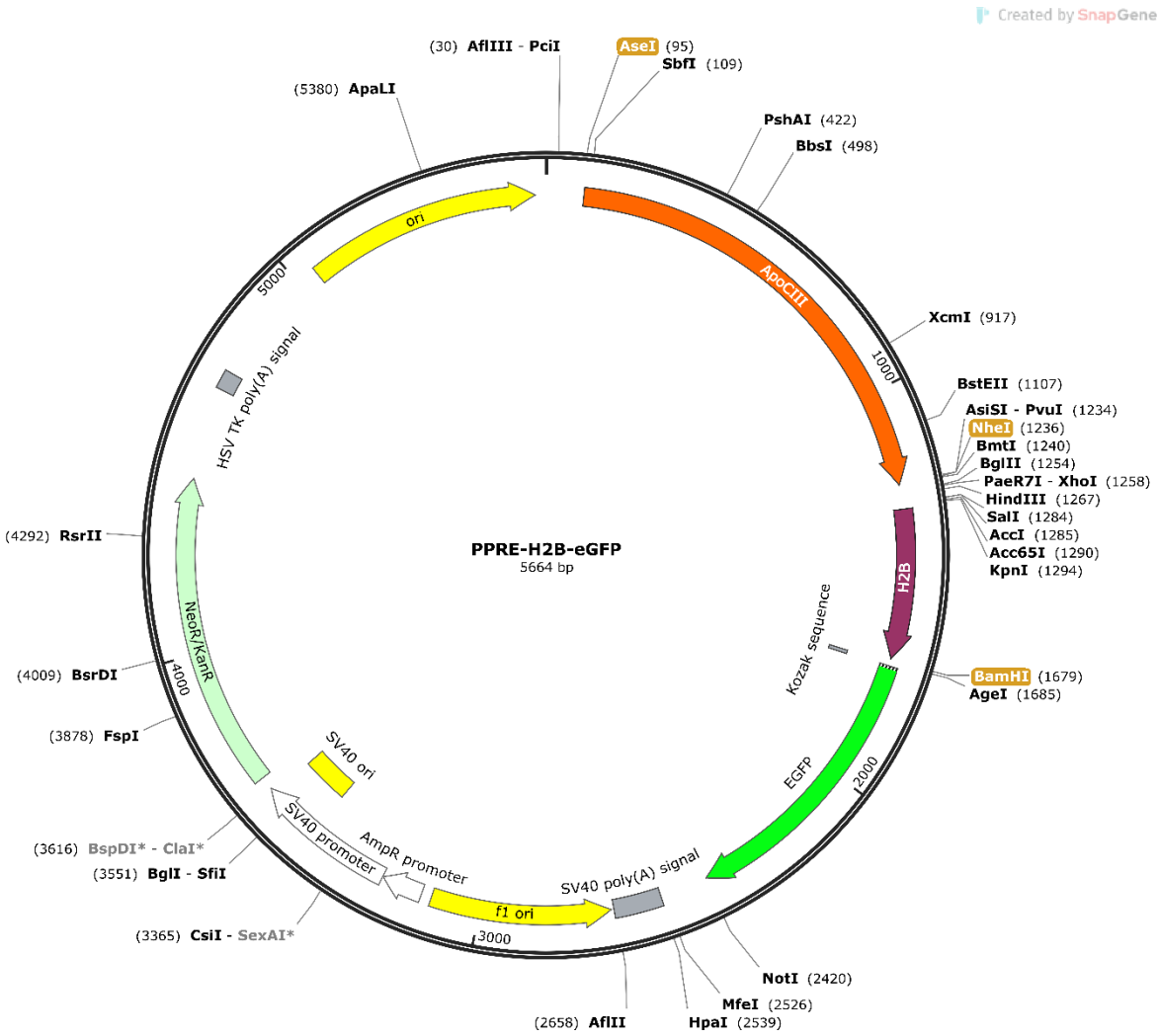


Figure 4.1 - Plasmid map of PPRE-H2B-eGFP, showing restriction enzyme recognition sites and key features or inserts. Restriction enzymes used for digestion in the present work are highlighted in gold. Generated with SnapGene Viewer (GSL Biotech, USA).

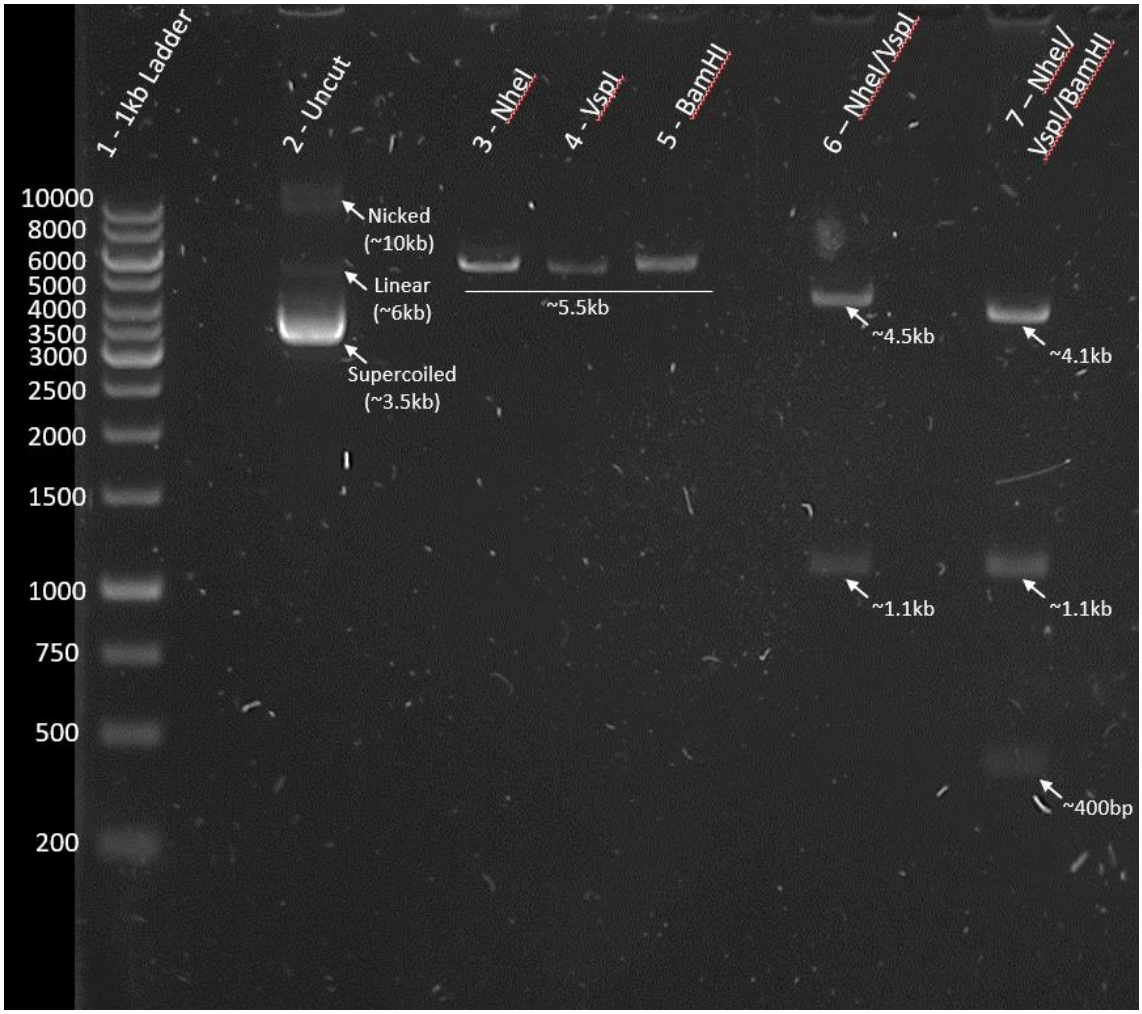


Figure 4.2 – Gel image of restriction enzyme digestion of PPRE-H2B-eGFP isolated from cultured, transformed DH5α *E.coli.* Approximate fragment sizes shown, 1% agarose gel, stained with Sybr safe DNA stain. All expected fragments were present, with correct sizing.
Lane 1: 1kb DNA ladder.
Lane 2: Uncut, native conformations of PPRE-H2B-eGFP plasmid.
Lanes 3 -5: Fragments resulting from digestions with single restriction enzymes (NheI, VspI, BamHI).
Lane 6: Fragments resulting from combined, dual digestions (NheI and VspI).
Lane 7: Fragments from a triple digest (NheI, VspI and BamHI).

Similarly, a plasmid map of PPRE-pNL1.3 was then used to identify expected fragment sizes following RE digestion (Figure 4.3). Digestion performed on PPRE-pNL1.3 with all four REs alone (BglII, KpnI, HindII and BamHI) produced single, distinct bands of approximately 4.5 kilobases (kb) in size (Figure 4.4, lanes 4-7), similar to the 4.3 kb size of the PPRE-pNL1.3 plasmid in a linear conformation.

A dual restriction enzyme digest was performed with BglII and KpnI, targeting RE recognition sites at either side of the ApoCIII insert (base 1112 to 4278). A plasmid map (Figure 4.3) was used to determine expected fragment sizes post-digestion, calculated as 1.14 kb for the PPRE ApoCIII insert and 3.2 kb for the remaining backbone. These predictions were matched experimentally, with a dual digest with BgIII and KpnI producing two bands of approximately 1.2 kb and 3.2kb (Figure 4.4, lane 8).

A dual digest with HindII and BamHI was performed to isolate the plasmid fragment containing the NLuc sequence (bases 1253 to 1766), responsible for producing a secreted nanoluciferase. Calculation of expected fragment sizes generated predictions of 906 bp for the NLuc sequence and 3.4 kb for the remaining plasmid. Dual digest with BamHII and HindII yielded fragments of approximately 3.5 kb and 1 kb (Figure 4.4, lane 9).

A quad digest was performed with BglII, KpnI, BamHII and HindII to identify that all plasmid fragments from previous dual digests could be produced from one single reaction. Approximate expected fragment sizes were a 1.2 kb PPRE ApoCIII insert, 900 bp NLuc sequence, a 2.3 kb backbone and small, 19 bp fragment from between the HindII and BglII sites. Quad digestion produced fragments of approximately 1.2, 1 and 2.5 kb (Figure 4.4, lane 10).

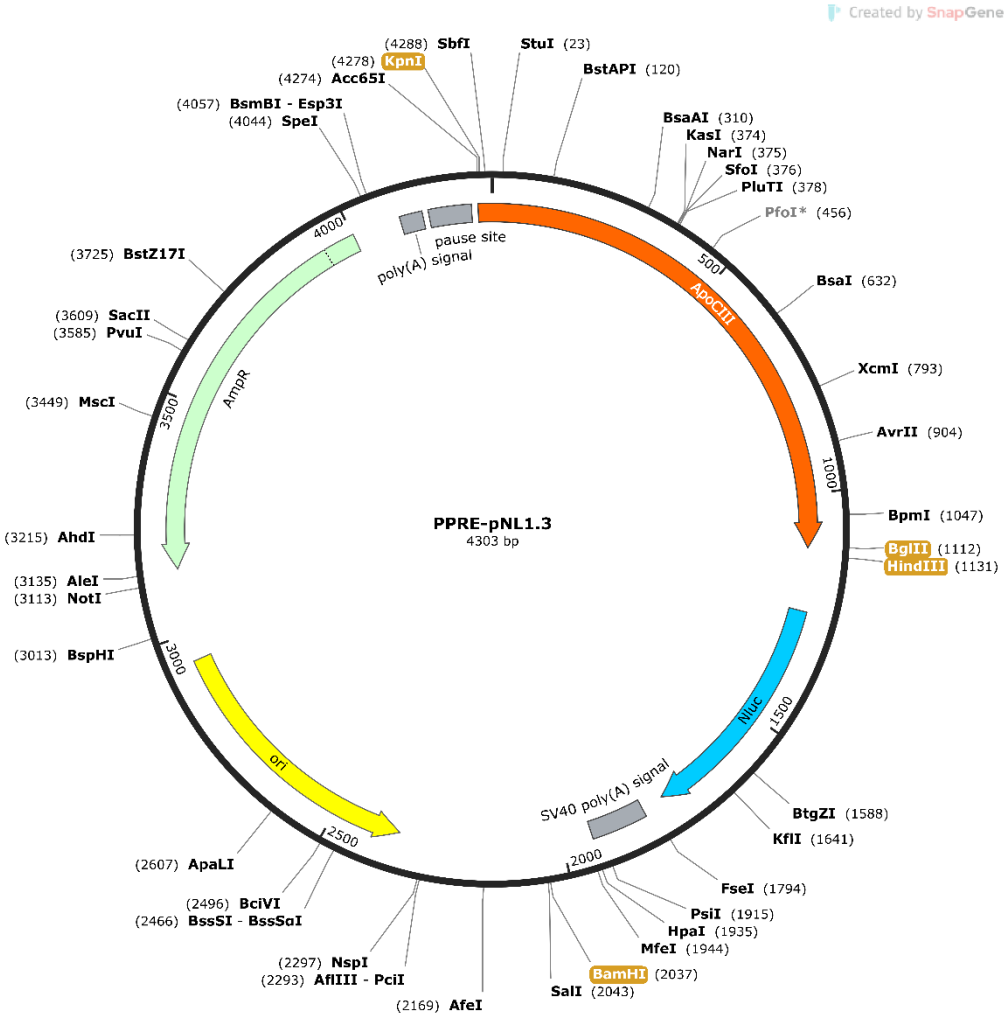


Figure 4.3 - Plasmid map of PPRE-pNL1.3, showing restriction enzyme recognition sites and key features or inserts. Restriction enzymes used for digestion in the present work are highlighted in gold. Generated using SnapGene Viewer (GSL Biotech, USA).

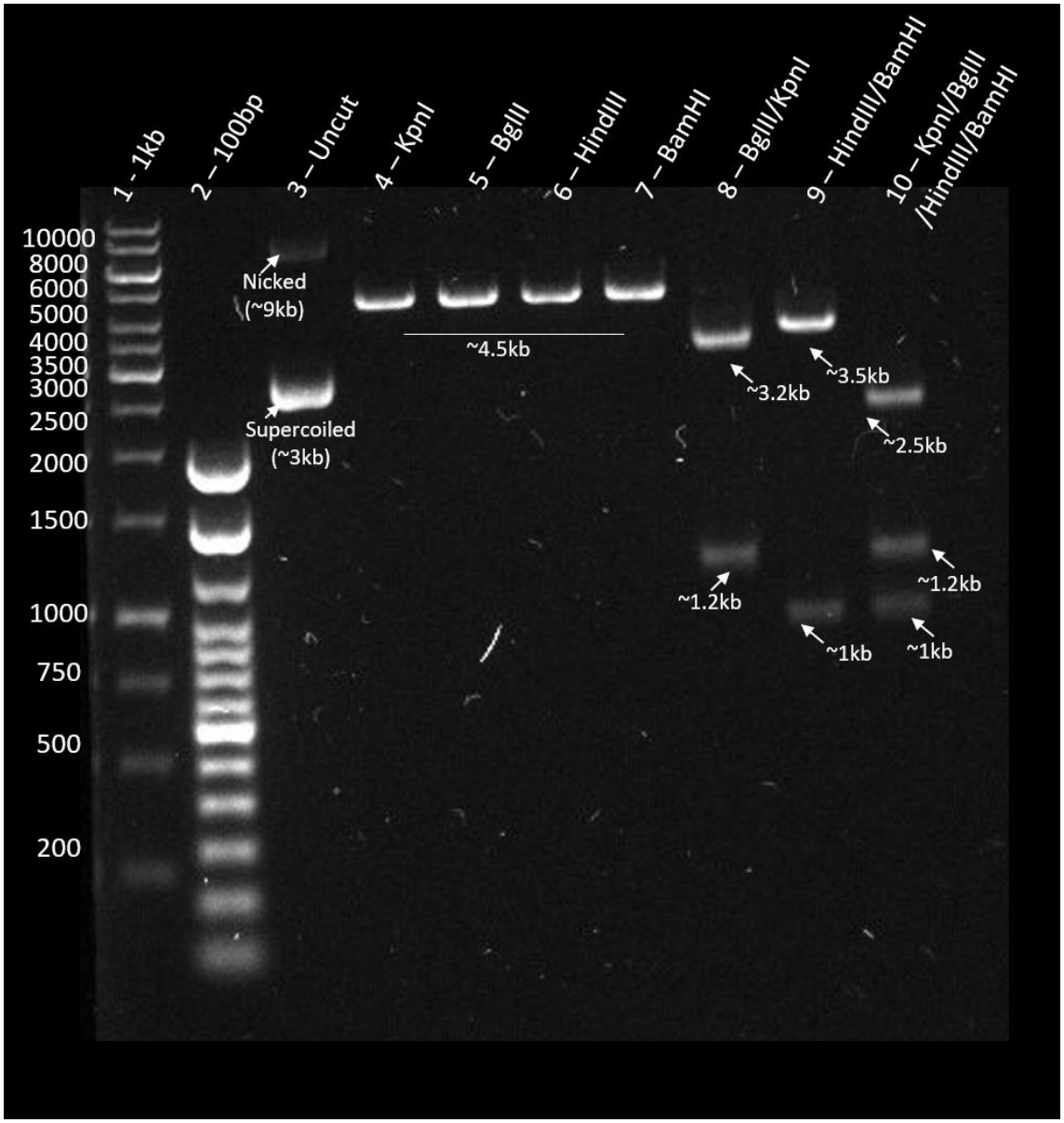


Figure 4.4 - Restriction enzyme digestion of PPRE-pNL1.3 isolated from cultured, transformed DH5α *E.coli.* Approximate fragment sizes shown following electrophoresis on a 1% agarose gel, stained with Sybr safe DNA stain.
Lane 1: 1kb DNA ladder.
Lane 2: 100bp DNA ladder.
Lane 3: Uncut, native conformations of PPRE-pNL1.3 plasmid.
Lanes 4 -7: Fragments resulting from digestions with single restriction enzymes.
Lanes 8 and 9: Fragments resulting from combined, dual digestions.
Lane 10: Fragments from a quad digest.

4.3. H400:PPRE-H2B-eGFP reporter line generation and testing

Purified PPRE-H2B-eGFP was then transfected into H400 OSCC cells, incubated for 18 hours, and exposed to the PPARγ agonist GW1929 at 1 µM for a further 24 hours (Section 2.4.1.6). Combined phase contrast and epifluorescence microscopy imaging transfected and PPARγ stimulated cells showed bright green fluorescence in a small proportion of cells, with varied intensity between cells. Qualitatively, cells appeared slightly rounded with some bleb formation, suggesting that either the transfection process or excitation with 405 nm light for epifluorescence microscopy were exerting cytotoxicity.

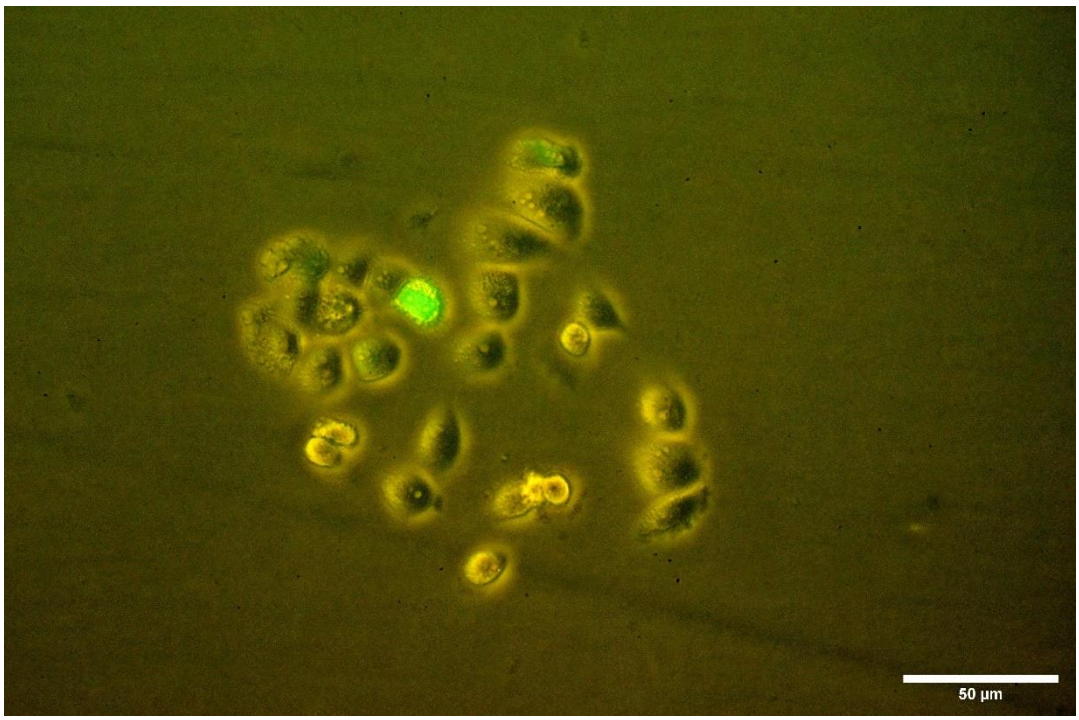


Figure 4.5 -Merged widefield epifluorescence and phase contrast photomicrograph of H400 cells transiently transfected with PPRE-H2B-eGFP plasmid. Cells exposed to 1 µM GW1929 for 24 hours prior to imaging. Green fluorescence can be seen in a small proportion of cells, matching the expected outcome. Fluorescence intensity is seen to vary between cells. Scale bar 50 µM.

Following initial verification of the transfection protocol as discussed above, growth curves were generated for both untransfected and PPRE-H2B-eGFP transfected H400 cells exposed to 500 µg/ml G418 (Section 2.3).

PPRE-H2B-eGFP transfected H400 cells exposed to 500 µg/ml G418 increased in number from day 0 to day 3, with further increases between day 3 and days 5 and 7. Cell number then decreased slightly at day 9. Conversely, untransfected H400 cells (Figure 4.6, blue datapoints) showed a flat growth profile, with a small increase in live cell number from day 0 to day 3, followed by a reduction to cells at day 5, and zero live cells thereafter.

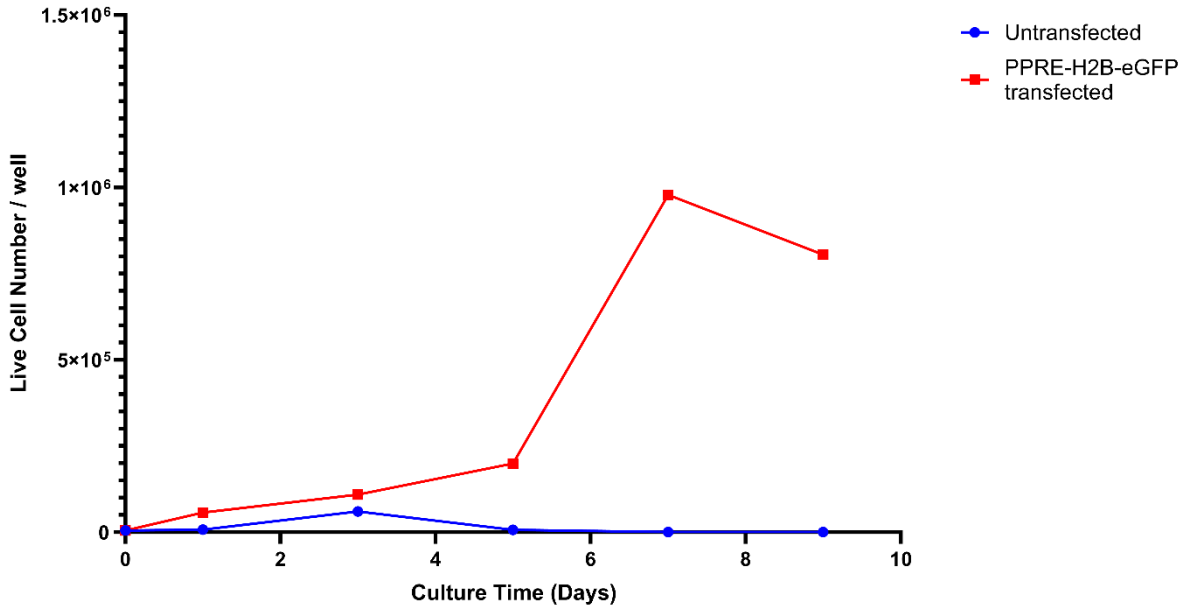


Figure 4.6 – Cell growth curves of untransfected (blue) and PPRE-H2B-eGFP transfected (red) H400 cells, exposed to 500 µg/ml Geneticin G418. A small increase in untransfected cells is shown, with a reduction to zero viable cells by day 7. This suggests strong toxicity from G418 in untransfected cells. In contrast, transfected cells appeared viable in G418-supplemented media, producing increases in cell number up to a maximum of 9.8×10^5 at day 7, suggesting that successful transfection of the *NeoR* gene occurred.
N=1, no statistical tests performed.

Following monoclonal selection and expansion of transfected cells shown to express eGFP, cellular fluorescence was quantified via a multimode plate reader, following exposure to a range of concentrations of GW1929 for 24 hours (Section 2.4.1.7). Unstimulated cells showed a slightly higher (13%) mean measured fluorescence, indicating a degree of basal eGFP expression. Treatment with GW1929 at 1, 10 and 20 μM led to small, dose-dependent increases of 3.75%, 7.44% and 11.5% in relative fluorescence units (RFU) compared with the transfected unstimulated control. However, variability between technical replicates was high, with overlap between multiple treatment groups. Further biological replicates were not performed due to replacement of the PPRE-H2B-eGFP reporter with the PPRE-pNL1.3 system. The limited sample size (N=1) of these data prevented statistical analyses, however qualitative assessment of the technical replicate variability and of the mean fluorescence provided an indication of the lack of utility of this assay.

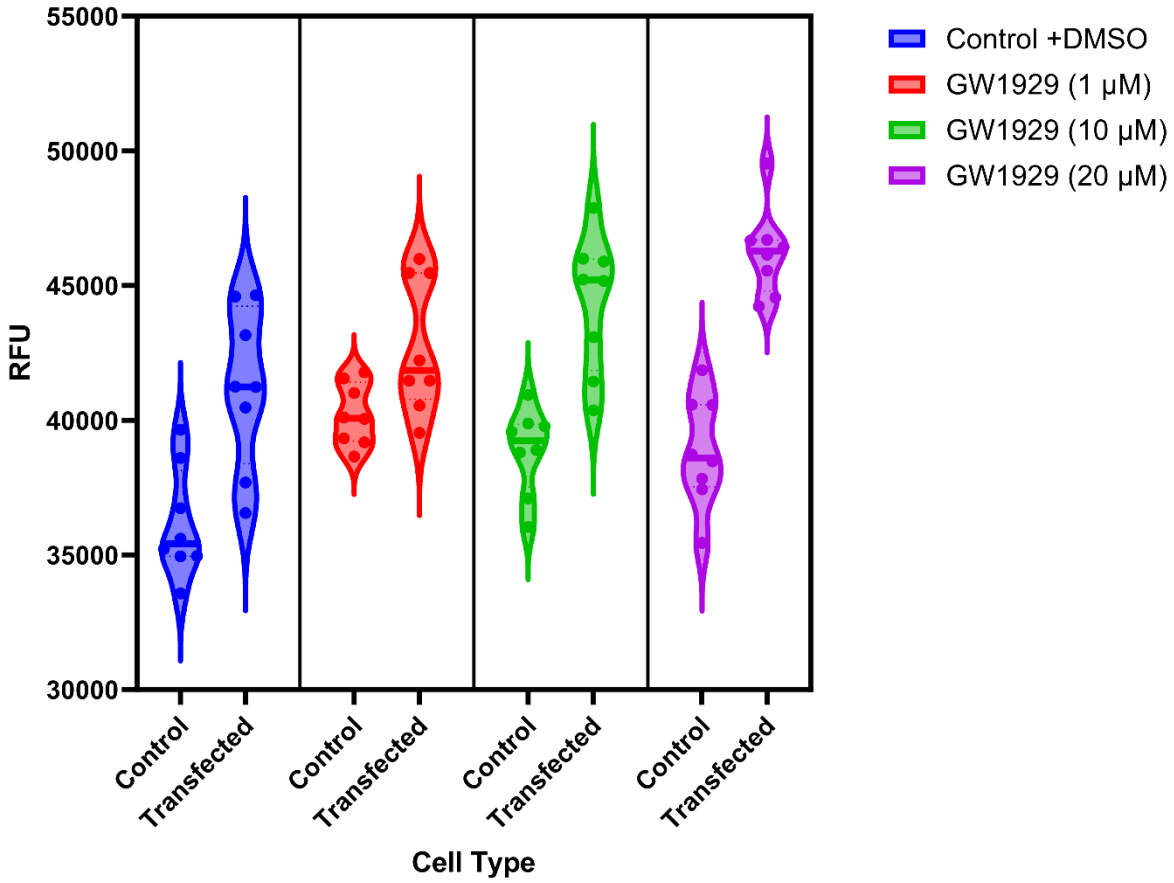


Figure 4.7 – eGFP fluorescence of untransfected control and PPRE-H2B-eGFP transfected H400 cells exposed to GW1929 at indicated concentrations. Violin plot represent technical replicates (n=6). Transfected H400 fluorescence (Ex 488, Em 522 nm) can be seen increasing slightly in a dose-dependent manner with increasing GW1929 concentration. High background fluorescence is noted, and high basal expression of eGFP in transfected but untreated H400s.
N=1, no statistical analysis performed.

4.4. H400:PPRE-pNL1.3 reporter line generation and testing

H400 and HaCaT cells were transfected with PPRE-pNL1.3 plasmid as described in Section 2.4.2. Following 24 hours of incubation post-transfection, the cells were exposed to agonists GW1929 and rosiglitazone, and antagonist GW9662 for 24 hours, prior to quantification of secreted luciferase activity. Control (untreated) H400 OSCC cells transfected with PPRE-pNL1.3 (Figure 4.8 A) generated a statistically significant increase in nanoluciferase activity compared with untransfected controls ($p < 0.0001$). Cells exposed to the PPARγ agonist 1 µM

GW1929 did not generate a significant change in luminescence ($p = 0.2427$), whilst 5 μM GW1929 led to a significant increase in luminescence of 36.7% ($p = 0.0077$). The thiazolidinedione-class PPARγ agonist rosiglitazone also produced a non-significant increase in luminescence of 16.0% ($p = 0.3302$). Unexpectedly, a statistically significant increase in luminescence of 37.9% was noted with the PPARγ antagonist GW9662 ($p = 0.0057$).

Control HaCaT cells transfected with PPRE-pNL1.3 (Figure 4.8 B) displayed a markedly different response to the selected test compounds. Whilst transfected control HaCaT cells showed a significant increase in luciferase activity compared with untransfected HaCaT cells ($p < 0.0001$), none of the treated cell populations showed a significant change in luciferase activity, with high variability between biological replicates. Interestingly, rosiglitazone did not generate a significant response in luminescence.

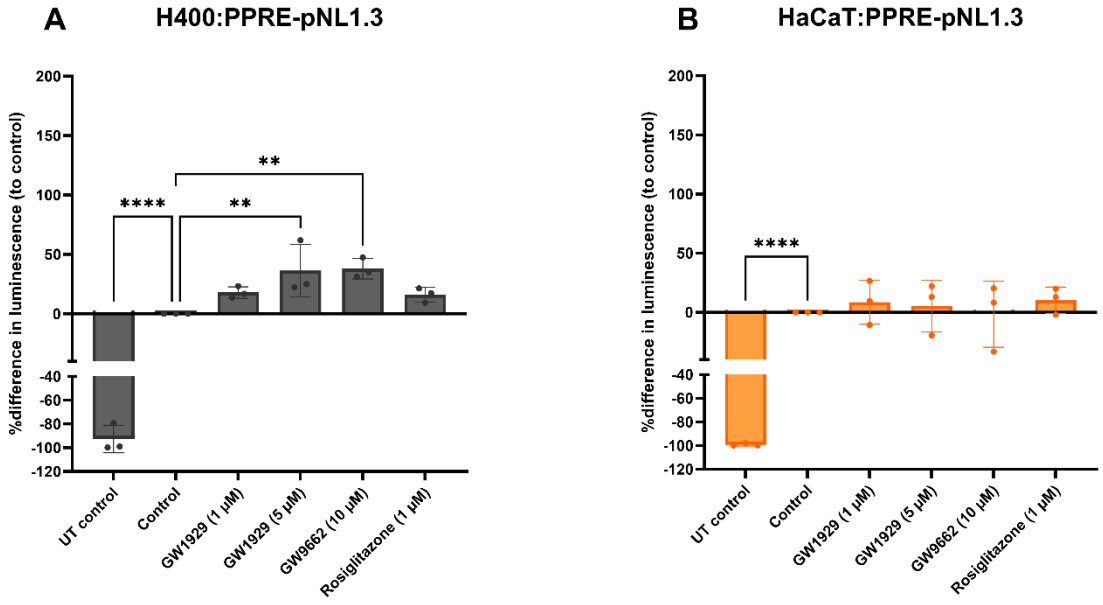


Figure 4.8 - Analysis of PPARγ activation using H400 cells (left, black) and HaCaT cells (right, orange) transfected with PPRE-pNL1.3.
Cells stimulated for 24 hours with known PPARγ agonists (GW1929 - PPARγ agonist, or rosiglitazone – thiazolidinedione class PPARγ agonist) or antagonists (GW9662 – irreversible inhibitor of PPARγ activation). Significant increases in PPARγ activation can be seen in H400 cells following 5 µM GW1929 and GW9662 stimulation, with smaller non-significant increases with 1 µM GW1929 and rosiglitazone stimulation. In contrast, transfected HaCaT cells showed minimal changes in PPARγ activation with all tested agents.
N=3, mean %difference in luminescence relative to transfected control ±SD, separate one-way ANOVAs with Dunnet's multiple comparisons post-hoc test (all to control).
* = $p < 0.05$. ** = $p < 0.01$. *** = $p < 0.001$. **** = $p < 0.0001$.

Transfected H400 cells were then cultured in media supplemented with charcoal stripped serum, as opposed to the foetal calf serum used in prior studies in this work. In the presence of CSS, all treatment groups of cells in CSS supplemented culture media showed marked differences in luminescence signal confirming activation of the nanoluciferase reporter, however with high inter-replicate variability (Figure 4.9). Mean luminescence relative to control cells appeared greater in CSS-supplemented cells treated with 5 µM GW1929 (50.1%), GW9662 (68.5%) and rosiglitazone (74.2%) than in FCS-supplemented cells (Figure

4.8 A). However, these two datasets were not directly comparable and thus no statistical analysis was performed.

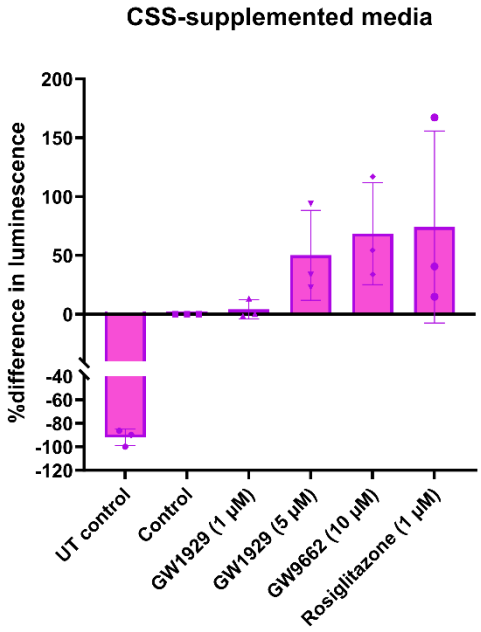


Figure 4.9 - PPARγ activation in H400:PPRE-pNL1.3 cells in charcoal stripped serum (CSS) supplemented media.
Cells stimulated for 24 hours with known PPARγ agonists (GW1929 - PPARγ agonist, or rosiglitazone – thiazolidinedione class PPARγ agonist) or antagonists (GW9662 – irreversible inhibitor of PPARγ activation). High mean PPARγ activation was noted with 5 µM GW1929, GW9662 and rosiglitazone, but high inter-replicate variability led to no statistical significance being detected.
N=3, mean %difference in luminescence relative to transfected control ±SD, separate one-way ANOVA with Dunnet's multiple comparisons post-hoc test (all to control).

4.5. Screening of compounds for PPARγ agonist activity

Following the generation and testing of PPARγ reporter systems, compounds commonly found in cosmetic and oral care products (Table 2.3) were screened for PPARγ activity. H400 cells transfected with PPRE-pNL1.3 were used as a reporter. However, cytotoxicity testing was first undertaken, exposing H400 cells to a range of concentrations between $1x10^{-3}$ µg/ml and $1x10^{1}$ µg/ml of each compound for 24 hours. In these studies, a redox-based CCK8

assays was performed, in which a reduction in absorbance correlates with a reduction in viable cell number.

Only the highest concentration of 10 µg/ml produced statistically significant reductions in absorbance of four of the compounds; Hydroxystearic acid (HSA), pTeroPure®, palmitoylethanolamide (PEA) and SabiWhite®. Treatment with 10 µg/ml HSA generated a reduction in absorbance (450 nm) from 0.501 to 0.232 ($p = 0.0366$), pTeroPure® a reduction from 0.441 to 0.196 ($p = 0.0366$), PEA from 0.457 to 0.182 ($p = 0.0164$) and SabiWhite® from 0.472 to 0.239 ($p = 0.0449$), as shown in Figure 4.10.

The remaining compounds did not produce statistically significant reductions in absorbance compared with the control group when tested at 10 µg/ml, or at any other concentrations .

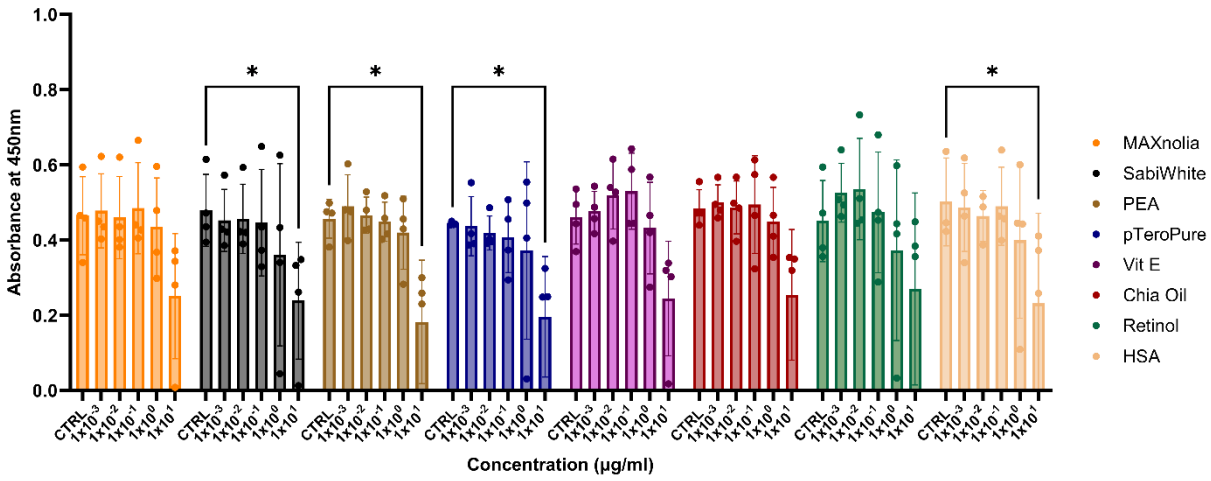


Figure 4.10 – CCK-8 cytotoxicity assay of cosmetic compounds under investigation as PPARγ agonists, following 24 hours of exposure. Each compound was tested at $1x10^{-3}$, $1x10^{-2}$, $1x10^{-1}$, 1 and $1x10^{1}$ µg/ml in culture media. Test agents were dissolved in DMSO, and the control samples were exposed to maximum concentration of DMSO (0.1% v/v). CCK-8 reagent incubated for one hour at room temperature. Statistically significant ($p < 0.05$) reduction in absorbance was only noted at the highest (10 µg/ml) concentration of HSA, pTeroPure®, PEA and SabiWhite®, with no marked toxicity seen in any other tested concentrations.
HSA = hydroxystearic acid, PEA = palmitoylethanolamide.

N=4, mean ±SD, two-way ANOVA with Dunnett's multiple comparisons post-hoc test (all to control).
* = $p < 0.05$.

Cosmetic compounds were applied to the H400:PPRE-pNL1.3 assay. Based upon the previously discussed cytotoxicity testing, a concentration of 1 µg/ml of each compound was selected to assess PPARγ activation.

Luminescence (proportional to PPARγ activation) in untransfected control (UTC) H400 cells was lower by 94.6% when compared with transfected control (CTRL) cells ($p < 0.0001$) (Figure 4.11 A) and by 96.7% when using the lysed cell assay ($p = 0.0001$) (Figure 4.11 B). Similarly, blank wells (culture media only) showed a reduction of 94.2% ($p = 0.0001$) and 97.0% ($p = 0.0005$) with the secreted and lytic systems, respectively.

Treatment of H400 cells with GW1929 (5 µM) resulted in marked increases in luminescence relative to unstimulated control cells. In the secreted luciferase assay, a statistically significant increase of 59.3% was recorded ($p = 0.0007$), with no significant increase noted with the lysed cell NanoGlo assay.

When assessed using the secreted NanoGlo assay (Figure 4.11A), none of the tested cosmetic compounds produced statistically significant changes in luminescence relative to unstimulated control cells. Similarly, no significant differences in mean luminescence occurred following stimulation with any tested cosmetic compound when assessed with the luciferase assay as performed on cell lysis products (Figure 4.11 B). Qualitatively, inter-replicate variability appeared greater than that in the secreted NanoGlo assay (Figure 4.11 A), shown by the larger standard deviation.

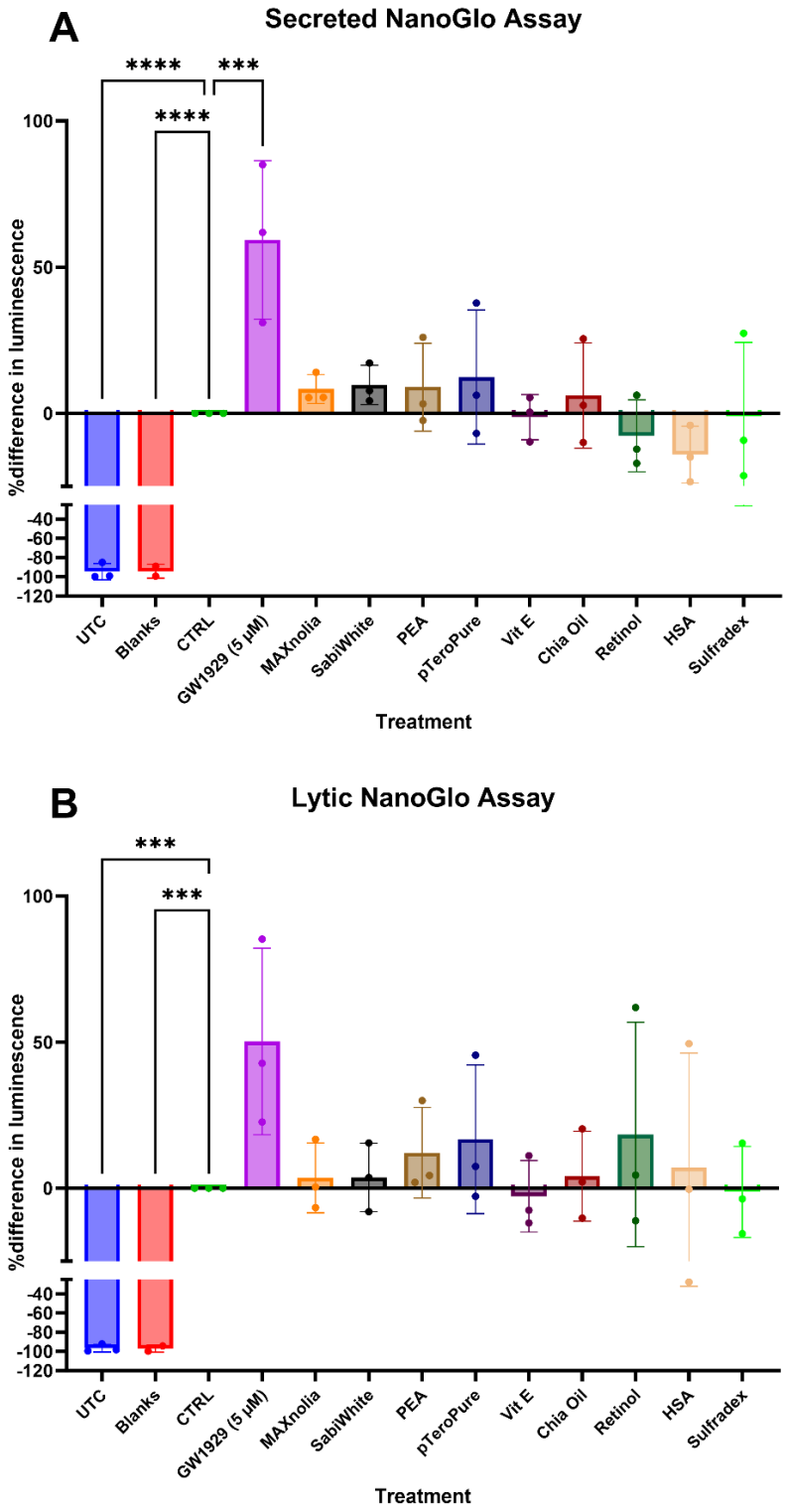


Figure 4.11 – NanoGlo assay of H400 cells transfected with PPRE-pNL1.3 reporter and treated with cosmetic compounds for 24 hours (1 µg/ml for all), showing that no tested compound generated a significant increase in PPARγ activation. A) NanoGlo performed on culture supernatant only and B) on the same cell population following lysis.

A) Significant reductions in luminescence relative to transfected control cells were detected in untransfected control (UTC) H400 cells and blank (culture media only) wells, while a significant increase occurred with 5 μM GW1929.
B) Significant reductions in luminescence relative to control were detected in UTC H400s and blank wells. No significant increase is produced following GW1929 treatment, though a relatively large non-significant increase was noted.
No significant increases or decreases in luminescence (relative to transfected, control H400 cells) were produce by any test compound cells at the tested concentration in either assay approach (secreted or lytic assay).
UTC = untransfected control, HSA = hydroxystearic acid, PEA = palmitoylethanolamide.

N=3, mean ±SD, one-way ANOVA with Dunnett's multiple comparisons post-hoc test (all to control). *** = $p < 0.001$, **** = $p < 0.0001$.

4.6. Investigation of paradoxical PPARγ activation by the irreversible antagonist GW9662

With previous studies within this project identifying paradoxical activation of PPARγ by the antagonist GW9662 (Figure 4.8 A), it was hypothesised that this aberrant response may have been generated by mutation of the PPARγ ligand binding domain (LBD), with particular interest in the site covalently bound to by GW9662 (Leesnitzer *et al.*, 2002). PCR-product Sanger sequencing was undertaken to verify the correct nucleotide sequence was present within this region of the PPARγ LBD in H400 cells.

PCR amplification of the PPARγ LBD after 25 PCR amplification cycles produced a single band of low intensity with a size of approximately 300 bp (Figure 4.12, lane 4), increasing to a higher intensity after 32 PCR cycles (Figure 4.12, lane 6) on a DNA electrophoresis gel. No signal was seen in either no template control (NTC) well (Figure 4.12, lanes 3 and 5).

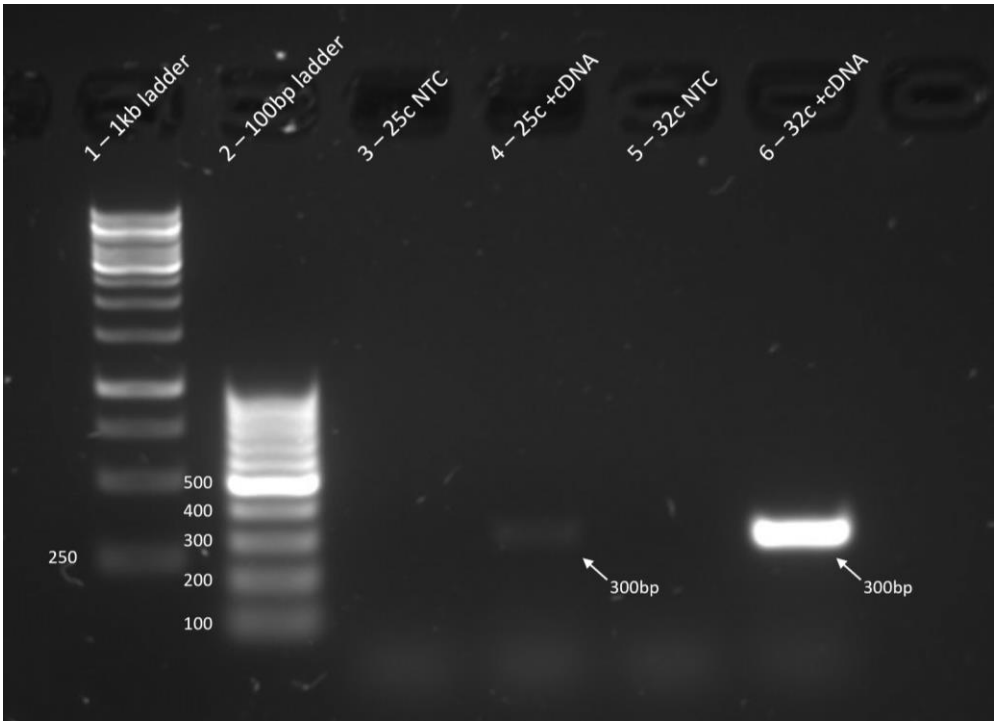


Figure 4.12 - DNA electrophoresis of PCR products for sequencing of the GW9662-modifable region of the PPARγ ligand binding domain in H400 cells. DNA ladder fragment labels shown in basepairs (bp). 2% agarose gel, stained with Sybr safe DNA dye.
Lane 1: 1kb DNA ladder.
Lane 2: 100bp DNA ladder.
Lane 3: 25 PCR cycles, reaction mix no template control.
Lane 4: 25 PCR cycles, 1 µl H400 cell cDNA.
Lane 5: 32 PCR cycles, reaction mix no template control.
Lane 6: 32 PCR cycles, 1 µl H400 cell cDNA.

PCR products were subjected to Sanger sequencing, and alignment of the resultant Sanger sequence with the canonical PPARG coding sequence (transcript variant PPARG-217) revealed no mismatches in the nucleotide sequence and no change in the predicted amino acid sequence of the translated protein (Figure 4.13).



Figure 4.13 – Sanger sequencing of PCR product aligned to canonical PPARG-217 coding sequence (CDS). Top sequence: PPARG-217, with nucleotide sequence and translated primary protein structure. Bottom sequence: Sanger sequenced product following alignment, with called nucleotides shown.
Grey rectangles above PPARG-217 CDS depict no mismatch, white rectangles depict uncalled bases in sequence and mismatches are marked by red rectangles. Figure generated using Benchling (Biology Software, 2023).

4.7. Discussion

The work described in present chapter aimed to produce and verify PPARγ reporter systems in relevant cell lines, to enable the screening of potential PPARγ ligands for further study. This resulted in the successful generation and validation of the H400:PPRE-pNL1.3 reporter system.

Initial work was undertaken to verify the identity of both the PPRE-H2B-eGFP and PPRE-pNL1.3 plasmids by restriction enzyme digestion (Section 4.2). Electrophoresis of digestion products revealed well defined bands for all fragments, which matched the expected fragment size calculated from plasmid maps (

Figure **4.1** and Figure 4.3). This suggested that both plasmids were correctly supplied from the repository and that relevant inserts were present. Colony PCR may be used to improve confidence in plasmid identity if required, employing oligonucleotide primers specific to the insert and allowing for verification of the successful cloning of the insert sequence. However, whilst being experimentally simple, colony PCR may fail to confirm the addition of the cloned sequence to the plasmid backbone, so backbone- or orientation-specific primers are often used to confirm a correctly oriented ligation of the insert to the backbone (Lu, 2003). Additionally, plasmids have widely been sequenced by Sanger sequencing (Zagursky *et al.*, 1985) for confirmation of plasmid identity. The plasmids employed in the present work were characterised by next-generation sequencing (NGS) upon deposition into the plasmid repository, producing an experimentally confirmed plasmid map. For this reason, diagnostic restriction enzyme digestion was suitable to rapidly provide sufficient evidence of the identity of the supplied plasmids.

Following successful verification of both plasmids, initial trials with the H400:PPRE-H2B-eGFP system were performed. Transfection of H400 oral squamous cell carcinoma cells with PPRE-H2B-eGFP (Section 4.3) was initially successful, with a proportion of these cells producing green fluorescence in response to 24 hours of stimulation with 1 µM GW1929 (Figure 4.5). The varied intensity of this fluorescent response may have been due to variability in the uptake of the PPRE-H2B-eGFP plasmid. Transfection efficiency with cationic lipids, as used in the present work, has been shown to be dependent on the experimental setup, with cell density, culture media constituents and DNA concentration leading to marked changes in efficiency (Dalby *et al.*, 2004). Whilst all these factors were controlled in the present work, verification of cell cycle position was not. Cell cycle has been shown to play a significant role in determining the efficiency of non-viral transfection, with

30-500 fold increases in efficiency when performed in S or G2 phases of the cell cycle, compared with G1 (Brunner *et al.*, 2000).

To reduce the variability of PPRE-dependent eGFP synthesis in transfected H400 cells, monoclonal selection and expansion was performed to produce a stably transfected cell line. The presence of a neomycin resistance gene (*neoR*) within the PPRE-H2B-eGFP plasmid (

Figure **4.1**) enabled selection of transfected cells by exposure to Geneticin G418, killing non-resistant cells and allowing only transfected cells to survive. As an additional benefit, stable transfection would also enable the use of the reporter line in organotypic co-cultures, as stable transfection negated the need for constant G418 exposure. This antibiotic, while required to maintain reporter transgene expression in transiently transfected cultures, would be toxic to other cells present, such as fibroblasts. Transiently transfected DNA has been shown to modify gene transcription for only 24-96 hours (Kim and Eberwine, 2010), insufficient for organotypic cultures which may require several weeks to differentiate and mature.

Previous work has shown that G418 exposure results in a 50% reduction in cell viability in a range of adherent mammalian cells at concentrations between 69 and 483 µg/ml, with the cytotoxic concentration heavily dependent on the cell line (Delrue *et al.*, 2018). Preliminary data from H400 cells exposed to 500 µg/ml G418 (Figure 4.6) while limited by the sample size of a single biological replicate, provided adequate evidence that G418, at the tested concentration of 500 µg/ml, was sufficient to trigger cell death in untransfected cells, providing a suitable approach for the selection of transfected cells.

Following selection and expansion to produce a stably transfected, monoclonal cell line, the synthesis of eGFP in response to GW1929 was assessed quantitatively using a fluorescence plate reader (Figure 4.7). Interestingly, unstimulated transfected cells showed an increase in

fluorescence compared with untransfected control cells. This suggested that PPRE-dependent eGFP production occurred even in the absence of an exogenous PPARγ agonist (GW1929, in this assay), indicating relatively high basal levels of PPARγ activation in these cells. Previous studies have also reported constitutive activation of PPARγ, likely by endogenous ligands such as fatty acids (Wang *et al.*, 2002; Zoete, Grosdidier and Michielin, 2007). Treatment of PPRE-H2B-eGFP-transfected H400 cells with 1 µM GW1929 produced no change in fluorescence, though a relatively small increase was detected with 10 and 20 µM treatments. However, recorded fluorescence was highly variable across technical replicates (as shown in Figure 4.7) and these data were unable to be reproduced due to high inter-replicate variability. Ultimately, high levels of variability and difficulties with quantifying the fluorescence, led to rejection of the H400:PPRE-H2B-eGFP cell line as a viable PPARγ reporter system.

The lack of utility of the H400:PPRE-H2B-eGFP reporter may have been caused by a range of factors, including issues with the PPARγ receptor, the stable transfection and selection process or due to experimental setup. H400 cells may have low levels of PPARγ expression, with endogenous ligands saturating all available PPARγ receptors, resulting in minimal increases in fluorescence following GW1929 stimulus. Similarly, depletion of cofactors and co-activators involved in PPARγ-dependent response element activation may reduce eGFP-mediated fluorescence, as these cofactors have been shown to be crucial to PPARγ function (Katsouri, Blondrath and Sastre, 2012).

Alternatively, it is possible that integration of the reporter plasmid into the H400 cell genome led to insertional mutagenesis or modification of DNA methylation, both of which have been reported to cause significant phenotypic changes with a wide range of viral and non-viral transfection systems (Baum *et al.*, 2006; Doerfler, 2011). Insertional mutations may have reduced transgene stability, resulting in gradual loss over successive passages of transfected

cells, explaining the data presented in Figure 4.7 were unable to be reproduced. In addition, variation in cell cycle, cell number and culture conditions prior to transfection may lead to insertion of the transgene at different locations and/or result in different levels of expression (Baum *et al.*, 2006). If monoclonal selection was then improperly performed by unintentionally culturing a population derived from more than a single cell, a cell population may have been produced within which reporter production (eGFP) differed.

However, while the H400:PPRE-H2B-eGFP system was deemed non-viable, an alternative reporter system was produced by transient transfection of H400 cells with PPRE-pNL1.3 (Section 4.4). Initially, both H400 and HaCaT cells were transfected to assess whether the choice of cell line played a significant role in the transfection success. As shown in Figure 4.8, a statistically significant increase in luminescence was observed between untransfected control and transfected cells in both H400 and HaCaT cells. These data indicated a high level of basal nanoluciferase expression, similar to that observed in the H400:PPRE-H2B-eGFP system; likely due to activation of PPARγ by endogenous ligands. However, unlike the H400:PPRE-H2B-eGFP reporter system, treatment of PPRE-pNL1.3-transfected H400 cells with 5 µM GW1929 produced a significant increase in luminescence compared with transfected control cells. Non-significant increases were also noted following stimulation with 1 µM GW1929 and with rosiglitazone, a known thiazolidinedione-class PPARγ agonist.

These results suggested that transient transfection with PPRE-pNL1.3 enabled successful nanoluciferase-mediated reporting of PPARγ activation in H400 cells. HaCaT cells appeared unsuitable for use in a PPARγ reporter system, demonstrating no marked change in luminescence relative to transfected controls. As was suggested for the H400:PPRE-H2B-eGFP reporter, it was possible that a low expression of PPARγ in HaCaT cells led to

saturation of all available receptors by endogenous ligands, suppressing the effects of the exogenous ligands.

In addition to investigating both HaCaT and H400 OSCC cells for use as PPARγ reporter cell lines, charcoal stripped serum (CSS) was also trialled as an alternative to FCS. CSS is widely used in nuclear receptor studies due to the prevalence of endogenous ligands in FCS, particularly fatty acids (Cao *et al.*, 2009). Removal of these ligands has been proposed to reduce basal activation of nuclear receptors. Application of CSS to the H400:PPRE-pNL1.3 reporter system (Figure 4.9 B) indeed resulted in greater mean increases in luminescence following treatment with 5 μM GW1929, GW9662 and rosiglitazone, however the data also showed much higher variability (Figure 4.9 A). For this reason, FCS-supplemented media was used in all successive applications of the PPRE-pNL1.3 reporter system.

Whilst H400:PPRE-pNL1.3 cells demonstrated responses to GW1929 and rosiglitazone which indicated PPARγ activation, unexpected significant increases in luminescence were also produced following stimulation with GW9662 (Figure 4.8). Initially, this was attributed to human error, but replacement of all agonist and antagonist stocks with newly purchased stocks (from different manufacturer batches) yielded a similar outcome. GW9662 is a potent, selective, irreversible antagonist of PPARγ, acting to covalently modify the ligand binding domain and prevent PPARγ activation (Leesnitzer *et al.*, 2002). Previous reports have indicated a slight reduction in PPARγ activation in 24-hour GW9662-stimulated villous cytotrophoblasts (VCTs) transfected with both PPRE-H2B-eGFP and PPRE-pNL1.3 (Degrelle, Shoaito and Fournier, 2017), suggesting that this paradoxical activation was not a failure of the reporter transgene.

Characterisation of the antagonist action of GW9662 has revealed that modification of the single cysteine residue in the LBD via covalent bonding inhibited ligand binding (Leesnitzer *et al.*, 2002). It was hypothesised that single point mutation of nucleotides coding for this residue may inhibit the binding and antagonistic activity of GW9662.

Sanger sequencing of the GW9662-modifiable region of the PPARγ ligand binding domain (LBD) (Figure 4.13) showed no single nucleotide polymorphisms or mutations within the small (~280bp) sequenced region. This cysteine residue (initially designated Cys^{285} but moved to Cys^{283} in more recent genome assemblies) was present in the sequenced PCR product from H400 cells. However, it is possible that mutation of other residues outside of the sequenced region may have changed the accessibility of the LBD to GW9662, preventing GW9662-dependent antagonism.

As previously shown (Figure 3.6), western blotting and RT-PCR of H400 OSCC cells revealed differential expression of two isoforms, PPARγ1 and γ2, due to alternate splicing of the PPARγ transcript. PPARγ2 has been shown to contain an extra 30 amino acids at the N-terminal end, within the A/B domain ligand-independent activation function (AF-1) (Bugge *et al.*, 2009). No previous work has been performed in which the response of PPARγ1 and γ2 to irreversible antagonists was characterised. However, the γ1 and γ2 variants have been suggested to have unique roles in lipid metabolism and insulin response (Omi *et al.*, 2005). These PPARγ isoforms have also been shown to have contradicting roles in prostate epithelial cell cancer, with expression of the γ1 isoform providing a proliferative stimulus, whilst γ2 has been shown to inhibit proliferation (Salgia *et al.*, 2019). Additionally, studies of PPARγ isoform expression in a range of tissues from goats have shown markedly greater γ1:γ2 ratios than the ~3:1 ratio shown here, suggesting that PPARγ2 expression in H400 OSCCs may be higher than other cell types (Li *et al.*, 2013). Unfortunately, no studies of PPARγ isoform

expression ratios in epithelial cells could be identified, preventing direct comparison to other epithelial cell types. However, it is highly possible that the antagonistic effect of GW9662 was modified in the presence of the first 30 additional amino acids in PPARγ2 (505 AAs, compared to 475 AAs for PPARγ1), especially if the expression ratio of γ2 to γ1 is higher than in other cell types. As these extra amino acids reside in the N-terminal activation function 1 (AF-1) domain, this may result in differences in activation of the longer γ2 variant compared with the γ1 variant. As previously discussed, the AF-1 domain is crucial in the interaction of the nuclear receptor with the basal transcriptional machinery, and in post-translation modification (Section 1.3). Indeed, previous studies of these two PPARγ isoforms identified a distinctly greater activation potency of the longer γ2 variant compared with γ1, even though the additional 30 amino acids possessed no activation capability in isolation (Werman *et al.*, 1997). Additional work would be required to further understand the paradoxical activation of PPARγ by the antagonist GW9662 shown here in what is clearly a complex interplay of two co-expressed isoforms. For example, isoform specific siRNA or CRISPR-Cas9 knock-down/out of PPARγ1 or γ2 transcripts may aid in identifying if the antagonistic effect of GW9662 is isoform-specific. However, even considering paradoxical GW9662-dependent PPARγ activation, H400 cells transfected with PPRE-pNL1.3 reporter still showed significant activation with the agonist GW1929, suggesting that this cell line was still suitable as a component in a PPARγ reporter system.

With a body of evidence that FCS-supplemented H400 cells transfected with PPRE-pNL1.3 presented a reproducible and suitably sensitive PPARγ reporter system, these cells were then utilized to test PPARγ-activation of compounds widely used in cosmetic formulations and oral care products. Prior to application to the reporter system, cytotoxicity testing was undertaken to establish the maximum non-toxic dose of each compound. Four tested

compounds (SabiWhite®, PEA, pTeroPure® and HSA) generated significant reductions in measured CCK-8 absorbance at 10 µg/ml, understood to correlate with a reduction in cell viability. All other tested compounds produced large but statistically insignificant reductions at the same concentration (Figure 4.10). The use of the colourimetric CCK-8/WST-8 cell viability assay enabled high-throughput screening of many compounds at a wide range of concentrations. However, colourimetric assays have been shown to have drawbacks compared with other methods of assessing cell viability. These assays have shown to inconsistently measure cell viability in cultures containing particulates, as these may cause optical interference or changes in absorption (Jiao *et al.*, 2015). The present work, however, required the testing of eight compounds with five concentrations (and one control) each, necessitating a high-throughput approach. Therefore, colourimetric testing was deemed more suitable than microscopy-based cell counts. Colourimetric testing typically uses redox-based reactions, wherein a reagent is reduced by metabolically active cells producing an insoluble salt (Berridge, Herst and Tan, 2005). While significantly more rapid and less subjective than microscopy-based cell counts with trypan blue, colourimetric testing results may be confounded by changes in cell metabolism induced by test agents or treatments (Ghasemi *et al.*, 2021) or by the presence of particulates in the culture media (Jiao *et al.*, 2015). However, the CCK-8 assay described in the present work was calibrated for possible optical interference from test compounds by the inclusion of appropriate control wells.

Following cytotoxicity testing, all test compounds were applied to the PPRE-pNL1.3 PPARγ reporter system at 1 µg/ml. Sulfradex was included at this stage without prior cytotoxicity testing and was applied to PPARγ activation studies at the same concentration (1 µg/ml) as all other compounds. None of the tested compounds produced statistically significant increases in measured luminescence, serving as an indicator of increased PPARγ activation. However,

several compounds produced modest but statistically non-significant increases, using assays for both secreted luciferase (Figure 4.11 A) and luciferase from lysed cells (Figure 4.11 B). While the PPRE-pNL1.3 system utilises a secreted nanoluciferase (England, Ehlerding and Cai, 2016), cell lysis was also trialled to ensure that a failure in protein packaging or export was not reducing assay sensitivity. This approach resulted in no marked change in recorded luminescence (representing PPARγ activation), suggesting that secretion of the nanoluciferase was not impeded, while GW1929 (acting as a positive control) produced increases in luminescence in both assay approaches used.

The lack of significant changes in PPARγ activation by the tested cosmetic compounds may have been due to a real effect or may be disguised by potentially low assay sensitivity. As previously discussed with respect to the H400:PPRE-H2B-eGFP reporter system, high basal PPARγ activation may have produced near-saturation of all available PPARγ receptors, reducing or masking the observed effect of supplementation with these compounds. To address this issue, future work may include the use of a cell line with lower basal PPARγ activity, enabling more pronounced activation of receptors by exogenous ligands, which may augment the sensitivity of the PPRE-pNL1.3 reporter system. Additionally, the sensitivity of a reporter in a specified application may be highly dependent on experimental design. It has previously been reported that the sensitivity of the nanoluciferase reporter transgene has significantly greater sensitivity than other luciferase-based bioluminescence assays (Hall *et al.*, 2012). However, further optimisation of timepoints, cell density and transfection protocols may improve the utility of the H400:PPRE-pNL1.3 reporter system in identifying novel PPARγ ligands with low activity.

In summary, the present work has described the generation and use of a PPARγ reporter system, comprising PPRE-pNL1.3-transfected H400 OSCC cells. The reporter system was used to identify a suitable ligand and ligand concentration to produce significant PPARγ activation in H400 cells, resulting in the selection of 5 µM GW1929 as a suitable stimulus for further work incorporating LPS-challenged H400 cells. This reporter was also applied to cosmetic compounds for the screening of PPARγ activation of these GRAS materials, showing that no tested compounds exhibited PPARγ ligand activity similar to GW1929.

5. DEVELOPMENT OF A NOVEL 3D PRINTED DEVICE FOR THE ORGANOTYPIC CULTURE OF GINGIVAL EPITHELIA EQUIVALENTS

5.1. Introduction

The following chapter was published in part as a publication, entitled "A novel 3D printed buoyant device for *in vitro* generation of stratified epithelial rafts at the air-liquid interface" (Hewitt *et al.*, 2022).

Monolayer cultures are widely used for *in vitro* studies on cellular responses, molecular pathways and cytocompatibility. These relatively simple cultures require short culture periods and may provide useful preliminary data but can fail to appropriately recapitulate the *in vivo* environment (Pezzulo *et al.*, 2011; Breslin and O'Driscoll, 2016). Previously described organotypic epithelia culture systems utilize Transwell inserts (Aufderheide and Mohr, 2000; Lin *et al.*, 2007) or a stainless-steel mesh, raising the cell scaffold from the surface of the culture flask to the air-liquid interface (ALI) (Prunieras, Regnier and Woodley, 1983; Bernstam, Vaughan and Bernstein, 1986). However, ALI maintenance requires frequent adjustments of media volume to account for both media evaporation and shrinkage of scaffolds due to fibroblast contraction. Any variation in ALI exposure of the epithelial layer between replicates may reduce experimental reproducibility, with the potential for resultant differences in differentiation or stratification. Mitigation of these variables is therefore needed if scientific rigour is to be maintained.

The novel approach described in this chapter comprised a 3D printed buoyant epithelial culture device (BECD), fabricated in polypropylene via a fused filament fabrication process. The BECD device had several key design requirements; to retain the fibroblast-seeded hydrogel without loss, to be easily sterilised and to continue to float (and thus maintain the ALI) even after prolonged periods of submersion. This unique approach enabled automatic maintenance of the ALI, thereby minimising variability between experimental replicates.

Additionally, a 3D-printed submerging ring was produced, used to force the device below the ALI to enable the generation of a confluent epithelial monolayer, prior to induction of the ALI by removal of the ring.

Potential materials for device fabrication were screened for a lack of reported cytotoxicity and a melting temperature suitable for FFF extrusion between 170-250°C. Four materials were chosen for initial characterisation with printing trials and autoclave testing: polypropylene (PP) (Fatou, 1971; Roy and Fleischman, 2003), poly-lactic acid (PLA) (Garlotta, 2001; Tsou *et al.*, 2017), polyethylene terephthalate-glycol modified (PETG) (Arany *et al.*, 2021; Hsueh *et al.*, 2021) and polycarbonate (PC) (Melo Pithon *et al.*, 2009; Greene, 2021). Subsequently, sterilised devices were exposed to HamsF12:DMEM for 14 days (or until failure, if this occurred before 14 days) to evaluate if constant exposure to culture media at 37°C caused failure of the polymer. Within these tests, failure was defined as the generation of cracks or voids, leading to media ingress and device submersion.

Following these trials, PP (BASF, Netherlands) was chosen for BECD fabrication in subsequent experiments, with the aim of identifying if the device geometry successfully generated stratified epithelia. PP-based BECDs were used to culture collagen hydrogels with an epithelial cell layer, which was then analysed histologically with Haematoxylin and eosin (H&E) staining (Fischer *et al.*, 2008) was used to assess epithelial architecture and cell viability. Consideration was given to the possibility of variability in epithelia thickness between independent biological replicates, or across the diameter of each raft.

In addition to stratification, epithelial tissues exhibit distinct patterns of spatial differentiation, key to the function of these tissues (Franke *et al.*, 1981). For this reason, immunofluorescence staining was used to provide a qualitative comparison of both the expression and localisation

of key differentiation markers in tissue cultured using the BECD system with healthy human control gingival tissue. These control tissues proved suitable for assessing epithelial differentiation markers, however, gingival tissue is highly differentiated, with a thick and distinct cornified layer and well demarcated spinous and granular layers (Oubayoun *et al.*, 1985). Artificial organotypic cultures generated using cancer cells were not expected to develop such a high level of maturation, but differentiation marker expression and localisation could still be compared.

5.2. BECD design and geometry

BECD design and geometry was produced to fit within standard 6-well plate culture dishes and to retain a collagen hydrogel, while containing an adequate volume of air within the device to float and maintain the ALI, as required to meet the design considerations. Engineering drawings (Figure 5.1) show relevant dimensions and features. Additionally, a 3D rendering of the complete BECD with submerging ring *in-situ*, as would be used for the three-day submersion period, is shown in Figure 5.1 G.

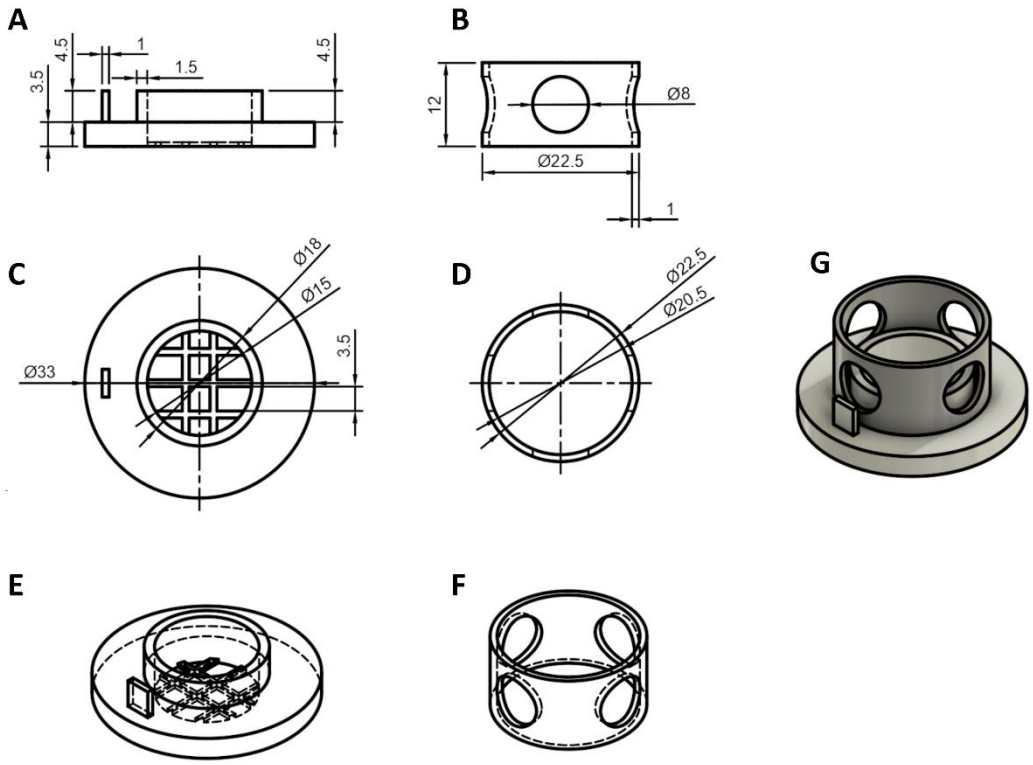


Figure 5.1 – Engineering drawings depicting the features and geometry of the BECD system.

A, C, E) Engineering drawings of the BECD construct with cross section, top-down and isometric views respectively.
B, D, F) Engineering drawings of the BECD submerging ring with cross section, top-down and isometric views respectively.
G) 3D rendering of the BECD with submerging ring in place. All units shown in millimetres.

5.3. Material selection trials and generation of stratified epithelia at the ALI

Polylactic acid (PLA) BECDs were produced successfully but exhibited a small amount of deformation immediately after sterilisation, with separation of printed walls and changes in device geometry (Figure 5.2 A). These geometry changes led to non-concentric or warped devices, which may have caused variation in the resultant size and shape of the collagen hydrogels. Delamination of some walls was also noted, which could lead to leakage of the

devices. Exposure to culture media for 7 days resulted in apparent crack formation, leading to a complete failure of structural integrity (Figure 5.2 B) and media ingress, at which point devices failed to maintain the ALI.

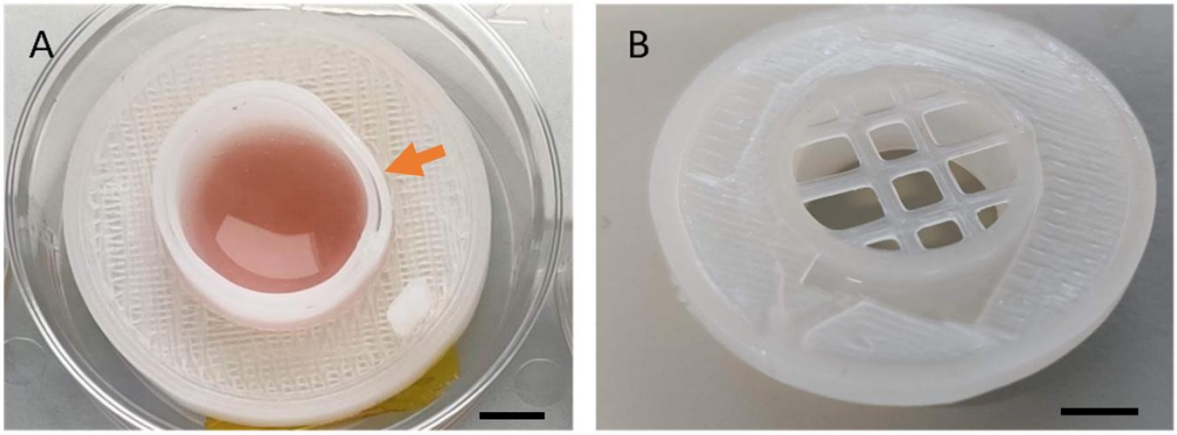


Figure 5.2 - PLA-based BECDs, demonstrating the two different failure modes observed in this study.
A) Deformation of inner chamber ring due to autoclave sterilisation, leading to a non-concentric inner chamber. Delamination of the inner chamber walls was also noted, marked by an orange arrow.
B) Cracking and delamination of the bottom surface of the device, following autoclaving and submersion in culture media for 7 days. Scale bars 5mm.

PETG BECDs exhibited significant issues with deformation following sterilisation, leading to unusable devices (data not shown) and PETG was therefore not used for further studies. PC was difficult to reliably print due to issues with adhesion to the printing bed, and not advanced beyond early printing trials (data not shown). The melting point of PP enabled both extrusion in consumer-grade FFF systems and autoclave sterilisation did not result in construct deformation. PP withstood relatively long periods (greater than 21 days) of incubation at 37˚C without obvious embrittlement, structural failure, or media absorption, as shown in Figure 5.3 C.



Figure 5.3 – Images of polypropylene (PP) 3D-printed BECD as used for *in vitro* trials.
A) PP BECD prior to use in *in vitro* trials, perspective view.
B) The same PP BECD shown in a top-down view.
C) PP BECD following 21 days of exposure to HamsF12 culture media at 37°C, bottom view. Minimal media ingress is noted, with no cracking or failure of the device. Scale bars 5mm where shown.

Following initial printing trials, the suitability of polypropylene-based BECDs (Figure 5.4 A-B) for epithelial cultures was assessed. Organotypic cultures using H400 OSCC cells and collagen-embedded 3T3 fibroblasts were established (as described in Section 582.5.2) and immersed in media for 72h using the submerging ring (Figure 5.4 C). After ring removal, the BECDs were allowed to float on the media surface at the ALI for 7, 14 and 21 days. The BECDs showed minimal media ingress and effective ALI maintenance at 21 days in culture (Figure 5.4 D), suggesting that the chosen geometry was appropriate for use *in vitro*.

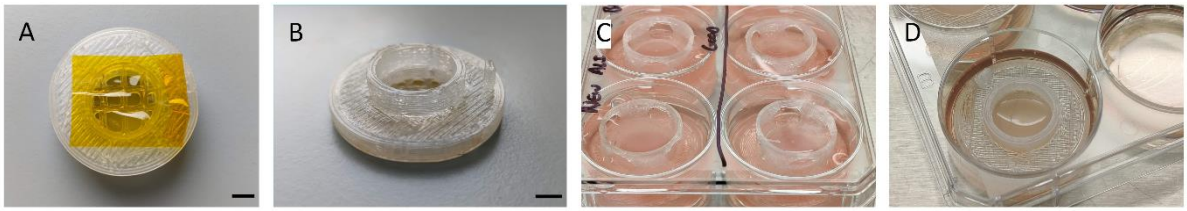


Figure 5.4 - Images of steps involved in the production and use of BECDs for stratified epithelial culture.
A) BECD with Kapton tape in-situ, prior to sterilisation by autoclave, bottom view.
B) BECD with Kapton tape in-situ, perspective view.
C) BECDs in culture with submerging ring in place for 3-day submersed incubation step.
D) BECD following 21 days of ALI culture. Minimal media ingress to BECD structure was noted, with the ALI appearing well maintained. Scale bars are 5mm where shown.

Following 7 days of ALI culture, a thin stratified epithelium was visible on the upper surface of collagen gels (Figure 5.5 A-B). There was an apparent increase in epithelial thickness from

7 to 14 days of ALI culture (Figure 5.5 C-D) and a further marked increase from 14 to 21 days (Figure 5.5 E-F), which indicated effective maintenance of the ALI when using the BECDs. However, no keratinization was noted after 21 days of culture at the ALI. BECD-cultured H400 cells kept at the ALI for 7 days showed some irregular stratification, which was noticeably reduced after 14 days culture at the ALI. Fibroblasts were observed throughout the collagen hydrogel and showed a homogenous distribution when observed by microscope. SIOX segmentation and thresholding of the H&E-stained micrographs enabled extraction of the epithelial tissue component with minimal false-positive selection when evaluated by microscope (Figure 5.5 B, D, F).

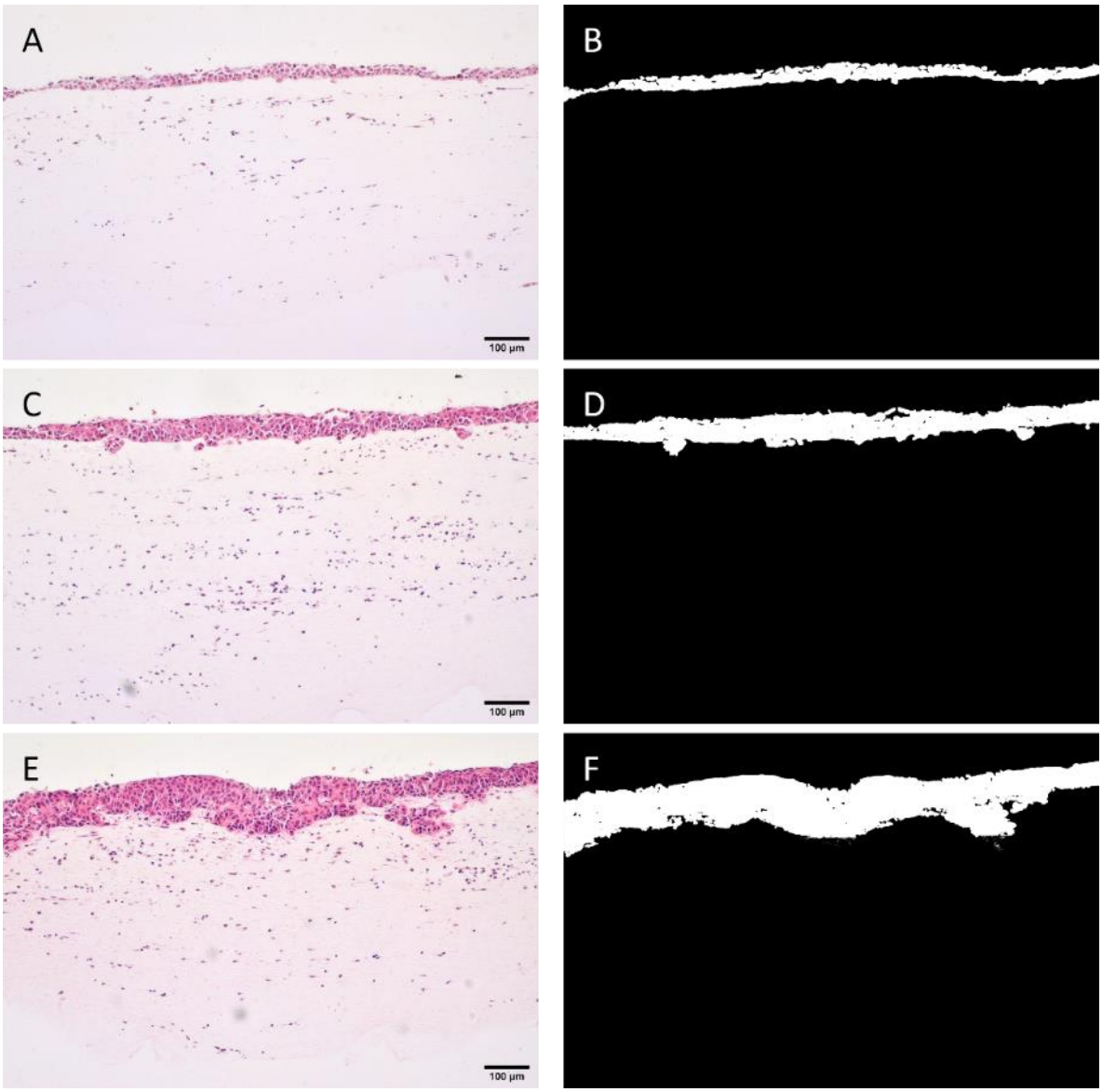


Figure 5.5 - Representative photomicrographs of H&E-stained sections of BECD-cultured H400 cells on a collagen-3T3 fibroblast gel for 7 (A), 14 (C) and 21 (E) days. B, D, F: The corresponding SIOX segmented image is shown for each micrograph, isolating the layers of epithelium shown in white. Scale bars = 100µm.

The output of material printing trials, autoclave sterilisation and *in vitro* use are summarised in Table 5.1.

Table 5.1 - Materials selection matrix depicting the outcome of printing, sterilisation and *in vitro* trials of PLA, PC, PETG and PC. N/A = Not tested due to failure in prior tests.

Material	Printing	Sterilisation	*In vitro use*
Polylactic acid (PLA)	Pass	Pass, with minor deformation	Fail - cracking
Polycarbonate (PC)	Fail	N/A	N/A
Polyethylene terephthalate, glycol modified (PETG)	Pass	Fail - deformation	N/A
Polypropylene (PP)	Pass	Pass	Pass

5.4. Assessment of BECD-cultured epithelial tissue thickness and reproducibility

While previous data (Figure 5.5) indicated a qualitative increase in epithelial thickness over time, quantitative measurement of these epithelia using SIOX and image analysis macros enabled statistical analysis of the response of H400 cells to the BECD system. To assesses epithelial thickness, epithelial cells were cultured on the upper surface of collagen hydrogels in BECDs for 7, 14 and 21 days. H&E staining, imaging and segmentation using SIOX were performed and the maximal epithelial thickness (MET) of each sample was analysed using an ImageJ macro, reducing bias and improving measurement reproducibility.

There was a significant increase in MET from 7 to 14 days of culture ($p < 0.05$), with an average MET of 50.34 µm, increasing to 91.66 µm after 14 days of culture (Figure 5.6 A). After 21 days, a further significant increase in MET was observed ($p < 0.01$), with the average MET being 137.04 µm. The range of MET values in the technical replicates was seen to increase at 14 and 21 days of ALI culture and indicated more variability during prolonged periods of culture, as expected.

To identify possible variability in MET between the central (inner) region of the hydrogel and the outer edges, sections were compared across the width of the BECD-cultured hydrogels (Figure 5.6 B). No significant difference was observed between the MET values of inner and outer hydrogel sections at the timepoints analysed ($p > 0.05$).

These data indicated that the BECD system successfully produced a stratified epithelial tissue using H400 cells and 3T3 fibroblasts in a collagen matrix and the thickness increased significantly at 7, 14 and 21 days of culture.

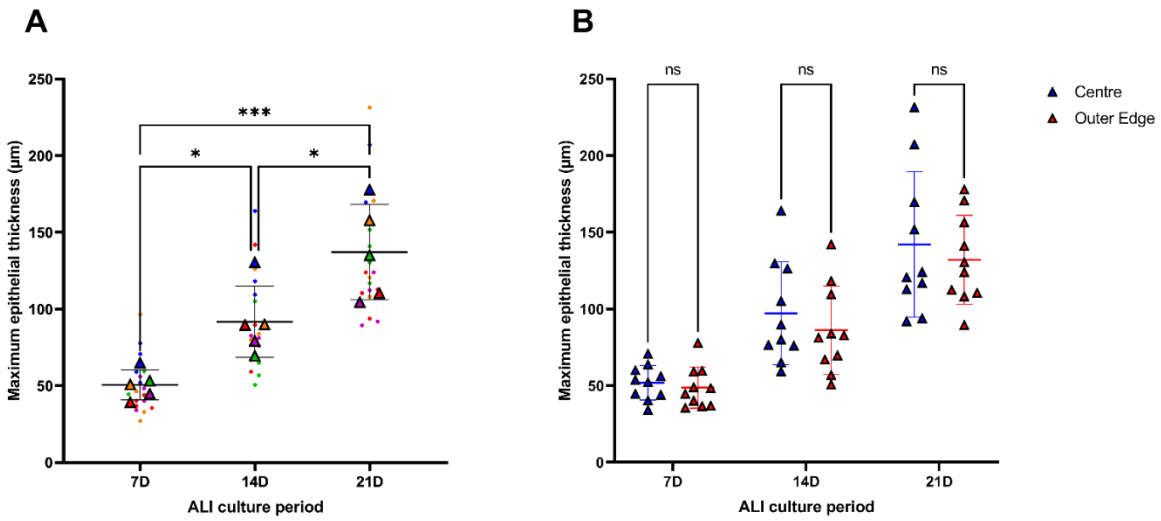


Figure 5.6 – A) Maximum epithelial thickness (MET) 'superplot' for H400 cells cultured at the ALI using BECDs. Biological replicates (triangle symbols) are colour matched with their respective technical replicates (small circle symbols).
N=5, 4 technical replicates per time point, mean ±SD, one-way ANOVA and Tukey's multiple comparisons test (all to all). * = $p < 0.05$, ** = $p < 0.01$, *** = $p < 0.001$.

B) MET comparison between histological sections from the inner region of the hydrogel (blue triangle symbols) and outer regions (red triangle symbols).
N=5, with 4 technical replicates from per timepoint, all technical replicates shown, with mean ±SD. Statistical analysis performed using two-way ANOVA and Šídák's multiple comparisons test. Ns = no significance.

5.5. Assessment of BECD-cultured epithelial tissue differentiation

Immunofluorescence staining for key epithelial differentiation markers was performed in both BECD-cultured tissues, and healthy gingival tissues obtained from oral surgery (Section 2.5.4). Staining for involucrin, a key marker of terminal epithelial cell differentiation, revealed expression in both control tissue and in BECD-cultured tissue by 21 days at the ALI (Figure 5.7 A, B). As expected, in control tissue involucrin expression was localised to the upper layers of the stratified epithelia, with limited fluorescence detected in the cells immediately above the basal epithelial cell layer. A similar pattern was observed in BECD-cultured tissue after 21 days at the ALI, with increased density of staining more distant from the basal layer. This localisation suggested terminal differentiation of epithelial cells in

BECD-cultured stratified epithelia was comparable with that observed *in vivo*. Cytokeratin 5 expression in control tissue (Figure 5.7 C) was limited to cells immediately adjacent to the basal cell layer and decreased in intensity as distance from the basal cell layer increased. Minimal expression was apparent in the uppermost cell layers. BECD-culture tissue (Figure 5.7 D) showed a similar trend, with the upper-most layers of cells showing minimal cytokeratin 5 expression, whilst cells adjacent to the basal layer showed highest expression. The transmembrane protein E-cadherin was selected as a marker of cell adhesion, with both control (Figure 5.7 E) and BECD-cultured tissues (Figure 5.7 F) showing staining for E-cadherin, localised to intercellular junctions. Expression was consistent from the basal cell layers to the more superficial cornified layers. These data indicated that H400-derived epithelial tissue cultured using the BECD system demonstrated similar differentiation patterns as the control gingival tissue.

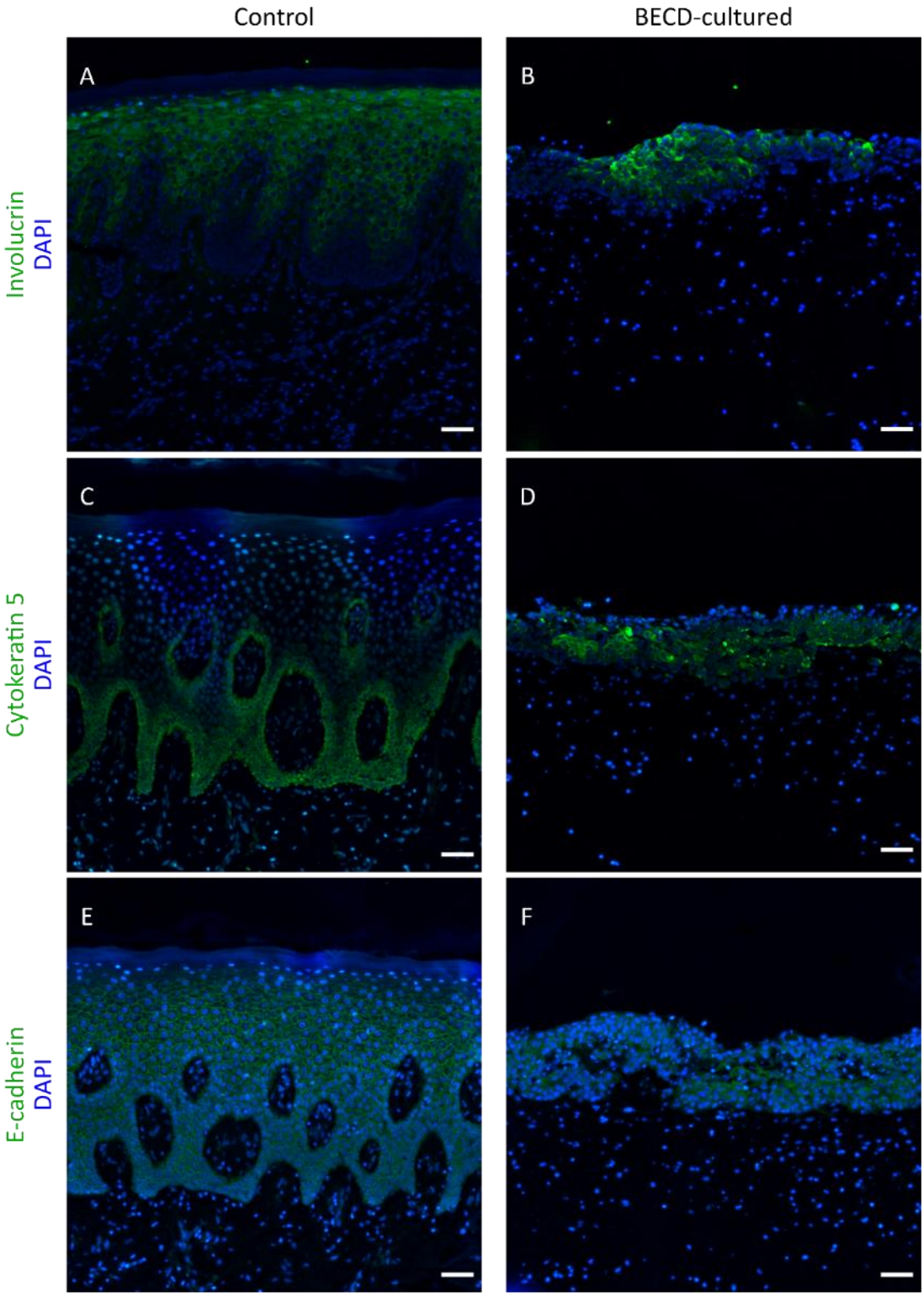


Figure 5.7 - Confocal micrographs of control human gingival tissue (A, C, E) and epithelia cultured in BECDs for 21 days (B, D, F). Involucrin was present and localised to the upper layers of the epithelia in control (A) and BECD-cultured H400s (B). In contrast, cytokeratin 5 was localised to the bottom layers of both control (C) and BECD-cultured cells (D). E-cadherin was also localised to intercellular junctions in both micrographs (E, F). AF488 (green) indicates protein of interest being stained, with DAPI (blue) used as a nuclear counterstain. Scale bars = 50 µm.

5.6. Discussion

The work described in this chapter aimed to develop and assess the utility of a novel device to produce epithelial tissue using easily fabricated devices and to reduce technique-sensitivity compared with existing methodologies. The buoyant epithelial culture device (BECD) enabled i) the establishment of epithelial cultures when immersed in media using the submerging ring, ii) a smooth and easy transition to the ALI environment, and iii) long term ALI cultures to be automatically maintained by floating on the media surface. BECDs considerably simplified typically highly technique-sensitive ALI culture, which has been shown to have high levels of inter-laboratory variability (Barosova *et al.*, 2021). It is also hypothesised that ALI culture is likely to have problematic levels of inter-user variability due to its technique sensitivity.

CAD and FFF technologies were jointly employed for the design and fabrication of BECDs, allowing for rapid amendment of the basic design, including simple geometry modifications, or more complex changes to include inserts or measurement probes, for example trans-epithelial electrical resistance readings for barrier function assessment. FFF has been increasingly used in laboratories with more 'open' and accessible approaches to science, often employed as a step in the production of *in vitro* devices (Yang *et al.*, 2016; Herreros-Pomares *et al.*, 2021), or for direct use *in vitro*, as described here. In addition, 3D bioprinting has been employed for use in developing tissue constructs and models (Vanderburgh, Sterling and Guelcher, 2016; Samavedi and Joy, 2017), though these approaches are markedly different compared with producing *in vitro* culture devices from polymers. The chosen design and device geometry (Figure 5.1) was printed with minimal errors and was sufficiently buoyant to maintain the ALI. The submerging ring effectively forced the device below the ALI to enable the formation of a confluent cell monolayer prior to ALI induction.

The selection of polymers for printing was primarily based on melting temperature and published cytotoxicity data. PC and PETG were subsequently excluded after initial trials of printing and sterilising the chosen design geometry. PC exhibited a prohibitively high melting temperature for the FFF 3D printer, producing issues with print quality and bed adhesion. Inversely, the lower melting temperature of PETG led to deformation following autoclave sterilisation. PLA was also trialled, passing initial printing and sterilisation trials with a small degree of deformation following autoclave treatment. Although PLA is used more widely than PP for consumer-grade FFF 3D-printing applications (Jones *et al.*, 2011), *in vitro* trials showed that PLA BECDs were prone to embrittlement and cracking after prolonged (14 day) periods immersed in culture media. PLA has been shown to be degraded by hydrolysis, leading to the formation of lactic acid, even in the absence of any catalytic enzymes (Garlotta, 2001). This hydrolysis may lead to device cracking and failure as noted (Figure 5.2 B), and the formation of lactic acid monomers may lead to cytotoxicity. There is a limited amount of research on the cytotoxicity of 3D-printed PLA constructs, but studies with human breast cancer cells grown in printed scaffolds showed no significant impact on cell viability (McAllister *et al.*, 2021). However, the noted issues with device cracking and structural failure led to the elimination of PLA for printing the devices.

Therefore, out of the four tested materials, only PP passed initial testing, and thus was used to fabricate BECDs and culture organotypic gingival epithelial equivalents. PP demonstrated a suitable melting temperature to enable extrusion by the FFF 3D printing system but avoided softening or melting at autoclave temperatures (Fatou, 1971). PP is also widely used in the production of *in vitro* cell cultureware, with high stability and low cytotoxicity (Roy and Fleischman, 2003).

Following selection of an appropriate material and design, 3D printed BECDs enabled growth of stratified epithelial tissues comparable with those obtained using traditional ALI methodologies including Transwell inserts (Rosdy and Clauss, 1990; Wang *et al.*, 2018) or stainless-steel mesh to raise the culture rafts (Prunieras, Regnier and Woodley, 1983; Bernstam, Vaughan and Bernstein, 1990). Previous work (Khan *et al.*, 2012) employing ALI-cultured H400 cells on a raised collagen gel demonstrated a similar epithelial tissue morphology and architecture following H&E staining compared with that presented in this study. It also showed no evidence of the generation of a cornified, keratinized apical cell layer following 21 days of ALI culture of H400 cells on a collagen hydrogel, similarly to the data presented in the current work. However, the use of DED as a substrate was shown to generate this cornified cell layer, suggesting that the scaffold used influences the degree of epithelial maturation. Modification of this scaffold material to more closely mimic epithelial dermis may be beneficial if this maturation is necessary or desired.

Thickness of the stratified epithelium produced with BECDs was studied at 7, 14 and 21 days of ALI culture. SIOX quantification provided a rapid, unbiased thresholding and segmentation technique to quantify the thickness of these epithelial cultures and thus this technique was subsequently used to automate the process of epithelial thickness assessment. The increasing thickness of the epithelial layer was apparent and statistically significant between these timepoints (Figure 5.5 and Figure 5.6A). BECDs did not appear to exert any cytotoxic effect on the cells, as cultures showed stratification and no marked changes in morphology. Additionally, the absence of a significant difference in MET between epithelia at the outer margin and inner sections of the hydrogels (Figure 5.6B) showed that epithelial thickness was constant across the width of the raft.

The thickness of the obtained epithelial tissues generated demonstrated reproducibility within both technical and biological repeats, which likely reflects the consistent ALI maintenance in BECDs. A minor increase in variability between replicates was noted at 14 and 21 days of culture (Figure 5.6A), which could be due to the shrinkage of the fibroblast-collagen matrix pulling some regions of epithelia below the ALI. Further work may identify a more dimensionally stable hydrogel replacement, reducing shrinkage in long term cultures (Bacakova *et al.*, 2019). Variability may also be reduced further by optimising print settings, leading to fewer voids through which media ingress may occur after prolonged submersion. The nature of FFF as a layer-by-layer additive manufacturing process means that water-tight components can prove challenging to fabricate. Higher resolution 3D printers and smaller diameter nozzles are likely to provide an improvement and reduce variability further. Additionally, the system is more economical than Transwell devices, with each BECD costing a fraction of these commercially available devices. Raw material cost for a complete system of a single BECD and submerging ring is in the order of £0.03 per device, about twenty times cheaper than a similar Transwell system.

Following initial histological assessments using H&E staining, immunofluorescence (Figure 5.7) was applied to produce a qualitative assessment of the expression and localisation of key epithelial markers. These were all detected in the cultured epithelial tissue, indicating that the differentiation shown in BECD-cultured tissue was similar to that of the control tissue. Involucrin expression in both control tissue and BECD-cultured tissue was localised predominantly to the uppermost layers of the stratified epithelium, a finding consistent with previous reports (Watt, 1983; Ekanayake-Mudiyanselage *et al.*, 1998). Involucrin is a widely used marker of terminal epithelial differentiation, playing a key role in barrier function in

healthy epithelia (Ye *et al.*, 2000), suggesting this function was likely to be maintained in these BECD-cultured tissues as is observed *in vivo*.

Expression of cytokeratin 5 was noted in BECD-cultured epithelial tissues, with maximal expression in the basal cells, though this localisation was not as clearly defined in cultured samples as in control tissue. These data, however, indicated that localisation of cytokeratin 5 was similar to that of *in vivo* tissues.

E-cadherin expression was also observed in BECD-cultured tissue. E-cadherin has been shown to be crucial for normal cell adhesion processes, spanning the intercellular space and providing a junction between adjacent cells via its transmembrane domains (Van Roy and Berx, 2008). The presence and localisation of E-cadherin in BECD-culture tissues provided evidence that cell adhesion was maintained as observed in control tissues.

Some variation in the demarcation and localisation of differentiation markers was expected when using ALI-based systems, which are relatively simple compared with the complex *in vivo* environment. It was notable that correctly stratified epithelia were developed despite the using the H400 cell line, which was derived from an alveolar process squamous cell carcinoma. The immortal, rapidly dividing nature of this cell line is useful for research purposes, however the differentiation and architectural arrangement of these cancer cells varies from the primary healthy human tissue (Prime *et al.*, 1990), or from tissues obtained with primary cells.

In summary, BECDs provide an economical and user-friendly approach to ALI culture with the potential to reduce variability within ALI-cultured tissues. This culturing approach is easily adaptable, allowing for rapid, reliable induction of ALI in any volume of culture media. A buoyant, self-levelling device is likely to reduce technique sensitivity with the possibility of

improved reproducibility compared with conventional methodologies, enhancing the suitability of the system for high-throughput applications.

BECDs may be used to elucidate the mechanisms of epithelial tissue disorders, or trial drug candidates in a more biomimetic system compared with a relatively simple monolayer culture, with application to periodontal disease, bacterial and viral infections and oral cancers. This system may be further used for the generation of other ALI-cultured tissues by modification of the cell types used, including cutaneous and bronchial epithelial tissues (Lin *et al.*, 2007). In addition to *in vitro* studies, the BECD system may also have utility in clinical tissue engineering applications, due to the versatility and ease of generation of stratified epithelial tissue. The devices could be increased in scale and throughput to enable the generation of oral mucosal or skin equivalents for use *in vivo*, for example replacing tissue lost to trauma, disease, burns or surgical intervention.

6. THE ROLE OF PPARγ ACTIVATION IN REDUCING THE EFFECTS OF LPS ON ORAL EPITHELIAL CELLS

6.1. Introduction

Following characterization of the effects of LPS on H400 OSCC gene expression and barrier function (Chapter 3), and development and testing of a PPARγ reporter system (Chapter 4), studies were conducted to identify the role of PPARγ stimulation in a model of gingival inflammation. While a range of PPARγ agonists exist, including TZD-class anti-diabetics and endogenous ligands such as 15d-PGJ2 (Li, Guo and Wu, 2019), the synthetic PPARγ agonist GW1929 was chosen for these studies. GW1929, when used at a concentration of 5 µM, had previously been shown to significantly increase PPARγ activation in the H400 OSCC reporter system (Section 4.4).

PPARγ activation has previously been shown to exert a wide variety of effects, suppressing inflammatory cytokine signalling in a variety of cell types (Jacob *et al.*, 2007; Martin, 2009) and upregulating tight junction-related genes (Ogasawara *et al.*, 2010). However, no studies have examined the role of PPARγ activation in improving barrier function following LPS challenge in gingival epithelial cells. For this reason, quantitative PCR was initially used to identify changes in the expression of genes relevant to inflammation, PPARγ signalling, barrier function and epithelial differentiation. H400 cells were then exposed to 2 µg/ml LPS for 24 hours, followed by 5 µM GW1929 with 2 µg/ml LPS. Control groups comprised vehicle control (DMSO solvent only), LPS only and GW1929 only. Following this, enzyme linked immunosorbent assays (ELISAs) were applied to monolayer cultured H400 cells to identify if interesting changes in the gene expression of two relevant cytokines translated to the protein level, and western blotting was performed to examine possible changes in tight junction related gene expression.

It was also hypothesized that responses to both LPS and PPARγ agonists may be different between epithelial cells cultured in simple monolayers, and those cultured in organotypic models. With previous data validating the generation of differentiated, stratified gingival epithelial models, the BECD system (as described in Chapter 5) was used to generate organotypic gingival epithelia. H400 OSCC cells were cultured at the ALI for 14 days in the BECD system and stimulated with the same concentrations of LPS and GW1929 as used for monolayer cultures. This approach enabled direct comparison of gene expression between these two approaches to gingival epithelial cell culture.

Additionally, barrier function analysis with TEER was performed on H400 OSCC cells cultured with both systems, and a FITC-dextran macromolecular tracer assay (Bischoff *et al.*, 2016) performed on monolayer cells. This approach allowed for analysis of the flux of ions and macromolecules through H400 cell layers, and RT-qPCR was performed to aid in developing a mechanistic understanding of the possible effect of PPARγ stimulation on barrier function.

6.2. Analysis of gene and protein expression in LPS-challenged H400 cells treated with PPARγ agonists

RT-qPCR, ELISAs and western blots were performed on monolayer and organotypically cultured H400 cells to identify changes in expression of genes and cytokine relevant to inflammation, barrier function and PPARγ signalling. Both groups of cells were exposed to LPS (1 µg/ml) for 24 hours, followed by LPS (2 µg/ml) and GW1929 (5 µM) for a further 24 hours prior to RNA / protein isolation.

6.2.1. LPS/GW1929 double treatment in monolayer H400 OSCC cells

RT-qPCR (shown in Figure 6.1) revealed that mean calibrated normalised relative quantity (CNRQ) for the pro-inflammatory cytokine interleukin 8 (*CXCL8*) showed no statistically significant increase between the control and any other treatment condition ($p > 0.05$). However, *CXCL8* CNRQ was significantly increased between GW1929-treated cells (mean CNRQ = 0.7) and cells exposed to LPS only (CNRQ = 3.52, $p = 0.0148$) and LPS+GW1929 (CNRQ = 3.45, $p = 0.0183$).

Pro-inflammatory cytokine interleukin 6 (*IL6*) was significantly increased from a mean CNRQ of 1.76 in the control population to 6.75 following LPS stimulation alone ($p < 0.0001$). Expression was significantly downregulated in cells exposed to both LPS and GW1929 when compared to LPS alone (CNRQ = 1.44, $p < 0.001$). Treatment with GW1929 in the absence of LPS produced no significant difference in *IL6* CNRQ relative to control cells ($p = 0.9721$). Conversely, expression of interleukin 11 (*IL11*), an anti-inflammatory cytokine, was only significantly upregulated in H400 cells exposed to LPS and GW1929, increasing from a mean CNRQ of 0.919 in control populations to 4.29 with LPS and GW1929 ($p = 0.0023$). No significant changes in IL11 CNRQ were detected following treatment with LPS or GW1929 in isolation (CNRQ = 1.86, $p = 0.7328$ and CNRQ = 1.55, $p = 0.8978$, respectively). Expression of tumour necrosis factor alpha (*TNFa*) and nuclear factor kappa beta (*NFKB*) were not significantly altered in any of the tested conditions compared to control cell populations ($p > 0.05$). Expression of interferon gamma (*IFNG)* was found to be very low, with CP values exceeding 40 amplification cycles, even after repetition to mitigate possible experimental error.

Within the group of genes relevant to PPARγ function and signalling, no significant changes in CNRQ of PPARγ (*PPARG*), prostaglandin-endoperoxide synthase 2 (*PTGS2* / *COX2*) or

aquaporin 3 (*AQP3*) were detected. PPARG expression remained stable, with a slight increase in populations exposed to GW1929 (both in isolation and with LPS), but with no significant differences between any experimental groups.

Barrier function related genes occludin (*OCLN*), claudin (*CLDN1*) and zona occludens 1/2 (*TJP1/2*), junctional adhesion molecule 1 and 3 (*JAM1* / *JAM3*) and differentiation markers involucrin (*IVL*) and keratin-10 (*KRT10*) also showed no relevant statistically significant differences. E-cadherin (*CDH1*) only showed one significantly different change in expression, with a greater expression following LPS exposure than following GW1929 exposure (CNRQ = 4.78 and 2.14 respectively, $p = 0.0026$).

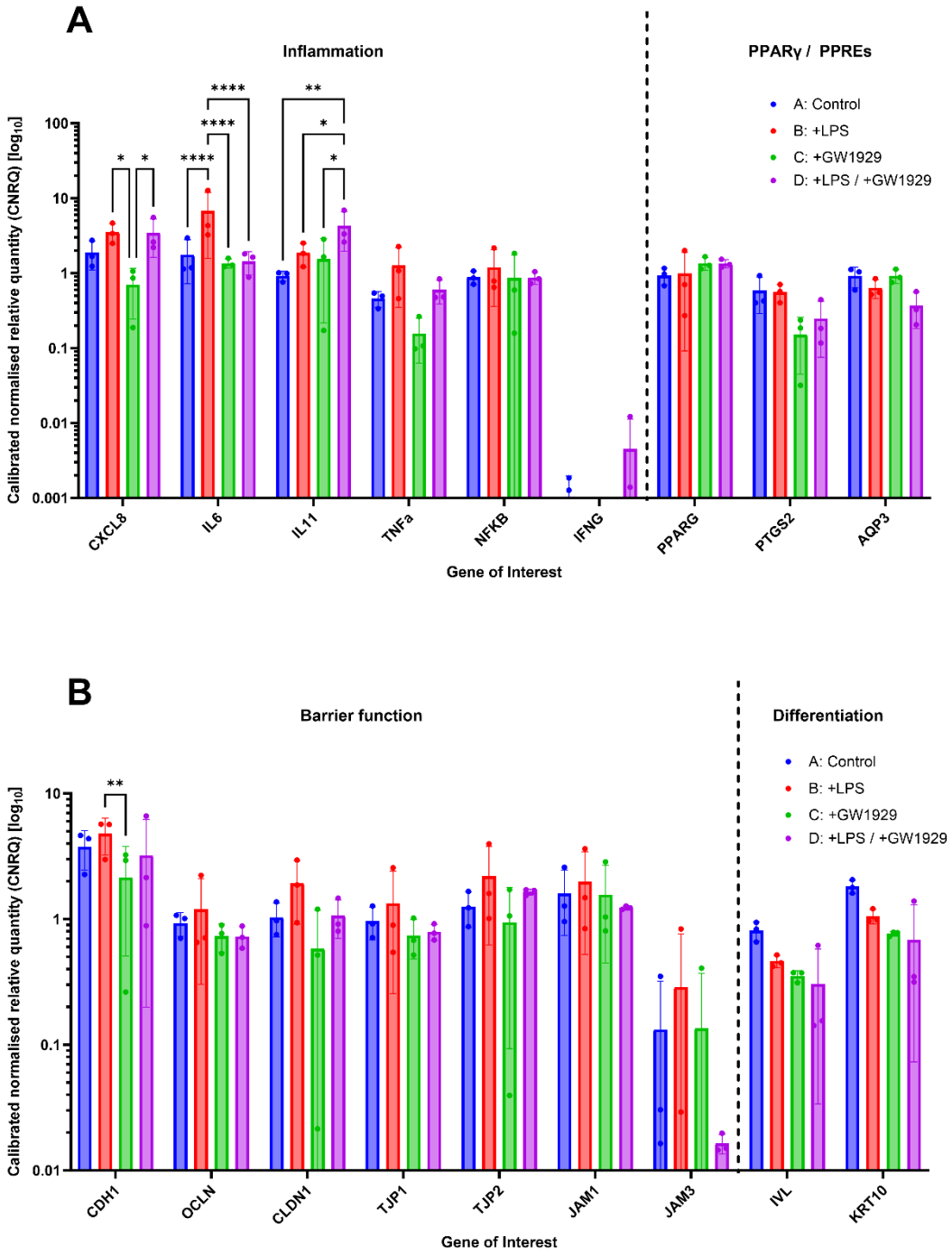


Figure 6.1 - RT-qPCR analysis of gene expression in monolayer cultured H400 cells, stimulated with LPS (2 µg/ml) and treated with GW1929 (5 µM).
CXCL8 = Interleukin 8, *IL6* = interleukin 6, *IL11* = interleukin 11, *TNFa* = tumour necrosis factor alpha, *NFKB* = nuclear factor kappa beta, *IFNG* = interferon gamma, *PPARG* = peroxisome proliferator activated receptor gamma, *PTGS2* = prostaglandin-endoperoxide synthase 2, *AQP3* = aquaporin 3, *CDH1* = e-cadherin, *OCLN* = occludin, *CLDN1* = claudin, *TJP1* = zona occludens 1, *TJP1* = zona occludens 2, *JAM1* = junctional adhesion molecule 1, *JAM3* = junctional adhesion molecule 3, *IVL* = involucrin, *KRT10* = cytokeratin 10

N=3, mean calibrated normalised relative quantity (CNRQ) ±SD, two-way ANOVA with Tukey's multiple comparisons post-hoc test (all to all). * = p < 0.05. ** = p < 0.01. *** = p < 0.001. **** = p < 0.0001.

RT-qPCR analysis of H400 cells stimulated with LPS and treated with GW1929 showed significant changes in the expression of interleukins 6 and 11. Therefore, enzyme-linked immunosorbent assays (ELISAs) were performed to identify if the noted changes in gene expression led to a change in protein expression by quantifying secreted IL-6 and IL-11 in the culture media. IL-6 ELISA showed cytokine production was below the limit of quantification (LOQ) of the assay system under all tested treatment conditions and across all biological replicates. A standard curve was produced with recombinant human IL-6 (from 9.38 to 600 pg/ml) and data fitted a quadratic polynomial, generating an R^2 value of 0.9992 (Figure 6.2). Recorded absorbance values for all samples are shown in

Table **6.1**.

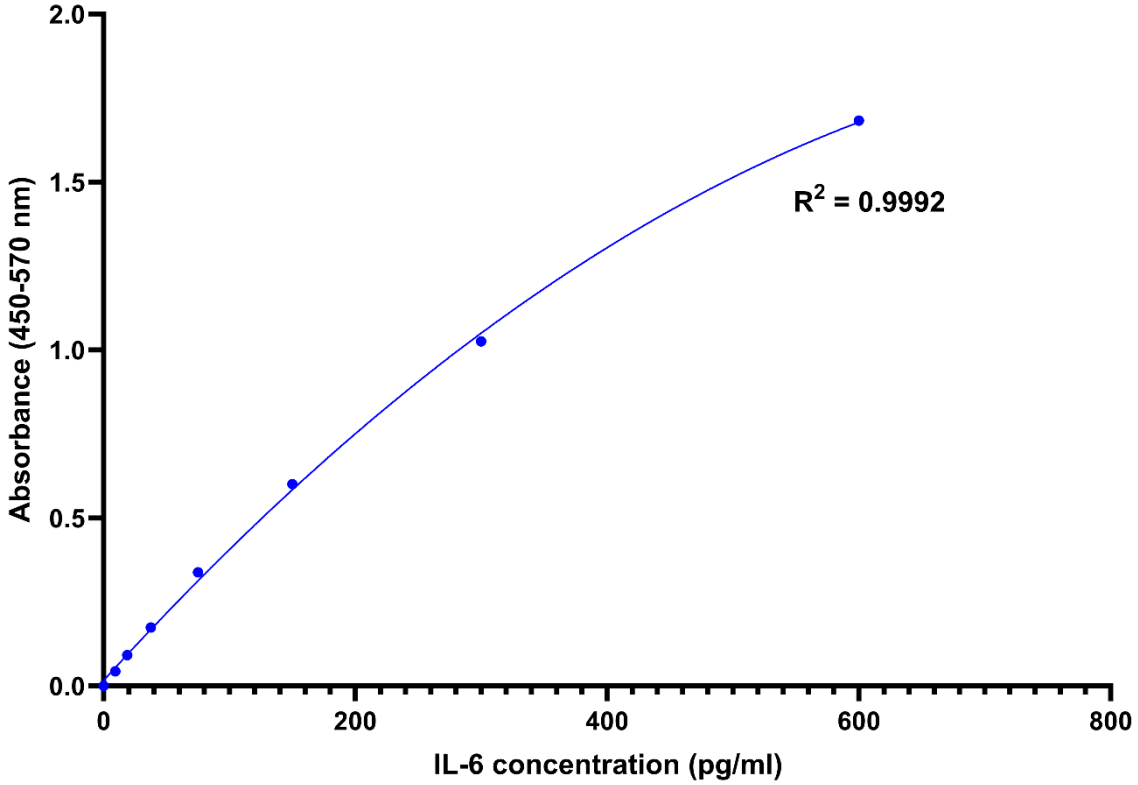


Figure 6.2 - Human IL-6 ELISA standard curve. Datapoints are mean of triplicate technical replicates. Data fit performed with a quadratic polynomial , $R^2 = 0.9992$.

Table 6.1 - Human IL-6 ELISA, recorded absorbance values of sample wells (450 - 570 nm). Mean of 3 technical replicates. Mean of biological replicates (±SD) shown.

	N1	N2	N3	Mean	SD
A – Control	0.002	0.003	0.001	0.002	0.001
B – LPS (2 µg/ml)	0.006	0.005	0.004	0.005	0.001
C – GW1929 (5 µM)	0.003	0	0	0.001	0.002
D – LPS and GW1929	0.003	0.003	0.003	0.003	0.000

ELISAs performed for IL-11 secreted by H400 OSCC cells generated no statistically significant change in expression in cells exposed to LPS and GW1929 compared with the control ($p > 0.05$) (Figure 6.3 B). Quadratic polynomial regression of standard curves generated for these assays produced a R^2 value of 0.9942 following linear regression (Figure 6.3 A)

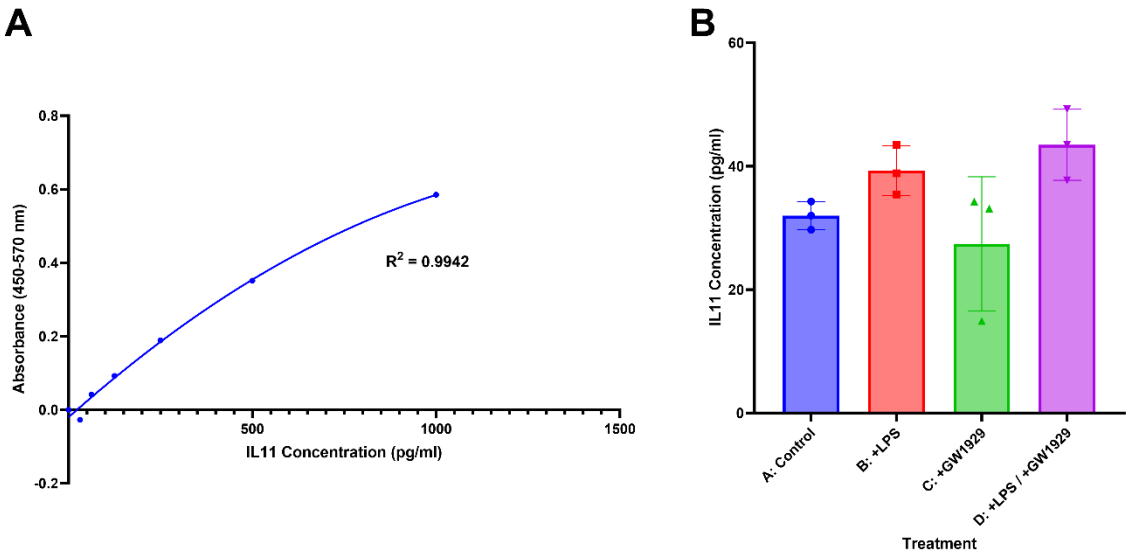


Figure 6.3 - IL-11 ELISA performed on H400 cells exposed to LPS and GW1929.
A) Standard curve generate from recombinant IL-11 protein standard, datapoints are mean of triplicate technical replicates. Quadratic poylnomail regression applied, $R^2 = 0.9942$.
B) Interpolated ELISA results, revealing a statistically significant increase in IL-11 expression between the control population and cells exposed to LPS (2 µg/ml) and GW1929 (5 µM).
N=3, mean concentration (pg/ml) ±SD, one-way ANOVA with Tukey's multiple comparisons post-hoc test (all to all). * = $p < 0.05$.

Whilst no statistically significant changes in expression of barrier function related genes was noted in RT-qPCR studies, western blotting was also performed to examine if any such changes occurred at the protein level. Due to constraints imposed by the size of SDS-PAGE gels, experiment group C (GW1929 only) was omitted from these data.

A western blot for zona occludens-1 (ZO-1), shown in Figure 6.4 A, generated one distinct band greater than 75 kDa in size, matching the expected size of ZO-1 (UniProt Q07157-1, 195 kDa). A second band was detected with a molecular weight of approximately 50 kDa, as expected for the beta actin loading control (41.7 kDa). No marked differences in expression of ZO-1 were observed in any treatment group. Quantification of band intensity was performed (Figure 6.4 B) and showed no significant changes in expression of ZO-1 between any tested treatment condition.

Similarly, western blotting for claudin-1 (Figure 6.4 C) generated a single band with a molecular weight of less than 25 kDa, matching the expected size of claudin-1 (UniProt O95832, 22.7 kDa), in addition to the beta actin loading control. Quantification of band intensity (Figure 6.4 D) showed no statistically significant change in claudin-1 expression ($p = 0.4609$).

A western blot for occludin (Figure 6.4 E) generated a single band of a molecular weight below 75 kDa, but greater than the 41.7 kDa beta-actin loading control. This fragment matched the expected size of occludin (UniProt Q16625-1, 59.1 kDa). Quantification of band intensity generated no statistically significant changes in expression in any tested condition (Figure 6.4 F).

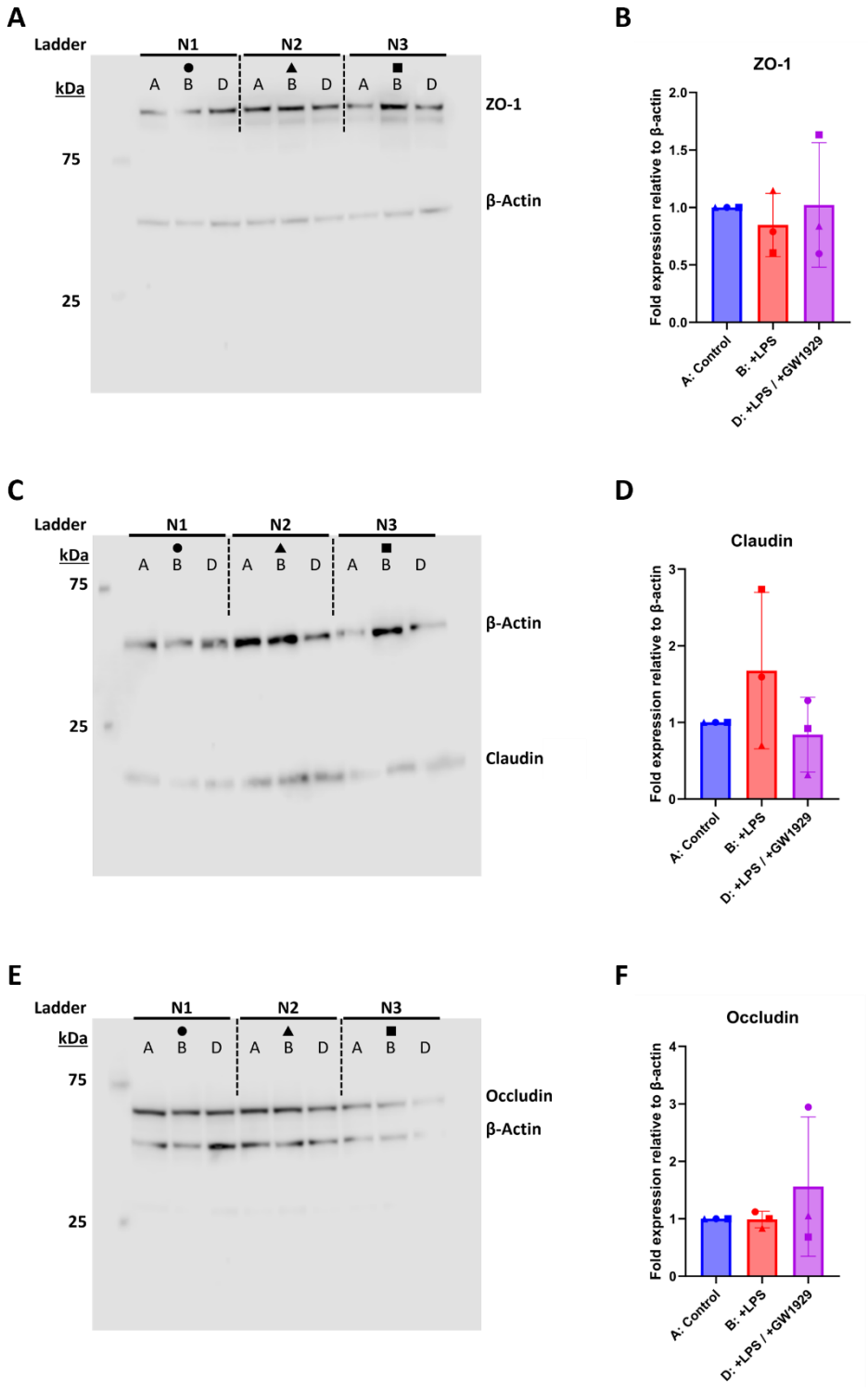


Figure 6.4 – Western blots and quantification of protein expression for tight junction proteins ZO-1 (A, B), claudin (C, D) and occludin (E, F). H400 cells exposed to LPS (2 µg/ml) and PPARγ agonist GW1929 (5 µM) prior to lysis and protein isolation. Quantification of protein expression was performed relative to loading control β-actin. No significant differences in tight junction protein expression were observed following treatment with LPS or LPS combined with GW1929. Western blots presented are unmodified except for the inclusion of annotations shown in black.
N=3, mean ±SD, one-way ANOVA with Tukey's multiple comparisons post-hoc test (all to all).

6.2.2. LPS/GW1929 double treatment in organotypically cultured H400 OSCC cells

Organotypically cultured H400 cells generated low gene expression responses following LPS treatment and GW1929 exposure, both in isolation and when combined. However, *JAM3* expression was significantly lower in control, LPS and GW1929-treated cultures than in combined LPS/GW1929 cultures. Expression fell from a CNRQ of 45.97 in LPS/GW1929 double treated cultures to 20.93 in the control ($p = 0.0070$), 20.68 in LPS treated cells ($p = 0.0064$), and 8.43 in GW1929 treated cells ($p < 0.0001$ for all). No other genes showed statistically significant expression changes between any tested conditions.

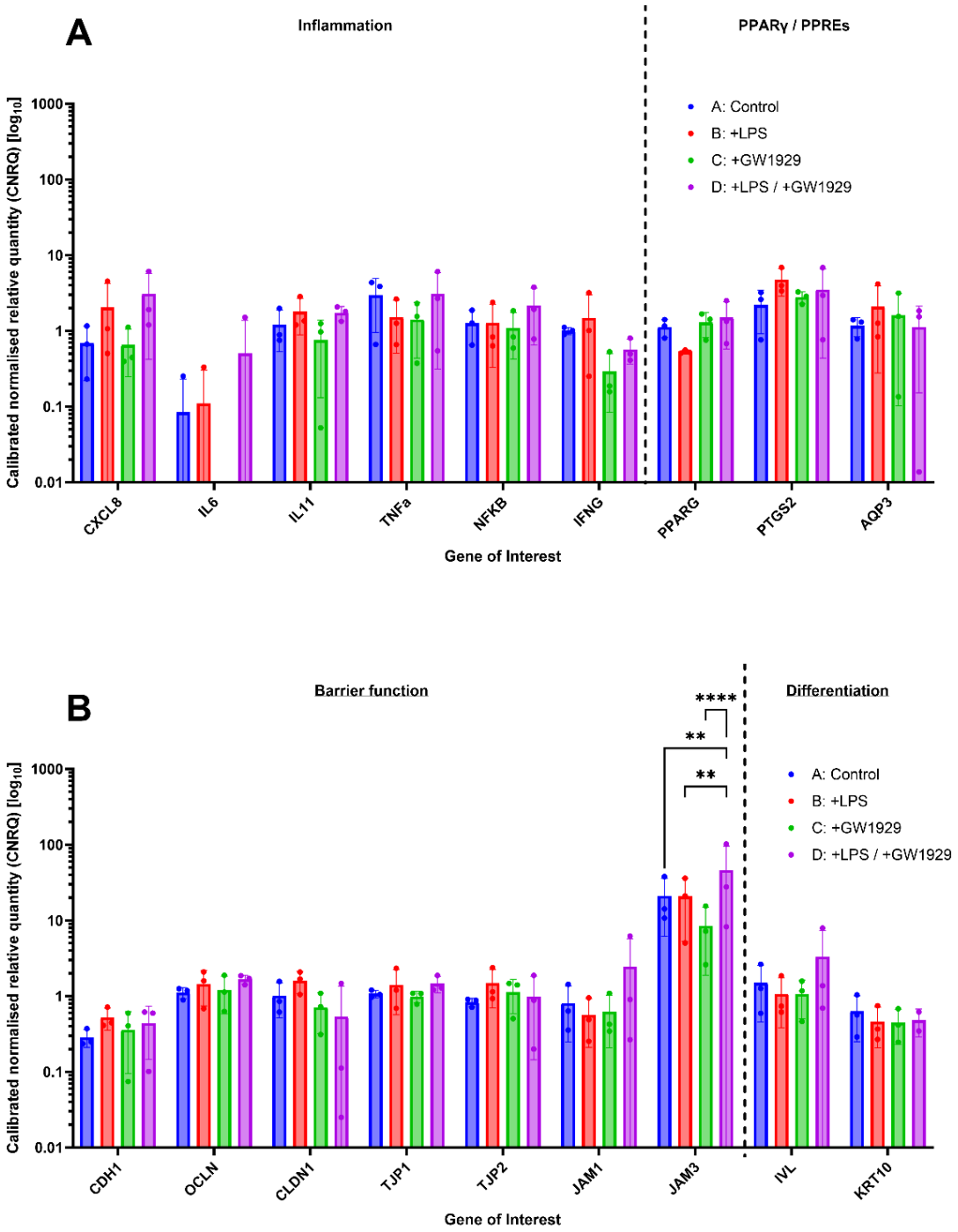


Figure 6.5 - RT-qPCR analysis of gene expression in BECD cultured H400 cells (14 days ALI), stimulated with LPS (2 µg/ml) and treated with GW1929 (5 µM).
CXCL8 = Interleukin 8, *IL6* = interleukin 6, *IL11* = interleukin 11, *TNFa* = tumour necrosis factor alpha, *NFKB* = nuclear factor kappa beta, IFNG = interferon gamma, *PPARG* = peroxisome proliferator activated receptor gamma, *PTGS2* = prostaglandin-endoperoxide synthase 2, *AQP3* = aquaporin 3, *CDH1* = e-cadherin, *OCLN* = occludin, *CLDN1* = claudin 1, *TJP1* = zona occludens 1, *TJP2* = zona occludens 2, *JAM1* = junctional adhesion molecule 1, *JAM3* = junctional adhesion molecule 3, *IVL* = involucrin, *KRT10* = cytokeratin 10
N=3, mean calibrated normalised relative quantity (CNRQ) ±SD, two-way ANOVA with Tukey's multiple comparisons post-hoc test (all to all). ** = $p < 0.01$, **** = $p < 0.0001$.

6.2.3. Comparison of gene expression between monolayer- and organotypically cultured cells

RT-qPCR was then used to directly compare the gene expression between H400 OSCC cells cultured in monolayer (2D) and organotypically (3D), with the same LPS challenge and PPARγ ligand (GW1929) treatments as described previously.

Interleukin 6 (*IL6*, Figure 6.6 B) expression appeared highly downregulated in 3D-cultured cells, but only GW1929-treated cells generated a significant difference in IL6 CNRQ, from 1.36 to 0.00 in 3D-cultured cells ($p = 0.0010$). TNFα (*TNFA*, Figure 6.6 D) expression appeared greater in 3D-cultured cells than in 2D, though these results were not statistically significant under any tested condition. Expression of interleukin 8 (*CXCL8*, Figure 6.6 A), interleukin 11 (IL11, Figure 6.6 C) and nuclear factor kappa beta (*NFKB*, Figure 6.6 E) was not found to be significantly different between 2D and 3D-cultured cells in any treatment group, and appeared relatively consistent between monolayer and 3D cultured cells.

Whereas *IL6* expression was markedly greater in 2D cultured cells than 3D, interferon gamma (*IFNG*, Figure 6.6 F) showed the opposite trend, with expression of IFNG appearing highly suppressed in 2D-cultured cells. Untreated control cells showed a statistically significant increase in CNRQ from 0.001 in 2D to 1.00 in 3D ($p = 0.0004$), and in combined LPS / GW1929-exposed cells (CNRQ = 0.0045 in 2D and 0.57 in 3D, $p = 0.0273$).

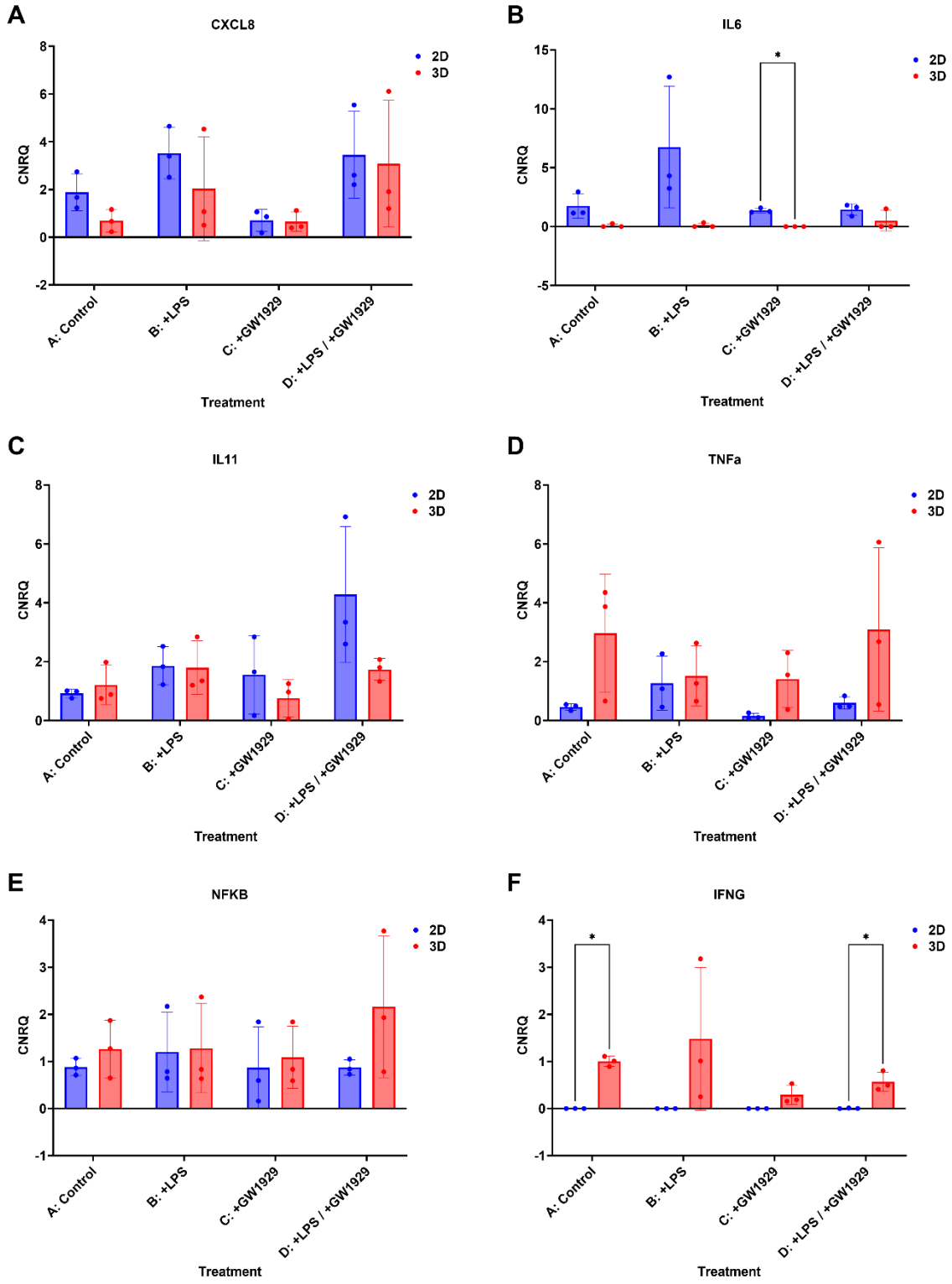


Figure 6.6 – Comparison of inflammation-related gene expression in monolayer (blue) and organotypic (red) H400 cells.
A) *CXCL8* (interleukin 8)
B) *IL6* (interleukin 6)
C) *IL11* (interleukin 11)
D) *TNFA* (tumour necrosis factor alpha)

E) *NFKB* (nuclear factor kappa beta)
F) *IFNG* (interferon gamma)
N=3, mean calibrated normalised relative quantity (CNRQ) ±SD, multiple unpaired t-tests with Holm-Šídák method. Alpha = 0.05. * = $p < 0.05$.

Expression of the peroxisome proliferator activated receptor gamma (*PPARG*, Figure 6.7 A) appeared relatively stable between 2D and 3D-cultured H400 cells at all tested conditions, with no statistically significant difference detected. Aquaporin (*AQP3,* Figure 6.7 B) expression was only significantly different in LPS and GW1929-stimulated cultures, where 3D-cultured cells showed greater expression (CNRQ = 1.69) than those cultured in 2D (CNRQ = 0.37) ($p = 0.0199$). Expression of prostaglandin-endoperoxide synthase 2 (*PTGS2*, Figure 6.7 *C*) was only statistically significant in cells exposed to GW1929, increasing from a CNRQ of 0.15 in 2D to 2.79 in 3D ($p = 0.0040$).

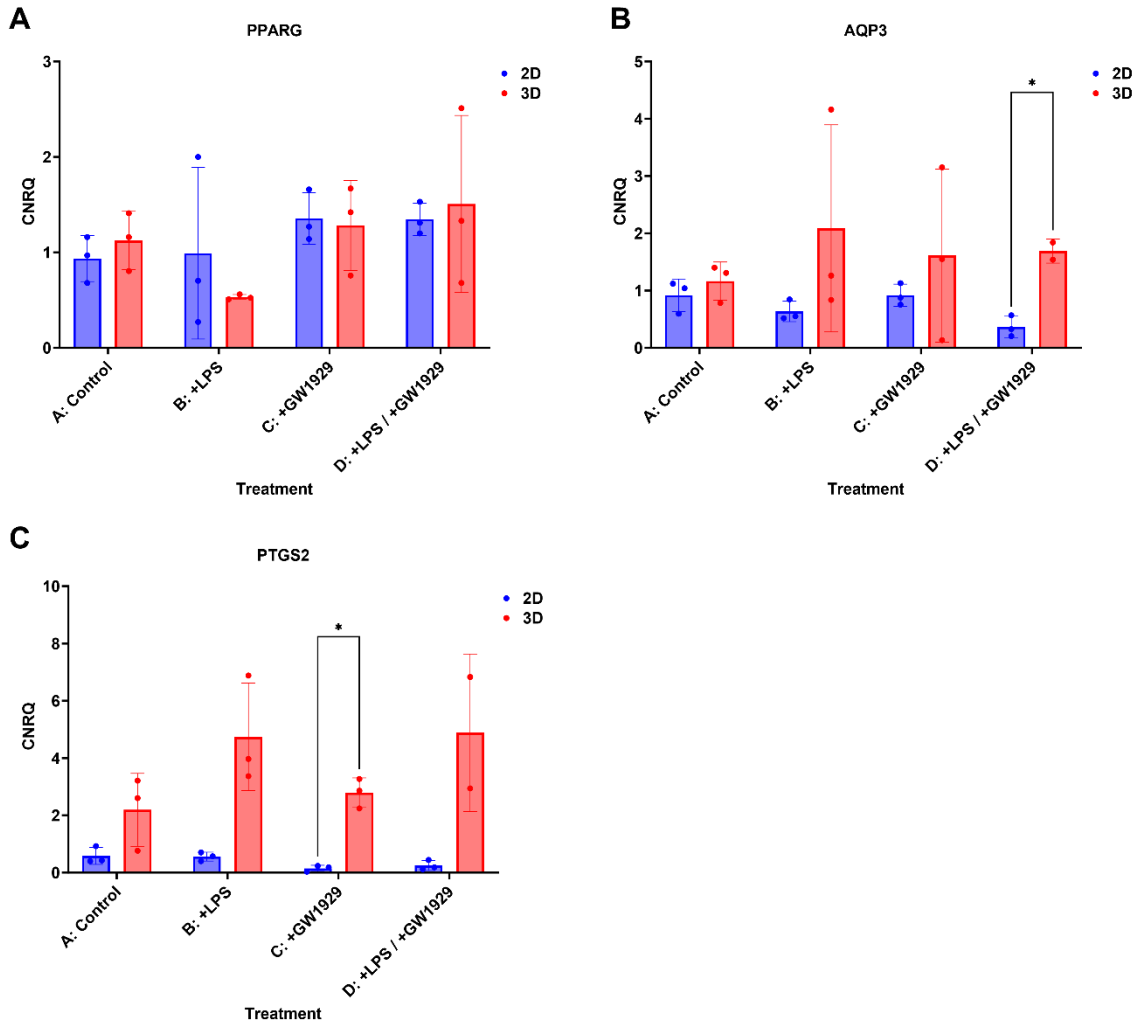


Figure 6.7 - Comparison of PPARγ and PPRE gene expression in monolayer (blue) and organotypic (red) H400 cells.
A) *PPARG* (peroxisome proliferator activated receptor gamma)
B) *AQP3* (aquaporin 3)
C) *PTGS2* (prostaglandin-endoperoxide synthase 2)
N=3, mean calibrated normalised relative quantity (CNRQ) ±SD, multiple unpaired t-tests with Holm-Šídák method. Alpha = 0.05. * = $p < 0.05$.

Expression of E-cadherin (CDH1) was significantly lower in organotypically cultured cells than monolayer cultured cells, in both the control group and cells exposed to LPS. In control cells, expression decreased from a CNRQ of 3.76 to 0.285 ($p = 0.0367$), and in LPS exposed cells expression decreased from a CNRQ of 4.78 to 0.52 ($p = 0.0367$). No significant change in expression was recorded for cells exposed to GW1929 and combined LPS / GW1929 treatment ($p = 0.2525$ for both). Occludin (*OCLN*) expression was shown to be significantly greater in organotypic cultures when exposed to LPS and GW1929 than in monolayer cultures, with an increase in CNRQ from 0.73 to 1.66 ($p = 0.0161$). JAM3 expression (Figure 6.8 F) appeared highly suppressed in 2D cultured cells compared with 3D cultures, though this was not a statistically significant finding ($p > 0.05$). No other tested barrier function genes showed statistically significant changes in expression between monolayer and organotypic cultures across any treatment condition.

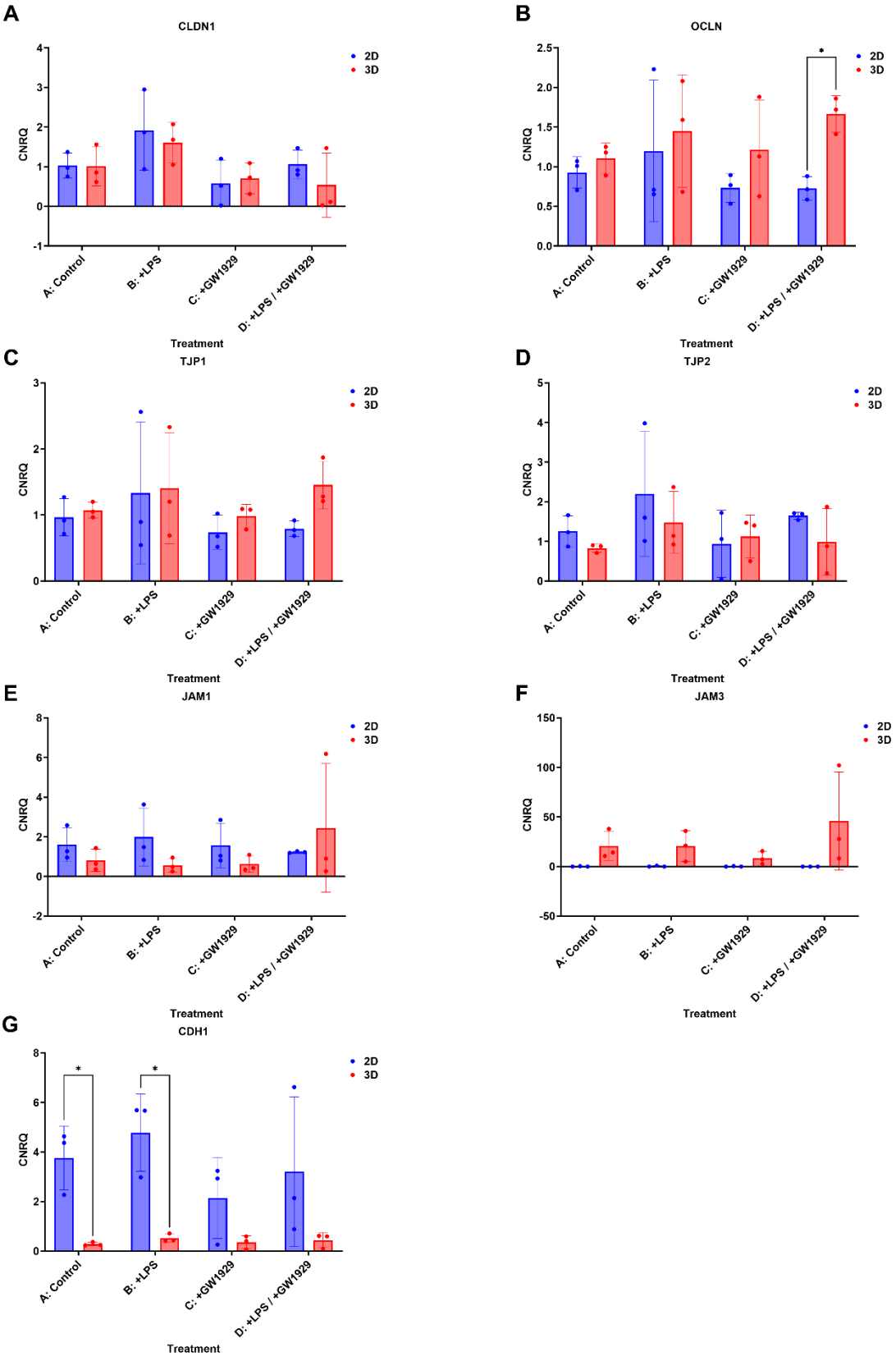


Figure 6.8 - Comparison of barrier function related gene expression in monolayer (blue) and organotypic (red) H400 cells.
A) *CLDN1* (claudin 1)

B) *OCLN* (occludin)
C) *TJP1* (tight junction protein 1 / zona occludens 1)
D) *TJP2* (tight junction protein 2 / zona occludens 2)
E) *JAM1* (junctional adhesion molecule 1)
F) *JAM3* (junctional adhesion molecule 3)
G) CDH1 (e-cadherin)
N=3, mean calibrated normalised relative quantity (CNRQ) ±SD, multiple unpaired t-tests with Holm-Šídák method. Alpha = 0.05. * = p < 0.05.

A reduction in expression of cytokeratin 10 (KRT10) was only statistically significant in the control group (Figure 6.9 A), where expression fell in 3D cultures from a CNRQ of 1.82 to 0.63 (p = 0.0384). Changes in expression of involucrin (IVL) was not statistically significant in any treatment group (Figure 6.9 B).

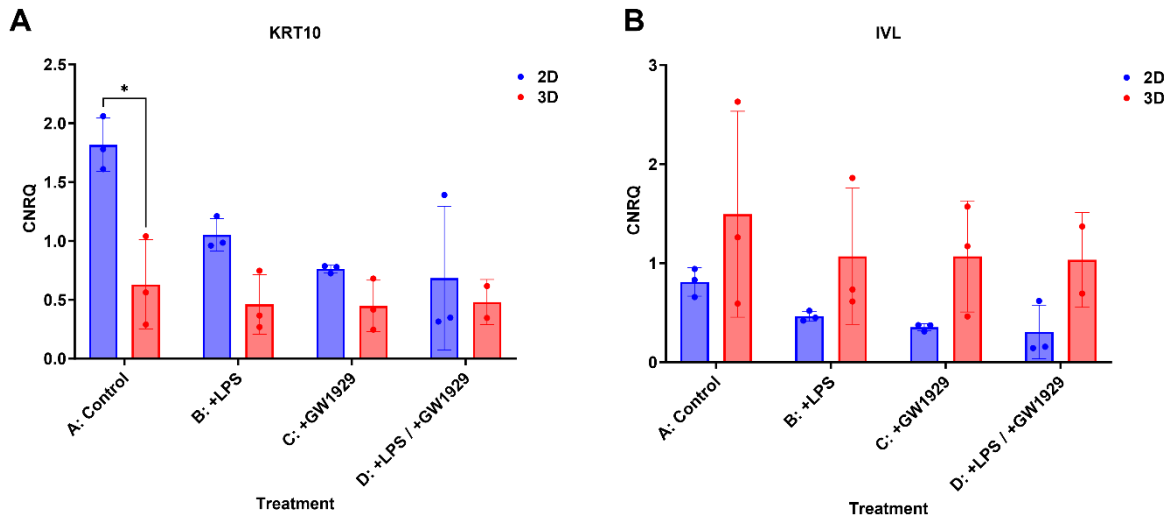


Figure 6.9 - Comparison of epithelial differentiation marker gene expression in monolayer (blue) and organotypic (red) H400 cells.
A) *KRT10 (*Cytokeratin 10*)*
B) *IVL* (Involucrin)
N=3, mean calibrated normalised relative quantity (CNRQ) ±SD, multiple unpaired t-tests with Holm-Šídák method. Alpha = 0.05. * = p < 0.05.

6.3. Barrier function assays in LPS-challenged H400 cells treated with a PPARγ agonist

Following the studies of gene and protein expression in monolayer and organotypically cultured H400 OSCC cells, barrier function studies were conducted. TEER and FITC-dextran macromolecular tracer (MMT) assays were performed on cells again challenged as previously described with LPS (2 μg/ml) for 24 hours, and then treated with LPS (2 μg/ml) in conjunction with the PPARγ agonist GW1929 (5 μM) for a further 24 hours. MMT and TEER assays were limited by a sample size of 2, preventing statistical analysis.

MMT assays performed on monolayer (2D) cell cultures indicated a 34% increase in tracer flux (measured as fluorescence) in LPS stimulated cells compared with the control (Figure 6.10 A). TEER performed on the same cells (Figure 6.10 B) showed a 30% reduction in mean electrical resistance from 192 $\Omega.cm^2$ in control cells, to 151 $\Omega.cm^2$ following LPS stimulation. This impact on barrier function was not reduced in cells exposed to LPS and GW1929 when assessed by MMT, with similar recorded fluorescence levels for LPS and LPS+GW1929 cells. However, TEER values for cells exposed to LPS+GW1929 returned to close to the baseline set by the control, indicating a recovery of barrier function.

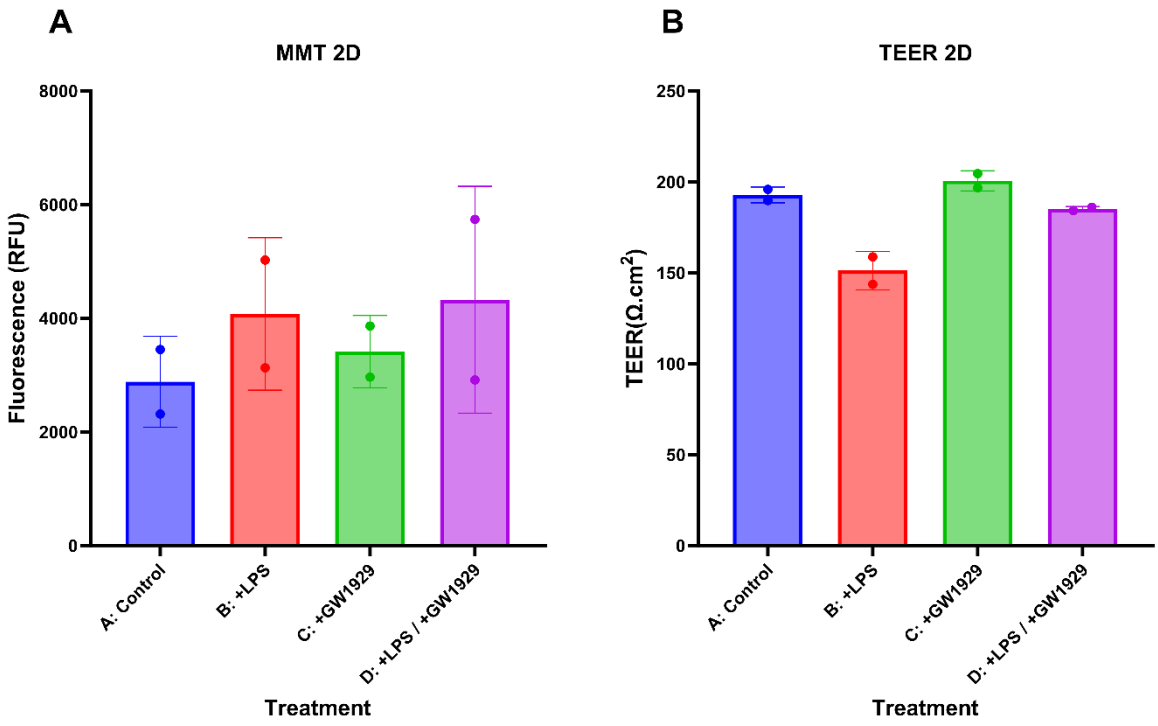


Figure 6.10 – Barrier function assays performed in monolayer H400 cells exposed to 2 µg/ml LPS and the PPARγ agonist GW1929 (5 µM). Cells were exposed to LPS for 24 hours, followed by a further 24 hours of LPS +/- GW1929 exposure.
A) FITC-dextran macromolecular tracer assay (MMT), showing a slight increase in fluorescence in LPS-treated cells compared with the control, with a similar level of fluorescence recorded in cells exposed to LPS and GW1929.
B) Transepithelial electrical resistance (TEER) measurements performed on the same samples. A decrease in TEER is noted in cells exposed to LPS alone, compared to control cells. An increase is also noted from LPS-exposed cells to cells treated with LPS and GW1929, suggesting a recovery in barrier function with GW1929 treatment.
N=2, mean ±SD, no statistical tests performed due to sample size.

TEER assays performed on organotypically (3D) cultured H400 cells using the BECD system reflected the same trends shown in TEER performed on monolayer H400 cells. TEER in untreated control cultures was recorded as 319 $\Omega.cm^2$, falling to 305 $\Omega.cm^2$ following LPS exposure. Cell cultures exposed to LPS and GW1929 generated TEER readings of 329 $\Omega.cm^2$.

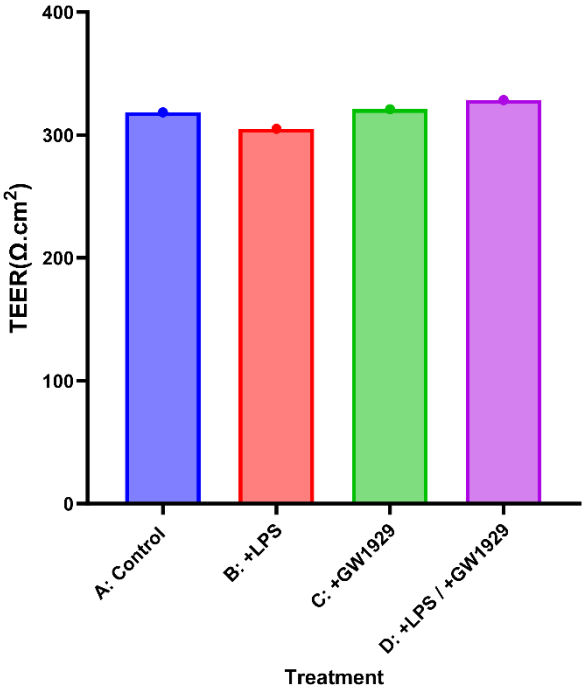


Figure 6.11 - TEER assay performed on organotypically cultured H400 cells exposed to 2 µg/ml LPS and the PPARγ agonist GW1929 (5 µM). Cells were exposed to LPS for 24 hours, followed by a further 24 hours of LPS +/- GW1929 exposure.
N=1, no statistical tests performed due to sample size.

6.4. Discussion

RT-qPCR of monolayer-cultured H400 cells exposed to *E. coli* LPS and the PPARγ agonist GW1929 (Figure 6.1) revealed interesting changes in inflammation-linked gene expression in monolayer H400 cells. The pro-inflammatory cytokine interleukin 6 (*IL6*) was significantly upregulated in LPS-treated H400 cells compared to control H400 cells, with PPARγ activation reducing this back to baseline levels, suggesting that PPARγ activation may act to ameliorate some of the inflammatory signalling induced by LPS. This finding was supported by previous studies showing that interleukin 6 gene expression can be significantly reduced

by PPARγ activation in LPS-stimulated cutaneous keratinocytes (Mastrofrancesco *et al.*, 2014).

Inversely, expression of the anti-inflammatory cytokine interleukin 11 (*IL11*) was shown to be significantly upregulated in H400 cells exposed to LPS and GW1929 simultaneously when compared with both untreated control cells and LPS-only cells. Interleukin 11 has been shown to strongly dampen the inflammatory response, reducing the expression of *TNFA* and *IL6* in macrophages (Schwertschlag *et al.*, 1999), though no effect was seen on TNFα expression in the present work. No studies were identified which directly examined the influence of PPARγ activation on interleukin 11 expression, though interleukins 6 and 11 have been shown to exist within the same family and share activation pathways (Garbers and Scheller, 2013), suggesting that PPARγ may modulate the expression of both interleukins via a common mechanism.

Enzyme-linked immunosorbent assays (ELISAs) were performed to identify how the changes in *IL6* and *IL11* gene expression translated to expression at the protein level. Unfortunately, IL6 ELISA failed to quantify IL6 protein across multiple repetitions of the protocol and any tested culture condition (Figure 6.2 and

Table **6.1**). This observation has previously been reported when studying IL6 production in H400 OSCC cells stimulated with heat killed bacteria (Grant *et al.*, 2023 - supplemental information), suggesting an issue with the export of IL6 protein from H400 cells, or a failure of the ELISA antibodies to detect IL6 produced by these cells. Such an issue was not noted with IL11 ELISAs, but no significant change in expression was noted with any tested condition. Overall, RT-qPCR studies for interleukins 6 and 11 suggested that PPARγ stimulation with GW1929 may reduce pro-inflammatory cytokine gene expression, while

simultaneously increasing anti-inflammatory cytokine expression in monolayer H400 cells. However, the possible immunomodulatory effect of PPARγ activation was not reflected in the gene expression of *CXCL8* and *TNFA*, as has been reported in both cutaneous keratinocytes (Mastrofrancesco *et al.*, 2014) and other cells (Ohama *et al.*, 2008). These distinctions may be due to differences in *CXCL8* and *TNFA* expression and regulation in oral gingival epithelial cells, or due to the study design, including differences in the inflammatory stimulus or PPARγ agonists used.

Interestingly, the gene expression responses shown by *CXCL8*, *IL6* and *IL11* cultured as a monolayer (Figure 6.1) were not seen in H400 cells cultured organotypically in the BECD system (Chapter 5) with no significant differences between any tested conditions in any gene (Figure 6.5). Comparison of inflammation-linked gene expression in monolayer (2D) and organotypic (3D) culture (Figure 6.6) suggests a marked difference in response to the LPS stimulus between these models. For example, *IL6* expression appeared heavily suppressed in 3D-cultured cells (Figure 6.6 B), while inversely interferon gamma (*IFNG)* expression was found to be significantly suppressed in 2D-cultured cells (Figure 6.6 F). Indeed, *IFNG* is not typically expressed in keratinocytes (Jiang *et al.*, 2020), suggesting that organotypic culture may have altered the transcriptional profile of the tested H400 OSCC cells. This effect was also shown in the expression of *PTGS2*, a possible response element of PPARγ (Hotta *et al.*, 2010). These data suggested that the transcriptional response of monolayer and organotypically cultured H400 cells to LPS was markedly different, and the LPS concentration used in these assays failed to produce a suitably strong inflammatory stimulus in organotypic cell cultures.

It is possible that the concentration of LPS used was too low to induce inflammatory signalling due to the greater number of cells found in organotypic cultures than monolayers, resulting from the more complex tissue architecture found in these models. Moreover, previous work has shown that the innate immune responses of airway epithelial cells are dependent on cellular differentiation state (Chan *et al.*, 2010). It is possible that the presence of differentiated epithelial cells in ALI cultures (as shown in Chapter 5, Section 5.5) may lead to modified immune responses compared to undifferentiated monolayer epithelial cells. Furthermore, the collagen hydrogel itself may act as a reservoir by absorbing LPS and reducing the concentration of LPS accessible by epithelial cells. It is suggested that further studies in LPS-exposed organotypic cultures may benefit from screening a wider range of LPS concentrations to identify how organotypic models may reduce the efficacy of LPS as an inflammatory stimulus, when compared with monolayer cells.

In addition to using a relatively low LPS concentration, a further limitation of the present work was the use of long treatment periods prior to RNA isolation for RT-qPCR. The studies performed in Sections 6.2 and 6.3 employed a 24-hour LPS pretreatment, followed by a further 24 hours of LPS with PPARγ agonist exposure, mimicking the possible clinical application of PPARγ agonists to treat inflamed gingival epithelial tissues *in vivo*. This relatively long period of LPS exposure prior to RNA or protein isolation may result in a failure to detect changes in the expression of some genes, wherein expression has begun to normalise, so shorter treatment periods may be more appropriate in future studies. The use of 48 hours of overall LPS exposure also prevents any comparison between the studies presented in the present chapter and Chapter 3.

With regards to epithelial barrier function, E-cadherin (*CDH1*) occludin (*OCLN*), claudin (*CLDN1*), junctional adhesion molecule 1 (*JAM1*) and zona occludens 1 and 2 (ZO-1/2,

TJP1/2) showed no significant changes in expression under any tested treatment condition, in both monolayer (Figure 6.1) and organotypic culture (Figure 6.5). However, in 3D cultures, expression of *JAM3* was significantly greater following dual LPS/GW1929 treatment than in any other condition. Direct comparison between expression of barrier function genes in monolayer and organotypic cultures (Figure 6.8) revealed significantly greater expression of E-cadherin (*CDH1*) in monolayers than stratified epithelia. This finding was unexpected, as it was hypothesised that stratified epithelia would show greater *CDH1* expression due to the involvement of E-cadherin both stratification beyond 5-7 cell layers (Jensen *et al.*, 1997) and tight junction formation in the epidermis (Tunggal *et al.*, 2005). However, this finding may be explained by the close proximity between near-confluent cells leading to the initial formation of intracellular junctions, upregulating E-cadherin.

It was also hypothesised that expression of some or all tight junction genes (claudin, ZO-1/2 and occludin) would be greater in organotypic cultures than monolayer due to the formation of a greater number of tight junctions throughout the epithelial layers. However, no significant difference was seen in transcript expression, or in protein expression, as assessed using western blots and depicted in Figure 6.4 (excluding ZO-2, for which western blotting was not performed). This finding may be due to the presence of a consistent ratio of tight junctions per cell between monolayer and organotypically cultured epithelial cells, resulting in no significant difference when expression was normalised to expression of housekeeping genes or loading control proteins. Expression of ZO-1 RNA has previously been shown to be significantly downregulated by 1 µg/ml LPS in endothelial cells (Zou *et al.*, 2022), but not in intestinal epithelial cells treated with the same LPS concentration (He *et al.*, 2019) or at 10 µg/ml (Omonijo *et al.*, 2019), suggesting such a response may be dependent on cell type. No studies of ZO-1 expression following PPARγ stimulation were identified, particularly in

epithelial cells. However, *in vivo* studies in rats identified an increase in peritoneal epithelial cell ZO-1 expression following injection with rosiglitazone, a TZD-class PPARγ agonist (Zhang *et al.*, 2018), a finding which was not reflected in the present work. Expression of occludin (Guo *et al.*, 2018; He *et al.*, 2019) and claudin (Wu *et al.*, 2020) have been shown to be significantly reduced in intestinal epithelial cells following treatment with LPS. Studies of rat periodontal sulcular epithelium exposed to LPS have shown reduced expression of claudin and a corresponding reduction in TEER (Fujita *et al.*, 2012). While no studies were identified examining the effect of PPARγ stimulation following LPS exposure, studies of nasal epithelial cells demonstrated upregulation of both occludin and claudin following treatment with PPARγ agonists (Ogasawara *et al.*, 2010). These studies suggest that treatment with PPARγ agonists may upregulate barrier function genes in some models. Whilst this effect was not observed in RT-qPCR or western blot studies in the present work, previous studies employing 50 µg/ml LPS have shown modification of the spatial arrangement of ZO-1 within tight junctions, correlating with increased TJ permeability (Richter *et al.*, 2016), suggesting that LPS may physically disrupt TJs. This suggests that the anti-barrier function effect of LPS may not be mediated purely by LPS-induced downregulation of TJ-critical genes, thought this possible TJ rearrangement has not been explored in the present work.

Nonetheless, even in the absence of significant changes in barrier function genes and proteins, TEER barrier function assays in monolayer cells suggested an amelioration of LPS-induced barrier function damage in cells exposed to PPARγ agonist (Figure 6.10 B). TEER was seen to decrease in LPS-exposed cells (suggesting a reduction in barrier function), but cells exposed to LPS and the PPARγ agonist GW1929 generated a TEER value close to that seen in the control cell population, suggesting barrier function was maintained. This effect may

have been reflected in TEER assays performed in organotypically cultured H400 cells, as shown in Figure 6.11, though the N = 1 data prevent any useful conclusions. TEER values for organotypic cultures were generally greater than those generated by monolayer cell cultures by approximately 100 $\Omega.cm^2$, as was expected due to the presence of a stratified epithelium and a collagen hydrogel. Again, TEER was greater in cells exposed to LPS and GW1929 than in cells exposed to LPS alone, suggesting that PPARγ activation may reduce LPS-induced epithelial barrier function damage.

Interestingly, while this trend was consistently noted throughout TEER studies in both monolayer and organotypic cultures, it was not observed in FITC-dextran MMT assays on monolayer cells. As shown in Figure 6.10 A, MMT fluorescence was recorded as being approximately equal in LPS and LPS+GW1929 cultures, suggesting that PPARγ activation had no impact on LPS-induced reduction in barrier function. However, these data should be cautiously analysed due to the use of only two biological replicates. This trend in barrier permeability was also shown in an MMT assay of organotypically cultured H400 cells (Figure 6.11), though the single biological replicate of this experiment limits the usefulness of these data. It has been suggested that the dual-mode action of tight junctions in forming both charge and size-selective channels (Krug, Schulzke and Fromm, 2014) may lead to different observed responses in TEER (assessing ion flux) and MMT assays (assessing macromolecule flux). Further work may be performed with a range of different inflammatory stimuli or incorporating macromolecular tracers of different sizes, aiming to identify how this may influence experimental outcomes. For example, lucifer yellow has been widely used for MMT assays (Zhao *et al.*, 2019) in the same way that FITC-dextran was applied in the present work. With a molecular weight of 457 Da (Gomes *et al.*, 2016), it is possible that barrier function

assays with lucifer yellow may generate different responses than assays performed with larger molecules such as FITC-dextran.

In conclusion, studies conducted within the present chapter have identified the possible role of PPARγ activation in reducing pro-inflammatory cell signalling and barrier function damage in LPS-stimulated gingival epithelial cells. However, the mechanism for the pro-barrier effect of PPARγ in the present work is still unclear and may be elucidated with further work. These studies have also highlighted the importance of studies comparing the responses between organotypically cultured cells and simple monolayers, with the present work showing marked differences shown in the immune response to bacterial LPS between these conditions.

7. CONCLUSIONS AND FUTURE WORK

7.1. Summary of findings

Gingivitis and periodontitis are highly prevalent periodontal diseases, causing a reduction in quality of life and requiring significant resources from healthcare systems (Batchelor, 2014). These periodontal diseases are inflammatory in nature, triggered by a build-up of plaque biofilm, but perpetuated by an aberrant, overactive host immune response. Conventional treatment options for the early stage of gingivitis prior to progression to periodontitis typically involve patient education of proper oral hygiene routines. The success of patient education is highly variable and dependent on the quality of advice given by the dental professional (Newton and Asimakopoulou, 2015). Pharmacological interventions for gingivitis are remarkably rare. For example, antibiotic therapy is typically only prescribed in cases of necrotizing ulcerative gingivitis (Malek *et al.*, 2017). NSAIDs have been studied to reduce gingival inflammation with the goal of preventing the inflammatory damage to deeper tissues, though issues with dose application and side effects have been noted (Heasman and Hughes, 2014).

The present work aimed to initially model and characterise gingival inflammation *in vitro*, using simple monolayer cultures and bacterial LPS. The nuclear hormone receptor PPARγ, implicated in a diverse range of inflammatory pathways, was chosen as a potential therapeutic target, with the aim of identifying the role of PPARγ activation on both inflammation and barrier function. Initial studies presented in Chapter 2.10 showed no change in growth rate or viability was noted at any of the tested LPS concentrations, even with chronic exposure for up to 9 days, suggesting the tested concentrations are non-toxic. Barrier function testing showed a reduction in TEER and increase in macromolecule flux (assessed by FITC-dextran MMT assay), suggesting a reduction in barrier function with LPS stimulation. Gene expression

analysis with RT-qPCR indicated increases in pro-inflammatory cytokine gene expression, and a possible reduction in barrier function-linked genes.

With strong evidence that LPS induced inflammation and reduced barrier function in H400 OSCC cells, studies were then conducted to identify the function of PPARγ in ameliorating some of this damage. Prior to combing LPS-stimulated cells with PPARγ agonists, it was important to first verify that the chosen cell line expressed PPARγ, as expression has previously been shown to be highly tissue specific (Chawla, 1994; Fajas *et al.*, 1997). Analysis with western blotting and semi-quantitative RT-PCR identified expression of two isoforms of PPARγ, γ1 and γ2 (Section 0). Two PPARγ reporter cell lines were then generated by genetic modification with plasmid transfection, introducing PPARγ-response element promoters linked to nuclear-localised eGFP (PPRE-H2B-eGFP, Section 4.3) and secreted luminescent (PPRE-pNL1.3, Section 4.4) protein expression. Studies with the PPRE-H2B-eGFP reporter system were halted due to issues with quantification, but PPRE-pNL1.3-transfected cells were successfully used to show that the synthetic PPARγ ligand GW1929 significantly activated PPARγ in H400 cells.

Following this, LPS-challenged monolayer H400 cells were treated with GW1929, generating a reduction in pro-inflammatory cytokine gene expression, an increase in anti-inflammatory gene expression (Section 6.2), and a possible reduction in damage to epithelial barrier function compared with cells exposed to LPS alone (Section 6.3). These findings further validated the hypothesis that PPARγ stimulation could act to reduce the negative effects of LPS in gingival epithelial cells.

Additional work was then performed to identify how the response of such cells may differ when cultured organotypically, compared with simple monolayer assays. Previous work has

shown that organotypic culture is important for generating representative genotypical models of epithelial tissue (Pezzulo *et al.*, 2011), which are typically cultured using an air-liquid interface (ALI) model. As part of the present work, a novel ALI culture device was conceptualised and developed for use in *in vitro*. This 3D-printed buoyant epithelial culture device (BECD) was designed to float in culture media whilst retaining a fibroblast-seeded collagen hydrogel, mimicking the sub-dermal tissues, with an epithelial layer seeded atop. These devices eliminated the requirement for manual ALI maintenance and aimed to improve both ease of use and experimental reproducibility. The device design and geometry was extensively tested (Section 5.2) and trialled with a variety of polymers to identify a suitable material for device fabrication. Polypropylene was found to be the most suitable polymer, both mechanically following autoclave sterilisation, and biologically, generating highly stratified epithelia after ALI culture (Section 5.3). Automated extraction and quantification revealed these epithelia significantly increased in epithelial thickness between 7, 14 and 21 days of ALI culture, with no significant variation between epithelial thickness as the edge of the hydrogel (Section 5.4). Immunofluorescence staining of these sections revealed appropriately localised expression of key epithelial differentiation markers involucrin, cytokeratin 5 and E-cadherin (Section 5.5). These studies suggested that the BECD system enabled the production of highly stratified, well differentiated organotypic models of the gingival epithelia.

These organotypic models were then applied to the same LPS-challenged, PPARγ-agonist treatments as previously described for monolayer studies. Interestingly, quantitative RT-PCR demonstrated minimal pro-inflammatory cytokine production following LPS addition, suggesting marked differences in immune response between monolayer and organotypic cultures (Section 6.2.3). These studies indicated that higher LPS doses may be required to

offset the higher cell numbers found in organotypic cultures compared with monolayers, or that differentiated epithelial cultures may respond differently to LPS than undifferentiated monolayers. Whilst preventing in-depth analysis of cytokine expression in organotypic cultures, this interesting finding may be explored in future work.

Overall, the present work provides evidence of the involvement of PPARγ in models of LPS-induced gingivitis and presents a translational opportunity to identify how the inclusion of PPARγ ligands in oral care projects could limit gingival inflammation.

7.2. Future work

Whilst the present work has provided evidence for the role of PPARγ in reducing gingival inflammation and improving barrier function, there remain some limitations and the potential for further studies to be undertaken:

- Within the present work, the role of LPS as an inducer of inflammation was extensively explored. However, LPS is one of many such pro-inflammatory agents implicated in periodontal disease, and other agents may alter the response of inflamed gingival epithelia to PPARγ stimulation, as described throughout this thesis. The inclusion of relevant planktonic bacteria or bacterial biofilm may generate a more representative model of the periodontal environment *in vivo*.
- While the generation of a PPARγ reporter system in oral epithelial cells was successful, paradoxical activation of PPARγ with a widely documented PPARγ antagonist (GW9662) was also observed. Although this did not appear to interfere with the ability of the reporter system to respond to agonists, this was still an unexpected finding. Initial analyses of this problem by sequencing the relevant section of the PPARγ gene did not find any mutation or frameshifts, suggesting that further

investigation is needed. Studies with other PPARγ antagonists may be performed to identify if this effect is specific to GW9662. Additionally, the present work identified a higher-than-expected ratio of expression between PPARγ isoforms γ1 and γ2. As these two isoforms have been shown to have differences in their activation function domains, isoform specific knock-down of one isoform would enable studies to identify the role of these two isoforms in models of gingivitis.

- Within PPARγ reporter studies, basal PPARγ activity was consistently high, potentially masking the effects of cosmetic compounds screened for PPARγ activation. The use of a cell type with lower basal PPARγ activity may provide a more suitable system for screening such compounds.
- Throughout the present work, H400 oral squamous cell carcinoma cells were the predominant cell line studied due to their relevancy and ease of use in the laboratory. While these cells were initially isolated from the alveolar mucosa, H400 cells are cancer derived, which may generate non-representative findings. Further work may employ either a more suitable immortalised gingival cell line, or primary cells derived from patient tissue.
- Finally, the overarching goal of the present work was to identify how the response of gingival epithelial cells differs between monolayer cultures and stratified, organotypic models. Initial work identified PPARγ activation was able to reduce the expression of LPS-induced inflammatory cytokines and reduce barrier function damage. However, replication of these data in organotypic models was limited by the generation of a sub-optimal inflammatory response. Further work could investigate this phenomenon by exploring higher concentrations of LPS, adding whole bacteria, or attempting to

identify how differentiated epithelial cells may respond differently to inflammatory stimuli than undifferentiated cells.

7.3. Concluding remarks

In conclusion, this work has generated evidence that bacterial lipopolysaccharide stimulates a significant immune response and reduction in barrier function in monolayer gingival epithelial cells. Additionally, activation of the nuclear hormone receptor PPARγ was shown to reduce these inflammatory markers and reduce LPS-induced barrier function damage. A novel, 3D-printed *in vitro* culture system was developed within the present work. These buoyant epithelial culture devices (BECDs) were shown to generate stratified, organotypic gingival epithelia with epithelial differentiation markers present and correctly localised. This system has significant utility in a range of *in vitro* studies of stratified epithelial tissues. Within the present work, it was applied to the same LPS-challenge trials as used for monolayer cultures. Interestingly, LPS generated a sub-optimal inflammatory response in these organotypic cultures, suggesting a marked difference in response compared with monolayer cultures. These findings may provide the basis for the use of isoform specific, topically applied PPARγ agonists in the treatment of gingivitis, reducing the excessive immune inflammatory response and loss of barrier function which can lead to periodontal ligament damage and eventual tooth loss.

8. LIST OF REFERENCES

Abdulkareem, A. A. *et al.* (2018a) 'Periodontal pathogens promote epithelial-mesenchymal transition in oral squamous carcinoma cells in vitro', *Cell Adhesion and Migration*, 12(2), pp. 127–137. doi: 10.1080/19336918.2017.1322253.

Abdulkareem, A. A. *et al.* (2018b) 'Potential role of periodontal pathogens in compromising epithelial barrier function by inducing epithelial-mesenchymal transition', *Journal of Periodontal Research*, 53(4), pp. 565–574. doi: 10.1111/jre.12546.

Abe-Yutori, M. *et al.* (2017) 'Decreased expression of E-cadherin by Porphyromonas gingivalis-lipopolysaccharide attenuates epithelial barrier function', *Journal of Periodontal Research*, 52(1), pp. 42–50. doi: 10.1111/jre.12367.

Alexander, F. A., Eggert, S. and Wiest, J. (2018) 'Skin-on-a-Chip: Transepithelial Electrical Resistance and Extracellular Acidification Measurements through an Automated Air-Liquid Interface', *Genes 2018, Vol. 9, Page 114*, 9(2), p. 114. doi: 10.3390/GENES9020114.

Al-Shehri, S. S. (2021) 'Reactive oxygen and nitrogen species and innate immune response', *Biochimie*, 181, pp. 52–64. doi: 10.1016/j.biochi.2020.11.022.

Angrisano, T. *et al.* (2010) 'LPS-induced IL-8 activation in human intestinal epithelial cells is accompanied by specific histone H3 acetylation and methylation changes', *BMC Microbiology*, 10(1), pp. 1–8. doi: 10.1186/1471-2180-10-172/FIGURES/4.

Aranda, A. and Pascual, A. (2001) 'Nuclear Hormone Receptors and Gene Expression', *Physiological Reviews*, 81, pp. 1269–1304.

Arany, P. *et al.* (2021) 'Biocompatibility and Dissolution Profile of FDM 3D Printed PETG Tablets', *Acta Pharmaceutica Hungarica*, 91(3–4), pp. 171–172. doi: 10.33892/aph.2021.91.171-172.

Armitage, G. C. (2004) 'The complete periodontal examination', *Periodontology 2000*, 34, pp. 22–33.

Asadi, M. *et al.* (2022) 'Caspase-3: Structure, function, and biotechnological aspects', *Biotechnology and Applied Biochemistry*, 69(4), pp. 1633–1645. doi: 10.1002/BAB.2233.

Atanasov, A. G. *et al.* (2013) 'Honokiol: A non-adipogenic PPARγ agonist from nature', *Biochimica et Biophysica Acta (BBA) - General Subjects*, 1830(10), pp. 4813–4819. doi: 10.1016/J.BBAGEN.2013.06.021.

Aufderheide, M. and Mohr, U. (2000) 'CULTEX - An alternative technique for cultivation and exposure of cells of the respiratory tract to airborne pollutants at the air/liquid interface', *Experimental and Toxicologic Pathology*, 52(3), pp. 265–270. doi: 10.1016/S0940-2993(00)80044-5.

Axelsson, P., Paulander, J. and Lindhe, J. (1998) 'Relationship between smoking and dental status in 35-, 50-, 65-, and 75-year-old individuals', *Journal of Clinical Periodontology*, 25(4), pp. 297–305. doi: 10.1111/J.1600-051X.1998.TB02444.X.

Bacakova, M. *et al.* (2019) 'A two-layer skin construct consisting of a collagen hydrogel reinforced by a fibrin-coated polylactide nanofibrous membrane', *International Journal of Nanomedicine*, 14, p. 5033. doi: 10.2147/IJN.S200782.

Bahekar, A. A. *et al.* (2007) 'The prevalence and incidence of coronary heart disease is significantly increased in periodontitis: A meta-analysis', *American Heart Journal*, 154(5), pp. 830–837. doi: 10.1016/J.AHJ.2007.06.037.

Bain, D. L. *et al.* (2007) 'Nuclear Receptor Structure: Implications for Function', *Annual Review of Physiology*, 69(1), pp. 201–220. doi: 10.1146/annurev.physiol.69.031905.160308.

Bals, R. *et al.* (2004) 'Isolation and air–liquid interface culture of human large airway and bronchiolar epithelial cells', *Journal of Cystic Fibrosis*, 3(SUPPL. 2), pp. 49–51. doi: 10.1016/J.JCF.2004.05.010.

Bandyopadhyay, U., Das, D. and Banjeree, R. K. (1999) 'Reactive oxygen species: Oxidative damage and pathogenesis on JSTOR', *Current Science*, 77(5), pp. 658–666. Available at: https://www.jstor.org/stable/24102839 (Accessed: 2 September 2022).

Baniahmad, A. (2005) 'Nuclear hormone receptor co-repressors', *The Journal of Steroid Biochemistry and Molecular Biology*, 93(2–5), pp. 89–97. doi: 10.1016/J.JSBMB.2004.12.012.

Banks-Schlegel, S. and Green, H. (1981) 'Involucrin synthesis and tissue assembly by keratinocytes in natural and cultured human epithelia', *The Journal of cell biology*, 90(3), pp. 732–737. doi: 10.1083/JCB.90.3.732.

Barosova, H. *et al.* (2021) 'Inter-laboratory variability of A549 epithelial cells grown under submerged and air-liquid interface conditions', *Toxicology in Vitro*, 75. doi: 10.1016/J.TIV.2021.105178.

Bartold, P. M., Walsh, L. J. and Narayanan, A. S. (2000) 'Molecular and cell biology of the gingiva', *Periodontology 2000*, 24(1), pp. 28–55. doi: 10.1034/J.1600-0757.2000.2240103.X.

Batchelor, P. (2014) 'Is periodontal disease a public health problem?', *British Dental Journal*, 217(8), pp. 405–409. doi: 10.1038/sj.bdj.2014.912.

Bateman, A. *et al.* (2023) 'UniProt: the Universal Protein Knowledgebase in 2023', *Nucleic Acids Research*, 51(D1), pp. D523–D531. doi: 10.1093/NAR/GKAC1052.

Batista, A. *et al.* (2023) 'Chia (Salvia hispanica L.) oil supplementation ameliorates liver oxidative stress in high-fat diet-fed mice through PPAR-γ and Nrf2 upregulation', *Journal of Functional Foods*, 102, p. 105462. doi: 10.1016/J.JFF.2023.105462.

Baum, C. *et al.* (2006) *Mutagenesis and Oncogenesis by Chromosomal Insertion of Gene Transfer Vectors, HUMAN GENE THERAPY*. Available at: www.liebertpub.com.

Bein, A. *et al.* (2017) 'LPS Induces Hyper-Permeability of Intestinal Epithelial Cells', *Journal of Cellular Physiology*, 232(2), pp. 381–390. doi: 10.1002/JCP.25435.

Belibasakis, G. N. *et al.* (2015) 'The expression of gingival epithelial junctions in response to subgingival biofilms', *Virulence*, 6(7), pp. 704–709. doi: 10.1080/21505594.2015.1081731.

Bernstam, L. I., Vaughan, F. L. and Bernstein, I. A. (1986) 'Keratinocytes grown at the air-liquid interface', *In Vitro Cellular and Developmental Biology - Animal*, 22(12), pp. 695–705. doi: 10.1007/bf02621086.

Bernstam, L. I., Vaughan, F. L. and Bernstein, I. A. (1990) 'Stratified cornified primary cultures of human keratinocytes grown on microporous membranes at the air-liquid interface', *Journal of Dermatological Science*, 1(3), pp. 173–181. doi: 10.1016/0923-1811(90)90129-2.

Berridge, M. V., Herst, P. M. and Tan, A. S. (2005) 'Tetrazolium dyes as tools in cell biology: New insights into their cellular reduction', *Biotechnology Annual Review*, 11(SUPPL.), pp. 127–152. doi: 10.1016/S1387-2656(05)11004-7.

Biology Software (2023) 'Benchling'. San Francisco, USA: Biology Software.

Bischoff, I. *et al.* (2016) 'Pitfalls in assessing microvascular endothelial barrier function: Impedance-based devices versus the classic macromolecular tracer assay', *Scientific Reports*, 6(1), pp. 1–11. doi: 10.1038/srep23671.

Black, B. E. *et al.* (2001) 'DNA binding domains in diverse nuclear receptors function as nuclear export signals', *Current Biology*, 11(22), pp. 1749–1758. doi: 10.1016/S0960-9822(01)00537-1.

Bongartz, T. *et al.* (2005) 'Treatment of active psoriatic arthritis with the PPAR ligand pioglitazone: an open-label pilot study', *Rheumatology*, 44(1), pp. 126–129. doi: 10.1093/rheumatology/keh423.

Brandner, J. M. *et al.* (2002) 'Organization and formation of the tight junction system in human epidermis and cultured keratinocytes', *European Journal of Cell Biology*, 81(5), pp. 253–263. doi: 10.1078/0171-9335-00244.

Brandner, J. M., Haftek, M. and Niessen, C. M. (2010) 'Adherens Junctions, Desmosomes and Tight Junctions in Epidermal Barrier Function ', *The Open Dermatology Journal*, 4, pp. 14–20.

Brasil-Oliveira, R. *et al.* (2020) 'Corticosteroid Use and Periodontal Disease: A Systematic Review', *European Journal of Dentistry*, 14(3), p. 496. doi: 10.1055/S-0040-1713954.

Breslin, S. and O'Driscoll, L. (2016) 'The relevance of using 3D cell cultures, in addition to 2D monolayer cultures, when evaluating breast cancer drug sensitivity and resistance', *Oncotarget*, 7(29), p. 45745. doi: 10.18632/ONCOTARGET.9935.

British Society of Periodontology (2016) *The Good Practitioner's Guide to Periodontology*. Available at: https://www.bsperio.org.uk/assets/downloads/good_practitioners_guide_2016.pdf (Accessed: 19 April 2023).

Brownlee, M. (2005) 'The pathobiology of diabetic complications: a unifying mechanism', *Diabetes*, 54(6). Available at: https://diabetesjournals.org/diabetes/article-abstract/54/6/1615/14015 (Accessed: 15 November 2023).

Brunner, S. *et al.* (2000) 'Cell cycle dependence of gene transfer by lipoplex, polyplex and recombinant adenovirus', *Gene Therapy 2000 7:5*, 7(5), pp. 401–407. doi: 10.1038/sj.gt.3301102.

Bugge, A. *et al.* (2009) 'The PPARγ2 A/B-Domain Plays a Gene-Specific Role in Transactivation and Cofactor Recruitment', *Molecular Endocrinology*, 23(6), pp. 794–808. doi: 10.1210/ME.2008-0236.

Bugge, T. H. *et al.* (1992) 'RXR alpha, a promiscuous partner of retinoic acid and thyroid hormone receptors.', *The EMBO Journal*, 11(4), pp. 1409–1418. doi: 10.1002/j.1460-2075.1992.tb05186.x.

Camp, H. S. *et al.* (2000) 'Differential activation of peroxisome proliferator-activated receptor-gamma by troglitazone and rosiglitazone.', *Diabetes*, 49(4), pp. 539–547. doi: 10.2337/DIABETES.49.4.539.

Cao, Z. *et al.* (2009) 'Effects of Resin or Charcoal Treatment on Fetal Bovine Serum and Bovine Calf Serum', *http://dx.doi.org/10.3109/07435800903204082*, 34(4), pp. 101–108. doi: 10.3109/07435800903204082.

Celik, B. *et al.* (2016) 'CXCl8, IL-1β and sCD200 are pro-inflammatory cytokines and their levels increase in the circulation of breast carcinoma patients', *Biomedical Reports*, 5(2), pp. 259–263. doi: 10.3892/BR.2016.709/HTML.

Celinski, K. *et al.* (2011) 'Effects of peroxisome proliferator-activated receptors-gamma ligands on dextran sodium sulphate-induced colitis in rats', *Journal of physiology and pharmacology : an official journal of the Polish Physiological Society*, 62(3), pp. 347–356. Available at: http://europepmc.org/abstract/MED/21893696.

Cha, B. S. *et al.* (2001) 'Peroxisome Proliferator-Activated Receptor (PPAR) γ and Retinoid X Receptor (RXR) agonists have complementary effects on glucose and lipid metabolism in human skeletal muscle', *Diabetologia*, 44(4), pp. 444–452. doi: 10.1007/S001250051642/METRICS.

Chae, B. S. (2018) ‘Pretreatment of Low-Dose and Super-Low-Dose LPS on the Production of In Vitro LPS-Induced Inflammatory Mediators’, *Toxicological Research 2018 34:1*, 34(1), pp. 65–73. doi: 10.5487/TR.2018.34.1.065.

Chan, R. W. Y. *et al.* (2010) ‘Influenza H5N1 and H1N1 Virus Replication and Innate Immune Responses in Bronchial Epithelial Cells Are Influenced by the State of Differentiation’, *PLoS ONE*, 5(1), p. e8713. doi: 10.1371/journal.pone.0008713.

Chapple, I. L. C. *et al.* (2015) ‘Primary prevention of periodontitis: Managing gingivitis’, *Journal of Clinical Periodontology*, 42(S16), pp. S71–S76. doi: 10.1111/JCPE.12366.

Chawla, A. (1994) ‘Peroxisome proliferator-activated receptor (PPAR) gamma: adipose-predominant expression and induction early in adipocyte differentiation’, *Endocrinology*, 135(2), pp. 798–800. doi: 10.1210/en.135.2.798.

Chen, S. and Schoen, J. (2019) ‘Air-liquid interface cell culture: From airway epithelium to the female reproductive tract’, *Reproduction in Domestic Animals*, 54(S3), pp. 38–45. doi: 10.1111/rda.13481.

Chin, A. C. *et al.* (2006) ‘The role of caspase-3 in lipopolysaccharide-mediated disruption of intestinal epithelial tight junctions’, *Canadian Journal of Physiology and Pharmacology*, 84(10), pp. 1043–1050. doi: 10.1139/y06-056.

Chinnathambi, S. *et al.* (2003) ‘Recapitulation of oral mucosal tissues in long-term organotypic culture’, *The Anatomical Record Part A: Discoveries in Molecular, Cellular, and Evolutionary Biology*, 270A(2), pp. 162–174. doi: 10.1002/AR.A.10021.

Ciapetti, G. *et al.* (1993) ‘In vitro evaluation of cell/biomaterial interaction by MTT assay’, *Biomaterials*, 14(5), pp. 359–364. doi: 10.1016/0142-9612(93)90055-7.

Clarke, N. G., Shephard, B. C. and Hirsch, R. S. (1981) ‘The effects of intra-arterial epinephrine and nicotine on gingival circulation’, *Oral surgery, oral medicine, and oral pathology*, 52(6), pp. 577–582. doi: 10.1016/0030-4220(81)90071-2.

Colley, H. E. *et al.* (2013) ‘Tissue-engineered oral mucosa to study radiotherapy-induced oral mucositis’, *International Journal of Radiation Biology*, 89(11), pp. 907–914. doi: 10.3109/09553002.2013.809171.

Colony, P. C. and Neutra, M. R. (1985) ‘Macromolecular transport in the fetal rat intestine’, *Gastroenterology*, 89(2), pp. 294–306. doi: 10.1016/0016-5085(85)90329-4.

Coutinho, A. E. and Chapman, K. E. (2011) ‘The anti-inflammatory and immunosuppressive effects of glucocorticoids, recent developments and mechanistic insights’, *Molecular and Cellular Endocrinology*, pp. 2–13. doi: 10.1016/j.mce.2010.04.005.

Cugini, M. A. *et al.* (2000) ‘The effect of scaling and root planing on the clinical and microbiological parameters of periodontal diseases: 12-month results’, *Journal of Clinical Periodontology*, 27(1), pp. 30–36. doi: 10.1034/J.1600-051X.2000.027001030.X.

Dalby, B. *et al.* (2004) ‘Advanced transfection with Lipofectamine 2000 reagent: primary neurons, siRNA, and high-throughput applications’, *Methods*, 33(2), pp. 95–103. doi: 10.1016/J.YMETH.2003.11.023.

Damek-Poprawa, M. *et al.* (2013) ‘Cell junction remodeling in gingival tissue exposed to a microbial toxin’, *Journal of Dental Research*, 92(6), pp. 518–523. doi: 10.1177/0022034513486807.

Degrelle, S. A., Shoaito, H. and Fournier, T. (2017) ‘New Transcriptional Reporters to Quantify and Monitor PPARγ Activity’, *PPAR Research*, 2017. doi: 10.1155/2017/6139107.

Delcourt-Huard, A. *et al.* (1997) ‘Reconstituted human gingival epithelium: Nonsubmerged in vitro model’, *In Vitro Cellular and Developmental Biology - Animal*, 33(1), pp. 30–36. doi: 10.1007/S11626-997-0019-0/METRICS.

Delrue, I. *et al.* (2018) ‘Determination of the Selection Capacity of Antibiotics for Gene Selection’, *Biotechnology Journal*, 13(8), p. 1700747. doi: 10.1002/BIOT.201700747.

Dizdar, O. *et al.* (2017) ‘Increased cancer risk in patients with periodontitis’, *https://doi.org/10.1080/03007995.2017.1354829*, 33(12), pp. 2195–2200. doi: 10.1080/03007995.2017.1354829.

Doerfler, W. (2011) ‘Epigenetic consequences of foreign DNA insertions: de novo methylation and global alterations of methylation patterns in recipient genomes’, *Reviews in Medical Virology*, 21(6), pp. 336–346. doi: 10.1002/RMV.698.

Ekanayake-Mudiyanselage, S. *et al.* (1998) ‘Expression of Epidermal Keratins and the Cornified Envelope Protein Involucrin is Influenced by Permeability Barrier Disruption’, *Journal of Investigative Dermatology*, 111(3), pp. 517–523. doi: 10.1046/J.1523-1747.1998.00318.X.

Elbrecht, A. *et al.* (1996) ‘Molecular Cloning, Expression and Characterization of Human Peroxisome Proliferator Activated Receptors gamma1 and gamma2’, *BIOCHEMICAL AND BIOPHYSICAL RESEARCH COMMUNICATIONS*, 224, pp. 431–437.

Ellis, S. D. *et al.* (1998) ‘Factors for progression of periodontal diseases’, *Journal of Oral Pathology & Medicine*, 27(3), pp. 101–105. doi: 10.1111/j.1600-0714.1998.tb01923.x.

England, C. G., Ehlerding, E. B. and Cai, W. (2016) ‘NanoLuc: A Small Luciferase Is Brightening Up the Field of Bioluminescence’, *Bioconjugate Chemistry*, 27(5), pp. 1175–1187. doi: 10.1021/acs.bioconjchem.6b00112.

Escriva, H., Delaunay, F. and Laudet, V. (2000) ‘Ligand Binding and Nuclear Receptor Evolution’, *BioEssays*, 22, pp. 717–727.

European Medicines Agency (2010) ‘European Medicines Agency recommends suspension of Avandia, Avandamet and Avaglim’, *European Medicines Agency*.

Evans, R. M. (2005) ‘The nuclear receptor superfamily: A Rosetta stone for physiology’, *Molecular Endocrinology*, pp. 1429–1438. doi: 10.1210/me.2005-0046.

Fajas, L. *et al.* (1997) ‘The Organization, Promoter Analysis, and Expression of the Human PPARγ Gene’, *Journal of Biological Chemistry*, 272(30), pp. 18779–18789. doi: 10.1074/jbc.272.30.18779.

Fanning, A. S. *et al.* (1998) ‘The tight junction protein ZO-1 establishes a link between the transmembrane protein occludin and the actin cytoskeleton’, *Journal of Biological Chemistry*, 273(45), pp. 29745–29753. doi: 10.1074/jbc.273.45.29745.

Fatou, J. G. (1971) ‘Melting temperature and enthalpy of isotactic polypropylene’, *European Polymer Journal*, 7(8), pp. 1057–1064. doi: 10.1016/0014-3057(71)90138-8.

Feldman, A. T. and Wolfe, D. (2014) ‘Tissue processing and hematoxylin and eosin staining’, *Methods in Molecular Biology*, 1180, pp. 31–43. doi: 10.1007/978-1-4939-1050-2_3.

Feldman, G. J., Mullin, J. M. and Ryan, M. P. (2005) ‘Occludin: Structure, function and regulation’, *Advanced Drug Delivery Reviews*, 57(6), pp. 883–917. doi: 10.1016/J.ADDR.2005.01.009.

Fischer, A. H. *et al.* (2008) ‘Hematoxylin and eosin staining of tissue and cell sections’, *Cold Spring Harbor Protocols*, 3(5), p. pdb.prot4986. doi: 10.1101/pdb.prot4986.

Flemmig, T. F. (1999) ‘Periodontitis’, *Annals of Periodontology*, 4(1), pp. 32–37. doi: 10.1902/annals.1999.4.1.32.

Forman, B. M. *et al.* (1992) ‘Half-site spacing and orientation determines whether thyroid hormone and retinoic acid receptors and related factors bind to DNA response elements as monomers, homodimers, or heterodimers.’, *Molecular Endocrinology*, 6(3), pp. 429–442. doi: 10.1210/MEND.6.3.1316541.

Forman, B. M. *et al.* (1995) ‘15-Deoxy-Δ12,14-Prostaglandin J2 is a ligand for the adipocyte determination factor PPARγ’, *Cell*, 83(5), pp. 803–812. doi: 10.1016/0092-8674(95)90193-0.

Franke, W. W. *et al.* (1981) ‘Diversity of cytokeratins’, *Journal of Molecular Biology*, 153(4), pp. 933–959. doi: 10.1016/0022-2836(81)90460-5.

Fujita, T. *et al.* (2012) ‘Loss of claudin-1 in lipopolysaccharide-treated periodontal epithelium’, *Journal of Periodontal Research*, 47(2), pp. 222–227. doi: 10.1111/j.1600-0765.2011.01424.x.

Funosas, E. *et al.* (2012) ‘Alteration of hemostasis in patients treated with subgingival NSAIDs during periodontal therapy’, *Acta Odontol Latinoam*, 25(1), pp. 103–108.

Garbers, C. and Scheller, J. (2013) ‘Interleukin-6 and interleukin-11: same same but different’, *Biological Chemistry*, 394(9), pp. 1145–1161. doi: 10.1515/hsz-2013-0166.

Garlotta, D. (2001) ‘A Literature Review of Poly(Lactic Acid)’, *Journal of Polymers and the Environment 2001 9:2*, 9(2), pp. 63–84. doi: 10.1023/A:1020200822435.

Garrod, D. and Chidgey, M. (2008) ‘Desmosome structure, composition and function’, *Biochimica et Biophysica Acta (BBA) - Biomembranes*, 1778(3), pp. 572–587. doi: 10.1016/j.bbamem.2007.07.014.

Ghasemi, M. *et al.* (2021) ‘The mtt assay: Utility, limitations, pitfalls, and interpretation in bulk and single-cell analysis’, *International Journal of Molecular Sciences*, 22(23). doi: 10.3390/IJMS222312827/S1.

Ghisletti, S. *et al.* (2007) ‘Molecular Cell Parallel SUMOylation-Dependent Pathways Mediate Gene-and Signal-Specific Transrepression by LXRs and PPARg’, *Molecular Cell*, 25, pp. 57–70. doi: 10.1016/j.molcel.2006.11.022.

Giepmans, B. N. G. and van IJzendoorn, S. C. D. (2009) ‘Epithelial cell-cell junctions and plasma membrane domains’, *Biochimica et Biophysica Acta - Biomembranes*, 1788(4), pp. 820–831. doi: 10.1016/J.BBAMEM.2008.07.015.

Gomes, M. J. *et al.* (2016) ‘Cell-based in vitro models for studying blood–brain barrier (BBB) permeability’, in *Concepts and Models for Drug Permeability Studies*. Elsevier, pp. 169–188. doi: 10.1016/B978-0-08-100094-6.00011-0.

Grant, M. M. *et al.* (2023) ‘Pre-conditioning of gingival epithelial cells with sub-apoptotic concentrations of curcumin prevents pro-inflammatory cytokine release’, *Journal of Periodontal Research*, 58(3), pp. 634–645. doi: 10.1111/jre.13114.

Green, K. J. *et al.* (2010) ‘Intercellular junction assembly, dynamics, and homeostasis.’, *Cold Spring Harbor perspectives in biology*. doi: 10.1101/cshperspect.a000125.

Green, K. J. and Jones, J. C. R. (1996) ‘Desmosomes and hemidesmosomes: structure and function of molecular components’, *The FASEB Journal*, 10(8), pp. 871–881. doi: 10.1096/fasebj.10.8.8666164.

Greene, J. P. (2021) ‘Microstructures of Polymers’, *Automotive Plastics and Composites*, pp. 27–37. doi: 10.1016/B978-0-12-818008-2.00009-X.

Grimaldi, B. *et al.* (2010) ‘PER2 controls lipid metabolism by direct regulation of PPARγ’, *Cell Metabolism*, 12(5), pp. 509–520. doi: 10.1016/j.cmet.2010.10.005.

Groeger, S. and Meyle, J. (2019) ‘Oral Mucosal Epithelial Cells’, *Frontiers in Immunology*, 10. doi: 10.3389/fimmu.2019.00208.

Grygiel-Górniak, B. (2014) ‘Peroxisome proliferator-activated receptors and their ligands: nutritional and clinical implications - a review’, *Nutrition Journal*, 13(1), p. 17. doi: 10.1186/1475-2891-13-17.

Güntsch, A. *et al.* (2006) ‘Effect of smoking on crevicular polymorphonuclear neutrophil function in periodontally healthy subjects’, *Journal of Periodontal Research*, 41(3), pp. 184–188. doi: 10.1111/j.1600-0765.2005.00852.x.

Guo, W. *et al.* (2018) ‘Analysis of differential expression of tight junction proteins in cultured oral epithelial cells altered by Porphyromonas gingivalis, Porphyromonas gingivalis lipopolysaccharide, and extracellular adenosine triphosphate’, *International Journal of Oral Science*, 10(1), pp. e8–e8. doi: 10.1038/ijos.2017.51.

Guth, K. *et al.* (2015) ‘Suitability of skin integrity tests for dermal absorption studies in vitro’, *Toxicology in Vitro*, 29(1), pp. 113–123. doi: 10.1016/J.TIV.2014.09.007.

Hagiu, A. *et al.* (2019) ‘Dose-dependent green tea effect on decrease of inflammation in human oral gingival epithelial keratinocytes: in vitro study’, *Clinical Oral Investigations*, 24, pp. 2375–2383. doi: 10.1007/s00784-019-03096-4/Published.

Hajishengallis, G. (2014) ‘Periodontitis: from microbial immune subversion to systemic inflammation’, *Nature Reviews Immunology 2015 15:1*, 15(1), pp. 30–44. doi: 10.1038/nri3785.

Hajishengallis, G. (2020) ‘New developments in neutrophil biology and periodontitis’, *Periodontology 2000*, 82(1), pp. 78–92. doi: 10.1111/prd.12313.

Hall, M. P. *et al.* (2012) ‘Engineered luciferase reporter from a deep sea shrimp utilizing a novel imidazopyrazinone substrate’, *ACS Chemical Biology*, 7(11), pp. 1848–1857. doi: 10.1021/cb3002478.

Hara-Chikuma, M. and Verkman, A. S. (2005) ‘Aquaporin-3 functions as a glycerol transporter in mammalian skin’, *Biology of the Cell*, 97(7), pp. 479–486. doi: 10.1042/BC20040104.

Hassell, T. M. (1993) ‘Tissues and cells of the periodontium’, *Periodontology 2000*, 3(1), pp. 9–38. doi: 10.1111/J.1600-0757.1993.TB00230.X.

He, C. *et al.* (2019) ‘Vitamin A inhibits the action of LPS on the intestinal epithelial barrier function and tight junction proteins’, *Food & Function*, 10(2), pp. 1235–1242. doi: 10.1039/C8FO01123K.

He, W. *et al.* (2013) ‘LPS induces IL-8 expression through TLR4, MyD88, NF-kappaB and MAPK pathways in human dental pulp stem cells’, *International endodontic journal*, 46(2), pp. 128–136. doi: 10.1111/J.1365-2591.2012.02096.X.

Heasman, P. A. and Hughes, F. J. (2014) ‘Drugs, medications and periodontal disease’, *British Dental Journal*, 217(8), pp. 411–419. doi: 10.1038/sj.bdj.2014.905.

Helsen, C. *et al.* (2012) ‘Structural basis for nuclear hormone receptor DNA binding’, *Molecular and Cellular Endocrinology*, 348(2), pp. 411–417. doi: 10.1016/J.MCE.2011.07.025.

Henke, B. R. *et al.* (1998) 'N-(2-Benzoylphenyl)-l-tyrosine PPARγ Agonists. 1. Discovery of a Novel Series of Potent Antihyperglycemic and Antihyperlipidemic Agents', *Journal of Medicinal Chemistry*, 41(25), pp. 5020–5036. doi: 10.1021/jm9804127.

Hermann-Kleiter, N. *et al.* (2015) 'The Nuclear Orphan Receptor NR2F6 Is a Central Checkpoint for Cancer Immune Surveillance', *Cell Reports*, 12(12), pp. 2072–2085. doi: 10.1016/j.celrep.2015.08.035.

Herreros-Pomares, A. *et al.* (2021) '3D printing novel in vitro cancer cell culture model systems for lung cancer stem cell study', *Materials Science and Engineering C*, 122. doi: 10.1016/J.MSEC.2021.111914.

Hewitt, B. J. *et al.* (2022) 'A 3D Printed Device for In Vitro Generation of Stratified Epithelia at the Air-Liquid Interface', *Tissue Engineering - Part C: Methods*, 28(11), pp. 599–609. doi: 10.1089/TEN.TEC.2022.0130.

Hodgkins, J. F. W., Watkins, R. and Walker, D. M. (1978) 'Correlated scanning and transmission electron microscopy of cell surfaces at various levels in human gingival epithelium', *Archives of Oral Biology*, 23(5), pp. 355–360. doi: 10.1016/0003-9969(78)90092-4.

Hormia, M., Owaribe, K. and Virtanen, I. (2001) 'The Dento-Epithelial Junction: Cell Adhesion by Type I Hemidesmosomes in the Absence of a True Basal Lamina', *Journal of Periodontology*, 72(6), pp. 788–797. doi: 10.1902/JOP.2001.72.6.788.

Hotta, M. *et al.* (2010) 'Carvacrol, a component of thyme oil, activates PPARα and γ and suppresses COX-2 expression', *Journal of Lipid Research*, 51(1), pp. 132–139. doi: 10.1194/JLR.M900255-JLR200.

Howell, T. H. *et al.* (1991) 'Effect of the NSAID piroxicam, topically administered, on the development of gingivitis in Beagle dogs', *Journal of Periodontal Research*, 26(3), pp. 180–183. doi: 10.1111/j.1600-0765.1991.tb01643.x.

Hsieh, C. C., Huang, C. J. and Lin, B. F. (2006) 'Low and high levels of α-tocopherol exert opposite effects on IL-2 possibly through the modulation of PPAR-γ, IκBα, and apoptotic pathway in activated splenocytes', *Nutrition*, 22(4), pp. 433–440. doi: 10.1016/J.NUT.2005.10.001.

Hsueh, M. H. *et al.* (2021) 'Effect of Printing Parameters on the Thermal and Mechanical Properties of 3D-Printed PLA and PETG, Using Fused Deposition Modeling', *Polymers 2021, Vol. 13, Page 1758*, 13(11), p. 1758. doi: 10.3390/POLYM13111758.

Huang, S. *et al.* (2014) 'Predictive modeling of gingivitis severity and susceptibility via oral microbiota', *The ISME Journal 2014 8:9*, 8(9), pp. 1768–1780. doi: 10.1038/ismej.2014.32.

Iacopino, A. M. (2001) 'Periodontitis and Diabetes Interrelationships: Role of Inflammation', *Annals of Periodontology*, 6(1), pp. 125–137. doi: 10.1902/ANNALS.2001.6.1.125.

Idrees, M. M. *et al.* (2014) 'Prevalence and severity of plaque-induced gingivitis in a Saudi adult population', *Saudi Medical Journal*, 35(11), p. 1373. Available at: /pmc/articles/PMC4362151/ (Accessed: 11 April 2023).

IJpenberg, A. *et al.* (1997) 'Polarity and Specific Sequence Requirements of Peroxisome Proliferator-activated Receptor (PPAR)/Retinoid X Receptor Heterodimer Binding to DNA', *Journal of Biological Chemistry*, 272(32), pp. 20108–20117. doi: 10.1074/jbc.272.32.20108.

Ishiyama, M. *et al.* (1996) 'A combined assay of cell viability and in vitro cytotoxicity with a highly water-soluble tetrazolium salt, neutral red and crystal violet', *Biological & pharmaceutical bulletin*, 19(11), pp. 1518–1520. doi: 10.1248/BPB.19.1518.

Ivanov, A. I., Parkos, C. A. and Nusrat, A. (2010) 'Cytoskeletal Regulation of Epithelial Barrier Function During Inflammation', *The American Journal of Pathology*, 177(2), pp. 512–524. doi: 10.2353/ajpath.2010.100168.

Jacob, A. *et al.* (2007) 'Mechanism of the anti-inflammatory effect of curcumin: PPAR-γ activation', *PPAR Research*. doi: 10.1155/2007/89369.

Jakubovics, N. S. *et al.* (2021) 'The dental plaque biofilm matrix', *Periodontology 2000*, 86(1), pp. 32–56. doi: 10.1111/prd.12361.

Jensen, P. J. *et al.* (1997) 'E-cadherin and P-cadherin have partially redundant roles in human epidermal stratification', *Cell and Tissue Research*, 288(2), pp. 307–316. doi: 10.1007/s004410050816.

Jiang, Y. *et al.* (2020) 'Cytokinocytes: the diverse contribution of keratinocytes to immune responses in skin', *JCI Insight*, 5(20). doi: 10.1172/jci.insight.142067.

Jiang, Y. J. *et al.* (2011) 'PPARgamma activators stimulate aquaporin 3 expression in keratinocytes/epidermis', *Experimental Dermatology*, 20(7), pp. 595–599. doi: 10.1111/J.1600-0625.2011.01269.X.

Jiao, G. *et al.* (2015) 'Limitations of MTT and CCK-8 assay for evaluation of graphene cytotoxicity', *RSC Advances*, 5(66), pp. 53240–53244. doi: 10.1039/C5RA08958A.

Jin, L. and Li, Y. (2010) 'Structural and functional insights into nuclear receptor signaling', *Advanced Drug Delivery Reviews*, 62(13), pp. 1218–1226. doi: 10.1016/J.ADDR.2010.08.007.

Johnson, G. K. *et al.* (2010) 'Interleukin-1 and interleukin-8 in nicotine- and lipopolysaccharide-exposed gingival keratinocyte cultures', *Journal of Periodontal Research*, 45(4), pp. 583–588. doi: 10.1111/j.1600-0765.2009.01262.x.

Jones, R. *et al.* (2011) 'RepRap – the replicating rapid prototyper', *Robotica*, 29(1), pp. 177–191. doi: 10.1017/S026357471000069X.

Kalinin, A. E., Kajava, A. V. and Steinert, P. M. (2002) 'Epithelial barrier function: Assembly and structural features of the cornified cell envelope', *BioEssays*, pp. 789–800. doi: 10.1002/bies.10144.

Kameyama, S. *et al.* (2009) 'Air exposure causes oxidative stress in cultured bovine tracheal epithelial cells and produces a change in cellular glutathione systems', *http://dx.doi.org/10.1080/01902140390240113*, 29(8), pp. 567–583. doi: 10.1080/01902140390240113.

Kantarci, A., Oyaizu, K. and Van Dyke, T. E. (2003) 'Neutrophil-Mediated Tissue Injury in Periodontal Disease Pathogenesis: Findings from Localized Aggressive Periodontitis', *Journal of Periodontology*, 74(1), pp. 66–75. doi: 10.1902/jop.2003.74.1.66.

Katsouri, L., Blondrath, K. and Sastre, M. (2012) 'Peroxisome proliferator-activated receptor-γ cofactors in neurodegeneration', *IUBMB Life*, pp. 958–964. doi: 10.1002/iub.1097.

Khan, E. *et al.* (2012) 'Architectural characterization of Organotypic cultures of H400 and primary rat keratinocytes', *Journal of Biomedical Materials Research - Part A*, 100 A(12), pp. 3227–3238. doi: 10.1002/jbm.a.34263.

Khorasanizadeh, S. and Rastinejad, F. (2001) 'Nuclear-receptor interactions on DNA-response elements', *Trends in Biochemical Sciences*, 26(6), pp. 384–390. doi: 10.1016/S0968-0004(01)01800-X.

Kim, E. Y. and Moudgil, K. D. (2008) 'Regulation of autoimmune inflammation by pro-inflammatory cytokines', *Immunology Letters*, 120(1–2), pp. 1–5. doi: 10.1016/J.IMLET.2008.07.008.

Kim, T. K. and Eberwine, J. H. (2010) 'Mammalian cell transfection: The present and the future', *Analytical and Bioanalytical Chemistry*, 397(8), pp. 3173–3178. doi: 10.1007/S00216-010-3821-6/FIGURES/3.

Kirschner, N. and Brandner, J. M. (2012) 'Barriers and more: Functions of tight junction proteins in the skin', *Annals of the New York Academy of Sciences*, 1257(1), pp. 158–166. doi: 10.1111/j.1749-6632.2012.06554.x.

Kistler, J. O. *et al.* (2013) 'Bacterial Community Development in Experimental Gingivitis', *PLoS ONE*, 8(8), p. e71227. doi: 10.1371/journal.pone.0071227.

Klepsch, V. *et al.* (2018) 'Nuclear orphan receptor NR2F6 as a safeguard against experimental murine colitis', *Gut*, 67(8), pp. 1434–1444. doi: 10.1136/gutjnl-2016-313466.

Koide, A. *et al.* (2007) 'Identification of Regions within the F Domain of the Human Estrogen Receptor α that Are Important for Modulating Transactivation and Protein-Protein Interactions', *Molecular Endocrinology*, 21(4), pp. 829–842. doi: 10.1210/me.2006-0203.

Koster, M. I. and Roop, D. R. (2007) ‘Mechanisms Regulating Epithelial Stratification’, *Annual Review of Cell and Developmental Biology*, 23(1), pp. 93–113. doi: 10.1146/annurev.cellbio.23.090506.123357.

Kozak, M. *et al.* (2020) ‘Cytokines and Their Genetic Polymorphisms Related to Periodontal Disease’, *Journal of Clinical Medicine 2020, Vol. 9, Page 4045*, 9(12), p. 4045. doi: 10.3390/JCM9124045.

Kraus, W. L. and Wong, J. (2002) ‘Nuclear receptor-dependent transcription with chromatin’, *European Journal of Biochemistry*, 269, pp. 2275–2283. doi: 10.1046/j.1432-1033.2002.02889.x.

Krug, S. M., Schulzke, J. D. and Fromm, M. (2014) ‘Tight junction, selective permeability, and related diseases’, *Seminars in Cell & Developmental Biology*, 36, pp. 166–176. doi: 10.1016/J.SEMCDB.2014.09.002.

Krumova, K. and Cosa, G. (2016) ‘Chapter 1 Overview of Reactive Oxygen Species’, pp. 1–21. doi: 10.1039/9781782622208-00001.

Kubota, H. *et al.* (2001) ‘Retinoid X receptor α and retinoic acid receptor γ mediate expression of genes encoding tight-junction proteins and barrier function in F9 cells during visceral endodermal differentiation’, *Experimental Cell Research*, 263(1), pp. 163–172. doi: 10.1006/excr.2000.5113.

Kuenzli, S. and Saurat, J.-H. (2003) ‘Effect of Topical PPARβ/δ and PPARγ Agonists on Plaque Psoriasis’, *Dermatology*, 206(3), pp. 252–256. doi: 10.1159/000068897.

Kuo, W. T. *et al.* (2021) ‘The Tight Junction Protein ZO-1 Is Dispensable for Barrier Function but Critical for Effective Mucosal Repair’, *Gastroenterology*, 161(6), pp. 1924–1939. doi: 10.1053/J.GASTRO.2021.08.047.

Lang, N. P., Schätzle, M. A. and Löe, H. (2009) ‘Gingivitis as a risk factor in periodontal disease’, *Journal of Clinical Periodontology*, 36(s10), pp. 3–8. doi: 10.1111/j.1600-051X.2009.01415.x.

Lavery, D. N. and Mcewan, I. J. (2005) ‘Structure and function of steroid receptor AF1 transactivation domains: induction of active conformations’, *Biochemical Journal*, 391(3), pp. 449–464. doi: 10.1042/BJ20050872.

Lechler, T. and Fuchs, E. (2005) ‘Asymmetric cell divisions promote stratification and differentiation of mammalian skin’, *Nature*, 437(7056), pp. 275–280. doi: 10.1038/nature03922.

Leesnitzer, L. M. *et al.* (2002) ‘Functional consequences of cysteine modification in the ligand binding sites of peroxisome proliferator activated receptors by GW9662’, *Biochemistry*, 41(21), pp. 6640–6650. doi: 10.1021/BI0159581.

Lennon, A. M. *et al.* (2002) 'MAP Kinase Cascades Are Activated in Astrocytes and Preadipocytes by 15-Deoxy-Δ12–14-prostaglandin J2 and the Thiazolidinedione Ciglitazone through Peroxisome Proliferator Activator Receptor γ-independent Mechanisms Involving Reactive Oxygenated Species', *Journal of Biological Chemistry*, 277(33), pp. 29681–29685. doi: 10.1074/jbc.M201517200.

Li, J., Guo, C. and Wu, J. (2019) '15-Deoxy-Δ-12,14 -Prostaglandin J2 (15d-PGJ2), an Endogenous Ligand of PPARγ: Function and Mechanism', *PPAR Research*, 2019, pp. 1–10. doi: 10.1155/2019/7242030.

Li, L. *et al.* (2013) 'Expression patterns of peroxisome proliferator-activated receptor gamma 1 versus gamma 2, and their association with intramuscular fat in goat tissues', *Gene*, 528(2), pp. 195–200. doi: 10.1016/j.gene.2013.07.013.

Li, X. *et al.* (2016) 'Mitochondrial reactive oxygen species mediate the lipopolysaccharide-induced pro-inflammatory response in human gingival fibroblasts', *Experimental Cell Research*, 347(1), pp. 212–221. doi: 10.1016/J.YEXCR.2016.08.007.

Li, Y. *et al.* (2010) 'Prevalence and severity of gingivitis in American adults', *American Journal of Dentistry*, 23(1), pp. 9–13.

Lin, H. *et al.* (2007) 'Air-Liquid Interface (ALI) culture of human bronchial epithelial cell monolayers as an in vitro model for airway drug transport studies', *Journal of Pharmaceutical Sciences*, 96(2), pp. 341–350. doi: 10.1002/jps.20803.

Löe, H. (1967) 'The Gingival Index, the Plaque Index and the Retention Index Systems', *The Journal of Periodontology*, 38(6), pp. 610–616. doi: 10.1902/JOP.1967.38.6.610.

Loryman, C. and Mansbridge, J. (2008) 'Inhibition of keratinocyte migration by lipopolysaccharide', *Wound Repair and Regeneration*, 16(1), pp. 45–51. doi: 10.1111/j.1524-475X.2007.00290.x.

LoVerme, J. *et al.* (2005) 'The search for the palmitoylethanolamide receptor', in *Life Sciences*, pp. 1685–1698. doi: 10.1016/j.lfs.2005.05.012.

Lu, S. (2003) 'Rapid Screening of Recombinant Plasmids', in *E. coli Plasmid Vectors. Methods in Molecular Biology*. Humana Press, pp. 169–174.

MacCallum, D. K. and Lillie, J. H. (1990) 'Evidence for Autoregulation of Cell Division and Cell Transit in Keratinocytes Grown on Collagen at an Air-Liquid Interface', *Skin Pharmacology and Physiology*, 3(2), pp. 86–96. doi: 10.1159/000210855.

MacKlis, P. *et al.* (2020) 'The Association Between Oral Health and Skin Disease', *The Journal of Clinical and Aesthetic Dermatology*, 13(6), p. 48. Available at: /pmc/articles/PMC7442307/ (Accessed: 18 December 2023).

Malek, R. *et al.* (2017) 'Necrotizing Ulcerative Gingivitis', *Contemporary Clinical Dentistry*, 8(3), p. 496. doi: 10.4103/CCD.CCD_1181_16.

Malinowski, J. M. and Bolesta, S. (2000) ‘Rosiglitazone in the treatment of type 2 diabetes mellitus: a critical review’, *Clinical Therapeutics*, 22(10), pp. 1151–1168. doi: 10.1016/S0149-2918(00)83060-X.

Man, M. Q. *et al.* (2004) ‘Peroxisome-Proliferator-Activated Receptor (PPAR)-γ Activation Stimulates Keratinocyte Differentiation’, *Journal of Investigative Dermatology*, 123(2), pp. 305–312. doi: 10.1111/J.0022-202X.2004.23235.X.

Mangelsdorf, D. J. *et al.* (1995) ‘The Nuclear Receptor Superfamily: The Second Decade’, *Cell*, 83(6), pp. 835–839.

Maquera-Huacho, P. M. *et al.* (2023) ‘Effect of Hesperidin on Barrier Function and Reactive Oxygen Species Production in an Oral Epithelial Cell Model, and on Secretion of Macrophage-Derived Inflammatory Mediators during Porphyromonas gingivalis Infection’, *International Journal of Molecular Sciences*, 24(12), p. 10389. doi: 10.3390/ijms241210389.

Martin, H. (2009) ‘Role of PPAR-gamma in inflammation. Prospects for therapeutic intervention by food components’, *Mutation Research/Fundamental and Molecular Mechanisms of Mutagenesis*, 669(1–2), pp. 1–7. doi: 10.1016/j.mrfmmm.2009.06.009.

Mastrofrancesco, A. *et al.* (2014) ‘Preclinical Studies of a Specific PPARγ Modulator in the Control of Skin Inflammation’, *Journal of Investigative Dermatology*, 134(4), pp. 1001–1011. doi: 10.1038/JID.2013.448.

Mavropoulos, A., Aars, H. and Brodin, P. (2003) ‘Hyperaemic response to cigarette smoking in healthy gingiva’, *Journal of Clinical Periodontology*, 30(3), pp. 214–221. doi: 10.1034/J.1600-051X.2003.10284.X.

McAllister, B. *et al.* (2021) ‘Abstract 2637: The use of 3D-printed Polylactic acid scaffolds (PLA) as a substrate for growth of MCF7 human breast cancer cells’, *Cancer Research*, 81(13_Supplement), pp. 2637–2637. doi: 10.1158/1538-7445.AM2021-2637.

McClenahan, D. *et al.* (2008) ‘Effects of lipopolysaccharide and Mannheimia haemolytica leukotoxin on bovine lung microvascular endothelial cells and alveolar epithelial cells’, *Clinical and Vaccine Immunology*, 15(2), pp. 338–347. doi: 10.1128/CVI.00344-07.

McKenna, N. J. and O’Malley, B. W. (2002) ‘Minireview: Nuclear Receptor Coactivators—An Update’, *Endocrinology*, 143(7), pp. 2461–2465. doi: 10.1210/ENDO.143.7.8892.

Melo Pithon, M. *et al.* (2009) ‘Cytotoxicity of polycarbonate orthodontic brackets’, *Brazilian Journal of Oral Sciences*, 8(2), pp. 84–87. doi: 10.20396/BJOS.V8I2.8642232.

Michalik, L. *et al.* (2002) *PPAR expression and function during vertebrate development*, *Int. J. Dev. Biol*. Available at: www.ijdb.ehu.es.

Michaud, D. S. *et al.* (2017) ‘Periodontal Disease, Tooth Loss, and Cancer Risk’, *Epidemiologic Reviews*, 39(1), pp. 49–58. doi: 10.1093/EPIREV/MXX006.

Mittal, R. *et al.* (2009) 'Efficacy and safety of combination acitretin and pioglitazone therapy in patients with moderate to severe chronic plaque-type psoriasis: A randomized, double-blind, placebo-controlled clinical trial', *Archives of Dermatology*, 145(4), pp. 387–393. doi: 10.1001/archdermatol.2009.5.

Montaigne, D., Butruille, L. and Staels, B. (2021) 'PPAR control of metabolism and cardiovascular functions', *Nature Reviews Cardiology*, 18(12), pp. 809–823. doi: 10.1038/s41569-021-00569-6.

Moras, D. and Gronemeyert, H. (1998) 'The nuclear receptor ligand-binding domain: structure and function', *Current Opinion in Cell Biology*, 10, pp. 384–391. Available at: http://biomednet.com/elecref/0955067401000384 (Accessed: 6 September 2023).

Mukherjee, R. *et al.* (1997) 'Identification, Characterization, and Tissue Distribution of Human Peroxisome Proliferator-activated Receptor (PPAR) Isoforms PPARγ2 versus PPARγ1 and Activation with Retinoid X Receptor Agonists and Antagonists', *Journal of Biological Chemistry*, 272(12), pp. 8071–8076. doi: 10.1074/jbc.272.12.8071.

Nagarakanti, S. *et al.* (2007) 'Differential Expression of E-Cadherin and Cytokeratin 19 and Net Proliferative Rate of Gingival Keratinocytes in Oral Epithelium in Periodontal Health and Disease', *Journal of Periodontology*, 78(11), pp. 2197–2202. doi: 10.1902/jop.2007.070070.

Nagy, L. and Schwabe, J. W. R. (2004) 'Mechanism of the nuclear receptor molecular switch', *Trends in Biochemical Sciences*, 29(6), pp. 317–324. doi: 10.1016/j.tibs.2004.04.006.

Nalayanda, D. D. *et al.* (2009) 'An open-access microfluidic model for lung-specific functional studies at an air-liquid interface', *Biomedical Microdevices*, 11(5), pp. 1081–1089. doi: 10.1007/s10544-009-9325-5.

Newton, J. T. and Asimakopoulou, K. (2015) 'Managing oral hygiene as a risk factor for periodontal disease: a systematic review of psychological approaches to behaviour change for improved plaque control in periodontal management', *Journal of Clinical Periodontology*, 42(S16). doi: 10.1111/jcpe.12356.

Ni, Y. *et al.* (2017) 'TNFα alters occludin and cerebral endothelial permeability: Role of p38MAPK', *PLOS ONE*, 12(2), p. e0170346. doi: 10.1371/journal.pone.0170346.

Nibali, L. *et al.* (2007) 'Severe periodontitis is associated with systemic inflammation and a dysmetabolic status: a case–control study', *Journal of Clinical Periodontology*, 34(11), pp. 931–937. doi: 10.1111/J.1600-051X.2007.01133.X.

Niessen, C. M. (2007) 'Tight Junctions/Adherens Junctions: Basic Structure and Function', *Journal of Investigative Dermatology*, 127(11), pp. 2525–2532. doi: 10.1038/sj.jid.5700865.

Nishio, K. *et al.* (2013) 'Attenuation of lipopolysaccharide (LPS)-induced cytotoxicity by tocopherols and tocotrienols', *Redox Biology*, 1(1), pp. 97–103. doi: 10.1016/j.redox.2012.10.002.

Offenbacher, S. *et al.* (2009) ‘Gingival Transcriptome Patterns During Induction and Resolution of Experimental Gingivitis in Humans’, *Journal of Periodontology*, 80(12), pp. 1963–1982. doi: 10.1902/jop.2009.080645.

Ogasawara, N. *et al.* (2010) ‘PPARγ agonists upregulate the barrier function of tight junctions via a PKC pathway in human nasal epithelial cells’, *Pharmacological Research*, 61, pp. 489–498. doi: 10.1016/j.phrs.2010.03.002.

Ohama, Y. *et al.* (2008) ‘Peroxisome proliferator-activated receptor-γ ligand reduced tumor necrosis factor-α-induced interleukin-8 production and growth in endometriotic stromal cells’, *Fertility and Sterility*, 89(2), pp. 311–317. doi: 10.1016/j.fertnstert.2007.03.061.

Olefsky, J. M. (2000) ‘Treatment of insulin resistance with peroxisome proliferator–activated receptor γ agonists’, *Journal of Clinical Investigation*, 106(4), pp. 467–472. doi: 10.1172/JCI10843.

De Oliveira, S., Rosowski, E. E. and Huttenlocher, A. (2016) ‘Neutrophil migration in infection and wound repair: going forward in reverse’, *Nature reviews. Immunology*, 16(6), p. 378. doi: 10.1038/NRI.2016.49.

Omi, T. *et al.* (2005) ‘Identification and characterization of novel peroxisome proliferator-activated receptor-gamma (PPAR-γ) transcriptional variants in pig and human’, *Journal of Animal Breeding and Genetics*, 122(1), pp. 45–53. doi: 10.1111/J.1439-0388.2005.00508.X.

Omonijo, F. A. *et al.* (2019) ‘Thymol Improves Barrier Function and Attenuates Inflammatory Responses in Porcine Intestinal Epithelial Cells during Lipopolysaccharide (LPS)-Induced Inflammation’, *Journal of Agricultural and Food Chemistry*, 67(2), pp. 615–624. doi: https://doi.org/10.1021/acs.jafc.8b05480.

O’Neill, C. A. and Garrod, D. (2011) ‘Tight junction proteins and the epidermis’, *Experimental Dermatology*, 20(2), pp. 88–91. doi: 10.1111/J.1600-0625.2010.01206.X.

Osafo, N. *et al.* (2017) ‘Mechanism of Action of Nonsteroidal Anti-Inflammatory Drugs’, in Al-kaf, A. G. A. (ed.) *Nonsteroidal Anti-Inflammatory Drugs*. InTech. doi: 10.5772/65816.

Ostermann, G. *et al.* (2002) ‘JAM-1 is a ligand of the β2 integrin LFA-1 involved in transendothelial migration of leukocytes’, *Nature Immunology*, 3(2), pp. 151–158. doi: 10.1038/ni755.

Otani, T. *et al.* (2019) ‘Claudins and JAM-A coordinately regulate tight junction formation and epithelial polarity’, *Journal of Cell Biology*, 218(10), pp. 3372–3396. doi: 10.1083/JCB.201812157.

Oubayoun, J.-P. *et al.* (1985) ‘Cytokeratin patterns of human oral epithelia: Differences in cytokeratin synthesis in gingival epithelium and the adjacent alveolar mucosa’, *Differentiation*, 30(2), pp. 123–129. doi: 10.1111/j.1432-0436.1985.tb00523.x.

Owen, G. I. and Zelent, A. (2000) ‘Origins and evolutionary diversification of the nuclear receptor superfamily’, *Cell. Mol. Life Sci*, 57, pp. 809–827.

Page, R. C. (1986) ‘Gingivitis’, *Journal of Clinical Periodontology*, 13(5), pp. 345–355. doi: 10.1111/J.1600-051X.1986.TB01471.X.

Palmer, N. A. O. *et al.* (2000) ‘A study of therapeutic antibiotic prescribing in National Health Service general dental practice in England’, *British Dental Journal*, 188(10), pp. 554–558. doi: 10.1038/SJ.BDJ.4800538.

Palumbo-Zerr, K. *et al.* (2015) ‘Orphan nuclear receptor NR4A1 regulates transforming growth factor-β 2 signaling and fibrosis’, *Nature Medicine*, 21(2), pp. 150–158. doi: 10.1038/nm.3777.

Papayannopoulos, V. (2017) ‘Neutrophil extracellular traps in immunity and disease’, *Nature Reviews Immunology 2017 18:2*, 18(2), pp. 134–147. doi: 10.1038/nri.2017.105.

De Pascale, M. C. *et al.* (2006) ‘Increased expression of transglutaminase-1 and PPARγ after vitamin E treatment in human keratinocytes’, *Archives of Biochemistry and Biophysics*, 447(2), pp. 97–106. doi: 10.1016/J.ABB.2006.02.002.

Pascual, G. *et al.* (2005) ‘A SUMOylation-dependent pathway mediates transrepression of inflammatory response genes by PPAR-γ’, *Nature*, 437(7059), pp. 759–763. doi: 10.1038/nature03988.

Patel, B., Mann, G. E. and Chapple, S. J. (2018) ‘Concerted redox modulation by sulforaphane alleviates diabetes and cardiometabolic syndrome’, *Free Radical Biology and Medicine*. Elsevier Inc., pp. 150–160. doi: 10.1016/j.freeradbiomed.2018.02.004.

Paterniti, I. *et al.* (2013) ‘Molecular evidence for the involvement of PPAR-δ and PPAR-γ in anti-inflammatory and neuroprotective activities of palmitoylethanolamide after spinal cord trauma’, *Journal of Neuroinflammation*, 10. doi: 10.1186/1742-2094-10-20.

de Pereda, J. M. *et al.* (2009) ‘Advances and perspectives of the architecture of hemidesmosomes: Lessons from structural biology’, *Cell Adhesion & Migration*, 3(4), pp. 361–364. doi: 10.4161/cam.3.4.9525.

Peruzzo, D. C. *et al.* (2016) ‘Impact of smoking on experimental gingivitis. A clinical, microbiological and immunological prospective study’, *Journal of Periodontal Research*, 51(6), pp. 800–811. doi: 10.1111/jre.12363.

Pezzulo, A. A. *et al.* (2011) ‘The air-liquid interface and use of primary cell cultures are important to recapitulate the transcriptional profile of in vivo airway epithelia’, *American Journal of Physiology - Lung Cellular and Molecular Physiology*, 300(1), pp. 25–31. doi: 10.1152/ajplung.00256.2010.

Picard, D. and Yamamoto, K. R. (1987) ‘Two signals mediate hormone-dependent nuclear localization of the glucocorticoid receptor.’, *The EMBO Journal*, 6(11), pp. 3333–3340. doi: 10.1002/J.1460-2075.1987.TB02654.X.

Piipponen, M., Li, D. and Landén, N. X. (2020) ‘The Immune Functions of Keratinocytes in Skin Wound Healing’, *International Journal of Molecular Sciences 2020, Vol. 21, Page 8790*, 21(22), p. 8790. doi: 10.3390/IJMS21228790.

Pistrosch, F. *et al.* (2005) ‘PPARγ-agonist rosiglitazone increases number and migratory activity of cultured endothelial progenitor cells’, *Atherosclerosis*, 183(1), pp. 163–167. doi: 10.1016/j.atherosclerosis.2005.03.039.

Pivarcsi, A., Kemény, L. and Dobozy, A. (2004) ‘Innate Immune Functions of the Keratinocytes’, *Acta Microbiologica et Immunologica Hungarica*, 51(3), pp. 303–310. doi: 10.1556/AMicr.51.2004.3.8.

Poenar, D. P. *et al.* (2020) ‘Low-Cost Method and Biochip for Measuring the Trans-Epithelial Electrical Resistance (TEER) of Esophageal Epithelium’, *Materials 2020, Vol. 13, Page 2354*, 13(10), p. 2354. doi: 10.3390/MA13102354.

Polak, D. *et al.* (2015) ‘Are anti-inflammatory agents effective in treating gingivitis as solo or adjunct therapies? A systematic review’, *Journal of Clinical Periodontology*, 42(S16), pp. S139–S151. doi: 10.1111/JCPE.12340.

Polak, D. and Shapira, L. (2018) ‘An update on the evidence for pathogenic mechanisms that may link periodontitis and diabetes’, *Journal of Clinical Periodontology*, 45(2), pp. 150–166. doi: 10.1111/jcpe.12803.

Preber, H. and Bergström, J. (1985) ‘Occurrence of gingival bleeding in smoker and non-smoker patients’, *Acta Odontologica Scandinavica*, 43(5), pp. 315–320. doi: 10.3109/00016358509046515.

Preethanath, R. S., Ibraheem, W. I. and Anil, A. (2020) ‘Pathogenesis of Gingivitis’, in *Oral Diseases*. IntechOpen. doi: 10.5772/intechopen.91614.

Preshaw, P. M. *et al.* (2012) ‘Periodontitis and diabetes: a two-way relationship’, *Diabetologia*, 55(1), pp. 21–31. doi: 10.1007/s00125-011-2342-y.

Preshaw, P. M. and Bissett, S. M. (2019) ‘Periodontitis and diabetes’, *British Dental Journal*, 227(7), pp. 577–584. doi: 10.1038/s41415-019-0794-5.

Presland, R. B. and Jurevic, R. J. (2002) ‘Making Sense of the Epithelial Barrier: What Molecular Biology and Genetics Tell Us About the Functions of Oral Mucosal and Epidermal Tissues’, *Journal of Dental Education*, 66(4), pp. 564–574. doi: 10.1002/j.0022-0337.2002.66.4.tb03536.x.

Prime, S. *et al.* (1990) ‘The behaviour of human oral squamous cell carcinoma in cell culture’, *The Journal of pathology*, 160(3), pp. 259–269. doi: 10.1002/PATH.1711600313.

Prunieras, M., Regnier, M. and Woodley, D. (1983) 'Methods for cultivation of keratinocytes with an air-liquid interface', *Journal of Investigative Dermatology*, 81(1 Suppl.), pp. S28–S33. doi: 10.1111/1523-1747.ep12540324.

Rangwala, S. M. and Lazar, M. A. (2004) 'Peroxisome proliferator-activated receptor γ in diabetes and metabolism', *Trends in Pharmacological Sciences*, 25(6), pp. 331–336. doi: 10.1016/j.tips.2004.03.012.

Rao, R. (2009) 'Occludin Phosphorylation in Regulation of Epithelial Tight Junctions', *Annals of the New York Academy of Sciences*, 1165(1), pp. 62–68. doi: 10.1111/j.1749-6632.2009.04054.x.

Rastinejad, F. *et al.* (2013) 'Understanding nuclear receptor form and function using structural biology', *Journal of Molecular Endocrinology*, 51(3), pp. T1–T21. doi: 10.1530/JME-13-0173.

Rawlings, A. V. *et al.* (2021) 'Effect of regioisomers of hydroxystearic acids as peroxisomal proliferator-activated receptor agonists to boost the anti-ageing potential of retinoids', *International Journal of Cosmetic Science*, 43(5), pp. 619–626. doi: 10.1111/ICS.12730.

Reiche, J., Schumann, M. and Richter, J. F. (2018) 'The Sandwich Assay: A Method for Subcellular Visualization of Paracellular Macromolecule Passage in Epithelial Sheets', *Current Protocols in Cell Biology*, 78(1). doi: 10.1002/cpcb.42.

Ren, D. *et al.* (2002) 'PPARγ knockdown by engineered transcription factors: exogenous PPARγ2 but not PPARγ1 reactivates adipogenesis', *Genes & Development*, 16(1), pp. 27–32. doi: 10.1101/GAD.953802.

Richter, B. *et al.* (2007) 'Rosiglitazone for type 2 diabetes mellitus', *Cochrane Database of Systematic Reviews*. doi: 10.1002/14651858.CD006063.pub2.

Richter, J. F. *et al.* (2016) 'A novel method for imaging sites of paracellular passage of macromolecules in epithelial sheets', *Journal of Controlled Release*, 229, pp. 70–79. doi: 10.1016/J.JCONREL.2016.03.018.

Ricote, M. *et al.* (1998) 'The peroxisome proliferator-activated receptor-γ is a negative regulator of macrophage activation', *Nature Letters*, 391, pp. 79–82. doi: https://doi.org/10.1038/34178.

Rimando, A. M. *et al.* (2005) 'Pterostilbene, a New Agonist for the Peroxisome Proliferator-Activated Receptor α-Isoform, Lowers Plasma Lipoproteins and Cholesterol in Hypercholesterolemic Hamsters', *Journal of Agricultural Food Chemistry*, 52(9), pp. 3403–3407. doi: 10.1021/JF0580364.

Roehlen, N. *et al.* (2020) 'Tight Junction Proteins and the Biology of Hepatobiliary Disease', *International Journal of Molecular Sciences 2020, Vol. 21, Page 825*, 21(3), p. 825. doi: 10.3390/IJMS21030825.

Rosdy, M. and Clauss, L. C. (1990) 'Terminal epidermal differentiation of human keratinocytes grown in chemically defined medium on inert filter substrates at the air-liquid interface', *Journal of Investigative Dermatology*, 95(4), pp. 409–414. doi: 10.1111/1523-1747.ep12555510.

Rosenthal, R. *et al.* (2010) 'Claudin-2, a component of the tight junction, forms a paracellular water channel', *Journal of Cell Science*, 123(11), pp. 1913–1921. doi: 10.1242/JCS.060665.

Van Roy, F. and Berx, G. (2008) 'The cell-cell adhesion molecule E-cadherin', *Cellular and Molecular Life Sciences*, pp. 3756–3788. doi: 10.1007/s00018-008-8281-1.

Roy, S. and Fleischman, A. J. (2003) 'Cytotoxicity Evaluation of Microsystems Materials Using Human Cells', *Sensors and Materials*, 15(6), pp. 335–340.

Royer, C. and Lu, X. (2011) 'Epithelial cell polarity: a major gatekeeper against cancer?', *Cell Death & Differentiation 2011 18:9*, 18(9), pp. 1470–1477. doi: 10.1038/cdd.2011.60.

Rübsam, M. *et al.* (2017) 'E-cadherin integrates mechanotransduction and EGFR signaling to control junctional tissue polarization and tight junction positioning', *Nature Communications*, 8(1), p. 1250. doi: 10.1038/s41467-017-01170-7.

Safe, S. *et al.* (2016) 'Nuclear receptor 4A (NR4A) family - Orphans no more', *Journal of Steroid Biochemistry and Molecular Biology*, 157, pp. 48–60. doi: 10.1016/j.jsbmb.2015.04.016.

Salas, P. J., Forteza, R. and Mashukova, A. (2016) 'Multiple roles for keratin intermediate filaments in the regulation of epithelial barrier function and apico-basal polarity', *Tissue Barriers*, 4(3), p. e1178368. doi: 10.1080/21688370.2016.1178368.

Salgia, M. M. *et al.* (2019) 'Different roles of peroxisome proliferator-activated receptor gamma isoforms in prostate cancer', *American Journal of Clinical and Experimental Urology*, 7(3), p. 98. Available at: /pmc/articles/PMC6627550/ (Accessed: 8 November 2023).

Samavedi, S. and Joy, N. (2017) '3D printing for the development of in vitro cancer models', *Current Opinion in Biomedical Engineering*, 2, pp. 35–42. doi: 10.1016/J.COBME.2017.06.003.

Sapna, N. and Vandana, K. L. (2011) 'Evaluation of hyaluronan gel (Gengigel®) as a topical applicant in the treatment of gingivitis', *Journal of Investigative and Clinical Dentistry*, 2(3), pp. 162–170. doi: 10.1111/j.2041-1626.2011.00064.x.

Sawada, N. (2013) 'Tight junction-related human diseases', *Pathology International*, 63(1), pp. 1–12. doi: 10.1111/PIN.12021.

Scheller, J., Garbers, C. and Rose-John, S. (2014) 'Interleukin-6: From basic biology to selective blockade of pro-inflammatory activities', *Seminars in Immunology*, 26(1), pp. 2–12. doi: 10.1016/J.SMIM.2013.11.002.

Schincaglia, G. P. *et al.* (2017) 'Clinical, Immune, and Microbiome Traits of Gingivitis and Peri-implant Mucositis', *Journal of Dental Research*, 96(1), pp. 47–55. doi: 10.1177/0022034516668847.

Schindelin, J. *et al.* (2012) 'Fiji: An open-source platform for biological-image analysis', *Nature Methods*. Nature Publishing Group, pp. 676–682. doi: 10.1038/nmeth.2019.

Schwarzberg, K. *et al.* (2014) 'The Personal Human Oral Microbiome Obscures the Effects of Treatment on Periodontal Disease', *PLOS ONE*, 9(1), p. e86708. doi: 10.1371/JOURNAL.PONE.0086708.

Schwertschlag, U. *et al.* (1999) 'Hematopoietic, immunomodulatory and epithelial effects of interleukin-11', *Leukemia*, 13(9), pp. 1307–1315. doi: 10.1038/sj.leu.2401514.

Seargent, J. M., Yates, E. A. and Gill, J. H. (2004) 'GW9662, a potent antagonist of PPARγ, inhibits growth of breast tumour cells and promotes the anticancer effects of the PPARγ agonist rosiglitazone, independently of PPARγ activation', *British Journal of Pharmacology*, 143(8), p. 933. doi: 10.1038/SJ.BJP.0705973.

Sentis, S. *et al.* (2005) 'Sumoylation of the Estrogen Receptor α Hinge Region Regulates Its Transcriptional Activity', *Molecular Endocrinology*, 19(11), pp. 2671–2684. doi: 10.1210/ME.2005-0042.

Sever, R. and Glass, C. K. (2013) 'Signaling by nuclear receptors', *Cold Spring Harbor Perspectives in Biology*, 5(3). doi: 10.1101/cshperspect.a016709.

Shafiq, N. *et al.* (2005) 'Pilot trial: Pioglitazone versus placebo in patients with plaque psoriasis (the P6)', *International Journal of Dermatology*, 44(4), pp. 328–333. doi: 10.1111/j.1365-4632.2005.02504.x.

Shang, L. *et al.* (2018) 'Multi-species oral biofilm promotes reconstructed human gingiva epithelial barrier function', *Scientific Reports*, 8(1), p. 16061. doi: 10.1038/s41598-018-34390-y.

Sharifi, A. M., Hoda, F. E. and Noor, A. M. (2010) 'Studying the effect of LPS on cytotoxicity and apoptosis in PC12 neuronal cells: Role of Bax, Bcl-2, and Caspase-3 protein expression', *Toxicology Mechanisms and Methods*, 20(6), pp. 316–320. doi: 10.3109/15376516.2010.486420.

Shetty, N., Thomas, B. and Ramesh, A. (2008) 'Comparison of neutrophil functions in diabetic and healthy subjects with chronic generalized periodontitis', *Journal of Indian Society of Periodontology*, 12(2), p. 41. doi: 10.4103/0972-124X.44089.

Sikora, M. J. *et al.* (2016) 'Endocrine Response Phenotypes Are Altered by Charcoal-Stripped Serum Variability', *Endocrinology*, 157(10), pp. 3760–3766. doi: 10.1210/EN.2016-1297.

Smith, M. A. and Bidochka, M. J. (1998) ‘Bacterial fitness and plasmid loss: the importance of culture conditions and plasmid size’, *Canadian Journal of Microbiology*, 44(4), pp. 351–355. Available at: https://pubmed.ncbi.nlm.nih.gov/9674107/ (Accessed: 19 May 2023).

Socransky, S. S. *et al.* (1998) ‘Microbial complexes in subgingival plaque’, *Journal of Clinical Periodontology*, 25(2), pp. 134–144. doi: 10.1111/J.1600-051X.1998.TB02419.X.

Srinivasan, B. *et al.* (2015) ‘TEER Measurement Techniques for In Vitro Barrier Model Systems’, *Journal of Laboratory Automation*. SAGE Publications Inc., pp. 107–126. doi: 10.1177/2211068214561025.

Steinert, P. M. (2000) ‘The complexity and redundancy of epithelial barrier function’, *Journal of Cell Biology*. Rockefeller University Press, pp. 5–7. doi: 10.1083/jcb.151.2.f5.

Stevens, L. J. and Page-McCaw, A. (2012) ‘A secreted MMP is required for reepithelialization during wound healing’, *Molecular Biology of the Cell*, 23(6), pp. 1068–1079. doi: 10.1091/MBC.E11-09-0745/ASSET/IMAGES/LARGE/1068FIG7.JPEG.

Studer, R. and Potchen, J. (1971) ‘The radioisotopic assessment of regional microvascular permeability to macromolecules’, *Microvascular Research*, 3(1), pp. 35–48. doi: 10.1016/0026-2862(71)90005-7.

Summers, A. (2009) ‘Gingivitis: diagnosis and treatment’, *Emergency Nurse*, 17(1), pp. 18–20.

Supino, R. (1995) ‘In Vitro Toxicity Testing Protocols’, in Walker, J. M. (ed.) *Methods in Molecular Biology*. Humana Press, pp. 137–149.

Takahara, T. *et al.* (2022) ‘TGFB1 mRNA expression is associated with poor prognosis and specific features of inflammation in ccRCC’, *Virchows Archiv*, 480(3), pp. 635–643. doi: 10.1007/S00428-021-03256-6/FIGURES/3.

Takahashi, N. *et al.* (2019) ‘Gingival epithelial barrier: regulation by beneficial and harmful microbes’, *https://doi.org/10.1080/21688370.2019.1651158*, 7(3). doi: 10.1080/21688370.2019.1651158.

Tanos, B. and Rodriguez-Boulan, E. (2008) ‘The epithelial polarity program: machineries involved and their hijacking by cancer’, *Oncogene 2008 27:55*, 27(55), pp. 6939–6957. doi: 10.1038/onc.2008.345.

Tarannum, F. and Faizuddin, M. (2012) ‘Effect of gene polymorphisms on periodontal diseases’, *Indian Journal of Human Genetics*, 18(1), p. 9. doi: 10.4103/0971-6866.96638.

Tatara, T. *et al.* (2018) ‘3D Culture Represents Apoptosis Induced by Trastuzumab Better than 2D Monolayer Culture’, *Anticancer Research*, 38(5). doi: 10.21873/anticanres.12528.

The British Society of Periodontology (2018) *Implementing the 2017 classification of periodontal diseases to reach a diagnosis in clinical practice*.

Thomson, A. *et al.* (2019) 'The Ussing chamber system for measuring intestinal permeability in health and disease', *BMC Gastroenterology*, 19. doi: 10.1186/s12876-019-1002-4.

Timmerman, M. F. and van der Weijden, G. A. (2006) 'Risk factors for periodontitis', *International Journal of Dental Hygiene*, 4(1), pp. 2–7. doi: 10.1111/J.1601-5037.2006.00168.X.

Treuter, E. and Venteclef, N. (2011) 'Transcriptional control of metabolic and inflammatory pathways by nuclear receptor SUMOylation', *Biochimica et Biophysica Acta (BBA) - Molecular Basis of Disease*, 1812(8), pp. 909–918. doi: 10.1016/J.BBADIS.2010.12.008.

Tsou, C. H. *et al.* (2017) 'Antibacterial Property and Cytotoxicity of a Poly(lactic acid)/Nanosilver-Doped Multiwall Carbon Nanotube Nanocomposite', *Polymers 2017, Vol. 9, Page 100*, 9(3), p. 100. doi: 10.3390/POLYM9030100.

Tunggal, J. A. *et al.* (2005) 'E-cadherin is essential for in vivo epidermal barrier function by regulating tight junctions', *The EMBO Journal*, 24(6), pp. 1146–1156. doi: 10.1038/sj.emboj.7600605.

Vanderburgh, J., Sterling, J. A. and Guelcher, S. A. (2016) '3D Printing of Tissue Engineered Constructs for In Vitro Modeling of Disease Progression and Drug Screening', *Annals of Biomedical Engineering 2016 45:1*, 45(1), pp. 164–179. doi: 10.1007/S10439-016-1640-4.

Vane, J. R. and Botting, R. M. (1998) 'Mechanism of Action of Nonsteroidal Anti-inflammatory Drugs', *The American Journal of Medicine*, 104(3), pp. 2S-8S. doi: 10.1016/S0002-9343(97)00203-9.

Waddington, R., Moseley, R. and Embery, G. (2008) 'Periodontal Disease Mechanisms: Reactive oxygen species: a potential role in the pathogenesis of periodontal diseases', *Oral Diseases*, 6(3), pp. 138–151. doi: 10.1111/j.1601-0825.2000.tb00325.x.

Wang, C. *et al.* (2001) 'Direct Acetylation of the Estrogen Receptor α Hinge Region by p300 Regulates Transactivation and Hormone Sensitivity', *Journal of Biological Chemistry*, 276(21), pp. 18375–18383. doi: 10.1074/jbc.M100800200.

Wang, H. *et al.* (2018) 'Establishment and comparison of air-liquid interface culture systems for primary and immortalized swine tracheal epithelial cells', *BMC Cell Biology*, 19(1), pp. 1–10. doi: 10.1186/s12860-018-0162-3.

Wang, N. *et al.* (2002) 'Constitutive activation of peroxisome proliferator-activated receptor-γ suppresses pro-inflammatory adhesion molecules in human vascular endothelial cells', *Journal of Biological Chemistry*, 277(37), pp. 34176–34181. doi: 10.1074/jbc.M203436200.

Watkins, S. M. *et al.* (2002) 'Lipid metabolome-wide effects of the PPARγ agonist rosiglitazone', *Journal of Lipid Research*, 43(11), pp. 1809–1817. doi: 10.1194/jlr.M200169-JLR200.

Watt, F. M. (1983) ‘Involucrin and Other Markers of Keratinocyte Terminal Differentiation’, *Journal of Investigative Dermatology*, 81(1), pp. S100–S103. doi: 10.1111/1523-1747.EP12540786.

Weigel, N. L. (1996) ‘Steroid hormone receptors and their regulation by phosphorylation’, *Biochemical Journal*, 319(3), pp. 657–667. doi: 10.1042/BJ3190657.

Van der Weijden, F. A. *et al.* (2015) ‘Can Chemical Mouthwash Agents Achieve Plaque/Gingivitis Control?’, *Dental Clinics of North America*, 59(4), pp. 799–829. doi: 10.1016/j.cden.2015.06.002.

Wenzl, K. *et al.* (2015) ‘The Nuclear Orphan Receptor NR4A1 and NR4A3 as Tumor Suppressors in Hematologic Neoplasms’, *Current Drug Targets*, 16(1), pp. 38–46.

Werman, A. *et al.* (1997) ‘Ligand-independent Activation Domain in the N Terminus of Peroxisome Proliferator-activated Receptor γ (PPARγ)’, *Journal of Biological Chemistry*, 272(32), pp. 20230–20235. doi: 10.1074/jbc.272.32.20230.

Wertz, P. W. (2021) ‘Roles of Lipids in the Permeability Barriers of Skin and Oral Mucosa’, *International Journal of Molecular Sciences*, 22(10), p. 5229. doi: 10.3390/ijms22105229.

Westin, S., Rosenfeld, M. G. and Glass, C. K. (1999) ‘Nuclear Receptor Coactivators’, *Advances in Pharmacology*, 47(C), pp. 89–112. doi: 10.1016/S1054-3589(08)60110-6.

White, P. C. *et al.* (2018) ‘Cigarette smoke modifies neutrophil chemotaxis, neutrophil extracellular trap formation and inflammatory response-related gene expression’, *Journal of Periodontal Research*, 53(4), pp. 525–535. doi: 10.1111/jre.12542.

Woelber, J. P. *et al.* (2019) ‘The influence of an anti-inflammatory diet on gingivitis. A randomized controlled trial’, *Journal of Clinical Periodontology*, 46(4), pp. 481–490. doi: 10.1111/jcpe.13094.

Wohlfeil, M. *et al.* (2009) ‘Degree of gingivitis correlates to systemic inflammation parameters’, *Clinica Chimica Acta*, 401(1–2), pp. 105–109. doi: 10.1016/j.cca.2008.11.017.

Wu, J. *et al.* (2020) ‘Betaine attenuates LPS-induced downregulation of Occludin and Claudin-1 and restores intestinal barrier function’, *BMC Veterinary Research*, 16(1), pp. 1–8. doi: 10.1186/S12917-020-02298-3/TABLES/1.

Xu, H. E. *et al.* (1999) ‘Molecular Recognition of Fatty Acids by Peroxisome Proliferator-Activated Receptors’, *Molecular Cell*, 3, pp. 397–403.

Yamamoto, Y. and Gaynor, R. (2005) ‘Role of the NF-kB Pathway in the Pathogenesis of Human Disease States’, *Current Molecular Medicine*, 1(3), pp. 287–296. doi: 10.2174/1566524013363816.

Yang, L. *et al.* (2016) ‘An in vitro vascular chip using 3D printing-enabled hydrogel casting’, *Biofabrication*, 8(3), p. 035015. doi: 10.1088/1758-5090/8/3/035015.

Ye, P., *et al.* (2000) ‘Expression patterns of E-cadherin, involucrin, and connexin gap junction proteins in the lining epithelia of inflamed gingiva’, *The Journal of Pathology*, 192, pp. 58–66.

Yeh, T.-H. *et al.* (2007) ‘Increased Communication Among Nasal Epithelial Cells in Air-Liquid Interface Culture’, *The Laryngoscope*, 117(8), pp. 1439–1444. doi: 10.1097/MLG.0b013e318063e84f.

Zagursky, R. J. *et al.* (1985) ‘Rapid and easy sequencing of large linear double-stranded DNA and supercoiled plasmid DNA’, *Gene Analysis Techniques*, 2(5), pp. 89–94. doi: 10.1016/0735-0651(85)90011-1.

Zaidi, M. R. (2019) ‘The Interferon-Gamma Paradox in Cancer’, *Journal of Interferon and Cytokine Research*, 39(1), pp. 30–38. doi: 10.1089/JIR.2018.0087/ASSET/IMAGES/LARGE/FIGURE1.JPEG.

Zhang, J. *et al.* (2004) ‘Selective disruption of PPARγ2 impairs the development of adipose tissue and insulin sensitivity’, *Proceedings of the National Academy of Sciences of the United States of America*, 101(29), pp. 10703–10708. doi: 10.1073/PNAS.0403652101.

Zhang, Y. *et al.* (2018) ‘PPAR-γ agonist rosiglitazone ameliorates peritoneal deterioration in peritoneal dialysis rats with LPS-induced peritonitis through up-regulation of AQP-1 and ZO-1’, *Bioscience Reports*, 38(3). doi: 10.1042/BSR20180009/57923.

Zhao, W. *et al.* (2019) ‘Lucifer Yellow - A Robust Paracellular Permeability Marker in a Cell Model of the Human Blood-brain Barrier’, *Journal of Visualized Experiments*, (150). doi: 10.3791/58900.

Zheng, X., Zhang, W. and Hu, X. (2018) ‘Different concentrations of lipopolysaccharide regulate barrier function through the PI3K/Akt signalling pathway in human pulmonary microvascular endothelial cells’, *Scientific Reports*, 8(1). doi: 10.1038/s41598-018-28089-3.

Zhu, Y. *et al.* (1995) ‘Structural organization of mouse peroxisome proliferator-activated receptor gamma (mPPAR gamma) gene: alternative promoter use and different splicing yield two mPPAR gamma isoforms.’, *Proceedings of the National Academy of Sciences*, 92(17), pp. 7921–7925. doi: 10.1073/PNAS.92.17.7921.

Zingarelli, B. *et al.* (2003) ‘Peroxisome Proliferator Activator Receptor-γ Ligands, 15-Deoxy-Δ12,14-Prostaglandin J2 and Ciglitazone, Reduce Systemic Inflammation in Polymicrobial Sepsis by Modulation of Signal Transduction Pathways’, *The Journal of Immunology*, 171(12), pp. 6827–6837. doi: 10.4049/jimmunol.171.12.6827.

Zoete, V., Grosdidier, A. and Michielin, O. (2007) ‘Peroxisome proliferator-activated receptor structures: Ligand specificity, molecular switch and interactions with regulators’, *Biochimica et Biophysica Acta (BBA) - Molecular and Cell Biology of Lipids*, 1771(8), pp. 915–925. doi: 10.1016/J.BBALIP.2007.01.007.

Zou, P. *et al*. (2022) ‘Lipopolysaccharide downregulates the expression of ZO-1 protein through the Akt pathway’, *BMC Infectious Diseases*, 22(1). doi: 10.1186/s12879-022-07752-1.

9. APPENDICES

9.1. Publications arising from this thesis

This chapter comprises research completed during the course of study for this PhD, for which I am the major contributor and first author. This article is reused under license from the publisher, Mary Ann Liebert, Inc.

TISSUE ENGINEERING: Part C
Volume 28, Number 11, 2022
© Mary Ann Liebert, Inc.
DOI: 10.1089/ten.tec.2022.0130

termis
Tissue Engineering
& Regenerative Medicine
International Society

Open camera or QR reader and
scan code to access this article
and other resources online.



METHODS ARTICLE

A 3D Printed Device for *In Vitro* Generation of Stratified Epithelia at the Air–Liquid Interface

Benjamin Hewitt, BMedSc,[1] Joanna Batt, BDS, PhD,[1] Richard M. Shelton, BDS, PhD,[1]
Paul R. Cooper, PhD,[2] Gabriel Landini, PhD,[1] Robert A. Lucas, PhD,[3]
Malgorzata Wiench, PhD,[1,4] and Michael R. Milward, BDS, PhD[1]

Downloaded by Birmingham University from www.liebertpub.com at 07/08/23. For personal use only.

Air–liquid interface (ALI) cultures are used to produce stratified epithelial tissues *in vitro*, notably for the production of oral mucosal equivalents. Currently, there are few purpose-built devices, which aim to enhance the ease and reproducibility of generating such tissue. Most ALI cultures utilize stainless steel grids or cell culture inserts to elevate the matrix or scaffold to the surface of the culture media. In this study, a novel buoyant epithelial culture device (BECD) was designed to both contain a fibroblast-seeded collagen hydrogel and float in culture media, thereby automatically maintaining the ALI without further user intervention. BECDs aim to mitigate several issues associated with ALI culture; reducing the chance of media flooding the epithelial layer from physical disturbance, reducing technique sensitivity for less-experienced users, and improving the reproducibility of the epithelia generated. H400 oral squamous cell carcinoma cells cultured in BECDs for 7, 14, and 21 days showed continuous increase in epithelial tissue thickness with expected localization of epithelial differentiation markers: cytokeratin 5, involucrin, and E-cadherin. Fused filament fabrication three-dimensional printing with polypropylene used in BECD production allows for rapid turnover and design iteration, presenting a versatile, adaptable, and useful tool for application in *in vitro* cell culture.

Keywords: air–liquid interface, epithelial rafts, fused filament fabrication, oral mucosal equivalents, stratified epithelial tissue

Impact Statement

Developing pharmaceuticals and improving understanding of cell biology requires biomimetic models, ranging from two-dimensional cell cultures to *in vivo* animal studies. Three-dimensional (3D) cultures provide a cellular architecture resembling *in vivo* tissue, with a reduced need for expensive and ethically questioned animal studies. This article outlines a 3D printed device for producing stratified epithelia typically found in cutaneous and mucosal tissues. These devices were designed to improve ease of use and reproducibility, while reducing cost compared with current methods and are shown to produce tissue with histological structure and differentiation similar to *in vivo* stratified epithelia.

[1]School of Dentistry, Institute of Clinical Sciences, University of Birmingham, Birmingham, United Kingdom.
[2]Department of Oral Sciences, Faculty of Dentistry, Sir John Walsh Research Institute, University of Otago, Dunedin, New Zealand.
[3]GlaxoSmithKline Consumer Healthcare, Weybridge, United Kingdom.
[4]Institute of Cancer and Genomic Sciences, University of Birmingham, Birmingham, United Kingdom.

Downloaded by Birmingham University from www.liebertpub.com at 07/08/23. For personal use only.

Introduction

Stratified epithelial tissue is found in the epidermis, oral mucosa, cornea,[1] urinary tract,[2] esophagus, and trachea.[3] Stratified epithelia typically form a homeostatic barrier, with the characteristic multilayered structure protecting against ultraviolet radiation,[4] forming a waterproof and abrasion-resistant layer[5] and providing both passive resistance and active immune response to bacterial ingress and colonization.[6] Compromising the epithelium integrity may result in homeostatic imbalance and bacterial infection of the deeper tissues, as commonly seen in burn victims. Barrier function compromise also occurs during epithelial–mesenchymal transition, and is suggested as a pathogenic mechanism in periodontitis.[7]

Stratified epithelia are separated from underlying connective tissue by a basement membrane (BM). Proliferative cells adjacent to the BM form the basal layer and give rise to a spinous cell layer[8] predominantly expressing cytokeratins 5 and 14.[9] Cells obtain an increasingly mature phenotype while migrating away from the basal layer, differentiating further into granular and cornified cells predominantly expressing cytokeratins 1 and 10.[10] The terminally differentiated cornified cell layer is most superficially located and provides resistance to physical and chemical attack, especially from abrasion, requiring that this layer is replenished by continued epithelial stratification.[9] Involucrin expression is a key marker of these terminally differentiated epithelial cells, forming a protein precursor for the insoluble cornified cell envelope.[11,12]

The production of stratified epithelial tissue *in vitro* provides a useful model for studying the function of normal epithelium as well as the changes that accompany a wide range of epithelial diseases. This allows for more representative cytotoxicity and biocompatibility testing than is provided by simple monolayer cultures,[13] as cell differentiation, morphology, and signaling are shown to more closely represent cells or tissue *in vivo* when cultured organotypically.[14,15] For this reason, organotypic oral mucosal equivalents are considered more advanced in the study of cancers, periodontal disease, and high-throughput *in vitro* drug efficacy studies.

Air–liquid interface (ALI) cultures produce stratified epithelia *in vitro*, with a fibroblast-seeded matrix (or other supporting scaffold) submerged in media and keratinocyte layer exposed to air.[16] While the exact mechanism of ALI-induced stratification is unknown, this approach is widely understood to be an effective method to produce stratified epithelia. A proposed mechanism is that direct exposure to oxygen triggers oxidative stress, increasing cellular glutathione levels, promoting cell growth and differentiation.[17]

Current ALI culture systems utilize Transwell inserts[18,19] or stainless steel mesh, raising the cell scaffold from the surface of the culture dish.[16,20] ALI maintenance requires frequent adjustments of media volume to account for evaporation and scaffold shrinkage due to fibroblast contraction. Variation in ALI may cause inconsistent differentiation or stratification, and mitigation of this is essential to maintain scientific rigor.

The use of a buoyant system could improve both the ease of generation and reproducibility of ALI culture by simultaneously retaining a fibroblast-seeded collagen hydrogel and maintaining the ALI.

Materials and Methods

Ethical approval

Ethical approval was gained under NHS South West–Central Bristol research ethics committee (REC) code 19/SW/0198.

Design considerations and requirements

The system comprises a buoyant epithelial culture device (BECD) and submerging ring, both fabricated through a fused filament fabrication (FFF) process in polypropylene (PP). The submerging ring is placed over the upper surface of the BECD, forcing the BECD under the culture media once the plate lid is applied. This allows for a period of submersion to enable the epithelial cells to grow to confluency, before removing the submerging ring and bringing the epithelium to the ALI.

Thermoplastics selected for such device are required to be noncytotoxic and compatible with extrusion, sterilization, and culture conditions. Potential materials were screened for a lack of reported cytotoxicity and a melting temperature suitable for FFF extrusion between 170°C and 250°C. Three materials were chosen for initial characterization: PP,[21,22] poly-lactic acid (PLA),[23,24] and polycarbonate (PC)[25,26]

Following initial printing trials, PP (BASF, Netherlands) was chosen for BECD fabrication in subsequent experiments. BECD design files are openly available and can be found in the Supplementary Materials.

Buoyant epithelial culture device design and fabrication

ALI culture devices were developed using a computer-aided design (CAD) package (Fusion 360, Autodesk, USA) with an internal diameter of 15 mm and outer diameter of 33 mm. STL files for the devices were exported by slicing into .gcode format (Ultimaker Cura 4.6, Ultimaker, the Netherlands). Engineering drawings and three-dimensional (3D) renderings of the devices were generated within the same CAD package (Fusion 360, Autodesk).

BECDs and submerging rings were fabricated on a bespoke FFF system with a brass 0.6 mm diameter nozzle (E3D, United Kingdom), 0.5 mm initial layer height, 0.32 mm successive layer height, 40 mm/s print speed, 240°C extrusion temperature, and 80°C bed in 1.75 mm PP filament (UltraFuse/BASF, Netherlands). Three top layers and one skin layer were incorporated to reduce the risk of voids forming in the upper surface, which could allow media ingress. The heated borosilicate bed was covered with PP tape for increased part adhesion.

BECDs and submerging rings were immersed in 70% ethanol overnight to aid in removal of any build surface residue and begin the decontamination process before sterilization (Fig. 1A–C). Twenty-five-millimeter-wide Kapton tape (RS Electronics, United Kingdom) was applied across the base of the BECD to prevent leakage during the collagen matrix gelling process (Fig. 1D). The submerging rings and BECDs—with tape *in situ*—were then autoclaved (MLS-3781L, Sanyo, Japan) at 121°C, 101 kPa for 15 min.

Cross-section (Fig. 1Ei), top–down (Eii), and isometric (Eiii) engineering drawings of the BECD are shown, depicting relevant dimensions and features. Corresponding views are also shown of the submerging ring (Fi–iii). A 3D rendering of the complete BECD with submerging ring *in situ*, as would be used for the 3-day submersion period, is shown in Figure 1G.

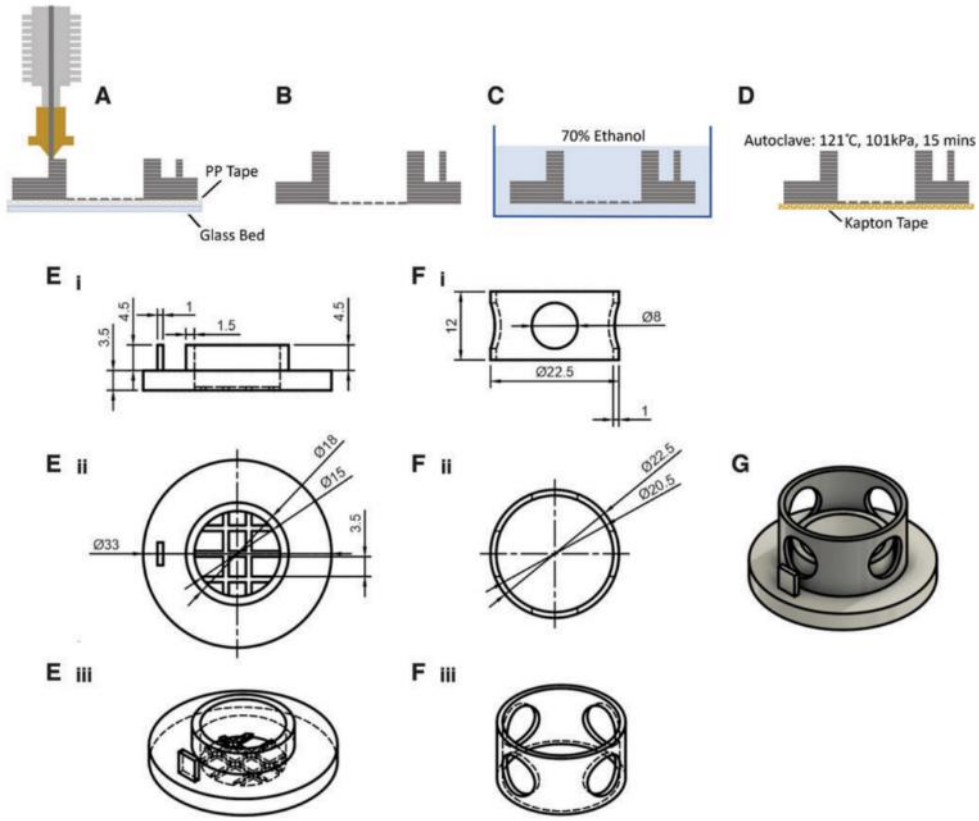


FIG. 1. Schematic diagrams and engineering drawings showing the BECD design and steps involved in the production and processing of 3D printed BECDs. **(A)** 3D printing through fused filament fabrication with polypropylene material on a heated borosilicate glass bed. Heated bed was coated in PP tape for increased part adhesion. **(B)** Construct with PP tape removed. **(C)** Immersion in 70% ethanol for removal of tape residue and initial decontamination. **(D)** Addition of Kapton polyamide tape before sterilization by autoclave. Kapton tape provided a sealing film, preventing the leakage of collagen solution before gelling. **(E)** Engineering drawings of the BECD construct with side **(i)**, top **(ii)**, and isometric **(iii)** views. All units shown in millimeters. **(F)** Engineering drawings of the submerging ring with side **(i)**, top **(ii)**, and isometric **(iii)** views. All units shown in millimeters. **(G)** 3D rendering of the BECD with submerging ring in place. 3D, three-dimensional; BECD, buoyant epithelial culture device; PP, polypropylene.

Downloaded by Birmingham University from www.liebertpub.com at 07/08/23. For personal use only.

Cell culture

Murine 3T3 fibroblasts (ECACC 85022108) were cultured in Dulbecco's modified Eagle's medium (DMEM; Gibco, United Kingdom) supplemented to final concentrations of 10% fetal calf serum (Gibco), 100 U/mL penicillin, 100 µg/mL streptomycin (both Gibco), and 1 mM L-glutamine (Thermo Fisher, United Kingdom).

H400 oral squamous cell carcinoma cells[27] (ECACC 06092006) were cultured in 1:1 Hams F12:DMEM, (Gibco), supplemented as above.

Human tissues were sourced following ethics approval under NHS ethics 19/SW/0198, collected as waste from surgical procedures at Birmingham Dental Hospital and School of Dentistry, Birmingham, United Kingdom.

Production of stratified epithelia using BECDs

A 10× reconstitution buffer was prepared by the addition of 1.1 g $NaHCO_3$ and 2.385 g HEPES (both Sigma-Aldrich, United Kingdom) to 50 mL dH_2O. A 10×DMEM and 10× reconstitution buffer was sterilized by passing through a 0.22 µm syringe filter. One milliliter of 3 mg/mL rat tail collagen (Thermo Fisher) was then added to 100 µL 10×

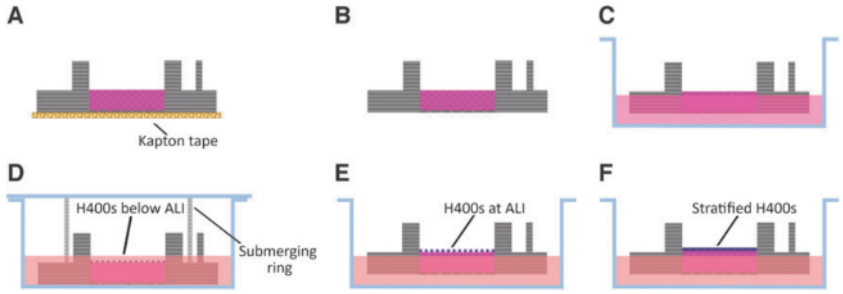


FIG. 2. Steps applied for the use of BECDs in establishing a fibroblast-seeded collagen gel and seeding keratinocytes on the surface for stratification through ALI culture. **(A)** Addition of 1.2 mL fibroblast seeded collagen. **(B)** 90 min incubation to allow for gelling, followed by removal of Kapton tape. **(C)** Overnight incubation in supplemented DMEM. **(D)** Addition of H400 cells onto surface to final concentration of 8×10^4 cells/culture. Three-day submersed incubation using 3D printed forced submersion ring. **(E)** Removal of submersion ring to enable ALI culture. **(F)** Incubation at 37°C, 5% CO_2 to enable epithelial stratification. Diagrams are not to scale. ALI, air–liquid interface; CO_2, carbon dioxide; DMEM, Dulbecco's modified Eagle's medium.

Downloaded by Birmingham University from www.liebertpub.com at 07/08/23. For personal use only.

DMEM (Gibco) and 100 µL 10×reconstitution buffer. One molar NaOH was added dropwise to produce a pink-colored solution, at pH 6.9, measured using a Beckman Φ40 pH meter (Beckman Coulter, USA). Viable 3T3 fibroblasts were counted using a hemocytometer and Trypan Blue dye exclusion. The 3T3 fibroblasts were added to the solution immediately after its preparation to a final concentration of 5×10^4 cells/mL and the solution mixed well by pipetting on ice.

Devices were placed in six-well plates and 1.2 mL buffered collagen solution with fibroblasts was added per BECD (Fig. 2A). Devices were incubated at 37°C, 5% carbon dioxide (CO_2) for 90 min until a firm gel had formed; Kapton tape was aseptically removed and devices were placed into a new six-well plate (Fig. 2B). Three milliliters of DMEM was added to each well. The BECDs were then incubated at 37°C, 5% CO_2 for 24 h to allow initial growth of 3T3 fibroblasts (Fig. 2C).

Culture medium was replaced with 2 mL supplemented Hams F12:DMEM. H400 cells were counted and diluted to a final concentration of 8×10^4 cells/mL, with 1 mL of suspension added to the upper gel surface, to a final 3 mL total media volume. Submerging rings were placed on top of the BECDs submerging the devices once the plate lid was applied (Fig. 2D), and incubated for 72 h at 37°C, 5% CO_2.

The submerging rings were removed and BECDs transferred to a plate containing 3 mL of Hams F12:DMEM per well. Removal of the submerging rings allowed the devices to float on the culture media, exposing the confluent H400 cell layer to air (Fig. 2E). Devices were cultured at the ALI for 7, 14, or 21 days, with media changes every second day. Five independent biological replicates were produced, with two technical replicates (BECD cultured rafts) for each biological replicate and time point.

Histological processing

Hydrogels were fixed overnight at room temperature (RT) in 10% neutral buffered formalin (Surgipath Europe Limited, United Kingdom), and dehydrated in a series of graded ethanol from 10% to 100%, 10 min each. The 100% alcohol step was repeated three times, followed by 2×10-min immersions in xylene and 24-h immersion in 60°C histological paraffin wax. Samples were moved through two changes of paraffin wax at 60°C before embedding and sectioning (4 µm sections) using a rotary microtome (RM2035, Leica Instruments, Germany). Sections were floated onto glass slides, heated in a 60°C oven for 1 h, dewaxed in xylene, and stained with Hematoxylin and Eosin (H&E), following standard protocols.[28]

Immunofluorescence staining

Sections prepared as described above were dewaxed and cells permeabilized by exposure to 0.25% Triton X-100 (Sigma-Aldrich, USA) in phosphate-buffered saline (PBS), 10 min, at RT, washed with PBS and blocked with goat serum (Sigma-Aldrich, UK) diluted 1:5 in PBS for 10 min at RT. Primary antibodies (anti-E-Cadherin [rabbit mAb, Ab76319], anti-Involucrin [mouse mAb, Ab80530], and anti-cytokeratin 5 [rabbit mAb, Ab52635]) were diluted 1:100 in PBST-BSA (10 mg/mLl BSA in PBS with 0.1% Tween 20 [Sigma-Aldrich, UK]) and incubated at RT for 1 h.

Samples were washed 3×in PBST for 5 min. Fluorophore-conjugated secondary antibodies were diluted either 1:200 (goat pAb anti-rabbit IgG, Ab150077) or 1:1000 (goat pAb anti-mouse IgG, Ab150113) with PBST-BSA supplemented to a final concentration of 10% type AB human plasma. Samples were incubated with secondary antibodies for 1 h at RT, washed three times in PBST for 2 min each and mounted in Fluoroshield mounting medium containing DAPI (Sigma-Aldrich, UK). All antibodies were supplied by Abcam (Cambridge, UK). Samples were imaged using a Zeiss LSM700 confocal microscope, maintaining the same imaging settings for all samples.

Image processing and analysis

Images were processed using Fiji,[29] with the simple interactive object extraction (SIOX) plugin utilized for segmentation of the epithelial cell layer. A SIOX preset was generated and applied to all images, ensuring unbiased

Downloaded by Birmingham University from www.liebertpub.com at 07/08/23. For personal use only.

segmentation. Approximately 5% of SIOX-segmented images presented some regions with false-positive selection, and segmentation was manually modified in these cases for these regions only.

The SIOX image was then processed through a macro within Fiji, wherein any holes in the segmented epithelium were filled and the Euclidean Distance Transform (EDT) was used to compute the distance from each epithelial tissue pixel to the closest epithelial boundary (i.e., superficial or basal). Since the maximum value of the EDT occurs at the thickest location(s) in the epithelium and its position is equidistant to both superficial and basal tissue boundaries, the EDT value was multiplied by two to give the maximal epithelial thickness and a precalculated pixel:μm calibration factor applied to produce thickness measurements in micrometers.

Statistical analyses

Statistical analyses were performed using GraphPad Prism 9.1.0 (GraphPad Software, San Diego, CA). Biological replicates are presented as mean values with standard deviation. Statistical analyses of inter- and intrareplicate maximum epithelial thickness was performed using two-way analysis of variance followed by Šídák's multiple comparisons test with significance level at $p < 0.05$.

For each biological replicate, two devices were cultured per time point, established with the same population of cells to provide technical replicates.

Two slides were produced for each technical replicate at each time point, with one section obtained ~2 mm and a second section obtained ~10 mm from the block face. This approach was employed to identify any changes in epithelial thickness across the diameter of the hydrogel. Data from both sections were incorporated into the final average for each biological replicate, giving four total technical replicates.

Experiment

Assessment of the suitability of PP-based BECDs to maintain long-term epithelial tissue culture.

PP, PLA, and PC were initially trialed for 3D printing of BECDs. PLA exhibited deformation immediately after sterilization and embrittlement after prolonged cell culture (data not shown). PC was difficult to reliably print due to substantial issues with bed adhesion. The melting point of PP enabled both extrusion in consumer-grade FFF systems and autoclave sterilization without deformation. PP withstood long periods of incubation at 37°C without obvious embrittlement, structural failure, or media absorption. PP-based BECDs were therefore used for epithelial cultures supported by collagen hydrogels with embedded fibroblasts (Fig. 3).

BECD cultures using H400 cells and collagen-embedded 3T3 fibroblasts were established by immersion in media for 72 h using the submerging ring (Fig. 3A–C). After ring removal, the BECDs were allowed to float on the media surface at the ALI for 7, 14, and 21 days. The BECDs showed minimal media ingress and effective ALI maintenance, even after 21 days in culture (Fig. 3D). Staining with H&E allowed for analysis and quantification of changes in epithelial thickness with time (Fig. 4A, C, E). Importantly, both fibroblasts and epithelial cells were viable after 7, 14, and 21 days of ALI culture confirming the low levels of cytotoxicity of PP-based BECDs in *in vitro* culture systems.[22,30]

Following 7 days of ALI culture, a thin stratified epithelium was visible on the upper surface of the collagen gel (Fig. 4A, B). There was a qualitative increase in epithelial thickness from 7 to 14 days of ALI culture (Fig. 4C, D) and a further marked increase from 14 to 21 days (Fig. 4E, F), indicating an effective maintenance of ALI environment when using the BECDs. However, no keratinization was noted after 21 days of culture at the ALI. BECD-cultured H400 cells exposed to the ALI for 7 days showed some irregular stratification, which was noticeably reduced after 14 days culture at the ALI. Fibroblasts could be observed throughout the collagen hydrogel and showed a visually homogeneous distribution.

SIOX segmentation and thresholding of the H&E-stained micrographs enabled extraction of the epithelial tissue component with minimal false-positive selection when evaluated visually (Fig. 4B, D, F). It presented a reproducible, objective approach for isolating and segmenting the epithelial tissue produced by BECDs, which was subsequently used to automate the process of epithelial thickness measurement.

Assessment of the reproducibility of BECD-grown epithelial tissue thickness

The performance of BECDs was next characterized by quantification of epithelial thickness and assessment of

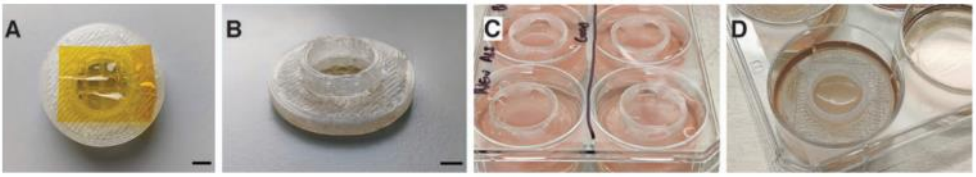


FIG. 3. Images of steps in production and use of BECDs for stratified epithelial culture. Scale bars are 5 mm where shown. **(A)** BECD with Kapton tape *in situ*, before sterilization by autoclave—*bottom* view. **(B)** BECD with Kapton tape *in situ*, perspective view. **(C)** BECDs in culture with submerging ring in place for 3-day submersed incubation step (Step D in Fig. 2). **(D)** BECD following 21 days of ALI culture. Minimal media ingress to BECD structure was noted, with ALI well maintained.

Downloaded by Birmingham University from www.liebertpub.com at 07/08/23. For personal use only.

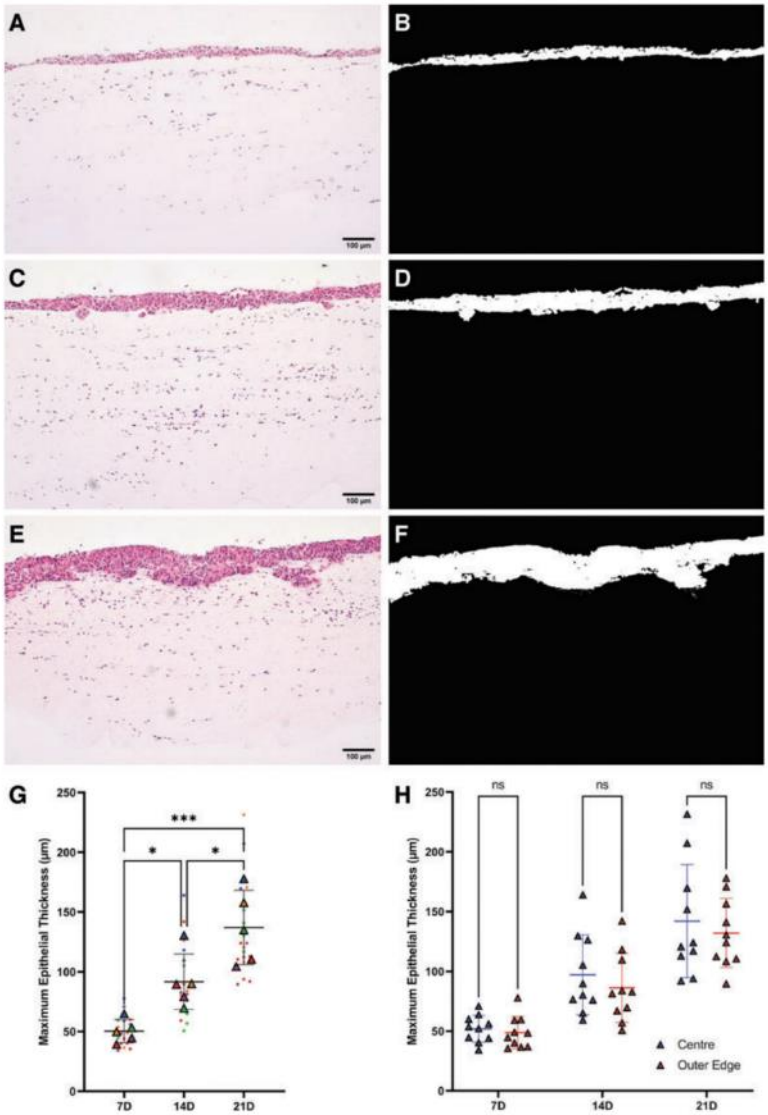


FIG. 4. **(A–F)** Representative photomicrographs of H&E-stained sections of BECD-cultured H400 cells on a collagen-3T3 fibroblast gel for 7 **(A)**, 14 **(C)**, and 21 **(E)** days. The corresponding SIOX segmented image is shown for each micrograph shown on the *right*-hand side, isolating the layers of epithelium, *white* **(B, D, E)**. Scale bars 100 µm. **(G)** Maximum epithelial thickness ''superplot'' for H400 cells cultured at the ALI using BECDs. Biological replicates (*triangle* symbols) are color matched to their respective technical replicates (small *circle* symbols). Statistical analyses performed through one-way ANOVA and Tukey's multiple comparisons test. $*p<0.05$, $**p<0.01$, $***p<0.001$. $N=5$, four technical replicates per time point, standard deviation shown. **(H)** MET comparison between microtome sections from the inner region of the hydrogel (*blue triangle* symbols) and outer regions (*red triangle* symbols). Data include all technical replicates ($N=5$) from all biological replicates of H400 epithelia cultured using the BECD system. Statistical analyses performed using two-way ANOVA and Šídák's multiple comparisons test. Ns, no significance. Standard deviation shown. ANOVA, analysis of variance; MET, maximal epithelial thickness; SIOX, simple interactive object extraction.

inter- or intrareplicate variability. Five biological replicates were cultured for 7, 14, and 21 days. Following H&E staining and segmentation using SIOX, the maximal epithelial thickness (MET) of each sample was analyzed using an automated macro procedure, reducing bias and improving measurement reproducibility.

There was a significant increase in MET from 7 to 14 days of culture ($p<0.05$), with an average MET of 50.34 μm, increasing to 91.66 μm after 14 days (Fig. 4G). After 21 days, a further significant increase in MET was observed ($p<0.01$), with the average MET of 137.04 μm. The range of MET values in the technical replicates was seen to increase at 14 and 21 days of ALI culture and indicated more variability during prolonged periods of culture, as expected.

To identify possible variability in MET between the central (inner) region of the hydrogel and the outer edges, the sections were compared across the width of the BECD-cultured hydrogels (Fig. 4H). No significant difference was observed between the MET values of inner and outer hydrogel sections at the tested time points ($p>0.05$).

These data indicate that the BECD system successfully produced a stratified epithelial tissue using H400 cells and 3T3 fibroblasts in a collagen matrix.

Qualitative assessment of epithelial markers' expression in BECD-cultured tissues

Immunofluorescence staining allowed for a qualitative comparison of the localization of key differentiation markers in tissue cultured using the BECD system compared with control human gingival tissue. Gingiva is a highly orthokeratinized tissue with a thick and distinct cornified layer and well demarcated spinous and granular layers. This provided a suitable positive control for assessing epithelial differentiation markers, although artificial organotypic cultures, especially using cancer cells, were not expected to develop such high level of maturation.

Involucrin, a key marker of epithelial cell differentiation, showed expression in both control tissue and BECD-cultured tissue by 21 days at the ALI (Fig. 5). In control tissue, involucrin expression was localized to the upper layers of the stratified epithelia, with limited fluorescence detected in the cells immediately above the basal epithelial cell layer. A similar pattern was seen in BECD-cultured tissue after 21 days at the ALI, with increased staining further from the basal layer. This localization suggested terminal differentiation of the epithelial cells in BECD-cultured stratified epithelia was comparable with that observed *in vivo*. Cytokeratin 5 expression in control tissue was limited to cells immediately above the basal cell layer, decreasing as distance from the basal cell layer increased. Minimal expression was apparent in the uppermost cell layers. BECD culture tissue showed a similar trend, with the uppermost layers of cells showing minimal cytokeratin 5 expression, whereas the cells adjacent to the basal layer showed highest expression.

The transmembrane protein E-cadherin was selected as a marker of cell adhesion, with both control and BECD-cultured tissues showing staining for E-cadherin, localized to intracellular junctions. Expression was consistent from the basal cell layers to the more superficial cornified layers. These data indicated that H400-derived epithelial tissue cultured using the BECD system showed similar differentiation patterns as the control gingival tissue.

Discussion

This study aimed to design, and assess the utility of, a novel device to produce epithelial tissue with easily fabricated devices and reduced technique sensitivity compared with existing methodologies. The BECD enabled (i) the establishment of epithelial cultures when submerged in media using the submerging ring, (ii) a smooth and easy transition to the ALI environment, and (iii) long-term ALI cultures to be automatically maintained by floating on the media surface. BECDs considerably simplified typically highly technique-sensitive ALI culture, which has been shown to have high levels of interlaboratory variability.[31] It is also hypothesized that ALI culture is likely to have problematic levels of interuser variability due to its technique sensitivity.

The use of BECDs resulted in a growth of stratified epithelial tissues comparable with those obtained using traditional ALI methodologies, including Transwell inserts[32,33] or stainless steel mesh to raise the culture rafts.[16,34]

Previous work employing ALI-cultured H400 cells on a raised collagen gel demonstrated a similar epithelial tissue morphology and architecture following H&E staining compared with that presented in this study.[10] Similarly, it also showed no evidence of keratinization of H400 cells following 21 days of ALI culture with conventional techniques on a relatively basic collagen hydrogel, suggesting that the scaffold used has some determination on the final level of epithelial maturation. Modification of this scaffold material to more closely mimic epithelial dermis may be beneficial if this maturation is necessary or desired.

An epithelial layer of increasing thickness from 7 to 14, and 14 to 21 days of culture was apparent (Fig. 4), while SIOX quantification provided a rapid, unbiased thresholding and segmentation technique to quantify the thickness of these epithelial cultures. BECDs did not appear to exert any cytotoxic effect on the cells, as cultures showed appropriate stratification and no marked changes in morphology. Additionally, the absence of a significant difference in MET between epithelia at the outer edge and inner sections of the hydrogels suggested that epithelial thickness was constant across the width of the raft.

The thickness of the produced epithelial tissues demonstrated good reproducibility within both technical and biological repeats, which could be attributed to the consistent ALI maintenance in BECDs. A small increase in variability between replicates was noted at 14 and 21 days of culture, likely due to the shrinkage of the fibroblast/collagen matrix pulling some regions of epithelia below the ALI. Further work may identify a more dimensionally stable hydrogel replacement, reducing shrinkage in long-term cultures.[35] Variability may also be reduced further

Downloaded by Birmingham University from www.liebertpub.com at 07/08/23. For personal use only.

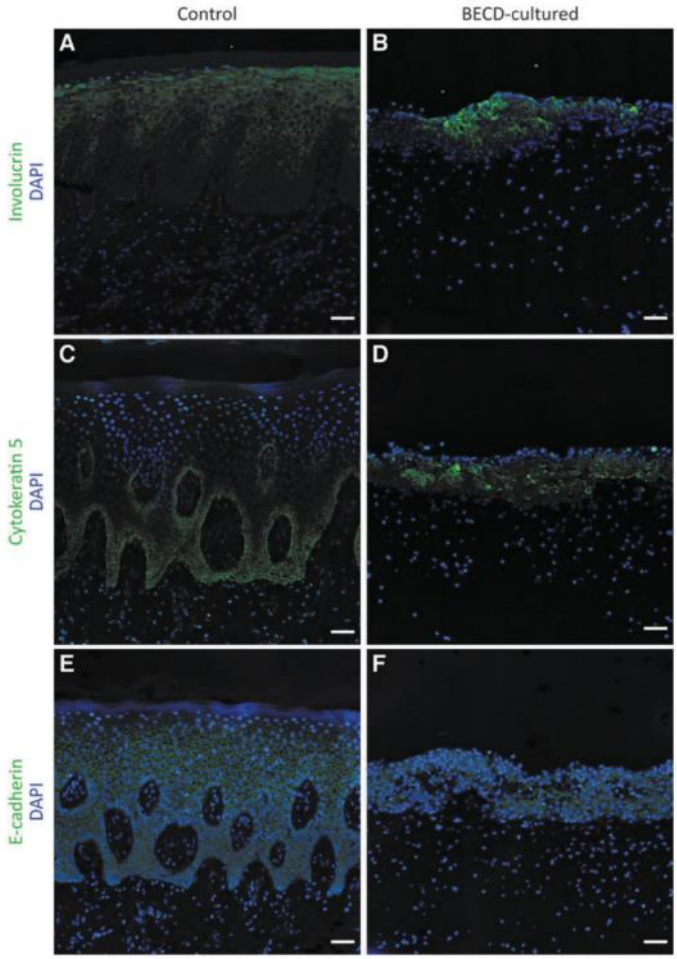


FIG. 5. Confocal images of control human gingival tissue **(A, C, E)** and epithelia cultured in BECDs for 21 days **(B, D, F)**. Involucrin is present and localized to the upper layers of the epithelia in control **(A)** and BECD-cultured H400s **(B)**. Inversely, cytokeratin 5 is localized to the *bottom* layers of both control **(C)** and BECD-cultured cells **(D)**. E-cadherin is also localized to intercellular junctions in both images **(E, F)**. AF488 (*green*) indicates protein of interest, with DAPI (*blue*) used as a nuclear counterstain. Scale bars: 50 μm.

Downloaded by Birmingham University from www.liebertpub.com at 07/08/23. For personal use only.

by optimizing print settings, leading to fewer voids, through which media ingress may occur after prolonged submersion. The nature of FFF as a layer-by-layer additive manufacturing process means that water-tight components can prove challenging to fabricate. Higher resolution 3D printers and smaller diameter nozzles are likely to provide an improvement and reduce variability even further.

Immunofluorescence staining allowed for a qualitative assessment of the expression and localization of key epithelial markers. These were all detected in the cultured epithelial tissue, indicating that the differentiation shown in BECD-cultured tissue was similar to that of the control tissue. Involucrin expression in both control tissue and BECD-cultured tissue was localized predominantly to the uppermost layers of the stratified epithelium, a finding consistent with previous reports.[11,36] Involucrin is a widely used marker of terminal epithelial differentiation, playing a key role in barrier function in healthy epithelia,[37] suggesting this function was likely to be maintained in these BECD-cultured tissues as observed *in vivo*.

Expression of cytokeratin 5 was noted in BECD-cultured epithelial tissues, with maximal expression in the basal cells, although this localization was not as clearly defined in cultured samples as in control tissue. These data, however, indicate that localization of cytokeratin 5 was similar to that of *in vivo* tissues.

E-cadherin has been shown to be crucial for normal cell adhesion processes, spanning the intracellular space and providing a junction between adjacent cells through its transmembrane domains.[38] E-cadherin expression was observed

Downloaded by Birmingham University from www.liebertpub.com at 07/08/23. For personal use only.

in BECD-cultured tissue, providing evidence that cell adhesion was maintained as observed in control tissues. As with cytokeratin 5 expression, E-cadherin expression in BECD-cultured tissue was not as clearly demarcated and localized as in control tissue. However, some variation is expected when using ALI-based systems, which are relatively simple compared with the complex *in vivo* environment.

It is notable that correctly stratified epithelia were developed despite the use of the H400 cell line, which was derived from an alveolar process squamous cell carcinoma. The immortal, rapidly dividing nature of this cell line is useful for research purposes, however, the differentiation and architectural arrangement of these cancer cells varies from the primary healthy human tissue.[27]

The BECD system is easily adaptable, allowing for rapid, reliable induction of ALI in any volume of culture media. A buoyant, self-leveling device is likely to reduce technique sensitivity with the possibility of improved reproducibility compared with conventional methodologies, improving the suitability of the BECD system for high-throughput applications. The system is more economical than Transwell devices, with each BECD costing a fraction of these commercially available devices. Raw material cost for a complete system of a single BECD and submerging ring is in the order of $0.05 per device, a cost $\sim 20\times$ less than a similar Transwell system. PP is readily available for use in FFF printers, providing a suitable mix of both material properties and low cytotoxicity.

The combination of CAD and FFF technologies allows for modification to include inserts or measurement probes, for example transepithelial electrical resistance readings for barrier function assessment. FFF has seen increasing use in the laboratory with a move to more ''open'' and accessible approaches to science, often employed as a step in the production of *in vitro* devices,[39,40] or for direct use *in vitro*, as described in this study.

In addition, 3D bioprinting has been employed for use in developing tissue constructs and models,[41,42] although these approaches are markedly different than producing *in vitro* culture devices from polymers.

In summary, BECDs provide an economical approach to ALI culture with the potential to reduce variability within ALI-cultured tissues. BECDs may be used to elucidate the mechanisms of epithelial tissue disorders, or trial drug candidates in a more realistic system than standard monolayer culture, with application to periodontal disease, epithelial tissue disorders, and oral cancers. The system may be used for the generation of other ALI-cultured tissues by modification of the cell types used, including cutaneous and bronchial epithelial tissues.[18] In addition to *in-vitro* studies, the BECD system may also find utility in clinical tissue engineering applications, due to the versatility and ease of generation of stratified epithelial tissue. The devices may be increased in scale to be used for the generation of oral mucosal equivalents for use *in vivo,* for example replacing tissue lost to trauma, disease, or surgical intervention.

Conclusion

The BECD system is a novel methodology for the production of stratified epithelial tissue with similar morphology and differentiation characteristics to *in vivo* tissue. Statistically significant epithelial stratification was noted between 7, 14, and 21 days of ALI culture. Key markers of epithelial differentiation and maturity were present and localized to regions of the epithelia that resembled control human tissue. These novel devices effectively produced epithelial tissue with reduced cost in comparison with current methods, in both financial input and researcher time. FFF is a suitable fabrication technique for these devices, employing a material with appropriate biological and material characteristics, while printing the devices at a scale suited to laboratory-based tissue culture. The devices have the potential for use in a wide range of *in vitro* studies of periodontal disease or oral cancer, and may also be modified to be used clinically to produce tissue equivalents for trauma victims.

Acknowledgment

The authors thank Dr Lauter Eston Pelepenko (Endodontics Division, Piracicaba Dental School FOP-Unicamp, Piracicaba, SP, Brazil), for his time and support proofreading this document.

Authors' Contributions

B.H.: Conceptualization (lead); methodology (lead); investigation (lead); writing—original draft (lead); and writing—review and editing (lead).

J.B.: Investigation (supporting); and writing—review and editing (supporting).

R.M.S. and P.R.C.: Writing—review and editing (supporting); and supervision (supporting).

G.L.: Formal analysis (supporting).

R.A.L.: Supervision (supporting); and writing—review and editing (supporting).

M.W. and M.R.M.: Supervision, lead (equal); project administration, lead (equal); writing—review and editing, and supporting.

Disclosure Statement

No competing financial interests exist.

Funding Information

This work was jointly supported by the Biotechnology and Biological Sciences Research Council (BBSRC; reference BB/T508329/1), and GlaxoSmithKline as part of an iCASE PhD studentship.

Supplementary Material

Supplementary Material

References

1. Gonzalez-Andrades M, Alonso-Pastor L, Mauris J, et al. Establishment of a novel in vitro model of stratified epithelial wound healing with barrier function. Sci Rep 2016;6(1):1–9; doi: 10.1038/srep19395
2. Sun T-T. Altered phenotype of cultured urothelial and other stratified epithelial cells: Implications for wound healing.

Downloaded by Birmingham University from www.liebertpub.com at 07/08/23. For personal use only.

Am J Physiol Physiol 2006;291(1):F9–F21; doi: 10.1152/ajprenal.00035.2006
3. Porter RM, Lunny DP, Ogden PH, et al. K15 expression implies lateral differentiation within stratified epithelial basal cells. Lab Investig 2000;80(11):1701–1710; doi: 10.1038/labinvest.3780180
4. Natarajan VT, Ganju P, Ramkumar A, et al. Multifaceted pathways protect human skin from UV radiation. Nat Chem Biol 2014;10(7):542–551; doi: 10.1038/nchembio.1548
5. Steinert PM. The complexity and redundancy of epithelial barrier function. J Cell Biol 2000;151(2):5–7; doi: 10.1083/jcb.151.2.f5
6. Presland RB, Jurevic RJ. Making sense of the epithelial barrier: What molecular biology and genetics tell us about the functions of oral mucosal and epidermal tissues. J Dent Educ 2002;66(4):564–574; doi: 10.1002/j.0022-0337.2002.66.4.tb03536.x
7. Abdulkareem AA, Shelton RM, Landini G, et al. Periodontal pathogens promote epithelial-mesenchymal transition in oral squamous carcinoma cells in vitro. Cell Adhes Migr 2018;12(2):127–137; doi: 10.1080/19336918.2017.1322253
8. Lechler T, Fuchs E. Asymmetric cell divisions promote stratification and differentiation of mammalian skin. Nature 2005;437(7056):275–280; doi: 10.1038/nature03922
9. Koster MI, Roop DR. Mechanisms regulating epithelial stratification. Annu Rev Cell Dev Biol 2007;23(1):93–113; doi: 10.1146/annurev.cellbio.23.090506.123357
10. Khan E, Shelton RM, Cooper PR, et al. Architectural characterization of organotypic cultures of H400 and primary rat keratinocytes. J Biomed Mater Res Part A 2012;100 A(12):3227–3238; doi: 10.1002/jbm.a.34263
11. Watt FM. Involucrin and other markers of keratinocyte terminal differentiation. J Invest Dermatol 1983;81(1):S100–S103; doi: 10.1111/1523-1747.EP12540786
12. Banks-Schlegel S, Green H. Involucrin synthesis and tissue assembly by keratinocytes in natural and cultured human epithelia. J Cell Biol 1981;90(3):732–737; doi: 10.1083/JCB.90.3.732
13. Pezzulo AA, Starner TD, Scheetz TE, et al. The air-liquid interface and use of primary cell cultures are important to recapitulate the transcriptional profile of in vivo airway epithelia. Am J Physiol Lung Cell Mol Physiol 2011;300(1):25–31; doi: 10.1152/ajplung.00256.2010
14. Breslin S, O'Driscoll L. The relevance of using 3D cell cultures, in addition to 2D monolayer cultures, when evaluating breast cancer drug sensitivity and resistance. Oncotarget 2016;7(29):45745; doi: 10.18632/ONCOTARGET.9935
15. Tatara T, Mukohara T, Tanaka R, et al. 3D culture represents apoptosis induced by trastuzumab better than 2D Monolayer Culture. Anticancer Res 2018;38(5):2831–2839; doi: 10.21873/anticanres.12528
16. Prunieras M, Regnier M, Woodley D. Methods for cultivation of keratinocytes with an air-liquid interface. J Invest Dermatol 1983;81(1 Suppl.):S28–S33; doi: 10.1111/1523-1747.ep12540324
17. Kameyama S, Kondo M, Takeyama K, et al. Air exposure causes oxidative stress in cultured bovine tracheal epithelial cells and produces a change in cellular glutathione systems. Exp Lung Res 2009;29(8):567–583; doi: 10.1080/01902140390240113
18. Lin H, Li H, Cho HJ, et al. Air-liquid interface (ALI) culture of human bronchial epithelial cell monolayers as an in vitro model for airway drug transport studies. J Pharm Sci 2007;96(2):341–350; doi: 10.1002/jps.20803
19. Aufderheide M, Mohr U. CULTEX: An alternative technique for cultivation and exposure of cells of the respiratory tract to airborne pollutants at the air/liquid interface. Exp Toxicol Pathol 2000;52(3):265–270; doi: 10.1016/S0940-2993(00)80044-5
20. Bernstam LI, Vaughan FL, Bernstein IA. Keratinocytes grown at the air-liquid interface. Vitr Cell Dev Biol Anim 1986;22(12):695–705; doi: 10.1007/bf02621086
21. Fatou JG. Melting temperature and enthalpy of isotactic polypropylene. Eur Polym J 1971;7(8):1057–1064; doi: 10.1016/0014-3057(71)90138-8
22. Roy S, Fleischman AJ. Cytotoxicity evaluation of microsystems materials using human cells. Sensors Mater 2003;15(6):335–340;
23. Garlotta D. A Literature review of poly(lactic acid). J Polym Environ 2001 92 2001;9(2):63–84; doi: 10.1023/A:1020200822435
24. Tsou CH, Yao WH, Lu YC, et al. Antibacterial property and cytotoxicity of a poly(lactic acid)/nanosilver-doped multiwall carbon nanotube nanocomposite. Polymers (Basel) 2017;9(3):100; doi: 10.3390/POLYM9030100
25. Greene JP. Microstructures of Polymers. In: Automotive Plastics and Composites. William Andrew Books; pp. 2021; 27–37.
26. Melo Pithon M, Lacerda R, Santos D, et al. Cytotoxicity of polycarbonate orthodontic brackets. Brazilian J Oral Sci 2009;8(2):84–87; doi: 10.20396/BJOS.V8I2.8642232
27. Prime S, Nixon S, Crane I, et al. The behaviour of human oral squamous cell carcinoma in cell culture. J Pathol 1990;160(3):259–269; doi: 10.1002/PATH.1711600313
28. Feldman AT, Wolfe D. Tissue Processing and Hematoxylin and Eosin Staining. In: Methods in Molecular Biology Humana Press Inc.; 2014; pp. 31–43; doi: 10.1007/978-1-4939-1050-2_3
29. Schindelin J, Arganda-Carreras I, Frise E, et al. Fiji: An open-source platform for biological-image analysis. Nat Methods 2012;9(7):676–682; doi: 10.1038/nmeth.2019
30. Ikarashi Y, Tsuchiya T, Nakamura A. Cytotoxicity of medical materials sterilized with vapour-phase hydrogen peroxide. Biomaterials 1995;16(3):177–183; doi: 10.1016/0142-9612(95)92115-M
31. Barosova H, Meldrum K, Karakocak BB, et al. Inter-laboratory variability of A549 epithelial cells grown under submerged and air-liquid interface conditions. Toxicol Vitr 2021;75:105178; doi: 10.1016/J.TIV.2021.105178
32. Rosdy M, Clauss LC. Terminal epidermal differentiation of human keratinocytes grown in chemically defined medium on inert filter substrates at the air-liquid interface. J Invest Dermatol 1990;95(4):409–414; doi: 10.1111/1523-1747.ep12555510
33. Wang H, He L, Liu B, et al. Establishment and comparison of air-liquid interface culture systems for primary and immortalized swine tracheal epithelial cells. BMC Cell Biol 2018;19(1):1–10; doi: 10.1186/s12860-018-0162-3
34. Bernstam LI, Vaughan FL, Bernstein IA. Stratified cornified primary cultures of human keratinocytes grown on microporous membranes at the air-liquid interface. J Dermatol Sci 1990;1(3):173–181; doi: 10.1016/0923-1811(90)90129-2

35. Bacakova M, Pajorova J, Broz A, et al. A two-layer skin construct consisting of a collagen hydrogel reinforced by a fibrin-coated polylactide nanofibrous membrane. Int J Nanomedicine 2019;14:5033; doi: 10.2147/IJN.S200782
36. Ekanayake-Mudiyanselage S, Aschauer H, Schmook FP, et al. Expression of epidermal keratins and the cornified envelope protein involucrin is influenced by permeability barrier disruption. J Invest Dermatol 1998;111(3):517–523; doi: 10.1046/J.1523-1747.1998.00318.X
37. Ye P, Chapple CC, Kumar RK, et al. Expression patterns of e-cadherin, involucrin, and connexin gap junction proteins in the lining epithelia of inflamed gingiva. J Pathol 2000; 192(1):58–66; doi: 10.1002/1096-9896(2000)9999:9999<::AID-PATH673>3.0.CO;2-T
38. Van Roy F, Berx G. The cell-cell adhesion molecule E-cadherin. Cell Mol Life Sci 2008;65(23):3756–3788; doi: 10.1007/s00018-008-8281-1
39. Yang L, Shridhar SV, Gerwitz M, et al. An in vitro vascular chip using 3d printing-enabled hydrogel casting. Biofabrication 2016;8(3):035015; doi: 10.1088/1758-5090/8/3/035015
40. Herreros-Pomares A, Zhou X, Calabuig-Fariñas S, et al. 3D printing novel in vitro cancer cell culture model systems for lung cancer stem cell study. Mater Sci Eng C 2021;122: 111914; doi: 10.1016/J.MSEC.2021.111914
41. Samavedi S, Joy N. 3D printing for the development of in vitro cancer models. Curr Opin Biomed Eng 2017;2:35–42; doi: 10.1016/J.COBME.2017.06.003
42. Vanderburgh J, Sterling JA, Guelcher SA. 3D printing of tissue engineered constructs for *in vitro* modeling of disease progression and drug screening. Ann Biomed Eng 2016;45(1):164–179; doi: 10.1007/S10439-016-1640-4

Address correspondence to:
Malgorzata Wiench, PhD
Birmingham Dental Hospital
5 Mill Pool Way
Birmingham B5 7EG
United Kingdom

E-mail: m.d.wiench@bham.ac.uk

Michael R. Milward, BDS, PhD
Birmingham Dental Hospital
5 Mill Pool Way
Birmingham B5 7EG
United Kingdom

E-mail: M.R.Milward@bham.ac.uk

Received: June 29, 2022
Accepted: August 26, 2022
Online Publication Date: October 14, 2022

Downloaded by Birmingham University from www.liebertpub.com at 07/08/23. For personal use only.